Numerical Methods for the Microscopic Cardiac Electrophysiology Model

Diane Fokoué

Thesis submitted in partial fulfillment of the requirements
for the Ph.D. degree in
Mathematics and Statistics[1]

Department of Mathematics and Statistics
Faculty of Science
University of Ottawa

[1]The Ph.D. program is a joint program with Carleton University, administered by the Ottawa-Carleton Institute of Mathematics and Statistics.

Abstract

The electrical activity of the heart is a well studied process. Mathematical modeling and computer simulations are used to study the cardiac electrical activity: several mathematical models exist, among them the microscopic model, which is based on the explicit representation of individual cells. The cardiac tissue is viewed as two separate domains: the intra-cellular and extra-cellular domains, Ω_i and Ω_e, respectively, separated by cellular membranes Γ. The microscopic model consists of a set of Poisson equations, one for each sub-domain, Ω_i and Ω_e, coupled on interfaces Γ with nonlinear transmission conditions involving a system of ODEs. The unusual transmission conditions on Γ make the model challenging to solve numerically.

In this thesis, we first focus on the dimensional analysis of the microscopic model. We then reformulate the problem on the interface Γ using a Steklov-Poincaré operator. We discretize the model in space using finite element methods. We prove the existence of a semi-discrete solution using a reformulation of the model as an ODE system on the interface Γ. We derive stability and error estimates for the finite element method. Afterwards, we consider five numerical schemes including the Godunov splitting method, two implicit methods, (Backward Euler (BE) and second order Backward Differentiation Formula (BDF2)), and two semi-implicit methods (Forward Backward Euler (FBE), and second order Semi-implicit Backward Differentiation Formula (SBDF2)). A convergence analysis of the implicit and semi-implicit methods is performed and the results are compared with manufactured solutions that we have proposed. Numerical results are presented to compare the stability, accuracy and efficiency of the methods. CPU times needed to solve the problem over a single cell using FBE, SBDF2 and Godunov splitting methods are reported. The results show that FBE and Godunov splitting methods achieve better numerical accuracy and efficiency than implicit and SBDF2 schemes, for a given computational time.

Finally, we solve the model using FBE and Domain Decomposition Method (DDM) for two cells connected to each other by a gap junction. We investigate the influence of the space discretization and we explore the differences between a conforming and non-conforming mesh on Γ. We compare the solutions obtained with both FBE and DDM methods. The results show that both methods give the same solution. Therefore, the DDM is capable of providing an accurate solution with a minimal number of sub-domain iterations.

Résumé

L'activité électrique du coeur fait l'objet de beaucoup de recherche. La modélisation mathématique et les simulations numériques sont utilisées pour étudier l'activité électrique cardiaque. Pour cette étude, plusieurs modèles mathématiques existent parmi lesquels le modèle microscopique. Ce dernier est basé sur la représentation explicite des cellules individuelles. Le tissu cardiaque est considéré comme deux domaines distincts : les domaines intra-cellulaire et extra-cellulaire, notés respectivement Ω_i et Ω_e, séparés par une membrane cellulaire notée Γ. Le modèle microscopique consiste en un ensemble d'équations de Poisson, une pour chaque sous-domaine Ω_i et Ω_e, couplées sur l'interface Γ par des conditions de transmission non linéaires impliquant un systme d'équations différentielles ordinaires (EDO). Les conditions de transmission non standards sur Γ rendent le modèle difficile à résoudre numériquement.

Dans cette thèse, nous faisons d'abord une analyse dimensionnelle du modèle. Ensuite, nous reformulons le problème sur Γ à l'aide d'un opérateur de Steklov-Poincaré. Nous discrétisons le modèle en espace en utilisant une méthode d'éléments finis. Nous prouvons l'existence d'une solution semi-discrète en utilisant une reformulation du modèle en un système d'EDO sur Γ. Nous dérivons des estimations d'erreur et de stabilité pour la méthode des éléments finis. Ensuite, nous considérons cinq discrétisations en temps, dont la méthode de Godunov, deux méthodes implicites (Euler implicite (BE) et Différentiation rétrograde (BDF2) du second ordre) et deux méthodes semi-implicites (Euler semi-implicite (FBE) et Différentiation rétrograde semi-implicite (SBDF2) du second ordre). Des estimés d'erreur sont obtenus pour les méthodes implicites et semi-implicites. Les résultats sont comparés aux solutions manufacturées que nous avons proposées. Des résultats numériques sont présentés pour comparer la stabilité, la précision et l'efficacité des méthodes. Les temps de calculs nécessaires pour résoudre le problème sur une cellule en utilisant les méthodes FBE, SBDF2 et le schéma de Godunov sont présentés. Les tests numériques montrent que la méthode de Godunov et le shéma FBE atteignent une meilleure précision et efficacité numériques que les schémas implicites et SBDF2, pour un temps de calcul donné.

Enfin, nous résolvons le modèle pour deux cellules interconnectées par une jonction de connection. Nous utilisons le shéma FBE et une méthode de décomposition de domaine (DDM). Nous étudions l'influence de la résolution du maillage et les différences entre un maillage conforme et non conforme sur Γ. Nous comparons les solutions obtenues avec les méthodes FBE et DDM. Les résultats numériques montrent que les deux méthodes donnent la même solution. Par conséquent, la méthode DDM est capable de fournir une solution précise avec un nombre minimal d'itérations de sous-domaines.

Acknowledgements

I would like to express my gratitude to Professor **Yves Bourgault** for having supervised my PhD thesis. I learned so many things from you. You are not only a great professional academics but also a wonderful person.
I am thankful to all members of my thesis committee: the external examiner Dr. Jean Deteix and the internal examiners Dr. Catherine Mavriplis, Dr. Emmanuel Lorin and Dr. Diane Guignard.
I am grateful to the Queen Elizabeth II Diamond Jubilee Scholarship (QES) program in partnership with the African Institute of Mathematical Sciences (AIMS) for funding part of my thesis.
A special thanks to the Natural Sciences and Engineering Research Council of Canada (NSERC) for supporting my research through a grant from the Collaborative Research and Training Experience (CREATE-481695-2016) program in Simulation-based Engineering Science (SBES).
I would like to thank Professor **Hubert Nnang** for introducing me to scientific world.
I am thankful to my officemates for the good times spent together in the office.
I am grateful to all my friends for being supportive and helpful throughout my doctoral studies.
Last but not least, I cannot say thank you enough to my lovely mom **Julienne Kwenbeu** for her prayers, tremendous support and neverending love. I would also like to express my deepest gratitude to my siblings, nephews and nieces Georgette, Simplice, Zéphirin, Gabriel, Guilène, Rachel, Dorgeline, Emérance, Géniale and Judicael.

Contents

Chapter 1

Basic Details of Cardiac Electrophysiology

Introduction

The heart is a muscular organ that propels the blood into the circulatory system through contractions of its muscle wall called myocardium. These contractions of the cardiac muscle result from numerous complex biochemical reactions and from some mechanical phenomena taking place in the muscle cells. These phenomena are initiated and are maintained by the electrical signals propagating through cells. Although the heart is one of the most important organs in the human body, the cardiac system is unfortunately vulnerable to breakdown and assault from various sources. The cardiovascular (heart) diseases, such as cardiac ischemia (restriction in blood supply to cardiac tissues) and heart arrhythmia (abnormal heart rhythm), can lead to heart failure and other heart-related complications. As reported by public-heath Canada, heart diseases are the second leading cause of death in Canada, claiming more than $51,500$ lives in 2015. About 2.4 million Canadians aged 20 years and older live with ischemic heart disease. According to the Cardiac Arrhythmia Network of Canada (CANet), heart arrhythmias kills about $40,000$ Canadians a year and are projected to be the leading cause of death in Canada by 2020. Many of those heart problems result from disturbances of the electrical activity. Therefore, a good-understanding of the electrical activity of the heart may help to treat those diseases and also to improve the precision of the tests that measure and record this activity, e.g. electrocardiogram(ECG). For more details about the link between the electrical activity and heart problems, see [33] and [23].

1.1 Cardiac Cells and Cardiac Action Potential

The heart has two types of cells: the cardiac muscle cells and the cardiac pacemaker cells. The latter cells have the ability to spontaneously generate and send out electrical signals. Furthermore, each cardiac cell is surrounded by a cellular membrane, that separates the intracellular space (the interior of a cell) from the extracellular space (the outside environment of a cell). The cell membrane consists of a lipid bilayer in which are embedded proteins. It contains ionic channels, which allow the flow of specific ions, mainly Na^+, Ca^{2+}, K^+, and Cl^-. Moreover, the cellular membrane serves as a gatekeeper and also as a barrier to the free flow of ions and maintains concentration differences of these ions. A potential difference, called resting transmembrane potential, exists across all cells membranes. In addition, the potential inside the cells is called intracellular potential and the one outside extracellular potential. At rest, the intracellular potential of cells is negative compared to the extracellular potential. Furthermore, the myocytes are excitable cells that are interconnected by regions called intercalated disks. These disks contain gap junctions, which are channels between cells that permit inter-cellular communications and that electrically couple adjacent cells. Thus, gap junctions allow solutes to pass from one cell to the next without having to pass through the cell membranes of the cells, see e.g. Figure 1.1(b). Further, excitable cells are capable of generating and transmitting electrochemical impulses, so they have the ability to respond actively to an electrical stimulus. However, stimulating an excitable cell leads to a change in transmembrane potential. If the change is small, the conductive properties of the membrane remain the same and the potential quickly returns to its resting value after the stimulus ends. On the other hand, if the stimulus is strong enough to raise the transmembrane potential above a certain threshold value, then the cell membrane depolarizes, that is, the transmembrane potential increases from its negative resting value to a value around, or above zero, then repolarizes, that is, the potential returs to its negative resting state. This phenomenum is called action potential (AP). In the following, we describe the five main phases of ventricular cell action potential, see Figure 1.1(a) for an illustration.

Phase 0: A rapid upstroke of the AP or fast depolarization
During this phase, some fast voltage-gated Na^+ channels are activated and open, allowing a large influx of Na^+ ions to enter the cell. This inward Na^+ flow causes the transmembrane potential to become less negative, and this results in a depolarization of the membrane. The membrane potential then increases further to about +40 mV from its resting value of about −85 mV.

Phase 1: Short repolarization
This is a brief initial repolarization caused by a decrease in inward Na^+ current due to closure of Na^+ channels. At the same time K^+ channels open, allowing a brief flow of K^+ ions out of the cell.

Phase 2: Plateau phase
During this phase, there is an increased Ca^{2+} conductance, causing inward Ca^{2+} flow. This creates an approximate balance between inward Ca^{2+} flow and outward K^+ flow.This phase is responsible for the long duration of cardiac action potentials.

Phase 3: Repolarization
This rapid repolarization results from the fact that Ca^{2+} channels close while K^+ channels are still open. The outward K^+ flow then exceeds the inward Ca^{2+} flow, causing a rapid decrease in the membrane potential.

Phase 4: Resting phase
The cell returns to its resting membrane potential characterized by an equilibrium between outward and inward ionic currents. Shortly after the repolarization, the cell is still in a *refractory period*, that is, a period of time during which the cell cannot be excited again till the ion concentrations and gating variables return to their equilibrium value.
For more details about cardiac action potential, see e.g.[34, 72, 64].

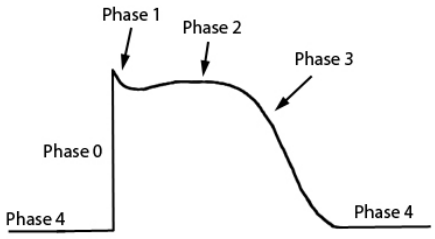

(a) Transmembrane potential as a function of time.

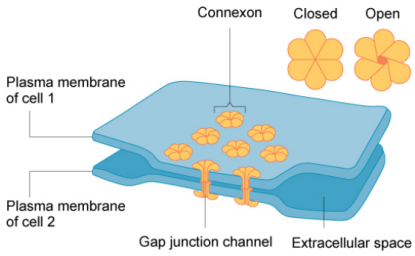

(b) Gap junction channels

Figure 1.1: Ventricular action potential and gap junction channels.

1.2 Membrane Ion Channel Gating

As mentioned above, the cell membrane contains ionic channels as well as pumps and transporters which allow the flow of specific ions accross the membrane. The movement of ions across the membrane is governed by the opening and closing of the ion channels in response to a change in transmembrane potential. The opening and closing of ion channels are the basis of electrical excitability. We introduce the formalism for modeling ion channel gating as described in [24] and [71]. The ionic current through a population of ionic channels is given per unit area of membrane surface by

$$\mathrm{I}_{ion} = \mathrm{G}(v,t)\phi(v),$$

where $\mathrm{G}(v,t)$ is the density of open channels per unit area of the membrane surface, which can be written as

$$\mathrm{G}(v,t) = \frac{\mathrm{N}}{\mathrm{S}} = \frac{\mathrm{N}_{total}}{\mathrm{S}}\frac{\mathrm{N}}{\mathrm{N}_{total}} = \frac{\mathrm{N}_{total}}{\mathrm{S}}w,$$

where $w = \frac{\mathrm{N}}{\mathrm{N}_{total}}$ is the gating variable that represents the percentage of open channels, N is the number of open channels on the membrane surface, N_{total} is the total number of membrane channels and S is the membrane surface area; $\phi(v)$ is the current-voltage relation of a single open channel, which can be written as $\phi(v) = g(v - v_{\mathrm{I}_0})$ where v is the transmembrane potential, g is the channel conductance and v_{I_0} is the Nernst equilibrium potential for a given ion, I_0,

$$v_{\mathrm{I}_0} = \frac{\mathrm{RT}}{z\mathrm{F}}\ln\left(\frac{[\mathrm{I}_0]_e}{[\mathrm{I}_0]_i}\right), \tag{1.1}$$

where R is Boltzmann's constant, T is the temperature, z is the charge of an electron, F is Faraday's constant, $[\mathrm{I}_0]_e$ and $[\mathrm{I}_0]_i$ denote the extra- and intracellular concentrations of the ion, I_0, respectively. Moreover, the models for the ion channels assume that the channels are composed of several sub-units. Each sub-unit may be either open or closed. We focus on ionic channels that consist of only one sub-unit with two states: the open state, O, and the close state, C. The change between the open and closed states may be written as

$$\mathrm{O} \underset{\beta(v)}{\overset{\alpha(v)}{\leftrightarrows}} \mathrm{C},$$

where α and β are the rate of opening and closing, respectively. The rate of change of w reads as follows

$$\frac{dw}{dt} = \alpha(v)(1-w) - \beta(v)w. \tag{1.2}$$

It is not possible to find a general solution of (1.2), since α and β depend on v. The equation (1.2) can be written as

$$\frac{dw}{dt} = \frac{(w_\infty - w)}{\tau_w}, \tag{1.3}$$

where $w_\infty = \frac{\alpha}{\alpha+\beta}$ is the asymptotic equilibrium state and $\tau_w = \frac{1}{\alpha+\beta}$ is the time constant. In general, the ionic channels are composed of several sub-units, which may be either open or closed, and which may depend on the state of the other sub-units, see e.g. [24].

1.3 Models for Ionic Activity in Cardiomyocytes

The ionic models are systems of ordinary differential equations (ODEs), that are used to describe from the basic to more complex levels, physiological processes occuring during the action potential. Several of these models exist and are grouped into three categories: the phenomenological models; the so-called first and second generation models, see e.g.[11, 23, 71] and the references therein. First of all, the cell membrane can be viewed as a capacitor, that separates ionic charges between the intra- and extracellular spaces. Moreover, the cell membrane contains ionic channels that act as resistors leading to ionic currents. The transmembrane current, I_m, is then the sum of the capacitive and the ionic current, I_{ion}, and must be equal to the applied current, I_{stim}, which reads as:

$$\mathrm{I}_m := \mathrm{C}_m \frac{dv}{dt} + \mathrm{I}_{\mathrm{ion}} \quad = \quad \mathrm{I}_{stim}, \tag{1.4}$$

where C_m is the capacitance of the membrane.
In the next sub-sections, we present the situation of a single myocyte, some models for ionic currents that could be useful in this work.

1.3.1 The Mitchell-Schaeffer Model

The model, proposed by Mitchell and Schaeffer [45], is a two-current model for a cardiac action potential that incorporates only an inward current (primarily carried by Na^+ and Ca^{2+}) and an outward current (primarily carried by K^+). Therefore, it requires a minimal set of currents to describe the process of excitation and recovery. The original Mitchell-Shaeffer (MS) model consists of two ordinary differential equations for the

transmembrane potential v and one gating variable w:

$$\begin{aligned}
\frac{\partial v}{\partial t} &= f(v,w) + \mathrm{I}_{stim}(t), \quad \text{with} \quad f(v,w) = \frac{1}{\tau_{in}} w v^2 (1-v) - \frac{1}{\tau_{out}} v, \\
\frac{\partial w}{\partial t} &= g(v,w), \quad \text{with} \quad g(v,w) = \begin{cases} \frac{1}{\tau_{open}}(1-w) & \text{if} \quad v < v_{gate}, \\ -\frac{1}{\tau_{close}} w & \text{if} \quad v \geq v_{gate}, \end{cases}
\end{aligned}$$

where $\mathrm{I}_{stim}(t)$ is an externally applied electrical stimulus, v_{gate} is the activation threshold potential and $\tau_{in}, \tau_{out}, \tau_{open}$ and τ_{close} are the four time constants that characterize the four main phases of the transmembrane action potential. The term $-f(v,w)$ represents the ionic current, I_{ion}, in (1.4) after rescaling this equation. The MS model is used in general to produce non-pacemaker cardiac AP. Several variations of the MS model have been proposed to address various purposes. In order to reproduce pacemaker cardiac action potential, Djabella et al. [18] proposed a modified model by introducing a tuning parameter in the MS model. They used a C^2 class function to describe the dynamics of the gating variable. Their modified MS model reads as

$$\begin{aligned}
\frac{\partial v}{\partial t} &= f(v,w) + \mathrm{I}_{stim}(t), \quad \text{with} \quad f(v,w) = \frac{1}{\tau_{in}} w (v+a)(v+a-\lambda)(1-v) - \frac{1}{\tau_{out}} v, \\
\frac{\partial w}{\partial t} &= g(v,w), \qquad\qquad \text{with} \quad g(v,w) = \tau(v,w)(w_\infty(v) - w),
\end{aligned}$$

$$\begin{aligned}
\tau(v,w) &= \frac{1}{\tau_{close}} + \frac{\tau_{close} - \tau_{open}}{\tau_{close}\tau_{open}} w_\infty(v) \\
w_\infty(v) &= \begin{cases} \frac{1}{2}(1 - \tanh(\frac{v - v_{gate}}{\eta_{gate}})) & \text{if} \quad \eta_{gate} \neq 0, \\ \frac{1}{2}(1 - \mathrm{sgn}(v - v_{gate})) & \text{if} \quad \eta_{gate} = 0, \end{cases}
\end{aligned}$$

where a, λ and η_{gate} are newly introduced parameters, that are used to control the excitability and pacemaker activity. In contrast, Corrado and Niederer [13] point out the fact that the transmembrane potential in the MS model, may cyclically depolarise and repolarise for certain values of the parameter τ, in the absence of any applied external stimulus. This unwanted behaviour, that they named "pacemaker cell behaviour" could be a problem in some clinical situation, see e.g. [13] and the references therein. To overcome this limitation, they introduce another modified version of the MS model that reads as

$$\begin{aligned}
\frac{\partial v}{\partial t} &= f(v,w) + \mathrm{I}_{stim}(t), \quad \text{with} \quad f(v,w) = \frac{1}{\tau_{in}} w v (v - v_{gate})(1-v) - \frac{1}{\tau_{out}} (1-w) v, \\
\frac{\partial w}{\partial t} &= g(v,w), \quad \text{with} \quad g(v,w) = \begin{cases} \frac{1}{\tau_{open}}(1-w) & \text{if} \quad v < v_{gate}, \\ -\frac{1}{\tau_{close}} w & \text{if} \quad v \geq v_{gate}. \end{cases}
\end{aligned}$$

Note that this model is obtained from the previous model by replacing $a = 0, \lambda = v_{gate}$, and introducing the factor $(1 - w)$ in the first equation.

Remark 1.3.2. *The potential v and the gating variable w are dimensionless and vary between 0 and 1. However, the voltage v can be scaled back to the original physiological values according to,*

$$\bar{v} = v(v_{max} - v_{rest}) + v_{rest}, \tag{1.5}$$

*where v_{rest} and v_{max} are the resting and maximum potentials, respectively. For example, we can choose $v_{rest} = -85mV$ and $v_{max} = +40mV$ as explained in the **Phase 0** of the action potential, Figure 1.1.*

1.3.3 The FitzHugh-Nagumo Model

The FitzHugh-Nagumo (FHN) model is a two-variable model, introduced by FitzHugh and Nagumo [22, 47], that is used to describe excitation and recovery during an action potential. The FHN model in its original formulatin consists of two ODEs for the trans-membrane potential v and a second variable, w, called recovery variable. The model equations are given by

$$\begin{aligned} \frac{\partial v}{\partial t} &= f(v,w), \quad \text{with} \quad f(v,w) = kv(v-\alpha)(1-v) - w, \\ \frac{\partial w}{\partial t} &= g(v,w), \quad \text{with} \quad g(v,w) = \varepsilon(v - \gamma w), \end{aligned}$$

where ε is chosen small, $0 < \alpha < \frac{1}{2}$, and γ is chosen so that the equation $k(v-\alpha)(1-v) - \frac{1}{\gamma} = 0$ has no real roots, that is, there is only one steady state solution, see e.g. [35].

1.3.4 The Hodgkin-Huxley Model

The Hodgkin-Huxley (HH) model, proposed by Hodgkin and Huxley [27], describes three ionic currents; a sodium current, a potassium current, and another one called leakage current made up by chloride and other ions. They are denoted by $\mathrm{I}_{Na}, \mathrm{I}_K$ and I_L, respectively, and are defined by

$$\mathrm{I}_{Na} = \bar{\mathrm{G}}_{Na} m^3 h (v - v_{Na}) \tag{1.6}$$

$$\mathrm{I}_K = \bar{\mathrm{G}}_K n^3 h (v - v_K) \tag{1.7}$$

$$\mathrm{I}_L = \bar{\mathrm{G}}_L (v - v_L) \tag{1.8}$$

where $\bar{\mathrm{G}}_{Na}$, $\bar{\mathrm{G}}_K$, $\bar{\mathrm{G}}_L$ are the maximum conductances for each current, that is, the currents one would obtain if all channels were open; v_{Na}, v_K, and v_L are the Nernst equilibrium potentials of the form (1.1), ; m, h, and n are three gating variables satisfying equation of the form (1.3). The total ionic current is then the sum of the three currents (1.6)-(1.8). The HH model reads as follows,

$$\begin{aligned}
\mathrm{C}_m\frac{dv}{dt} + \bar{\mathrm{G}}_{Na}m^3h(v-v_{Na}) &+ \bar{\mathrm{G}}_K n^3h(v-v_K) + \bar{\mathrm{G}}_L(v-v_L) = \mathrm{I}_{stim},\\
\frac{dm}{dt} &= \frac{m_\infty(v)-m}{\tau_m(v)}\,,\\
\frac{dh}{dt} &= \frac{h_\infty(v)-h}{\tau_h(v)}\,,\\
\frac{dn}{dt} &= \frac{n_\infty(v)-n}{\tau_n(v)}\,,
\end{aligned}$$

where the coefficients of the gating variables are given by equations of the form

$$\begin{aligned}
w_\infty &= \frac{\alpha_w}{\alpha_w+\beta_w}\,,\\
\tau_w &= \frac{1}{\alpha_w+\beta_w}\,,
\end{aligned}$$

for $w = m, h, n$, with

$$\begin{aligned}
\alpha_m &= \frac{0.1(25-v)}{\exp\left(0.1(25-v)\right)-1}\,, \qquad \beta_m = 4\exp\left(\frac{-v}{18}\right)\\
\alpha_n &= \frac{0.01(10-v)}{\exp\left(0.1(10-v)\right)-1}\,, \qquad \beta_n = 0.125\exp\left(\frac{-v}{80}\right)\\
\alpha_h &= 0.07\exp\left(\frac{-v}{20}\right)\,, \qquad \beta_h = \frac{1}{\exp\left(\frac{30-v}{10}\right)+1}.
\end{aligned}$$

The remaining parameters are

$$C_m = 1, \bar{G}_{Na} = 120, \bar{G}_K = 36, \bar{G}_L = 0.3, v_{Na} = 115, v_K = -12, v_L = 10.6\,.$$

The HH model describes the AP of a *squid giant axon*, which is a large nerve cell found in squids.

In 1977, Beeler and Reuter [6] proposed the first model of a mammalian ventricular cells. The model relies on the HH formalism and describes four ionic currents and the intracellular calcium concentration. The currents are controlled by six gating variables. Similarly, Luo and Rudy [44] introduced the so-called Luo Rudy 1 (LR1) model, which

is a new mammalian ventricular model based on the Beeler-Reuter model. The model included six ionic currents, which are controlled by seven gate variables in addition to a model for the intracellular calcium concentration. It is important to point out that HH, Beeler-Reuter and LR1 models are part of the first-generation models while MS and FHN models fall into the category of phenomenological models. The above models have a number of limitations. They aim to reproduce the AP, but uses a simplified formulation of the underlying physiological details. However, the so-called second-generation models fill the above-mentioned gaps by addressing a more detailed description of membrane currents as well as intracellular ionic concentrations. The second-generation models include more gating variables for ion channels, pumps and exchangers. In 1985, Difrancesco and Noble [16] proposed the first second-generation model of *Purkinje fibers*, which are large cardiac fibers specialized for rapid conduction along the endocardium of the ventricles. Other early second-generation models are the Luo Rudy dynamic (LRd) model [43] for guinea pig ventricular cells and the ten Tusscher-Noble-Noble-Panfilov (TNNP) model [73] for human ventricular tissue. As detailed as the second-generation models may be, they are computationally demanding. The following URL, `http://www.cellml.org/`, summarizes several other existing ionic models. In this work, we only focus on simple ionic models of ventricular cells, that capture the basic features of the cardiac AP.

1.4 Mathematical Models of Cardiac Tissue

The electrical activity of the heart is a well-studied process. Mathematical modelling and computer simulations are used for the study of the cardiac electrical activity. For this study, several mathematical models exist, among which the microscopic and macroscopic bidomain models.

The macroscopic model makes assumptions about the continuity of the cardiac tissue. The tissue is divided into two separate domains joined by the cell membrane: the intracellular and the extracellular domains. Since the muscle cells are connected via gap junctions, both domains are assumed to be continuous and fill the complete volume of the heart. The electrical potential in each of the two domains is then viewed as a quantity averaged over a small control volume. Therefore, every point in the heart muscle is assumed to be in both the intracellular and extracellular domains. Furthermore, the cardiac tissue has anisotropic conductive properties, since cardiac cells consist of fibers, and the conduction is higher in the direction of the fibers. In case the intracellular and extracellular domains have the same anisotropy ratio, the bidomain model can be re-

duced to the so-called monodomain model, see e.g.[71] and [23].
Although the bidomain model is widely used with many successful applications, it has some limitations. In fact, being an organ level model, the bidomain model does not provide details regarding the dynamics surrounding a single cell. Thus, the macroscopic bidomain model may fail to describe finer details of cardiac conduction, for example, it cannot address the ephaptic coupling of cardiac cells. Indeed, in the past some reasearchers believed that gap junctions are responsible for electrical impulse transmission between cardiomyocytes [60, 81]. However, recent experimental results have shown that AP conduction may still be possible in the absence of gap junctions channels [12, 36, 40, 65]. *Ephaptic coupling* is the expression used to describe AP conduction in the absence of gap junction channels.
On the other hand, at the microscopic level the cardiac tissue has a discrete structure. The cardiac structure consists of a collection of elongated cardiac cells, connected end-to-end or side-to-side by junctions, surrounded by the extracellular matrix. The microscopic model deals with an explicit representation of individual cells; the extracellular, the cell membrane and the intracellular domains are represented as separate geometrical spaces [76, 24, 67, 59, 79]. It is important to note, however, that some authors represent cardiomyocytes as a circuit diagram [12, 36, 40]. The microscopic model is of increasing significance, since it provides a more explicit and detailed framework for modeling cardiac tissue. For this reason, it is well suited to picture out the ephaptic coupling of cardiac cells and to simulate cell monoloyers. In fact, simulating cell monolayers is important in the development of human induced pluripotent stem cell-derived cardiomyocytes, which offer a powerful in vitro tool to investigate disease mechanisms and to perform patient-specific drug screening [38]. This model then fills the gaps of the macroscopic bidomain model, but does not claim to replace it. In the following, we mainly focus on the microscopic model, and we briefly present the macroscopic bidomain model.

1.4.1 Macroscopic Bidomain Model

At the macroscopic scale, the intracellular and the extracellular domains, Ω_i and Ω_e, respectively, are assumed to be continuous and fill the complete volume of the heart. Therefore, both domains are indistinguishable so that the domain, Ω, occupied by the heart is assimilated to $\Omega = \Omega_i = \Omega_e \subseteq \mathbb{R}^n$, $d = 2, 3$. Assuming that the heart is electrically insulated from its surroundings, the standard formulation of the bidomain

model consists in finding (v, u_e) such that

$$\begin{aligned} \nabla \cdot (\sigma_i \nabla v) + \nabla \cdot (\sigma_i \nabla u_e) &= \chi C_m \frac{\partial v}{\partial t} + \chi \mathrm{I}_{ion} \quad \text{in } \Omega, \\ \nabla \cdot (\sigma_i \nabla v) + \nabla \cdot ((\sigma_i + \sigma_e) \nabla u_e) &= 0 \quad \text{in } \Omega, \end{aligned}$$

with the boundary conditions

$$\begin{aligned} n \cdot (\sigma_i \nabla v + \sigma_i \nabla u_e) &= 0 \quad \text{on } \Gamma, \\ n \cdot (\sigma_e \nabla u_e) &= 0 \quad \text{on } \Gamma. \end{aligned}$$

In these equations, u_i is the intracellular potential, u_e is the extracellular potential; $v = u_i - u_e$ denotes the transmembrane potential, σ_i and σ_e are intracellular and extracellular conductivity 2-tensors, respectively; n is the unit exterior normal to the boundary of the heart Γ; C_m is the electrical capacitance of the membrane per unit area; χ represents the cell membrane area per unit volume; I_{ion} is the ionic current through the cell membrane per unit area. In case of equal anisotropy ratio, that is $\sigma_e = \lambda \sigma_i$ for some scalar λ, the bidomain can be reduced to the so-called monodomain model:

$$\frac{\lambda}{1+\lambda} \nabla \cdot (\sigma_i \nabla v) = \chi C_m \frac{\partial v}{\partial t} + \chi \mathrm{I}_{ion}, \quad \text{in } \Omega$$

with the boundary condition

$$n \cdot (\sigma_i \nabla v) = 0 \quad \text{on } \Gamma.$$

For rigorous details about the derivation of the bidomain model, see e.g. [48, 23, 71, 75].

1.4.2 Microscopic Model Based on Electrical Circuit

In the literature, several authors consider the flow of current through cardiomyocytes according to electrical circuits. Sperelakis et al. [51, 65] investigate the mechanism for transmission of excitation from one cell to the next within cardiac tissue by considering a circuit diagram of current along a strand of 10 cells, see Figure 1.2. They showed that successful transmission of excitation is possible without gap junctions, but is highly parameter dependent. More recently, Keener et al. [12, 36, 39, 40] followed the same framework as Sperelakis et al. [51, 65] to study the electrical coupling of cardiac cells in the absence of gap junctions. They consider the flow of current through cells according

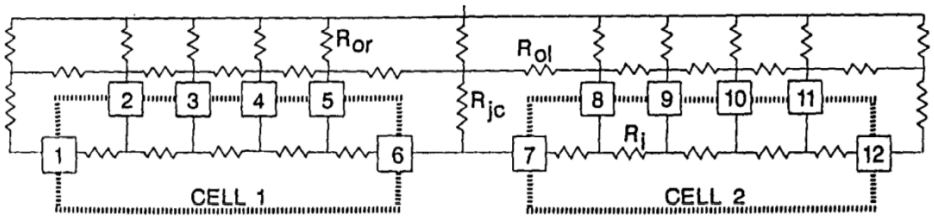

Figure 1.2: Electric circuit representing a strand of 2 cells separated by a narrow junctional cleft. Each cell is composed of six units: 4 surface membrane units, a pre-junctional and a post-junctional membrane units (reprinted from [51]).

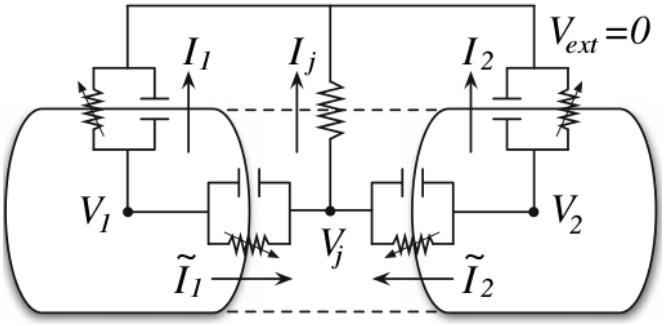

Figure 1.3: Circuit diagram of two cells coupled through a common junctional cleft space. The extracellular potential is set to be $V_{ext} = 0$ (reprinted from [12]).

to a circuit diagram. In the following, we only present the paper of Keener and Copene [12]. In this paper, they consider the flow of current through 2 cells, see Figure 1.3. They assume that the two cells with intracellular potentials V_1 and V_2, are isopotential. The extracellular potential, V_{ext}, is assumed to be constant in space and time. The potential V_{ext} is scaled to be $V_{ext} = 0$ so that V_1 and V_2 represent the nonjunctional transmembrane potentials. There is a difference in voltage between the junctional cleft space and extracellular space. The current which is driven between the two regions reads

$$I_j = \frac{1}{r_j} V_j, \tag{1.9}$$

where r_j is the resistance to current between the two spaces, and V_j is the junctional cleft potential which varies from the extracellular potential V_{ext}. The currents I_1 and I_2 (see Figure 1.3), accross the nonjunctional membranes of the two cells are the sum of

capacitive and ionic currents and are given by

$$\mathrm{I}_1 = \mathrm{A}\left(\mathrm{C}_m\frac{dV_1}{dt} + \mathrm{I}_{ion}(V_1)\right), \tag{1.10}$$

$$\mathrm{I}_2 = \mathrm{A}\left(\mathrm{C}_m\frac{dV_2}{dt} + \mathrm{I}_{ion}(V_2)\right). \tag{1.11}$$

Similarly, the currents, $\tilde{\mathrm{I}}_1$ and $\tilde{\mathrm{I}}_2$ (see, Figure 1.3), accross the junctional membrane of the two cells are obtained by

$$\tilde{\mathrm{I}}_1 = \tilde{\mathrm{A}}\left(\mathrm{C}_m\frac{d(V_1 - V_j)}{dt} + \tilde{\mathrm{I}}_{ion}(V_1 - V_j)\right), \tag{1.12}$$

$$\tilde{\mathrm{I}}_2 = \tilde{\mathrm{A}}\left(\mathrm{C}_m\frac{d(V_2 - V_j)}{dt} + \tilde{\mathrm{I}}_{ion}(V_2 - V_j)\right), \tag{1.13}$$

where $\tilde{\mathrm{A}}$ and A are the surface areas of the junctional and nonjunctional membranes, respectively; $\tilde{\mathrm{I}}_{ion}$ and I_{ion} are the sum of the junctional and nonjunctional ionic membrane currents, respectively. The potential differences $V_1 - V_j$ and $V_2 - V_j$ denote the transmembrane potentials of the junctional membranes. Applying Kirchhoff's circuit laws at each of the three nodes in the circuit diagram of Figure 1.3, we obtain

$$\mathrm{I}_1 = -\tilde{\mathrm{I}}_1 \tag{1.14}$$

$$\mathrm{I}_j = \tilde{\mathrm{I}}_1 + \tilde{\mathrm{I}}_2 \tag{1.15}$$

$$\mathrm{I}_2 = -\tilde{\mathrm{I}}_2. \tag{1.16}$$

For nondimensionlization purpose, they set

$$V_1 = u_1 V^* + V_{rest}, \tag{1.17}$$

$$V_2 = u_2 V^* + V_{rest}, \tag{1.18}$$

$$V_j = u_j V^*, \tag{1.19}$$

where $V^* = V_{peak} - V_{rest}$. Note that V_{rest} and V_{peak} are the resting and maximum potentials, respectively. The resulting non-dimensional system of equations is then given by

$$\frac{d}{d\tau}u_1 + \alpha\frac{d}{d\tau}(u_1 - u_j) = f(u_1) + \alpha\tilde{f}(u_1 - u_j), \tag{1.20}$$

$$\alpha\frac{d}{d\tau}(u_1 - u_j) + \alpha\frac{d}{d\tau}(u_2 - u_j) = \alpha\tilde{f}(u_1 - u_j) + \alpha\tilde{f}(u_2 - u_j) + \sigma u_j, \tag{1.21}$$

$$\frac{d}{d\tau}u_2 + \alpha\frac{d}{d\tau}(u_2 - u_j) = f(u_2) + \alpha\tilde{f}(u_2 - u_j); \tag{1.22}$$

where u_1 and u_2 are the nondimensional potentials of the two cells, and u_j is the nondimensional potential in the junctional cleft space between the two cells, $\alpha = \frac{\tilde{\mathrm{A}}}{\mathrm{A}}$ is the ration of the junctional membrane surface area to the nonjunctional membrane surface area, and $\sigma = \frac{t^*}{r_j \mathrm{A} C_m}$ is a nondimensional parameter with the rescaled time $t = t^* \tau$. The nonjunctional and junctional nondimensional ionic membrane currents are denoted by $f(u)$ and $\tilde{f}(u)$, respectively.

1.4.3 Microscopic Model Based on Electrodiffusion Equations

The electrodiffusion is a passive process by which charged particles are transported through a medium under the influence of both simultaneously a concentration gradient and an electric potential [25]. The Nernst-Planck equations describes the electrodiffusion process. Mori and Peskin [46] presented a model for cellular electrophysiology based on Nernst-Planck equations together with some boundary conditions. In the model, the tissue is partitioned into several non-overlapping intracellular compartments and multiple extracellular spaces. Intracellular and extracellular spaces are labeled by $\Omega_i^{(k)}$ and $\Omega_e^{(l)}$, respectively. The membrane separating the domains $\Omega_i^{(k)}$ and $\Omega_e^{(l)}$ is denoted by $\Gamma^{(kl)}$, see Figure 1.4. Let N be the total number of ion species; c_j and ϕ denote the j-th ion

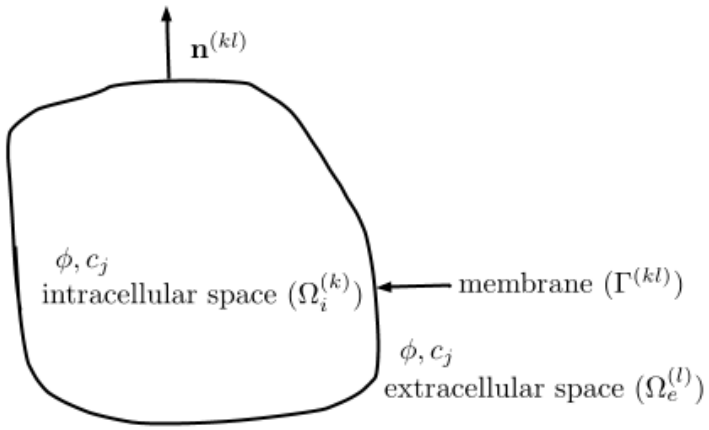

Figure 1.4: The membrane $\Gamma^{(kl)}$, the intra and extracellular domains $\Omega_i^{(k)}$ and $\Omega_e^{(l)}$, respectively, in which the variables c_j and ϕ are defined (reprinted from [46]).

concentration and electrostatic potential, respectively. In $\Omega_i^{(k)}$ and $\Omega_e^{(l)}$, the equations

satisfied by c_j and ϕ read as follows

$$\frac{\partial c_j}{\partial t} = -\nabla \cdot \mathbf{J}_j, \qquad \text{(ion conservation)} \qquad (1.23)$$

$$\mathbf{J}_j = -\mathrm{D}_j \left(\nabla c_j + \frac{q z_j c_j}{k_{\mathrm{B}} \mathrm{T}} \nabla \phi \right), \qquad \text{(drift-diffusion flux)} \qquad (1.24)$$

$$0 = \rho_0 + \sum_{j=1}^{\mathrm{N}} q z_j c_j, \qquad \text{(electroneutrality condition)} \qquad (1.25)$$

where $\mathbf{J}_j$ is the flux of the j-th species of ion; D_j is the diffusion coefficient of the j-th ion; q is the elementary charge; qz_j is the amount of charge on the j-th ion; k_{B} is the Boltzmann constant; T is the absolute temperature and ρ_0 is the fixed background charge density (if any). The flux $\mathbf{J}_j$ is expressed as a sum of two components: the diffusion component caused by the gradient of the ion concentration and the drift component which is driven by the electric field. Equations (1.23)-(1.25) are coupled with some boundary conditions on membranes $\Gamma^{(kl)}$, see [17, 52, 53] for more details. Poisson Nernst-Planck equations can be used in several biophysical models, including cardiac electrophysiology models. For instance, Mori et al. [46] used the electrodiffusion model to study the effect of gap junctions on the propagation of cardiac action potential.

1.4.4 Microscopic Model Based on Potential Equations

For the derivation of basic equations that govern the microscopic model, we follow the ideas of Veneroni [79]. We adopt the following notations, see Figure 1.5. We consider that Ω_i and Ω_e denote the intracellular and extracellular space, respectively, whose boundaries are $\partial\Omega_i$ and $\partial\Omega_e$, respectively. The set $\overline{\Gamma} = \partial\Omega_i \cap \partial\Omega_e$ is the surfacic cellular membrane that separates the two spaces, $\Gamma_i = \partial\Omega_i \setminus \Gamma$, and $\Gamma_e = \partial\Omega_e \setminus \Gamma$ stand for the remaining part of the boundary of Ω_i and Ω_e, respectively. The vectors n_i, n_e represent the unit exterior normals to the boundary of Ω_i and Ω_e, respectively. They satisfy $n = n_i = -n_e$ on Γ. We set $\Omega = \Omega_i \cup \Omega_e \cup \Gamma \subset \mathbb{R}^m$, $m = 2, 3$, to be the physical region occupied by the heart.

Assuming that $\mathrm{I}_{i,stim}$ and $\mathrm{I}_{e,stim}$ are the given stimulation currents applied to Ω_i and Ω_e, respectively, the potentials inside Ω_i and Ω_e could be obtained by solving the following Poisson's equations:

$$\begin{aligned} -\nabla \cdot (\sigma_i \nabla u_i) &= \mathrm{I}_{i,stim} \quad \text{in } \Omega_i, \\ -\nabla \cdot (\sigma_e \nabla u_e) &= \mathrm{I}_{e,stim} \quad \text{in } \Omega_e, \end{aligned}$$

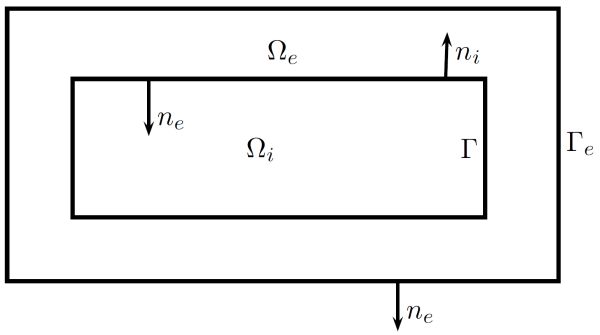

Figure 1.5: Sketch of a simplified computational domain; the intracellular space Ω_i, the cell membrane Γ, and the extracellular space Ω_e.

where u_i is the intracellular potential; u_e is the extracellular potential; σ_i and σ_e are intracellular and extracellular conductivities, respectively. In addition, the normal current flux though the membrane is continuous, due to the current conservation law. Then we have

$$\sigma_i \nabla u_i \cdot n_i + \sigma_e \nabla u_e \cdot n_e \;=\; 0 \quad \text{on } \Gamma.$$

The cell membrane can be viewed as a capacitor in parallel with a resistor leading to ionic currents, see e.g. [24, 37, 23, 79]. As stated above, the membrane current per unit area, I_m, is then the sum of the capacitive and ionic currents, and reads as follows

$$\mathrm{I}_m \;=\; \mathrm{C}_m \frac{\partial v}{\partial t} + f(v, w),$$

where C_m is the electrical capacitance of the membrane per unit area, $v = u_i - u_e$ denotes the transmembrane potential, f represents the ionic current through the cellular membrane Γ and w is the gating variable. It is worth recalling that f is one of the three functions given in Section 1.3.

The following Neumann boundary conditions (BCs) hold on the membrane Γ:

$$\sigma_e \nabla u_e \cdot n_e \;=\; -\sigma_i \nabla u_i \cdot n_i := \mathrm{I}_m \quad \text{on } \Gamma.$$

These Neumann BCs are complemented by

$$\sigma_i \nabla u_i \cdot n_i = g_i \quad \text{on } \Gamma_i \quad \text{and} \quad \sigma_e \nabla u_e \cdot n_e = g_e \quad \text{on } \Gamma_e,$$

or

$$u_i = 0 \quad \text{on } \Gamma_i \quad \text{and} \quad u_e = 0 \quad \text{on } \Gamma_e,$$

for some given functions g_i and g_e. Summarizing all these equations, the microscopic model equations read

$$\begin{aligned}
-\nabla \cdot (\sigma_i \nabla u_i) &= \mathrm{I}_{i,stim} \quad \text{in } \Omega_i, && (1.26)\\
-\nabla \cdot (\sigma_e \nabla u_e) &= \mathrm{I}_{e,stim} \quad \text{in } \Omega_e, && (1.27)\\
\mathrm{I}_m &:= \mathrm{C}_m \frac{\partial v}{\partial t} + f(v,w) \quad \text{on } \Gamma, && (1.28)\\
\sigma_e \nabla u_e \cdot n_e &= -\sigma_i \nabla u_i \cdot n_i = \mathrm{I}_m \quad \text{on } \Gamma, && (1.29)\\
v &= u_i - u_e \quad \text{on} \quad \Gamma, && (1.30)\\
\sigma_e \nabla u_e \cdot n_e &= g_e \quad \text{on } \Gamma_e, && (1.31)\\
\sigma_i \nabla u_i \cdot n_i &= g_i \quad \text{on } \Gamma_i. && (1.32)
\end{aligned}$$

To ensure wellposedness of the problem (1.26)-(1.32), a supplementary condition on u_e is needed. This will be discussed below. The model is coupled with the following system of ordinary differential equations

$$\frac{\partial w}{\partial t} = g(v,w) \quad \text{on} \quad \Gamma. \tag{1.33}$$

where g models the dynamics of the gating variable, w.

Veneroni [79] proved the existence of a solution for the microscopic model with two choices for the ionic current, that are the classical Hodgkin-Huxley model [27] and the Phase-I Luo-Rudy model [44]. In the same vein, Franzone and Savaré [24] derive, adapting the tools of abstract evolution equations in Hilbert spaces, existence, uniqueness and some regularity results for the model. They consider only the FitzHugh-Nagumo model as a membrane model for ionic currents. In the literature, several other authors have used the microscopic model for different purposes. For example, to assess the computational challenges of the microscopic modeling framework, Tveito et al. [76] solved, using a finite difference method (FDM) and two types of mixed finite element methods (FEM), a variant of the microscopic model (1.26)-(1.32). They first present the method in the case of two coupled cells, $\Omega_{i,1}$ and $\Omega_{i,2}$, that are connected by gap junctions $\Gamma_{1,2}$ and are surrounded by a connected extracellular space Ω_e, see Figure 1.6. The model assumes that there are no stimulation currents applied to $\Omega_{i,j}$ and Ω_e, the potentials $u_{i,j}$ and u_e inside $\Omega_{i,j}$ and Ω_e, respectively, are then obtained by solving the equation (1.26) in $\Omega_{i,j}$ and the equation (1.27) in Ω_e with $\mathrm{I}_{i,j} = 0$ and $\mathrm{I}_e = 0$ for $j = 1, 2$. On the membranes Γ_1 and Γ_2, the equations of the form (1.28) and (1.29) are solved, together with a Dirichlet boundary condition

$$u_e = 0 \quad \text{on} \quad \partial\Omega_e \setminus (\Gamma_1 \cup \Gamma_2). \tag{1.34}$$

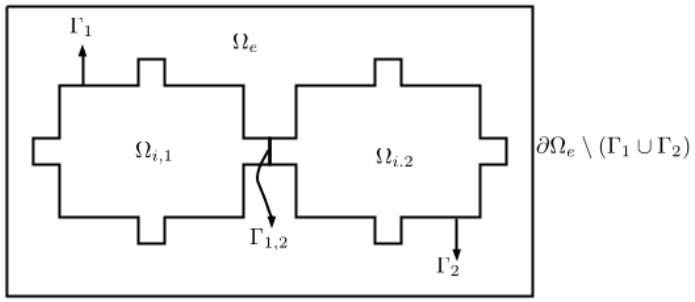

Figure 1.6: Sketch of an idealized computational domain: two idealized cells $\Omega_{i,1}$ and $\Omega_{i,2}$, connected by a gap junction $\Gamma_{1,2}$ and the surounding extracellular space Ω_e (reprinted from [76]).

Similarly, on the gap junction $\Gamma_{1,2}$ the following equations are considered

$$\begin{aligned} n_{i,2} \cdot \sigma_i \nabla u_{i,2} &= -n_{i,1} \cdot \sigma_i \nabla u_{i,1} \equiv \mathrm{I}_{1,2} && \text{on } \Gamma_{1,2}, \\ w &= u_{i,1} - u_{i,2} && \text{on } \Gamma_{1,2}, \\ \frac{\partial w}{\partial t} &= \frac{1}{\mathrm{C}_{1,2}}(\mathrm{I}_{1,2} - \mathrm{I}_{gap}) && \text{on } \Gamma_{1,2}, \end{aligned}$$

where $n_{i,j}$ is the normal pointing out from $\Omega_{i,j}$ for $j = 1, 2$, and I_{gap} is the gap junction current density, which can be represented by a passive membrane

$$\mathrm{I}_{gap}(w) = \frac{1}{\mathrm{R}_{gap}} w,$$

where R_{gap} represents the resistance of the passive membrane. For the computation, they introduced a two-step operator splitting method in order to handle the case of a nonlinear ionic current, I_{ion}. In the first (ODE) substep of the operator splitting scheme, they solved a system of ODEs of the form (1.28) on the membrane, with the membrane current, I_m, set equal to zero. In the second (PDE) substep, they solved the linear system arising from an implicit discretization in time and space of (1.26)-(1.29) with $u_e = 0$ on $\partial\Omega_e \setminus \Gamma$ and the term I_{ion} set to zero. For the discretization in time of (1.28), they used an implicit Euler scheme. They considered both a passive and an active model for the dynamics on the cell membrane between the intra and extracellular spaces. In the passive model, the ionic current is given by

$$\mathrm{I}_{ion}(v) = \frac{1}{\mathrm{R}_m}(v - v_{rest}), \tag{1.35}$$

where R_m is the resistance of the passive membrane and v_{rest} is the resting potential of the membrane. In the active model, I_{ion} is represented by the model of Grandi et al. [26]. Tveito et al. [76] proposed and compared three different approaches for the spatial discretization of PDEs arising from the second (PDE) substep, which are the finite difference method, the mortar finite element method [7] and Raviart-Thomas finite element method [55]. They first assess the accuracy of these numerical methods. In the case of the nonlinear ionic current, they explored convergence under mesh refirements: they compared, for two connected cells, the solutions obtained from the numerical methods using different spatial resolution. For the linear ionic current (1.35), they considered a simple model problem with known analytical solution. They consider then a 2D domain consisting of an extracellular domain and a single cell, see Figure 1.7. With linear ionic currents, all the discretizations provide converging numerical solutions. The convergence of the finite difference discretization is linear and this method is the least accurate. Compared to the FDM, the mortar FEM provides solutions with considerably smaller error, whereas the Raviart-Thomas FEM is the most accurate with errors much smaller than those of the mortar FEM. Furthermore, for the CPU requirements, Tveito et al. [76] were interested in the CPU time needed to solve the numerical problems, particularly the CPU time per physical cell.

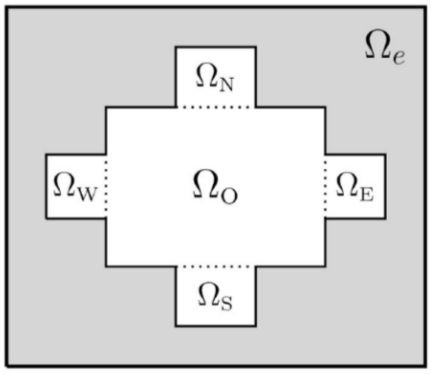

Figure 1.7: Sketch of a 2D version of a domain in the case of a single cell. Here $\Omega_i = \Omega_o \cup \Omega_W \cup \Omega_E \cup \Omega_S \cup \Omega_N$ (reprinted from [76]).

To study at the microscopic level the relationship between tissue morphology and the propagation of the depolarization wave, Henriquez et al. [67] introduced a 3D model of cardiac tissue. Figure 1.8 summarizes all the equations and boundary conditions used in the model.

In this figure, φ_i, φ_e and $\mathrm{I_{mem}}$ are equivalent to u_i, u_e and $\mathrm{I_{ion}}$, respectively, $\mathrm{I_{stim}}$ is an

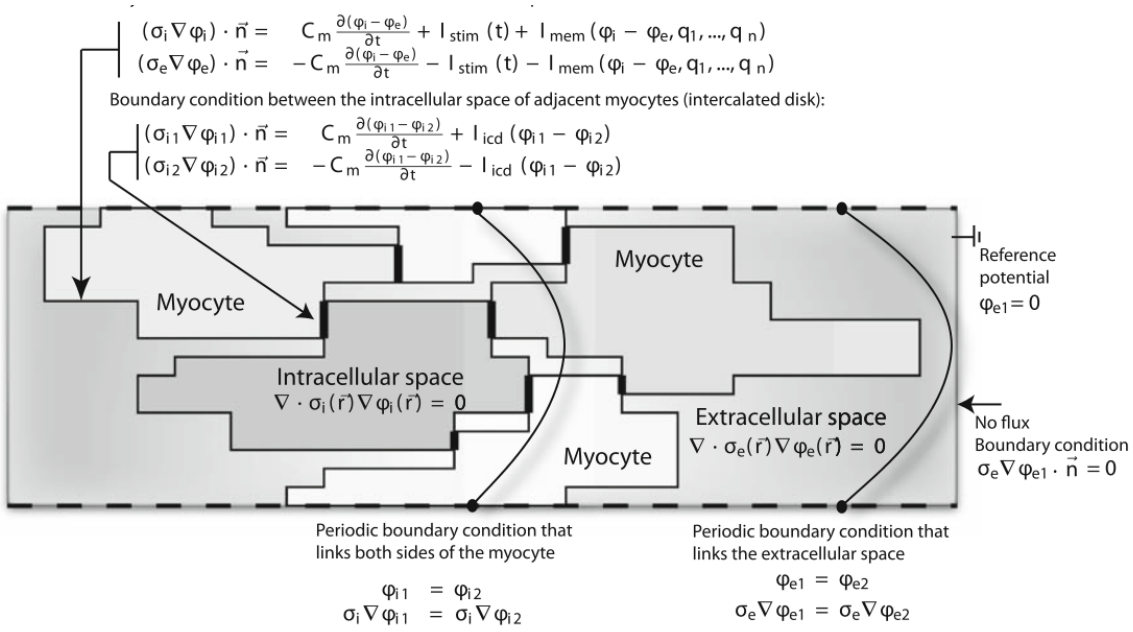

Figure 1.8: Summary of all the model equations and boundary conditions (reprinted from [67])

externally applied stimulus current, and $q_1, \cdots, q_n$ are the variables denoting the state of the membrane as a function of time. The term I_{icd} stands for the conductance of the intercalated disk. They consider a geometrical model that consists of an explicit description of the shape and stacking of all the myocytes that are located in a small piece of tissue to be stimulated. The intracellular and extracellular spaces are continuous spatially separated volumes that are defined inside the same cartesian space. The model assumes that myocytes are stacked inside an extracellular matrix so that at some locations, the myocytes touch neighboring myocytes, whereas at other locations small sheets of extracellular space separate the myocytes. Therefore, the tissue is subdivided into multiple non-overlapping compartments: a single compartment for the extracellular space and separated compartments for each myocyte. For their model, they constrain the shape of the cells to look like those captured in histology, see Figures 1.9 and 1.10. In Figure 1.9, each subdomain is represented with a different color to represent the different myocytes and the extracellular space left uncolored. Because a myocyte is surrounded

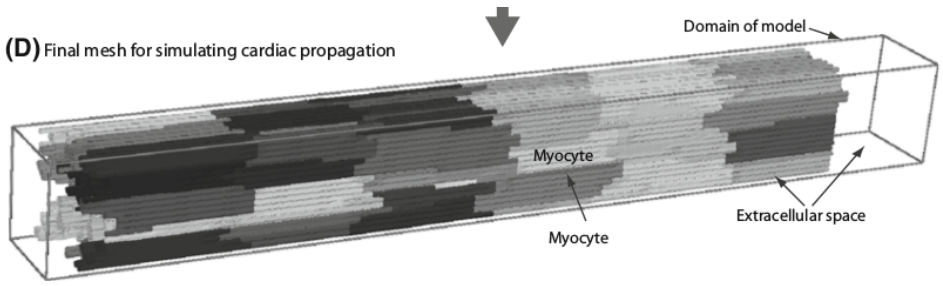

Figure 1.9: A 3D stack of myocytes (reprinted from [67])

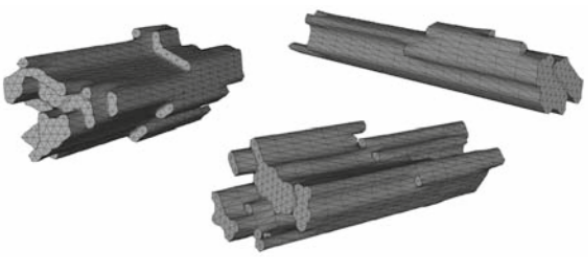

(a) Cell shapes in the computer generated model.

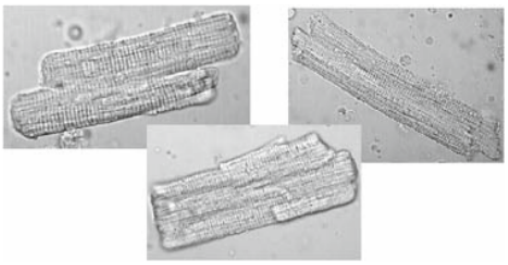

(b) Microscopic images of rat myocytes.

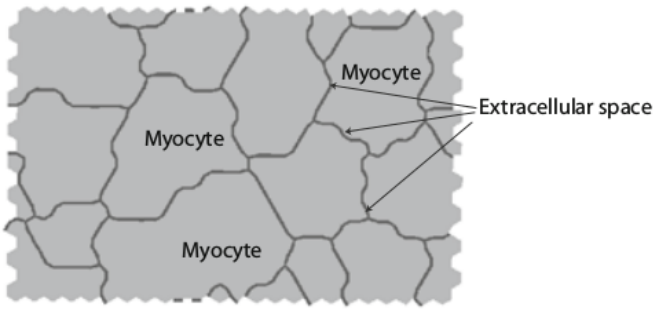

(c) Distribution of extracellular space around myocytes in the computer generated model.

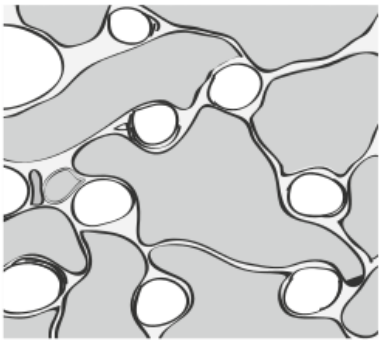

(d) Microscopic images of rat myocytes.

Figure 1.10: A comparaison between the computer generated tissue geometry and actual illustrations from histology (reprinted from [67]).

by extracellular space and neighboring myocytes, some interfaces are designated as intercalated disks, whereas other are designated as membranes. For interfaces separating two myocytes $\Omega_{i,1}$ and $\Omega_{i,2}$, the model assumes a surface resistance and capacitance that mimick a membrane infused with gap junctions, that is, a low resistive barrier between the two myocytes. Electrical potentials at the interface between $\Omega_{i,1}$ and $\Omega_{i,2}$ are denoted

by φ_{i1} and φ_{i2}, respectively, and conductivities by σ_{i1} and σ_{i2}, respectively. For the computation, they discretized their model in space using a mesh consisting of tetrahedral elements, and to solve for potentials, they use the finite element method with linear interpolation inside each element. Moreover, they use a semi-implicit Crank-Nicolson scheme to discretize in time and solved the linear set of equations resulting from the finite element method for each time step using the Minimal Residual Method (MINRES). As results, Henriquez et al. made a qualitative comparaison between shape and stacking of the myocytes as generated by their computational model and actual images of myocytes from histology. They also qualitatively compared the distributions of gap junctions and extracellular space with histological results, see Figure 1.10.

1.5 Existence of the Solution of Microscopic Problem

This section is devoted to reaction-diffusion systems associated with the microscopic model. We follow [79] and give a functional framework and a mathematical setting, where the wellposedness of the model can be established. We state the existence theorem for a solution. Let $]0, \mathrm{T}[$ be the evolution time interval. Let

$$\mathcal{Q}_{i,e} := \Omega_{i,e}\times]0,\mathrm{T}[, \quad \Sigma := \Gamma\times]0,\mathrm{T}[, \quad \Sigma_{i,e} := \Gamma_{i,e}\times]0,\mathrm{T}[.$$

Given

$$\begin{aligned} \mathrm{I}_{i,e} : \mathcal{Q}_{i,e} \;\to\; \mathbb{R}, \quad g_i : \Sigma_i \to \mathbb{R}, \quad \sigma_{i,e} : \overline{\Omega}_{i,e} \to \mathbb{M}^{3\times 3}, \\ v_0 : \Gamma \to \mathbb{R}, \quad \mathbf{w}_0 : \Gamma \;\to\; (0,+\infty)^k, \quad \mathbf{z}_0 : \Gamma \to (0,+\infty)^m, \end{aligned}$$

we seek

$$\begin{aligned} u_{i,e} : \mathcal{Q}_{i,e} \;\to\; \mathbb{R}, \quad \mathbf{w} = (w_1,\cdots,w_k) : \Sigma \to \mathbb{R}^k \\ v := u_i - u_e : \Sigma \;\to\; \mathbb{R}, \quad \mathbf{z} = (z_1,\cdots,z_m) : \Sigma \to (0,+\infty)^m, \end{aligned}$$

satisfying the equations

$$-\nabla\cdot(\sigma_{i,e}\nabla u_{i,e}) = \mathrm{I}_{i,e} \quad \text{in } \mathcal{Q}_{i,e}, \tag{1.36}$$

$$\sigma_i \nabla u_i \cdot n_i = g_i \quad \text{on } \Sigma_i, \tag{1.37}$$

$$u_e = 0 \quad \text{on } \Sigma_e, \tag{1.38}$$

$$\begin{aligned} \mathrm{I}_m &= \mathrm{C}_m \frac{\partial v}{\partial t} + \mathrm{I}_{\mathrm{ion}}(v, \mathbf{w}, \mathbf{z}) \quad \text{on } \Sigma, && (1.39)\\ \sigma_e \nabla u_e \cdot n_e &= -\sigma_i \nabla u_i \cdot n_i = \mathrm{I}_m \quad \text{on } \Sigma, && (1.40)\\ \frac{\partial \mathbf{w}}{\partial t} &= \mathbf{F}(v, \mathbf{w}) \quad \text{on } \Sigma, && (1.41)\\ \frac{\partial \mathbf{z}}{\partial t} &= \mathbf{G}(v, \mathbf{w}, \mathbf{z}) \quad \text{on } \Sigma, && (1.42) \end{aligned}$$

with initial data

$$\begin{aligned} v(x,0) &= v_0(x) \quad \text{on } \Gamma, && (1.43)\\ \mathbf{w}(x,0) &= \mathbf{w}_0(x) \quad \text{on } \Gamma, && (1.44)\\ \mathbf{z}(x,0) &= \mathbf{z}_0(x) \quad \text{on } \Gamma, && (1.45) \end{aligned}$$

where $\mathbb{M}$ is a $3 \times 3-$ matrix, $\mathbf{w}$ is the vector of gating variables, $\mathbf{F} = (F_1, \cdots, F_k)$ is the dynamics of the gating variable, $\mathbf{z}$ is the vector of intracellular ionic concentrations, and $\mathbf{G} = (G_1, \cdots, G_m)$ is the dynamics of the ionic concentrations.

Theorem 1.5.1. *Let be given*

$$\mathrm{I}_{i,e} \in \mathrm{H}^1(0,\mathrm{T};\mathrm{L}^2(\Omega_{i,e})), \quad g_i \in \mathrm{H}^1(0,\mathrm{T};\mathrm{H}^{-\frac{1}{2}}(\Gamma_i)), \quad v_0 \in \mathrm{H}^{\frac{1}{2}}(\Gamma),$$

$$\boldsymbol{z}_0 \in (\mathrm{L}^2(\Gamma))^m, \text{ with } \boldsymbol{\log z}_0 \in (\mathrm{L}^2(\Gamma))^m, \quad \boldsymbol{w}_0 : \Gamma \to [0,1]^k \text{ measurable},$$

$\sigma_{i,e} : \overline{\Omega}_{i,e} \to \mathbb{M}^{3\times 3}$, *are symmetric, positive definite, continuous tensors, and satisfy the uniform ellipticity condition*

$$\exists \underline{\sigma}, \overline{\sigma} > 0 : \quad \underline{\sigma}|\xi|^2 \le \sigma_{i,e}(x)\xi \cdot \xi \le \overline{\sigma}|\xi|^2 \quad \forall \xi \in \mathbb{R}^3, \quad \forall x \in \Omega_{i,e},$$

$F_j : \mathbb{R}^2 \to \mathbb{R}$, *is locally Lipschitz continuous for* $j = 1, \cdots, k$, *and* $G_i, i = 1, \cdots, m$, *are properly chosen, see [79] for more details.*
There exist $k + m + 2$ *functions* $w_1, \cdots, w_k, z_1, \cdots, z_m, u_i, u_e$ *such that*

$$u_i \in \mathrm{L}^2(0,\mathrm{T};\mathrm{H}^1(\Omega_i)), \quad u_e \in \mathrm{L}^2(0,\mathrm{T};\mathrm{H}^1_{\Gamma_e^0}(\Omega_e)),$$

$$v := (u_i - u_e)_{|\Gamma} \in \mathrm{H}^1(0,\mathrm{T};\mathrm{L}^2(\Gamma)) \cap \mathrm{L}^2(0,\mathrm{T};\mathrm{H}^{\frac{1}{2}}(\Gamma)),$$

$$\boldsymbol{w} : \Sigma \to [0,1]^k \text{ and } \boldsymbol{z} : \Sigma \to (0,+\infty)^m \text{ measurable},$$

$$w_j(x,\cdot) \in \mathrm{C}^1(0,\mathrm{T}) \cap \mathrm{C}^0[0,\mathrm{T}] \text{ for a.e } x \in \Gamma,\ j = 1, \cdots, k,$$

$$z_i(x,\cdot) \in \mathrm{C}^1(0,\mathrm{T}) \cap \mathrm{C}^0[0,\mathrm{T}] \text{ for a.e } x \in \Gamma,\ i = 1, \cdots, m,$$

$$\boldsymbol{w} \in \mathrm{L}^2(\Gamma;\mathrm{C}^0[0,\mathrm{T}])^k, \ \boldsymbol{z} \in \mathrm{H}^1(0,\mathrm{T};\mathrm{L}^2(\Gamma))^m, \ \boldsymbol{\log(z)} \in \mathrm{L}^2(\Gamma;\mathrm{C}^0[0,\mathrm{T}])^m,$$

which solve the problem (1.36)-(1.45).

The proof of the theorem can be found in[79]. A more detailed description of parabolic problems is presented in [54, 20, 56].
In this thesis, we deal with the Mitchell-Schaeffer model [45] for the ionic current model. As such, the vector of intracellular ionic concentrations $\mathbf{z}$ is not considered in our model. Moreover, the boundary conditions (1.38) are not Neuman boundary conditions (1.31) as in our model. Nevertheless, given the similarities between the two models, we assume on the basis of Theorem 1.5.1 that the model (1.26)-(1.33) admits a unique solution. We will clarify the functional setting for our model in Chapter 2.

1.6 Dimensional Analysis of the Model

We start with a dimensional analysis of the microscopic model (1.26)-(1.32). Dimensional analysis helps to derive the relationship between the different physical quantities involved in the model, which makes the system more analytically tractable. The non-dimensional variables and parameters will be denoted with a bar on the top.
The non-dimensional intracellular, extracellular, and transmembrane potentials, $\overline{u}_i, \overline{u}_e$ and $\overline{v}$ are rescaled as follows, respectively,

$$u_i = v_m \overline{u}_i + v_{rest}, \tag{1.46}$$
$$u_e = v_m \overline{u}_e + v_{rest}, \tag{1.47}$$
$$v = v_m \overline{v}, \tag{1.48}$$

where $v_m = v_{max} - v_{rest}$ is the characteristic transmembrane potential amplitude, v_{max} is the maximum membrane potential reached once the cell is depolarized, and v_{rest} is the resting membrane potential. We set the dimensionless variables, $\bar{t}$ and $\overline{x}$ as

$$\bar{t} = \frac{t}{\mathrm{T}}, \qquad \overline{x} = \frac{x}{\mathrm{L}},$$

where T and L represent the characteristic time and length, respectively. From the equation (1.28) we have

$$\begin{aligned} \mathrm{I_m} &= C_m \frac{\partial v}{\partial t} + f(v, w), \\ &= C_m v_m \frac{\partial \bar{v}}{\partial t} + f(v_m \bar{v}, \bar{w}), \quad \text{from (1.48)} \\ &= \frac{C_m v_m}{\mathrm{T}} \frac{\partial \bar{v}}{\partial \bar{t}} + f(v_m \bar{v}, \bar{w}). \end{aligned}$$

It follows that

$$\frac{\mathrm{T}}{C_m v_m}\mathrm{I_m} = \frac{\partial \overline{v}}{\partial \overline{t}} + \frac{\mathrm{T}}{C_m v_m} f(v_m \overline{v}, w),$$

since $\overline{w} = w$. It follows from equation (1.29) that

$$\frac{\mathrm{T}}{C_m \mathrm{L}}\sigma_e \bar{\nabla}\bar{u}_e \cdot n_e = -\frac{\mathrm{T}}{C_m \mathrm{L}}\sigma_i \bar{\nabla}\overline{u}_i \cdot n_i = \frac{\mathrm{T}}{C_m v_m}\mathrm{I_m}.$$

From now on, we assume that the interface Γ_i is empty. The nondimensional microscopic model reads

$$\begin{aligned}
-\bar{\nabla}\cdot(\bar{\sigma}_i\bar{\nabla}\bar{u}_i) &= \bar{\mathrm{I}}_{i,stim} \quad \text{in } \Omega_i, && (1.49)\\
-\bar{\nabla}\cdot(\bar{\sigma}_e\nabla\bar{u}_e) &= \bar{\mathrm{I}}_{e,stim} \quad \text{in } \Omega_e, && (1.50)\\
\bar{\mathrm{I}}_m &:= \frac{\partial \bar{v}}{\partial \bar{t}} + \bar{f}(\bar{v}, w) \quad \text{on } \Gamma, && (1.51)\\
\bar{\sigma}_e\bar{\nabla}\bar{u}_e \cdot n_e &= -\bar{\sigma}_i\bar{\nabla}\overline{u}_i \cdot n_i = \bar{\mathrm{I}}_m \quad \text{on } \Gamma, && (1.52)\\
\bar{v} &= \bar{u}_i - \bar{u}_e \quad \text{on} \quad \Gamma, && (1.53)\\
\bar{\sigma}_e\bar{\nabla}\bar{u}_e \cdot n_e &= \bar{g}_e \quad \text{on } \Gamma_e, && (1.54)
\end{aligned}$$

where $\Gamma_e = \partial\Omega_e \setminus \Gamma$. The relations between the scaled and the physical parameters are given by

$$\begin{aligned}
\bar{\sigma}_{i,e} &= \frac{\mathrm{T}}{\mathrm{C}_m \mathrm{L}}\sigma_{i,e}, \qquad \bar{\mathrm{I}}_{i,e,stim} = \frac{\mathrm{T}}{\mathrm{C}_m v_m}\mathrm{I}_{i,e,stim}, \qquad \bar{\mathrm{I}}_m = \frac{\mathrm{T}}{\mathrm{C}_m v_m}\mathrm{I}_m,\\
\bar{f}(\bar{v}, w) &= \frac{\mathrm{T}}{\mathrm{C}_m v_m} f(v_m\bar{v}, w), \qquad \bar{g}_e = \frac{\mathrm{T}}{\mathrm{C}_m v_m} g_e.
\end{aligned}$$

Note that the equation (1.51) can be rewritten

$$\frac{1}{\mathrm{T}}\bar{\mathrm{I}}_m(\bar{v}, w) = \frac{1}{\mathrm{T}}\frac{\partial \bar{v}}{\partial \bar{t}} + \frac{1}{\mathrm{T}}\bar{f}(\bar{v}, w),$$

where $\frac{1}{\mathrm{T}}\bar{f}(\bar{v}, w)$ represent the source term $f(v, w)$ in the MS model defined in section 1.3, see [57]. Therefore, the nondimensional microscopic model can be coupled with any nondimensional ionic model. From now on, we write the nondimensional variables and parameters without bars.

1.7 Objectives of the Thesis

In all the reviewed literature, few numerical methods are proposed for the microscopic model of cardiac electrophysiology. Simple test cases to verify numerical methods and

check their accuracy are also lacking. To our knowledge, the numerical analysis (e.g., stability, error estimates) is not yet available for any discretization method applied to the microscopic model. The purpose of this thesis is to explore various numerical methods for solving the microscopic model. A convergence analysis of the methods is performed and the results are compared to a manufactured solution that we have proposed. Numerical results are presented to compare the stability, accuracy and efficiency of the methods.

The rest of the thesis is organized as follows. In Chapter 2, we reformulate the problem on the interface using a Steklov-Poincaré oper- ator. We discretize the model in space using the finite element method (FEM). Afterwards, we prove the existence of a semi-discrete solution using a reformulation as an ODE system on the interface Γ. We derive stability and error estimates for the FEM. We propose a manufactured solution and we use it to perform numerical tests to verify that the order of convergence of the numerical method agrees with what is expected on the basis of the theoretical analysis of the convergence.

Note that Chapter 2 is presented in a draft paper format (in preparation for journal submission), while the subsequent chapters more closely follow the traditional thesis format.

In Chapter 3, we consider a variety of time-stepping methods applied to the microscopic model. A first class of methods directly addresses the fully coupled discrete problem through implicit and semi-implicit methods. Fully implicit methods studied are the Backward Euler (BE) method and second order Backward Differentiation Formula (BDF2). We use the Forward Backward Euler (FBE) method and the second order Semi-Implicit Backward Differentiation Formula (SBDF2) as representatives of the semi-implicit methods. The second class of methods is based on the Godunov splitting method. At each time step, we need to solve two separate problems, namely the nonlinear ODE models representing the ionic activity on Γ and coupled linear space propagation problems on the domains Ω_i and Ω_e. Under some assumptions on the nonlinear terms involved in the time-stepping methods, we prove the well-posedness of semi-discrete problems. We obtain theoretical convergence and error estimates in space and time, respectively. We first perform numerical tests using a manufactured solution that we have proposed to verify that the order of convergence of the methods agrees with the latter theoretical analysis. We then test the methods using a reference solution computed with the SBDF2 scheme. Numerical results are presented to compare the stability, accuracy and efficiency of the methods.

In Chapter 4, we provide an exploratory study aiming at extending the methods used in Chapter 3 in the case of the multi-cell model. We focus on the model consisting of two

cells connected to each other by a gap junction. We first consider a fixed, unstructured fine mesh that is conformal on the interfaces. We apply the FBE method to the model and we visualize the propagation of the action potential in both cells. We then investigate the influence of the space discretization, the conformity and the non-conformity of the mesh on the solution to determine if the results are mesh dependent or not. This will allow us to use meshes with as few nodes and elements as possible without altering the results. In addition to the FBE method, we solve the two-cell model using a non-overlapping time-splitting domain decomposition method (DDM). We estimate the error between two successive iterates of the DDM. Finally, we compare the solutions obtained with both FBE and DDM methods.

In Chapter 5, we present our conclusions and perspectives on the results obtained in the thesis.

Chapter 2

Numerical Methods for Microscopic Model

The electrical activity of the heart is a well-studied process. Several mathematical models are available for the simulation of the cardiac electrical activity at various scales. For instance, the bidomain model that is based on a homogenization process represents the cardiac action potential at the organ level, see e.g. [23, 48, 49, 71, 75]. For studying propagation between a smaller group of myocytes, the microscopic model is based on an explicit representation of individual cells. The cardiac tissue can be viewed as two separate domains: the intracellular and extracellular domains, Ω_i and Ω_e, respectively, the cellular membranes Γ are represented as separate geometrical spaces [24, 59, 67, 76, 78, 79]. The microscopic model is of increasing importance, since it is well suited to study the impact of some types of intercellular couplings and connections on the cardiac action potential (AP). In the literature, several authors have studied and used the microscopic model. Some of them consider the flow of current through cardiomyocytes using an analogy with electrical circuits. Sperelakis et al. [51, 65, 66] used this approach to investigate the mechanism for transmission of excitation from one cell to the next within cardiac tissue by considering a circuit diagram along a strand of cells. More recently, Keener et al. [12, 36, 39, 40] followed the same framework to study the electrical coupling of cardiac cells in the absence of gap junctions. In contrast, several other authors consider a microscopic model based on potential equations [5, 24, 31, 28, 59, 67, 76, 77, 79]. Tveito et al. [31] derived the bidomain model from the cell-based model and highlighted both similarities and differences between the models. To study at the microscopic level the relationship between tissue morphology and the propagation of the depolarization wave,

and to investigate the role of the distributions of the extracellular space around cells on the conduction velocity, Stinstra et al. [67, 68, 69] introduced a 3D model of cardiac tissue. Spiteri et al. [19] used the cell-based model to simulate the effects of a cardiac condition called long QT syndrome (LQTS). They compared simulations from data from healthy cells, cells that exhibit the syndrome, and cells that have been treated with a drug to restore healthy heart function. Veneroni [79] proved the existence of a solution for the microscopic model with two choices for the ionic current, that are the classical Hodgkin-Huxley model [27] and the Phase-I Luo-Rudy model [44]. In the same vein, Franzone and Savaré [24] derive, adapting the tools of abstract evolution equations in Hilbert spaces, existence, uniqueness and some regularity results for the model. They consider the FitzHugh-Nagumo model as a membrane model for ionic currents. Mori et al.[46] used the electrodiffusion model [25] to study the effect of gap junctions on the propagation of cardiac action potential.

From the mathematical standpoint, the microscopic model consists in a set of Poisson equations in two adjacent domains, coupled on interfaces with nonlinear transmission conditions involving a system of ODEs. The unusual coupling of PDEs and ODEs on the boundary makes the microscopic models challenging to solve numerically. Few numerical methods have been proposed in the litterature for the microscopic model [2, 5, 19, 28, 29, 31, 30, 76, 77]. Agudelo-Toro and Neef [2] presented numerical methods allowing detailed simulations of the electric activity of excitable cells and their interaction with extracellular potentials. They introduced an implicit time iteration scheme based on the Crank-Nicolson method and studied the numerical stability of the method. To assess the computational challenges of the microscopic modeling framework, Tveito et al. [76] solved the model using a finite difference method (FDM) and two types of mixed finite element methods (FEM) [7, 55]. In addition, they assess the accuracy of these numerical methods. Bécue [5] studied in his PhD thesis the impact of the presence and absence of different gap junctions models on the propagation of the AP. He developed a computational model of AP propagation through hand-crafted two- and three-dimensional networks of cells. He discretized the model in time using the Forward Backward Euler scheme. Tveito et al. [30] described the spatial operator splitting algorithm for splitting the model into separate equations. They outlined a finite difference discretization for the splitting approach and investigated the accuracy of the spatial splitting method.

In all the reviewed literature, few numerical methods are proposed and tested with simple test cases. The numerical analysis (e.g., stability, error estimates) is not yet available for any discretization method applied to the microscopic model. The goal of our paper is

to perform the numerical analysis of a finite element method for the microscopic model. We reformulate the problem on the interface Γ using Steklov-Poincaré operator. We discretize the model in space using the finite element method (FEM). Afterwards, we prove the existence of semi-discrete solutions using a formulation as an ODE system on the interface Γ. We derive stability and error estimates for the FEM. We perform numerical tests with a manufactured solution to verify that the order of convergence of the numerical method agrees with what is expected on the basis of the theoretical analysis of the convergence.

2.1 Formulations of the Microscopic Model

We consider the microscopic model [24, 79]

$$\begin{aligned} -\nabla\cdot(\sigma_i\nabla u_i) &= \mathrm{I}_{i,stim} \quad \text{in } \Omega_i, && (2.1)\\ -\nabla\cdot(\sigma_e\nabla u_e) &= \mathrm{I}_{e,stim} \quad \text{in } \Omega_e, && (2.2)\\ \mathrm{I}_m &:= \mathrm{C}_m\frac{\partial v}{\partial t} + f(v,w) \quad \text{on } \Gamma, && (2.3)\\ \sigma_e\nabla u_e\cdot n_e &= -\sigma_i\nabla u_i\cdot n_i = \mathrm{I}_m \quad \text{on } \Gamma, && (2.4)\\ [u] &= u_i - u_e = v \quad \text{on} \quad \Gamma, && (2.5)\\ \sigma_e\nabla u_e\cdot n_e &= g_e \quad \text{on} \quad \Gamma_e, && (2.6) \end{aligned}$$

where $\Omega=\Omega_i\cup\Omega_e\cup\Gamma\subset\mathbb{R}^m, m=2,3$, $\mathrm{I}_{i,stim}$ and $\mathrm{I}_{e,stim}$ are the given stimulation currents applied on Ω_i and Ω_e, respectively, f represents the ionic current through the cellular membrane Γ and g_e is a given function on $\Gamma_e=\partial\Omega_e\setminus\Gamma$. The model is coupled with the following system of ordinary differential equations describing the electrochemical process behind the opening/closing of the ionic channels through the membrane of the cell

$$\frac{\partial w}{\partial t} = g(v,w) \quad \text{on} \quad \Gamma, \tag{2.7}$$

where g models the dynamics of the gating variable, w. The following initial conditions are needed to close the system:

$$v(0) = v_0, \qquad w(0)=w_0 \qquad \text{on} \qquad \Gamma. \tag{2.8}$$

For the sake of simplicity, we assume below that $f=f(v)$ and $g=g(w)$ are independent from the gating variable w and membrane potential v, respectively. There are no essential difficulties in taking $f=f(v,w)$ and $g=g(v,w)$, only appropriate assumptions must be made about the dependence of f and g on the variables w and v, respectively, see [5]. We take $\mathrm{C}_m=1$.

2.1.1 Variational Formulation

We define a functional framework within which we derive the variational formulation of the problem (2.1)-(2.6). We set

$$u(x) = \begin{cases} u_i(x), \ x \in \Omega_i, \\ u_e(x), \ x \in \Omega_e, \end{cases} \quad \sigma(x) = \begin{cases} \sigma_i(x), \ x \in \Omega_i, \\ \sigma_e(x), \ x \in \Omega_e, \end{cases} \quad \mathrm{I_{stim}}(x) = \begin{cases} \mathrm{I}_{i,stim}(x), \ x \in \Omega_i, \\ \mathrm{I}_{e,stim}(x), \ x \in \Omega_e. \end{cases}$$

We define

$$\mathrm{W} = \left\{ u \in \mathrm{L}^2(\Omega) : u_{|\Omega_i} \in \mathrm{H}^1(\Omega_i), \, u_{|\Omega_e} \in \mathrm{H}^1(\Omega_e), \, \int_{\Omega_e} u_e dx = 0 \right\}, \tag{2.9}$$

equipped with the norm:

$$\|u\|_{\mathrm{W}} = \left(\|u\|^2_{\mathrm{H}^1(\Omega_i)} + \|u\|^2_{\mathrm{H}^1(\Omega_e)} \right)^{\frac{1}{2}}.$$

Then, W is a Hilbert space. Following Theorem 1.5.1, we assume that (2.1)-(2.6) admits a unique solution with

$$u \in \mathrm{L}^2(0,\mathrm{T};\mathrm{W}), \quad v = [u] \in \mathrm{H}^1(0,\mathrm{T};\mathrm{L}^2(\Gamma)) \cap \mathrm{L}^2(0,\mathrm{T};\mathrm{H}^{\frac{1}{2}}(\Gamma)), \quad \mathrm{I_{stim}} \in \mathrm{L}^2(0,\mathrm{T};\mathrm{L}^2(\Omega)),$$
$$\sigma \in \mathrm{L}^\infty(\Omega), \quad v_0 \in \mathrm{L}^2(\Gamma), \quad w_0 \in \mathrm{L}^2(\Gamma).$$

Multiplying the PDEs (2.1)-(2.2) by a test function $\varphi \in \mathrm{W}$, integrating over Ω, and using the Green formula yield

$$\begin{aligned} \int_{\Omega_i} \sigma_i \nabla u_i \cdot \nabla \varphi_i + \int_{\Omega_e} \sigma_e \nabla u_e \cdot \nabla \varphi_e + \int_\Gamma \frac{\partial [u]}{\partial t} [\varphi] \ &+ \ \int_\Gamma f([u])[\varphi] = \int_\Omega \mathrm{I}_{stim} \varphi \\ &+ \ \int_{\Gamma_e} g_e \varphi, \end{aligned} \tag{2.10}$$

where $[u] = u_{|\Omega_i} - u_{|\Omega_e} = u_i - u_e$ and $[\varphi] = \varphi_{|\Omega_i} - \varphi_{|\Omega_e} = \varphi_i - \varphi_e$ and $\dfrac{\partial [u]}{\partial t}$ is the weak derivative of $[u]$ in $\mathcal{D}'(0,\mathrm{T})$. We will reformulate the problem (2.10) into a variational formulation defined only on Γ. To do this, we will use the Steklov-Poincaré operator which links the potentials u_i and u_e with the transmembrane potential v. As such, we

split (2.1)-(2.6) into two coupled problems:

$$\begin{aligned}
-\nabla\cdot(\sigma_i\nabla u_i) &= \mathrm{I}_{i,stim} \quad \text{in} \quad \mathcal{D}'(\Omega_i), && (2.11)\\
-\nabla\cdot(\sigma_e\nabla u_e) &= \mathrm{I}_{e,stim} \quad \text{in} \quad \mathcal{D}'(\Omega_e), && (2.12)\\
\sigma_e\nabla u_e\cdot n_e &= -\sigma_i\nabla u_i\cdot n_i \quad \text{in} \quad \mathrm{H}^{-\frac{1}{2}}(\Gamma), && (2.13)\\
\sigma_e\nabla u_e\cdot n_e &= g_e \quad \text{in} \quad \mathrm{H}^{-\frac{1}{2}}(\Gamma_e), && (2.14)\\
[u] &= u_i-u_e=v, \quad \text{in} \quad \mathrm{H}^{\frac{1}{2}}(\Gamma) && (2.15)\\
\int_{\Omega_e} u_e\,dx &= 0, && (2.16)
\end{aligned}$$

and

$$\frac{\partial v}{\partial t}+f(v) = -\sigma_i\nabla \mathrm{S}_i(v)\cdot n_i \text{ on } \Gamma, \tag{2.17}$$

where S is an operator defined as follows:

$$\begin{aligned}
\mathrm{S}\colon \mathrm{H}^{\frac{1}{2}}(\Gamma) &\longrightarrow \mathrm{W} && (2.18)\\
v &\longmapsto \mathrm{S}(v):=(\mathrm{S}_i(v),\mathrm{S}_e(v))=u,
\end{aligned}$$

where $\mathrm{S}_i(v)=u_i$, $\mathrm{S}_e(v)=u_e$ and u is the solution of the problem (2.11)-(2.16).
There exists a linear lifting operator, see e.g. [54, 20]

$$\begin{aligned}
\mathrm{R}_i\colon \mathrm{H}^{\frac{1}{2}}(\Gamma) &\longrightarrow \mathrm{H}^1(\Omega_i), && (2.19)\\
\varphi &\longmapsto \mathrm{R}_i(\varphi),
\end{aligned}$$

such that $\mathrm{R}_i(\varphi)_{|\Gamma}=\varphi$ for all $\varphi\in\mathrm{H}^{\frac{1}{2}}(\Gamma)$ and

$$\|\mathrm{R}_i(\varphi)\|_{\mathrm{H}^1(\Omega_i)} \leq \mathrm{C}\|\varphi\|_{\mathrm{H}^{\frac{1}{2}}(\Gamma)}. \tag{2.20}$$

Fix $v\in\mathrm{H}^{\frac{1}{2}}(\Gamma)$, $\mathrm{R}_i(v)$ a lifting of v in $\mathrm{H}^1(\Omega_i)$, and define u_v a lifting of v in W as follows :

$$u_v=\begin{cases}\mathrm{R}_i(v) & \text{in } \Omega_i,\\ 0 & \text{in } \Omega_e,\\ v & \text{on } \Gamma.\end{cases} \tag{2.21}$$

Define

$$\mathrm{W}(v)=\left\{u\in\mathrm{L}^2(\Omega): u_{|\Omega_i}\in\mathrm{H}^1(\Omega_i),\ u_{|\Omega_e}\in\mathrm{H}^1(\Omega_e),\ [u]_{|\Gamma}=v,\ \int_{\Omega_e}u_e dx=0\right\},$$

where $[u]_{|\Gamma} = u_i - u_e$ on Γ. Then $\mathrm{W}(v) \neq \emptyset$ since $u_v \in \mathrm{W}(v)$. The space $\mathrm{W}(v)$ can be written

$$\mathrm{W}(v) = u_v + \mathrm{W}(0).$$

Therefore, $\mathrm{W}(v)$ is an affine space with vector space $\mathrm{W}(0) \subset \mathrm{H}^1(\Omega)$. The proposed variational formulation for (2.11)-(2.16) is:

$$\begin{cases} \text{Seek } u \in \mathrm{W}(v) \ \text{ such that} \\ \int_{\Omega_i} \sigma_i \nabla u_i \cdot \nabla \varphi_i + \int_{\Omega_e} \sigma_e \nabla u_e \cdot \nabla \varphi_e = \int_\Omega \mathrm{I}_{stim} \varphi + \int_{\Gamma_e} g_e \varphi_e, \\ \text{for all} \quad \varphi \in \mathrm{W}(0). \end{cases} \tag{2.22}$$

To show existence and uniqueness of the solution, we must first reformulate (2.22) on a vector subspace of $\mathrm{H}^1(\Omega)$ since it is defined on an affine subspace. We set $\tilde{u} = u - u_v \in \mathrm{W}(0)$. The problem (2.22) becomes

$$\begin{cases} \text{Seek } \tilde{u} \in \mathrm{W}(0) \ \text{ such that} \\ \int_\Omega \sigma \nabla \tilde{u} \cdot \nabla \varphi = \int_\Omega \mathrm{I}_{stim} \varphi + \int_{\Gamma_e} g_e \varphi_e - \int_{\Omega_i} \sigma \nabla u_v \cdot \nabla \varphi_i, \quad \text{for all} \quad \varphi \in \mathrm{W}(0). \end{cases} \tag{2.23}$$

Proposition 2.1.1. *Under the hypothesis that* $\mathrm{I}_{stim} \in \mathrm{L}^2(\Omega)$, *and* $g_e \in \mathrm{L}^2(\Gamma_e)$, *the problem* (2.23) *has a unique solution.*

Proof. Set

$$\begin{cases} a(\tilde{u}, \varphi) = \int_\Omega \sigma \nabla \tilde{u} \cdot \nabla \varphi. \\ \quad l(\varphi) = \int_\Omega \mathrm{I}_{stim} \varphi + \int_{\Gamma_e} g_e \varphi_e - \int_{\Omega_i} \sigma \nabla u_v \cdot \nabla \varphi_i, \quad \text{for all} \quad \varphi \in \mathrm{W}(0). \end{cases} \tag{2.24}$$

We want to show that $a(\cdot,\cdot)$ and $l(\cdot)$ satisfy the conditions of the Lax- Milgram theorem. Obviously, $a(\cdot,\cdot)$ is a continuous bilinear form on $\mathrm{W}(0) \times \mathrm{W}(0)$ and $l(\cdot)$ is a linear form on $\mathrm{W}(0)$. We show:

i) The bilinear form $a(\cdot,\cdot)$ is coercive on $\mathrm{W}(0)$. The set $\Omega_e \subset \Omega$ is of non-zero measure. Define

$$\mathbb{E} = \left\{ u \in \mathrm{H}^1(\Omega) : \frac{1}{\mathrm{meas}(\Omega_e)} \int_{\Omega_e} u_e dx = 0 \right\}.$$

Then $\mathbb{E}$ is a closed subspace of $\mathrm{H}^1(\Omega)$ and there exists a constant C such that

$$C\|u\|_{1,\Omega} \leqslant \|\nabla u\|_{\mathrm{L}^2(\Omega)}, \quad \forall u \in \mathbb{E}, \tag{2.25}$$

thanks to the Poincaré-Friedrichs inequality, see [20, Lemma B.66]. For all $u \in \mathrm{W}(0)$,

$$\begin{aligned} a(u,u) = \int_\Omega \sigma |\nabla u|^2 &\geq \operatorname*{ess\,inf}_{x\in\Omega} \sigma \|\nabla u\|^2_{\mathrm{L}^2(\Omega)} \\ &\geq \nu \|u\|^2_{\mathrm{H}^1(\Omega)}, \quad \text{from} \quad (2.25) \\ &= \nu \|u\|^2_{\mathrm{W}}, \end{aligned}$$

for some constants $\nu > 0$. It follows that the bilinear form $a(\cdot,\cdot)$ is coercive on $\mathrm{W}(0)$.

ii) The linear form $l(\cdot)$ is continuous on $\mathrm{W}(0)$. Using the continuity of 8the trace operators,

$$\begin{aligned} |l(\varphi)| &\leq \|\mathrm{I}_{stim}\|_{\mathrm{L}^2(\Omega)} \|\varphi\|_{\mathrm{L}^2(\Omega)} + \|g_e\|_{\mathrm{L}^2(\Omega)_e} \|\varphi_e\|_{\mathrm{L}^2(\Omega_e} + C \|\nabla u_v\|_{\mathrm{L}^2(\Omega_i)} \|\nabla\varphi\|_{\mathrm{L}^2(\Omega_i)} \\ &\leq C(\|\mathrm{I}_{stim}\|^2_{\mathrm{L}^2(\Omega)} + \|g_e\|^2_{\mathrm{L}^2(\Gamma_e)} + \|\nabla u_v\|^2_{\mathrm{L}^2(\Omega_i)})^{\frac{1}{2}} \\ &\quad (\|\varphi\|^2_{\mathrm{L}^2(\Omega)} + \|\varphi_e\|^2_{\mathrm{L}^2(\Gamma_e)} + \|\nabla\varphi_i\|^2_{\mathrm{L}^2(\Omega_i)})^{\frac{1}{2}} \\ &\leq C(\|\mathrm{I}_{stim}\|^2_{\mathrm{L}^2(\Omega)} + \|g_e\|^2_{\mathrm{L}^2(\Gamma_e)} + \|u_v\|^2_{\mathrm{H}^1(\Omega_i)})^{\frac{1}{2}} \|\varphi\|_{\mathrm{H}^1(\Omega)} \\ &= C\left(\|\mathrm{I}_{stim}\|^2_{\mathrm{L}^2(\Omega)} + \|g_e\|^2_{\mathrm{L}^2(\Gamma_e)} + \|\mathrm{R}_i(v)\|^2_{\mathrm{H}^1(\Omega_i)}\right)^{\frac{1}{2}} \|\varphi\|_{\mathrm{H}^1(\Omega)}, \quad \text{from } (2.21) \\ &\leq C\left(\|\mathrm{I}_{stim}\|^2_{\mathrm{L}^2(\Omega)} + \|g_e\|^2_{\mathrm{L}^2(\Gamma_e)} + \|v\|^2_{\mathrm{H}^{\frac{1}{2}}(\Gamma)}\right)^{\frac{1}{2}} \|\varphi\|_{\mathrm{H}^1(\Omega)}. \quad \text{from } (2.20). \end{aligned}$$

For the sake of simplicity, $C > 0$ represents some constant that may change from one line to the next. Therefore, the variational formulation problem (2.23) has a unique solution $\tilde{u}$ thanks to the Lax-Milgram theorem. Moreover, the solution $\tilde{u}$ satisfies:

$$\|\tilde{u}\|_{\mathrm{W}} \leqslant C\left(\|\mathrm{I}_{stim}\|^2_{\mathrm{L}^2(\Omega)} + \|g_e\|^2_{\mathrm{L}^2(\Gamma_e)} + \|v\|^2_{\mathrm{H}^{\frac{1}{2}}(\Gamma)}\right)^{\frac{1}{2}}. \tag{2.26}$$

□

Proposition 2.1.2. *Under the hypothesis that* $\mathrm{I}_{stim} \in \mathrm{L}^2(\Omega)$ *and* $g_e \in \mathrm{L}^2(\Gamma_e)$*, the problem* (2.22) *has a unique solution. Moreover, the solution* u *satisfies:*

$$\|u\|_{\mathrm{W}} \leqslant C\left(\|\mathrm{I}_{stim}\|^2_{\mathrm{L}^2(\Omega)} + \|g_e\|^2_{\mathrm{L}^2(\Gamma_e)} + \|v\|^2_{\mathrm{H}^{\frac{1}{2}}(\Gamma)}\right)^{\frac{1}{2}}. \tag{2.27}$$

Proof. From Proposition 2.1.1, there exists at least one solution $u = \tilde{u} + u_v \in \mathrm{W}(v)$. We show that the solution u is unique and independent from the lifting function u_v. Take

$u^1, u^2 \in \mathrm{W}(v)$ two solutions of (2.22). Then $u^1 - u^2 \in \mathrm{W}(0)$ since $[u^1 - u^2] = 0$ and is the solution of the problem

$$\int_\Omega \sigma \nabla (u^1 - u^2) \cdot \nabla \varphi \;=\; 0, \qquad \forall \varphi \in \mathrm{W}(0).$$

It follows from (2.26) that

$$\|u^1 - u^2\|_{\mathrm{W}} \;\leqslant\; C \|v - v\|_{\mathrm{H}^{\frac{1}{2}}(\Gamma)} = 0.$$

Thus

$$\|u^1 - u^2\|_{\mathrm{W}} = 0 \Longrightarrow u^1 = u^2.$$

Therefore the problem (2.22) has a unique solution. We have that

$$\big| \|u\|_{\mathrm{W}} - \|u_v\|_{\mathrm{H}^1(\Omega_i)} \big| \leqslant \|u - u_v\|_{\mathrm{W}} = \|\tilde{u}\|_{\mathrm{W}}.$$

It follows that

$$\begin{aligned} \|u\|_{\mathrm{W}} &\leqslant \|\tilde{u}\|_{\mathrm{W}} + \|u_v\|_{\mathrm{H}^1(\Omega_i)} \\ &\leqslant C \left(\|\mathrm{I}_{stim}\|^2_{\mathrm{L}^2(\Omega)} + \|g_e\|^2_{\mathrm{L}^2(\Gamma_e)} + \|v\|^2_{\mathrm{H}^{\frac{1}{2}}(\Gamma)} \right)^{\frac{1}{2}}, \quad \text{from (2.20) and (2.26).} \end{aligned}$$

We deduce that the problem (2.22) is well-posed. □

The next step consists of verifying that the solution of (2.22) is also a solution of (2.11)-(2.16) in the weak sense.

Proposition 2.1.3. *If u solves (2.22), then u solves the problem (2.11)-(2.16).*

Proof. Let $\varphi \in \mathcal{D}(\Omega)$, $\varphi = 0$ in Ω_e. Let u be a solution of the problem (2.22). Hence,

$$\begin{aligned} \langle -\nabla \cdot (\sigma \nabla u), \varphi \rangle_{\mathcal{D}'(\Omega_i), \mathcal{D}(\Omega_i)} &= \langle \sigma \nabla u, \nabla \varphi \rangle_{\mathrm{L}^2(\Omega_i), \mathrm{L}^2(\Omega_i)} \\ &= \int_{\Omega_i} \sigma_i \nabla u_i \cdot \nabla \varphi \\ &= \int_{\Omega_i} \mathrm{I}_{i,stim} \varphi. \end{aligned}$$

We deduce that $-\nabla \cdot (\sigma_i \nabla u_i) = \mathrm{I}_{i,stim}$ in $\mathcal{D}'(\Omega_i)$ and (2.11) follows. Similarly, taking $\varphi \in \mathcal{D}(\Omega)$, $\varphi = 0$ in Ω_i we deduce (2.12). Let $\varphi \in \mathcal{D}(\overline{\Omega})$, $\varphi \neq 0$ on Γ_e, $\varphi = 0$ on Γ and $\varphi = 0$ in Ω_i. Green's formula and problem (2.22) give,

$$\begin{aligned} -\int_{\Omega_e} \nabla \cdot (\sigma_e \nabla u_e) \varphi + \langle \sigma_e \nabla u_e \cdot n_e, \varphi \rangle_{\mathrm{H}^{-\frac{1}{2}}(\Gamma_e), \mathrm{H}^{\frac{1}{2}}(\Gamma_e)} &= \int_{\Omega_e} \sigma_e \nabla u_e \cdot \nabla \varphi \\ &= \int_{\Omega_e} \mathrm{I}_{e,stim} \varphi + \int_{\Gamma_e} g_e \varphi. \end{aligned}$$

It follows that

$$\langle \sigma_e \nabla u_e \cdot n_e, \varphi \rangle_{\mathrm{H}^{-\frac{1}{2}}(\Gamma_e), \mathrm{H}^{\frac{1}{2}}(\Gamma_e)} = \int_{\Gamma_e} g_e \varphi,$$

thanks to (2.12). Thus $\sigma_e \nabla u_e \cdot n_e = g_e$ on $\mathrm{H}^{-\frac{1}{2}}(\Gamma_e)$ which implies (2.14). We have

$$u \in \mathrm{W}(v) \Rightarrow u_i - u_e = v \text{ on } \Gamma \text{ and } \int_{\Omega_e} u_e = 0 \Leftrightarrow (2.15) \text{ and } (2.16).$$

Let us take $\varphi \in \mathcal{D}(\Omega)$, $\varphi = 0$ on $\partial\Omega \setminus \Gamma$ and $\varphi \neq 0$ on Γ. From Green's formula and problem (2.22) we have,

$$\begin{aligned} -\int_{\Omega_i} \nabla \cdot (\sigma_i \nabla u_i)\varphi \; - \; & \int_{\Omega_e} \nabla \cdot (\sigma_e \nabla u_e)\varphi + \langle \sigma_e \nabla u_e \cdot n_e + \sigma_i \nabla u_i \cdot n_i, \varphi \rangle_{\mathrm{H}^{-\frac{1}{2}}(\Gamma), \mathrm{H}^{\frac{1}{2}}(\Gamma)} \\ = \; & \int_{\Omega_i} \sigma_i \nabla u_i \cdot \nabla \varphi + \int_{\Omega_e} \sigma_e \nabla u_e \cdot \nabla \varphi \\ = \; & \int_{\Omega} \mathrm{I}_{stim} \varphi. \end{aligned}$$

This implies that for $\varphi \in \mathrm{W}$, with $\varphi = 0$ on Γ_e,

$$\langle \sigma_e \nabla u_e \cdot n_e + \sigma_i \nabla u_i \cdot n_i, \varphi \rangle_{\mathrm{H}^{-\frac{1}{2}}(\Gamma), \mathrm{H}^{\frac{1}{2}}(\Gamma)} = 0.$$

Thus

$$\sigma_e \nabla u_e \cdot n_e = -\sigma_i \nabla u_i \cdot n_i, \quad \text{on } \mathrm{H}^{-\frac{1}{2}}(\Gamma) \Longleftrightarrow (2.13).$$

Therefore the problem (2.22) is equivalent to the transmission problem (2.11)-(2.16). □

We are now interested in the problem (2.17). Let $u \in \mathrm{W}(v)$ be a solution of the problem (2.22). The variational formulation for (2.17) reads

$$\int_{\Gamma} \frac{\partial v}{\partial t} \varphi + \int_{\Gamma} f(v)\varphi + \langle \sigma_i \nabla \mathrm{S}_i(v) \cdot n_i, \varphi \rangle_{\mathrm{H}^{-\frac{1}{2}}(\Gamma), \mathrm{H}^{\frac{1}{2}}(\Gamma)} = 0, \quad \forall \varphi \in \mathrm{H}^{\frac{1}{2}}(\Gamma), \quad (2.28)$$

$$v(0) = v_0, \quad v_0 \in \mathrm{H}^{\frac{1}{2}}(\Gamma), \quad (2.29)$$

where from the definition of the duality product $\langle \cdot, \cdot \rangle_{\mathrm{H}^{-\frac{1}{2}}(\Gamma), \mathrm{H}^{\frac{1}{2}}(\Gamma)}$

$$\langle \sigma_i \nabla \mathrm{S}_i(v) \cdot n_i, \varphi \rangle_{\mathrm{H}^{-\frac{1}{2}}(\Gamma), \mathrm{H}^{\frac{1}{2}}(\Gamma)} = \int_{\Omega_i} \sigma_i \nabla \mathrm{S}_i(v) \cdot \nabla \mathrm{R}_i(\varphi) - \int_{\Omega_i} \mathrm{I}_{i,stim} \mathrm{R}_i(\varphi), \ \forall \varphi \in \mathrm{H}^{\frac{1}{2}}(\Gamma), \quad (2.30)$$

where S and R are defined as in (2.18) and (2.19), respectively. We want to show under some regularity properties that $v \in \mathrm{H}^{\frac{1}{2}}(\Gamma)$ and $u \in \mathrm{W}(v)$ solve (2.28) and (2.22), respectively, if and only if u solves (2.10).

Proposition 2.1.4. *The problem* (2.10) *is equivalent to problems* (2.22) *and* (2.28).

Proof. Let u be a solution of (2.10). Let us take $\varphi \in \mathrm{W}$, $\varphi_{|\Omega_e} = 0$ and $\varphi_{|\Omega_i} = \varphi$. We have

$$\int_{\Omega_i} \sigma_i \nabla u_i \cdot \nabla \varphi + \int_\Gamma \frac{\partial [u]}{\partial t} \varphi + \int_\Gamma f([u])\, \varphi \quad = \quad \int_\Omega \mathrm{I}_{i,stim} \varphi.$$

By considering (2.30), we deduce that

$$\int_\Gamma \frac{\partial [u]}{\partial t} \varphi + \int_\Gamma f([u])\, \varphi + \langle \sigma_i \nabla \mathrm{S}_i([u]) \cdot n_i, \varphi \rangle_{\mathrm{H}^{-\frac{1}{2}}(\Gamma), \mathrm{H}^{\frac{1}{2}}(\Gamma)} \quad = \quad 0,$$

where $[u] = u_i - u_e = v$. Then the problem (2.28) follows. Let $\varphi \in \mathrm{W}$, $\varphi_{|\Omega_e} = \varphi_e$ and $\varphi_{|\Omega_i} = \varphi_i$ such that $[\varphi] = \varphi_i - \varphi_e = 0$ on Γ. Then, $[u] = v$ which implies $u \in \mathrm{W}(v)$. We have

$$\int_{\Omega_i} \sigma_i \nabla u_i \cdot \nabla \varphi_i + \int_{\Omega_e} \sigma_e \nabla u_e \cdot \nabla \varphi_e = \int_\Omega \mathrm{I}_{stim} \varphi + \int_{\Gamma_e} g_e \varphi_e.$$

Therefore, we obtain the problem (2.22).
Conversely, let $v \in \mathrm{H}^{\frac{1}{2}}(\Gamma)$ and $u \in \mathrm{W}(v)$ be the solutions of (2.28) and (2.22), respectively. Let $\varphi \in \mathrm{W}$, $\varphi_{|\Omega_e} = \varphi_e$ and $\varphi_{|\Omega_i} = \varphi_i$. There exists an extension $\tilde{\varphi} \in \mathrm{H}^1(\Omega)$ such that $\tilde{\varphi}_{|\Omega_e} = \varphi_e$ and $[\tilde{\varphi}] = 0$ on Γ, see e.g. [8]. Then $\tilde{\varphi} = \varphi_e$ on Γ. Let us define $\tilde{\varphi}_i = \varphi_i - \tilde{\varphi}$ in Ω_i. The problems (2.22) and (2.28) give, respectively,

$$\int_{\Omega_i} \sigma_i \nabla u_i \cdot \nabla \tilde{\varphi} + \int_{\Omega_e} \sigma_e \nabla u_e \cdot \nabla \tilde{\varphi} = \int_\Omega \mathrm{I}_{stim} \tilde{\varphi} + \int_{\Gamma_e} g_e \tilde{\varphi}. \tag{2.31}$$

$$\int_{\Omega_i} \sigma_i \nabla u_i \cdot \nabla \tilde{\varphi}_i + \int_\Gamma \frac{\partial [u]}{\partial t} \tilde{\varphi}_i + \int_\Gamma f([u])\, \tilde{\varphi}_i \quad = \quad \int_\Omega \mathrm{I}_{i,stim} \tilde{\varphi}_i. \tag{2.32}$$

By adding up equations (2.31) and (2.32) we obtain

$$\int_{\Omega_i} \sigma_i \nabla u_i \cdot \nabla \varphi_i + \int_{\Omega_e} \sigma_e \nabla u_e \cdot \nabla \varphi_e + \int_\Gamma \frac{\partial [u]}{\partial t} [\varphi] + \int_\Gamma f([u])\, [\varphi] \quad = \quad \int_\Omega \mathrm{I}_{stim} \varphi + \int_{\Gamma_e} g_e \varphi,$$

since $\tilde{\varphi}_i = \varphi_i - \tilde{\varphi} = \varphi_i - \varphi_e$ on Γ. Then the problem (2.10) follows. □

We will need the following results later.

Proposition 2.1.5. *The operator* S *defined in* (2.18) *is Lipschitzian, that is, there exists* $\mathrm{L} > 0$ *such that*

$$\|\mathrm{S}(v_1) - \mathrm{S}(v_2)\|_{\mathrm{W}} \quad \leqslant \quad \mathrm{L} \|v_1 - v_2\|_{\mathrm{H}^{1/2}(\Gamma)}, \ \forall v_1, v_2 \in \mathrm{H}^{\frac{1}{2}}(\Gamma). \tag{2.33}$$

Proof. Fix $v_1, v_2 \in \mathrm{H}^{\frac{1}{2}}(\Gamma)$ and consider $u^1 \in \mathrm{W}(v_1)$ and $u^2 \in \mathrm{W}(v_2)$ solution of the problem (2.22) both with the same I_{stim} and g_e. Hence, $[u^1 - u^2] = v_1 - v_2$. We have that $u^1 - u^2 \in \mathrm{W}(v_1 - v_2)$ solves the problem

$$\int_{\Omega_i} \sigma_i \nabla(u_i^1 - u_i^2) \cdot \nabla \varphi_i + \int_{\Omega_e} \sigma_e \nabla(u_e^1 - u_e^2) \cdot \nabla \varphi_e \;=\; 0, \qquad \forall \varphi \in \mathrm{W}(0).$$

It follows from (2.27) that

$$\mathrm{S}(v_1) - \mathrm{S}(v_2)\|_{\mathrm{W}} = \|u^1 - u^2\|_{\mathrm{W}} \;\leqslant\; C\|v_1 - v_2\|_{\mathrm{H}^{1/2}(\Gamma)},$$

since $\|\mathrm{I}_{stim}\|_{0,\Omega} = 0$ and $\|g_e\|_{0,\Gamma_e} = 0$. □

Let S be defined as in (2.18). Let us define the following map

$$\begin{aligned} \gamma_1 \colon \mathrm{H}^{\frac{1}{2}}(\Gamma) &\longrightarrow \mathrm{H}^{-\frac{1}{2}}(\Gamma) \\ v &\longmapsto \sigma_i \nabla \mathrm{S}_i(v) \cdot n_i, \end{aligned} \tag{2.34}$$

where $\mathrm{S}_i(v) = u_{|\Omega_i} = u_i$ for u solution of the problem (2.22).

Proposition 2.1.6. *The map γ_1 given in (2.34) is Lipschitzian, that is, there exists $\tilde{\mathrm{L}} > 0$ such that*

$$\|\gamma_1(v_1) - \gamma_1(v_2)\|_{\mathrm{H}^{-\frac{1}{2}}(\Gamma)} \leqslant \tilde{\mathrm{L}} \|v_1 - v_2\|_{\mathrm{H}^{\frac{1}{2}}(\Gamma)}, \;\; \forall v_1, v_2 \in \mathrm{H}^{\frac{1}{2}}(\Gamma).$$

Proof. Fix $v_1, v_2 \in \mathrm{H}^{\frac{1}{2}}(\Gamma)$ and $\varphi \in \mathrm{H}^{\frac{1}{2}}(\Gamma)$. From (2.30) we have

$$\left| \langle \sigma_i \nabla \mathrm{S}_i(v_1) \cdot n_i - \sigma_i \nabla \mathrm{S}_i(v_2) \cdot n_i, \varphi \rangle_{\mathrm{H}^{-\frac{1}{2}}(\Gamma), \mathrm{H}^{\frac{1}{2}}(\Gamma)} \right| \;=\; \left| \int_{\Omega_i} \sigma_i \nabla \left(\mathrm{S}_i(v_1) - \mathrm{S}_i(v_2) \right) \cdot \nabla \mathrm{R}_i(\varphi) \right|.$$

Then

$$\begin{aligned} \left| \int_{\Omega_i} \sigma_i \nabla \left(\mathrm{S}_i(v_1) - \mathrm{S}_i(v_2) \right) \cdot \nabla \mathrm{R}_i(\varphi) \right| &\leq \|\sigma_i\|_{\mathrm{L}^\infty(\Omega_i)} \|\mathrm{S}_i(v_1) - \mathrm{S}_i(v_2)\|_{\mathrm{H}^1(\Omega_i)} \|\mathrm{R}_i(\varphi)\|_{\mathrm{H}^1(\Omega_i)}, \\ &\leq C \|\mathrm{S}(v_1) - \mathrm{S}(v_2)\|_{\mathrm{W}} \|\varphi\|_{\mathrm{H}^{\frac{1}{2}}(\Gamma)}, \quad \text{from (2.20)} \\ &\leq C \|v_1 - v_2\|_{\mathrm{H}^{\frac{1}{2}}(\Gamma)} \|\varphi\|_{\mathrm{H}^{\frac{1}{2}}(\Gamma)}, \quad \text{from (2.33)}. \end{aligned}$$

It follows that

$$\begin{aligned} \|\sigma_i \nabla \mathrm{S}_i(v_1) \cdot n_i - \sigma_i \nabla \mathrm{S}_i(v_2) \cdot n_i\|_{\mathrm{H}^{-\frac{1}{2}}(\Gamma)} &= \sup_{\varphi \neq 0} \frac{\left| \langle \sigma_i \nabla \left(\mathrm{S}_i(v_1) - \mathrm{S}_i(v_2) \right) \cdot n_i, \varphi \rangle_{\mathrm{H}^{-\frac{1}{2}}(\Gamma), \mathrm{H}^{\frac{1}{2}}(\Gamma)} \right|}{\|\varphi\|_{\mathrm{H}^{1/2}(\Gamma)}}, \\ &\leqslant C \|v_1 - v_2\|_{\mathrm{H}^{\frac{1}{2}}(\Gamma)}. \end{aligned}$$

Thus the map (2.34) is Lipschitzian. □

Proposition 2.1.7. *Assume that f in (2.28) is in $\mathrm{C}^1(\mathbb{R})$ and satisfies a global Lipschitz condition on $\mathbb{R}$, then $f\colon \mathrm{H}^{\frac{1}{2}}(\Gamma) \longrightarrow \mathrm{H}^{-\frac{1}{2}}(\Gamma)$ is Lipschitzian.*

Proof. Let $v \in \mathrm{H}^{\frac{1}{2}}(\Gamma) \subset \mathrm{L}^2(\Gamma)$ be arbitrary. We claim that $f(v) \in \mathrm{L}^2(\Gamma)$. Indeed, the function f satisfies a global Lipschitz condition on $\mathbb{R}$ which implies for a.e. $x \in \Gamma$

$$\begin{aligned} |f(v(x)) - f(0)| \leqslant \mathrm{L}_1|v(x)| \quad &\Longrightarrow \quad |f(v(x))| \leqslant \mathrm{L}_1|v(x)| + |f(0)|\,, \\ &\Longrightarrow \quad \int_\Gamma |f(v(x))|^2 \leqslant \mathrm{L}_2 \left(\|v\|^2_{\mathrm{L}^2(\Gamma)} + \int_\Gamma |f(0)|^2 \right) < \infty. \end{aligned}$$

Therefore $f(v) \in \mathrm{L}^2(\Gamma)$. Furthermore, f is Lipschitzian in $\mathrm{L}^2(\Gamma)$, that is,

$$\|f(v_1) - f(v_2)\|_{\mathrm{L}^2(\Gamma)} \leqslant \mathrm{L}_3\|v_1 - v_2\|_{\mathrm{L}^2(\Gamma)}, \ \forall v_1, v_2 \in \mathrm{L}^2(\Gamma), \tag{2.35}$$

for some constant $\mathrm{L}_3 > 0$.
Let $v_1, v_2 \in \mathrm{H}^{\frac{1}{2}}(\Gamma)$ and $\varphi \in \mathrm{H}^{\frac{1}{2}}(\Gamma)$ be arbitrary. Since $f(v_1), f(v_2) \in \mathrm{L}^2(\Gamma)$ we have

$$\begin{aligned} \left| \langle f(v_1) - f(v_2), \varphi \rangle_{\mathrm{H}^{-\frac{1}{2}}(\Gamma), \mathrm{H}^{\frac{1}{2}}(\Gamma)} \right| &= \left| \int_\Gamma [f(v_1) - f(v_2)]\, \varphi \right|, \\ &\leqslant \|f(v_1) - f(v_2)\|_{\mathrm{L}^2(\Gamma)} \|\varphi\|_{\mathrm{L}^2(\Gamma)}, \\ &\leqslant \mathrm{L}_3\|v_1 - v_2\|_{\mathrm{L}^2(\Gamma)} \|\varphi\|_{\mathrm{L}^2(\Gamma)}, \quad \text{from (2.35)} \\ &\leqslant \mathrm{L}_4\|v_1 - v_2\|_{\mathrm{H}^{\frac{1}{2}}(\Gamma)} \|\varphi\|_{\mathrm{H}^{\frac{1}{2}}(\Gamma)}, \ \text{since } \mathrm{H}^{\frac{1}{2}}(\Gamma) \hookrightarrow \mathrm{L}^2(\Gamma). \end{aligned}$$

It follows that

$$\begin{aligned} \|f(v_1) - f(v_2)\|_{\mathrm{H}^{-\frac{1}{2}}(\Gamma)} &= \sup_{\varphi \neq 0} \frac{\left| \langle f(v_1) - f(v_2), \varphi \rangle_{\mathrm{H}^{-\frac{1}{2}}(\Gamma), \mathrm{H}^{\frac{1}{2}}(\Gamma)} \right|}{\|\varphi\|_{\mathrm{H}^{1/2}(\Gamma)}}, \\ &\leqslant \mathrm{L}_4\|v_1 - v_2\|_{\mathrm{H}^{\frac{1}{2}}(\Gamma)}, \end{aligned}$$

for some constant $\mathrm{L}_4 > 0$. Therefore f is Lipschitzian. □

2.1.2 Space-Discretization of the Microscopic Model

We will present the methods in detail in the 2D case. However, the theory can be applied in 3D. We consider a spatial discretization of the problems (2.22) and (2.28) through finite element methods. Let $\mathcal{T}_h$ be a partition of the domain $\overline{\Omega} = \overline{\Omega}_i \cup \overline{\Omega}_e$ into triangular elements. The parameter h corresponds to the maximal size of the elements in the triangulation $\mathcal{T}_h$. Let us assume that the partition $\mathcal{T}_h = \mathcal{T}_{ih} \cup \mathcal{T}_{eh}$, where $\mathcal{T}_{ih}$ and

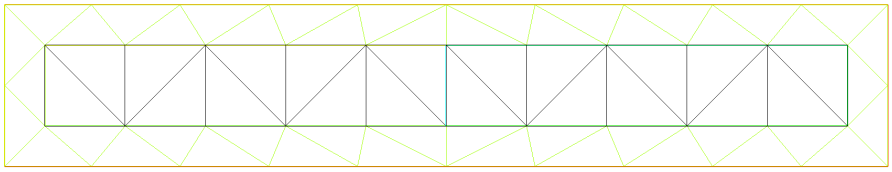

Figure 2.1: Sketch of a conformal mesh on the membrane Γ between the cell and the extracellular domain.

$\mathcal{T}_{eh}$ are triangular element meshes of Ω_i and Ω_e, respectively, and $\mathcal{T}_{ih} \cap \mathcal{T}_{eh} = \varnothing$. The meshes $\mathcal{T}_{ih}$ and $\mathcal{T}_{eh}$ can be conformal or nonconformal on the interface Γ, which means that the edges of adjacent triangles may or may not match on Γ, see Figures 2.1 and 2.2.

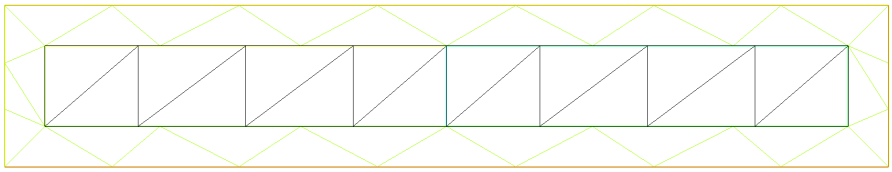

Figure 2.2: Sketch of a nonconformal mesh on the membrane Γ between the cell and the extracellular domain.

The $\mathbb{P}_d$ finite element spaces associated with the meshes $\mathcal{T}_{ih}$ and $\mathcal{T}_{eh}$ are defined as follows

$$\mathrm{V}_h^i = \left\{ u_{ih} \in \mathrm{C}(\overline{\Omega}_i) \ : \ u_{ih}|_{\mathrm{K}} \in \mathbb{P}_d(\mathrm{K}), \ \forall \mathrm{K} \in \mathcal{T}_{ih} \right\}, \tag{2.36}$$

$$\mathrm{V}_h^e = \left\{ u_{eh} \in \mathrm{C}(\overline{\Omega}_e) \ : \ u_{eh}|_{\mathrm{K}} \in \mathbb{P}_d(\mathrm{K}), \ \forall \mathrm{K} \in \mathcal{T}_{eh} \right\}, \tag{2.37}$$

where $\mathbb{P}_d(\mathrm{K})$ is the set of polynomials with real coefficients and of degree less than or equal to d on K. The corresponding $\mathbb{P}_d$ Lagrange interpolation operators are denoted by $\mathit{\Pi}_{\mathrm{h}}^{\mathrm{i}}$ and $\mathit{\Pi}_{\mathrm{h}}^{\mathrm{e}}$, respectively. Let $u_i \in \mathrm{H}^{l+1}(\Omega_i)$ and $u_e \in \mathrm{H}^{l+1}(\Omega_e)$ for $1 \leqslant l \leqslant d$. We have the following interpolation error estimates:

$$\|u_e - \mathit{\Pi}_{\mathrm{h}}^{\mathrm{e}} u_e\|_{\mathrm{H}^1(\Omega_e)} \leq \mathrm{C} h^l |u_e|_{\mathrm{H}^{l+1}(\Omega_e)}, \tag{2.38}$$

$$\|u_i - \mathit{\Pi}_{\mathrm{h}}^{\mathrm{i}} u_i\|_{\mathrm{H}^1(\Omega_i)} \leq \mathrm{C} h^l |u_i|_{\mathrm{H}^{l+1}(\Omega_i)}, \tag{2.39}$$

for some constant C > 0, where $|\cdot|_{\mathrm{H}^{l+1}(\Omega)}$ stands for the $\mathrm{H}^{l+1}(\Omega)-$ seminorm:

$$|v|_{\mathrm{H}^{l}(\Omega)} = \left(\sum_{|\alpha|=l} \|D^{\alpha} v\|^2_{\mathrm{L}^2(\Omega)} \right)^{1/2}. \tag{2.40}$$

The proof of these error estimates can be found in [10, 20, 56].
We define the following trace operators :

$$\begin{aligned} \gamma_0^i \colon \mathrm{H}^1(\Omega_i) &\longrightarrow \mathrm{L}^2(\Gamma) \\ u_i &\longmapsto u_{i|\Gamma}, \\ \gamma_0^e \colon \mathrm{H}^1(\Omega_e) &\longrightarrow \mathrm{L}^2(\Gamma) \\ u_e &\longmapsto u_{e|\Gamma}. \end{aligned}$$

The linear operators γ_0^i and γ_0^e are continuous, that is,

$$\|\gamma_0^i(u_i)\|_{\mathrm{L}^2(\Gamma)} \leq C\|u_i\|_{\mathrm{H}^1(\Omega_i)} \tag{2.41}$$

$$\|\gamma_0^e(u_e)\|_{\mathrm{L}^2(\Gamma)} \leq C\|u_e\|_{\mathrm{H}^1(\Omega_e)}, \tag{2.42}$$

for some constant C > 0.
Now we construct a mesh, $\mathcal{T}_{\Gamma h}$, on the interface Γ for both conformal and non-conformal cases. Let $\mathcal{S}_\Gamma^i$ and $\mathcal{S}_\Gamma^e$ be the collection of vertices on the inner and outer sides of Γ, respectively. Let us set

$$\begin{aligned} \mathcal{S}_\Gamma^i &= \{x_j^i,\ j = 1, \cdots, \mathrm{N}_i^\Gamma\}, \\ \mathcal{S}_\Gamma^e &= \{x_j^e,\ j = 1, \cdots, \mathrm{N}_e^\Gamma\}, \end{aligned}$$

where N_i^Γ and N_e^Γ denote the total number of nodes on the inner and outer sides of Γ, respectively. For simplicity, let $\mathcal{S}_\Gamma$ be the union of $\mathcal{S}_\Gamma^i$ and $\mathcal{S}_\Gamma^e$. The vertices in $\mathcal{S}_\Gamma$ are rearranged as follows:

$$\mathcal{S}_\Gamma = \mathcal{S}_\Gamma^i \cup \mathcal{S}_\Gamma^e = \{x_j,\ j = 1, \cdots, \mathrm{N}^\Gamma\}, \tag{2.43}$$

where N^Γ is the total number of nodes on Γ. To avoid curved boundaries, we assume that Γ is a polygonal simple curve, that is, it is the union of edges. We define the curve

$$\begin{aligned} \gamma \colon [0,1] &\longrightarrow \Gamma \\ s &\longmapsto \gamma(s), \qquad\qquad \gamma(0) = \gamma(1), \end{aligned}$$

and a partition $0 = s_0 < s_1 < \cdots < s_{\mathrm{N}^\Gamma} = 1$ such that $\gamma(s_j) = x_j$, $j = 1, \cdots, \mathrm{N}^\Gamma$. Using this ordering of the nodes on Γ, the mesh $\mathcal{T}_{\Gamma h}$ is composed of the elements $\mathrm{K} = [x_j, x_{j+1}] \subset \mathbb{R}^2$, edges of the polygonal curve Γ, that is,

$$\mathcal{T}_{\Gamma h} = \left\{ \mathrm{K} : \ \mathrm{K} = [x_j, x_{j+1}], \ x_j \in \mathcal{S}_\Gamma, \ j = 1, \cdots, \mathrm{N}^\Gamma \right\}.$$

For a conformal interface Γ, $\mathcal{S}_\Gamma = \mathcal{S}_\Gamma^i = \mathcal{S}_\Gamma^e = \{x_j, \ j = 1, \cdots, \mathrm{N}^\Gamma\}$ and the finite element space associated to $\mathcal{T}_{\Gamma h}$ reads:

$$\mathrm{V}_h^\Gamma \ = \ \gamma_0^i \left(\mathrm{V}_h^i \right) = \gamma_0^e \left(\mathrm{V}_h^e \right), \tag{2.44}$$

where γ_0^i and γ_0^e are the trace operators defined in (2.41) and (2.42).
For the nonconformal interface Γ, we define

$$\mathrm{V}_h^\Gamma = \left\{ v_h = u_{ih} - u_{eh} \in \mathrm{C}(\Gamma) : u_{ih} \in \mathrm{V}_{h|_\Gamma}^i, \ u_{eh} \in \mathrm{V}_{h|_\Gamma}^e, \ v_{h|_\mathrm{K}} \in \mathbb{P}_d(\mathrm{K}), \ \mathrm{K} \in \mathcal{T}_{\Gamma h} \right\}. \tag{2.45}$$

For both cases, we have $v_h = u_{ih_{|\Gamma}} - u_{eh_{|\Gamma}} \in \mathrm{V}_h^\Gamma$ for $u_{ih} \in \mathrm{V}_h^i$ and $u_{eh} \in \mathrm{V}_h^e$.
We are now in position to define the discrete version of the spaces W and $\mathrm{W}(v)$. Define

$$\mathrm{W}_h = \left\{ u_h \in \mathrm{L}^2(\Omega) : u_{h_{|\Omega_i}} \in \mathrm{V}_h^i, \ u_{h_{|\Omega_e}} \in \mathrm{V}_h^e, \ \int_{\Omega_e} u_{eh} \, dx = 0 \right\},$$

$$\mathrm{W}_h(v_h) = \left\{ u_h \in \mathrm{L}^2(\Omega) : u_{h_{|\Omega_i}} \in \mathrm{V}_h^i, \ u_{h_{|\Omega_e}} \in \mathrm{V}_h^e, \ [u_h] = v_h, \ \int_{\Omega_e} u_{eh} \, dx = 0 \right\},$$

where $[u_h] = u_{ih_{|\Gamma}} - u_{eh_{|\Gamma}} \in \mathrm{V}_h^\Gamma$, $u_{h_{|\Omega_i}} = u_{ih}$ and $u_{h_{|\Omega_e}} = u_{eh}$.
The discrete version of the problem (2.10) reads

$$\begin{aligned} \int_{\Omega_i} \sigma_i \nabla u_{ih} \cdot \nabla \varphi_{ih} + \int_{\Omega_e} \sigma_e \nabla u_{eh} \cdot \nabla \varphi_{eh} \ &+ \ \int_\Gamma \frac{\partial [u_h]}{\partial t} [\varphi_h] + \int_\Gamma f([u_h]) [\varphi_h] \\ &= \ \int_\Omega \mathrm{I}_{stim} \varphi_h + \int_{\Gamma_e} g_e \varphi_h, \end{aligned} \tag{2.46}$$

where $\varphi_h \in \mathrm{W}_h$, $[\varphi_h] = \varphi_{ih_{|\Gamma}} - \varphi_{eh_{|\Gamma}} \in \mathrm{V}_h^\Gamma$, $\varphi_{h_{|\Omega_i}} = \varphi_{ih}$ and $\varphi_{h_{|\Omega_e}} = \varphi_{eh}$.
The numerical method (2.46) can be used for both conformal and nonconformal cases, but we will restrict our analysis to the conformal case. In the following, we thus assume that we are in the conformal case for the analysis and the numerical tests. As before, we want to split the problem (2.46) into two problems. For this purpose, we introduce the following linear Scott-Zhang interpolation operator, see [20, Lemma 1.130]

$$\begin{aligned} \mathrm{SZ}_h \colon \mathrm{H}^1(\Omega_i) \ &\longrightarrow \ \mathrm{V}_h^i \subset \mathrm{H}^1(\Omega_i) \\ \varphi \ &\longmapsto \ \mathrm{SZ}_h(\varphi). \end{aligned} \tag{2.47}$$

The operator SZ_h possesses two key features. It preserves boundary values on Γ, that is, $\varphi_{|\Gamma} = g$ implies $\mathrm{SZ}_h(\varphi)_{|\Gamma} = g$ for $g \in \gamma_0^i(\mathrm{V}_h^i)$. It satisfies $\mathrm{SZ}_h(\varphi) = \varphi$ for all $\varphi \in \mathrm{V}_h^i$. Furthermore, the operator SZ_h is continuous, that is,

$$\|\mathrm{SZ}_h(\varphi)\|_{\mathrm{H}^1(\Omega_i)} \leq \mathrm{C}\|\varphi\|_{\mathrm{H}^1(\Omega_i)}, \tag{2.48}$$

for some constant $\mathrm{C} > 0$, independent from the mesh size h.
Further, we define the following lifting operator

$$\begin{aligned} \mathrm{R}_{ih} \colon \mathrm{V}_h^\Gamma \subset \mathrm{H}^{\frac{1}{2}}(\Gamma) &\longrightarrow \mathrm{V}_h^i \subset \mathrm{H}^1(\Omega_i), \\ v_h &\longmapsto \mathrm{R}_{ih}(v_h) = \mathrm{SZ}_h(\mathrm{R}(v_h)), \end{aligned} \tag{2.49}$$

where R is defined as in (2.19). We claim that R_{ih} is continuous, that is, there exists a constant $C > 0$ independent from the mesh size h such that

$$\|\mathrm{R}_{ih}(v_h)\|_{\mathrm{H}^1(\Omega_i)} \leq \mathrm{C}\|v_h\|_{\mathrm{H}^{\frac{1}{2}}(\Gamma)}. \tag{2.50}$$

In fact, we have

$$\begin{aligned} \|\mathrm{R}_{ih}(v_h)\|_{\mathrm{H}^1(\Omega_i)} &= \|\mathrm{SZ}_h(\mathrm{R}_i(v_h))\|_{\mathrm{H}^1(\Omega_i)} \\ &\leqslant \mathrm{C}_1\|\mathrm{R}_i(v_h)\|_{\mathrm{H}^1(\Omega_i)}, \quad \text{from (2.48)} \\ &\leqslant \mathrm{C}_2\|v_h\|_{\mathrm{H}^{\frac{1}{2}}(\Gamma)}, \quad \text{from (2.20)} \end{aligned}$$

for some constants $\mathrm{C}_1, \mathrm{C}_2 > 0$.
Fix $v_h \in \mathrm{V}_h^\Gamma$ and define $u_{v_h} \in \mathrm{W}_h(v_h)$ as follows:

$$u_{v_h} = \begin{cases} \mathrm{R}_{ih}(v_h) = \mathrm{SZ}_h(\mathrm{R}_i(v_h)) & \text{in } \Omega_i, \\ 0 & \text{in } \Omega_e, \\ v_h & \text{on } \Gamma. \end{cases} \tag{2.51}$$

Then we have $\gamma_0^i(u_{v_h}) = v_h$ since $\mathrm{SZ}_h(\mathrm{R}_i(v_h)) = \mathrm{R}_i(v_h) = v_h$ on Γ.
The space $\mathrm{W}_h(v_h)$ can be written as

$$\mathrm{W}_h(v_h) = u_{v_h} + \mathrm{W}_h(0).$$

The discrete version of (2.22) is

$$\begin{cases} \text{Seek } \ u_h \in \mathrm{W}_h(v_h) \ \text{ such that} \\ \int_{\Omega_i} \sigma_i \nabla u_{ih} \cdot \nabla \varphi_{ih} + \int_{\Omega_e} \sigma_e \nabla u_{eh} \cdot \nabla \varphi_{eh} = \int_\Omega \mathrm{I}_{stim}\varphi_h + \int_{\Gamma_e} g_e \varphi_{eh}, \\ \text{for all } \ \ \varphi_h \in \mathrm{W}_h(0). \end{cases} \tag{2.52}$$

Under the hypothesis of Proposition 2.1.2, one can show that the solution, $u_h = \tilde{u}_h + u_{v_h}$ of (2.52) is unique and independent from the lifting function u_{v_h}. Moreover, u_h satisfies

$$\|u_h\|_{\mathrm{W}} \leqslant C \left(\|\mathrm{I}_{stim}\|^2_{0,\Omega} + \|g_e\|^2_{0,\Gamma_e} + \|v_h\|^2_{\mathrm{H}^{\frac{1}{2}}(\Gamma)} \right)^{\frac{1}{2}}. \tag{2.53}$$

The discrete version of the operator S is

$$\begin{aligned} \mathrm{S}_h \colon \mathrm{V}_h^\Gamma &\longrightarrow \mathrm{W}_h \\ v_h &\longmapsto \mathrm{S}_h(v_h) := (\mathrm{S}_{ih}(v_h), \mathrm{S}_{eh}(v_h)) = u_h, \end{aligned} \tag{2.54}$$

where $\mathrm{S}_{ih}(v_h) = u_{ih}$, $\mathrm{S}_{eh}(v) = u_{eh}$ and u_h is the solution of the problem (2.52). Proceeding as in Proposition 2.1.5 and using (2.53) one can show that the operator S_h is Lipschitzian. We are now in position to write the discrete version of the problem (2.28). Let u_h be the the solution of the problem (2.52). The discrete version of the problem (2.28) consists in finding $v_h(t) = u_{ih_{|\Gamma}} - u_{eh_{|\Gamma}} \in \mathrm{V}_h^\Gamma$ such that

$$\int_\Gamma \frac{\partial v_h}{\partial t}\varphi_h + \int_\Gamma f(v_h)\varphi_h + \langle \sigma_i \nabla \mathrm{S}_{ih}(v_h) \cdot n_i, \varphi_h \rangle_{\mathrm{H}^{-\frac{1}{2}}(\Gamma), \mathrm{H}^{\frac{1}{2}}(\Gamma)} = 0, \quad \forall \varphi_h \in \mathrm{V}_h^\Gamma, \tag{2.55}$$

where

$$\langle \sigma_i \nabla \mathrm{S}_{ih}(v_h) \cdot n_i, \varphi_h \rangle_{\mathrm{H}^{-\frac{1}{2}}(\Gamma), \mathrm{H}^{\frac{1}{2}}(\Gamma)} = \int_{\Omega_i} \sigma_i \nabla \mathrm{S}_{ih}(v_h) \cdot \nabla \mathrm{R}_{ih}(\varphi_h) - \int_{\Omega_i} \mathrm{I}_{i,stim} \mathrm{R}_{ih}(\varphi_h), \tag{2.56}$$

where R_{ih} and S_h are defined as in (2.50) and (2.54), respectively.

Proposition 2.1.8. *The problem* (2.46) *is equivalent to problems* (2.52) *and* (2.55).

The proof of this proposition uses the same arguments as those of the Proposition 2.1.4.

2.2 Analysis of the Semi-Discrete Formulation

Let $\{\Phi_{i,l},\ l = 1, \cdots, \mathrm{N}_\Gamma, \mathrm{N}_\Gamma + 1, \cdots, \mathrm{N}_{ih}\}$ and $\{\Phi_{e,k},\ k = 1, \cdots, \mathrm{N}_\Gamma, \mathrm{N}_\Gamma + 1, \cdots, \mathrm{N}_{eh}\}$ be the usual basis of $\mathbb{P}_d$ hat functions associated with the vertices $\{x_l,\ 1 \leqslant l \leqslant \mathrm{N}_{ih}\}$ and $\{x_k,\ 1 \leqslant k \leqslant \mathrm{N}_{eh}\}$, respectively. Take V_h^Γ as in (2.44). Let $\Phi_l^\Gamma = \Phi_{i,l_{|\Gamma}}$, be the restriction of the basis function $\Phi_{i,l}$ on Γ, for $1 \leqslant l \leqslant \mathrm{N}_\Gamma$. Then $\{\Phi_l^\Gamma,\ 1 \leqslant l \leqslant \mathrm{N}_\Gamma\}$ is a basis for V_h^Γ. Write

$$v_h(t) = \sum_{k=1}^{\mathrm{N}_\Gamma} v_k(t) \Phi_k^\Gamma. \tag{2.57}$$

Taking $\varphi = \Phi_l^\Gamma$ in (2.55) for $t > 0$ and $1 \leqslant l \leqslant \mathrm{N}_\Gamma$ gives

$$\sum_{k=1}^{\mathrm{N}_\Gamma} \frac{dv_k(t)}{dt} \int_\Gamma \Phi_k^\Gamma \Phi_l^\Gamma = -\left\langle \sigma_i \nabla \mathrm{S}_{ih} \left(\sum_{k=1}^{\mathrm{N}_\Gamma} v_k(t) \Phi_k^\Gamma \right) \cdot n_i + f \left(\sum_{k=1}^{\mathrm{N}_\Gamma} v_k(t) \Phi_k^\Gamma \right), \Phi_l^\Gamma \right\rangle_{\mathrm{H}^{-\frac{1}{2}}(\Gamma), \mathrm{H}^{\frac{1}{2}}(\Gamma)}.$$

The previous equation can be written under matrix form:

$$\mathrm{M}_\Gamma \frac{d\mathrm{V}}{dt} = \mathrm{F}(\mathrm{V}), \tag{2.58}$$

$$\mathrm{V}(0) = \mathrm{V}_{0h}, \qquad \mathrm{V}_{0h} \in \mathrm{V}_h^\Gamma, \tag{2.59}$$

where

$$\begin{aligned}
(\mathrm{M}_\Gamma)_{lj} &= \int_\Gamma \Phi_j^\Gamma \Phi_l^\Gamma, \quad 1 \leqslant j, l \leqslant \mathrm{N}_\Gamma \\
\mathrm{V}(t) &= \left(v_1(t), v_2(t), \cdots, v_{\mathrm{N}_\Gamma}(t) \right)^{\mathrm{T}}, \\
(\mathrm{F}(\mathrm{V}))_l &= -\left\langle \sigma_i \nabla \mathrm{S}_{ih} \left(\sum_{k=1}^{\mathrm{N}_\Gamma} v_k(t) \Phi_k^\Gamma \right) \cdot n_i + f \left(\sum_{k=1}^{\mathrm{N}_\Gamma} v_k(t) \Phi_k^\Gamma \right), \Phi_l^\Gamma \right\rangle_{\mathrm{H}^{-\frac{1}{2}}(\Gamma), \mathrm{H}^{\frac{1}{2}}(\Gamma)}.
\end{aligned}$$

Proceeding as in Proposition 2.1.6 and Proposition 2.1.7 one can show that the map $v_h \longmapsto \sigma_i \nabla \mathrm{S}_{ih}(v_h) \cdot n_i$ from V_h^Γ to $\mathrm{H}^{-\frac{1}{2}}(\Gamma)$ and the function $f : \mathrm{V}_h^\Gamma \longrightarrow \mathrm{H}^{-\frac{1}{2}}(\Gamma)$ are Lipschitzian, respectively. In addition, the mass matrix M_Γ is invertible. Therefore, there exists $\mathrm{T} > 0$ such that $\mathrm{V} \in \mathrm{C}^1\left([0, \mathrm{T}]; \mathrm{V}_\mathrm{h}^\Gamma\right)$ is a unique solution of the problen (2.58)-(2.59) thanks to the Cauchy-Lipschitz Theorem, see e.g. [14, 50]. The 3D conformal case can be handled as above. However, the 2D and 3D nonconformal cases are challenging to deal with. A special analysis is needed in the spirit of what is done for the mortar finite element method.

2.2.1 Stability Estimates

We set $\mathrm{E} = \mathrm{H}^{\frac{1}{2}}(\Gamma)$, $\mathrm{H} = \mathrm{L}^2(\Gamma)$ endowed with their usual norms. Identifying H with its dual space H', we have the following continuous injections,

$$\mathrm{E} \hookrightarrow \mathrm{H} \simeq \mathrm{H}' \hookrightarrow \mathrm{E}',$$

where $\mathrm{E}' = \mathrm{H}^{-\frac{1}{2}}(\Gamma)$ denotes the dual space of E, see e.g. [1, 41, 42]. It follows that the duality product $\langle \cdot, \cdot \rangle_{\mathrm{E}',\mathrm{E}}$ and the scalar product $(\cdot, \cdot)$ defined in H coincide, that is,

$$\langle f, g \rangle_{\mathrm{E}',\mathrm{E}} = (f, g) = \int_\Omega f(x) g(x)\, dx, \quad \forall f \in \mathrm{H}, \quad \forall g \in \mathrm{E}. \tag{2.60}$$

We derive some stability estimates uniform in h. Let us first state the following lemma:

Lemma 2.2.1 (Gronwall Lemma)**.** *Let* $\mathrm{T} > 0$. *Let* $f \in \mathrm{L}^1(0,\mathrm{T})$ *be a non-negative function,* g *and* φ *be continuous functions on* $[0,\mathrm{T}]$. *Assume that* g *is non-decreasing. If* φ *satisfies*

$$\varphi(t) \leqslant g(t) + \int_0^{\mathrm{t}} f(\tau)\varphi(\tau) \qquad \forall t \in [0,\mathrm{T}], \tag{2.61}$$

then

$$\varphi(t) \leqslant g(t)\exp\left(\int_0^{\mathrm{t}} f(\tau)\right) \qquad \forall t \in [0,\mathrm{T}]. \tag{2.62}$$

The proof of this lemma can be found in [54]. The following stability estimates hold on v_h, u_{ih} and u_{eh}.

Proposition 2.2.2 (Stability Estimates)**.** *Let* $\mathrm{T} > 0$.*There exist positive constants* $\mathrm{C}_1, \mathrm{C}_2, \mathrm{C}_3$, *independent from* h *and depending only on* T, $v(0), f(0), \mathrm{I}_{stim}, g_e$, *the Lipschitz constant* L_f, *and the conductances* σ_i, σ_e, *such that*

$$\|v_h(t)\|^2_{\mathrm{L}^2(\Gamma)} \leqslant \mathrm{C}_1 \qquad \forall t \in [0,\mathrm{T}]\,, \tag{2.63}$$

$$\|u_{ih}\|_{\mathrm{L}^2(0,\mathrm{T};\mathrm{H}^1(\Omega_i))} + \|u_{eh}\|_{\mathrm{L}^2(0,\mathrm{T};\mathrm{H}^1(\Omega_e))} \leqslant \mathrm{C}_2, \tag{2.64}$$

$$\|v_h\|_{\mathrm{L}^2(0,\mathrm{T};\mathrm{H}^{\frac{1}{2}}(\Gamma))} \leqslant \mathrm{C}_3, \tag{2.65}$$

where $v_h(t)$ *is the solution of the Cauchy problem* (2.58)-(2.59), $u_{h_{|\Omega_i}}(t) = u_{ih}(t)$, *and* $u_{h_{|\Omega_e}}(t) = u_{eh}(t)$ *are the solution of the problem* (2.52).

Proof. Let us prove the inequality (2.63). Taking $\varphi_h = u_h$ in (2.46) we have

$$\begin{aligned}\int_{\Omega_i} \sigma_i \nabla u_{ih}\cdot\nabla u_{ih} + \int_{\Omega_e} \sigma_e \nabla u_{eh}\cdot\nabla u_{eh} &+ \int_\Gamma \frac{\partial v_h}{\partial t} v_h + \int_\Gamma f(v_h)\, v_h = \int_{\Omega_i} \mathrm{I}_{i,stim} u_{ih} \\ &+ \int_{\Omega_e} \mathrm{I}_{e,stim} u_{eh} + \int_{\Gamma_e} g_e u_{eh}.\end{aligned} \tag{2.66}$$

where $[u_h] = u_{ih_{|\Gamma}} - u_{eh_{|\Gamma}} = v_h$. Considering the identification (2.60), we have

$$\int_\Gamma \frac{\partial v_h}{\partial t} v_h = \frac{1}{2}\frac{d}{dt}\|v_h\|^2_{\mathrm{L}^2(\Gamma)}. \tag{2.67}$$

Thanks to the Cauchy-Schwarz inequality, we have

$$\left|\int_{\Omega_i} \mathrm{I}_{i,stim} u_{ih}\right| \leqslant \|\mathrm{I}_{i,stim}\|_{\mathrm{L}^2(\Omega_i)}\|u_{ih}\|_{\mathrm{L}^2(\Omega_i)} \leqslant \|\mathrm{I}_{i,stim}\|_{\mathrm{L}^2(\Omega_i)}\|u_{ih}\|_{\mathrm{H}^1(\Omega_i)}, \tag{2.68}$$

$$\left|\int_{\Omega_e} \mathrm{I}_{e,stim} u_{eh}\right| \leqslant \|\mathrm{I}_{e,stim}\|_{\mathrm{L}^2(\Omega_e)}\|u_{eh}\|_{\mathrm{L}^2(\Omega_e)} \leqslant \|\mathrm{I}_{e,stim}\|_{\mathrm{L}^2(\Omega_e)}\|u_{eh}\|_{\mathrm{H}^1(\Omega_e)}, \tag{2.69}$$

$$\left|\int_{\Gamma_e} g_e u_{eh}\, dx\right| \leqslant \|g_e\|_{\mathrm{L}^2(\Gamma_e)}\|u_{eh}\|_{\mathrm{L}^2(\Gamma_e)} \leqslant \alpha_2\|g_e\|_{\mathrm{L}^2(\Gamma_e)}\|u_{eh}\|_{\mathrm{H}^1(\Omega_e)}, \tag{2.70}$$

where $\alpha_2 > 0$ is a constant. The last inequality in (2.70) comes from the continuity of the trace operator $\gamma_{\Gamma_e} : \mathrm{H}^1(\Omega_e) \longrightarrow \mathrm{L}^2(\Gamma_e)$. Furthermore,

$$\beta \left(\|\nabla u_{ih}\|^2_{\mathrm{L}^2(\Omega_i)} + \|\nabla u_{eh}\|^2_{\mathrm{L}^2(\Omega_e)} \right) \leqslant \int_{\Omega_i} \sigma_i \nabla u_{ih} \cdot \nabla u_{ih} + \int_{\Omega_e} \sigma_e \nabla u_{eh} \cdot \nabla u_{eh}, \quad (2.71)$$

where $\beta = \min \left(\operatorname*{ess\,inf}_{x \in \Omega_i} \sigma_i, \ \operatorname*{ess\,inf}_{x \in \Omega_e} \sigma_e \right)$. Subtituting (2.67)-(2.71) in the equation (2.66) and using the Poincaré-Friedrichs inequality (2.25) and Young inequality, we obtain

$$\begin{aligned} \frac{\mathrm{C}\beta}{2} \left(\|u_{ih}\|^2_{\mathrm{H}^1(\Omega_i)} + \|u_{eh}\|^2_{\mathrm{H}^1(\Omega_e)} \right) &+ \frac{1}{2} \frac{d}{dt} \|v_h\|^2_{\mathrm{L}^2(\Gamma)} \leqslant \|f(v_h)\|_{\mathrm{L}^2(\Gamma)} \|v_h\|_{\mathrm{L}^2(\Gamma)} \quad (2.72) \\ &+ \frac{1}{2\mathrm{C}\beta} \|\mathrm{I}_{i,stim}\|^2_{\mathrm{L}^2(\Omega_i)} + \frac{1}{\mathrm{C}\beta} \|\mathrm{I}_{e,stim}\|^2_{\mathrm{L}^2(\Omega_e)} + \frac{\alpha_2^2}{\mathrm{C}\beta} \|g_e\|^2_{\mathrm{L}^2(\Gamma_e)}, \end{aligned}$$

for some constant $\mathrm{C} > 0$. Since f is Lipschitzian, the term $\|f(v_h)\|_{\mathrm{L}^2(\Gamma)} \|v_h\|_{\mathrm{L}^2(\Gamma)}$ is handled as follows

$$\begin{aligned} \|f(v_h)\|_{\mathrm{L}^2(\Gamma)} &\leqslant \|f(v_h) - f(0)\|_{\mathrm{L}^2(\Gamma)} + \|f(0)\|_{\mathrm{L}^2(\Gamma)} \\ &\leqslant \mathrm{L}_f \|v_h\|_{\mathrm{L}^2(\Gamma)} + \|f(0)\|_{\mathrm{L}^2(\Gamma)}. \quad (2.73) \end{aligned}$$

It follows that

$$\begin{aligned} \|f(v_h)\|_{\mathrm{L}^2(\Gamma)} \|v_h\|_{\mathrm{L}^2(\Gamma)} &\leqslant \mathrm{L}_f \|v_h\|^2_{\mathrm{L}^2(\Gamma)} + \|f(0)\|_{\mathrm{L}^2(\Gamma)} \|v_h\|_{\mathrm{L}^2(\Gamma)}, \\ &\leqslant \left(\mathrm{L}_f + \frac{1}{2} \right) \|v_h\|^2_{\mathrm{L}^2(\Gamma)} + \frac{1}{2} \|f(0)\|^2_{\mathrm{L}^2(\Gamma)}. \quad (2.74) \end{aligned}$$

The last inequality comes from the Young inequality.
Plugging in (2.74) into (2.72), we deduce that

$$\begin{aligned} \frac{d}{dt} \|v_h\|^2_{\mathrm{L}^2(\Gamma)} &\leqslant (2\mathrm{L}_f + 1) \|v_h\|^2_{\mathrm{L}^2(\Gamma)} + \|f(0)\|^2_{\mathrm{L}^2(\Gamma)} + \mathrm{C} \|\mathrm{I}_{i,stim}\|^2_{\mathrm{L}^2(\Omega_i)} \\ &+ \mathrm{C} \|\mathrm{I}_{e,stim}\|^2_{\mathrm{L}^2(\Omega_e)} + \mathrm{C} \|g_e\|^2_{\mathrm{L}^2(\Gamma_e)}. \quad (2.75) \end{aligned}$$

By integrating in time, we obtain

$$\begin{aligned} \|v_h(t)\|^2_{\mathrm{L}^2(\Gamma)} &\leqslant \|v_h(0)\|^2_{\mathrm{L}^2(\Gamma)} + \int_0^t \left(\|f(0)\|^2_{\mathrm{L}^2(\Gamma)} + \mathrm{C} \|\mathrm{I}_{i,stim}\|^2_{\mathrm{L}^2(\Omega_i)} \right) d\tau \\ &+ \mathrm{C} \int_0^t \left(\|\mathrm{I}_{e,stim}\|^2_{\mathrm{L}^2(\Omega_e)} + \|g_e\|^2_{\mathrm{L}^2(\Gamma_e)} \right) d\tau + \int_0^t (2\mathrm{L}_f + 1) \|v_h\|^2_{\mathrm{L}^2(\Gamma)} \, d\tau. \end{aligned}$$

From Lemma 2.2.1, we obtain

$$\begin{aligned} \|v_h(t)\|^2_{\mathrm{L}^2(\Gamma)} &\leqslant \mathrm{C} e^{(2\mathrm{L}_f + 1)\mathrm{T}} \left[\|v_h(0)\|^2_{\mathrm{L}^2(\Gamma)} + \mathrm{T} \|f(0)\|^2_{\mathrm{L}^2(\Gamma)} + \|\mathrm{I}_{i,stim}\|^2_{\mathrm{L}^2(0,\mathrm{T};\mathrm{L}^2(\Omega_i))} \right] \\ &+ \mathrm{C} e^{(2\mathrm{L}_f + 1)\mathrm{T}} \left[\|\mathrm{I}_{e,stim}\|^2_{\mathrm{L}^2(0,\mathrm{T};\mathrm{L}^2(\Omega_e))} + \|g_e\|^2_{\mathrm{L}^2(0,\mathrm{T};\mathrm{L}^2(\Gamma_e))} \right], \end{aligned}$$

a.e. on $[0, \mathrm{T}]$. It is worth noticing that the previous inequality implies

$$\|v_h\|_{\mathrm{L}^\infty(0,\mathrm{T};\mathrm{L}^2(\Gamma))} \leqslant \mathrm{C}_1, \tag{2.76}$$

for some constant $\mathrm{C}_1 > 0$.

We now prove the inequality (2.64). Substituting (2.74) into (2.72) and integrating from 0 to T yields

$$\begin{aligned} \mathrm{C}_2 \int_0^{\mathrm{T}} \left(\|u_{ih}\|^2_{\mathrm{H}^1(\Omega_i)} + \|u_{eh}\|^2_{\mathrm{H}^1(\Omega_e)} \right) dt &\leqslant \|v_h(0)\|^2_{\mathrm{L}^2(\Gamma)} + \mathrm{C} \int_0^{\mathrm{T}} \|v_h(t)\|^2_{\mathrm{L}^2(\Gamma)}\, dt \\ &+ \mathrm{C} \left(\mathrm{T}\|f(0)\|^2_{\mathrm{L}^2(\Gamma)} + \|\mathrm{I}_{i,stim}\|^2_{\mathrm{L}^2(0,\mathrm{T};\mathrm{L}^2(\Omega_i))} \right) \\ &+ \left(\|\mathrm{I}_{e,stim}\|^2_{\mathrm{L}^2(0,\mathrm{T};\mathrm{L}^2(\Omega_e))} + \|g_e\|^2_{\mathrm{L}^2(0,\mathrm{T};\mathrm{L}^2(\Gamma_e))} \right). \end{aligned}$$

Hence, there exists a constant $\mathrm{C} > 0$ such that

$$\|u_{ih}\|^2_{\mathrm{L}^2(0,\mathrm{T};\mathrm{H}^1(\Omega_i))} + \|u_{eh}\|^2_{\mathrm{L}^2(0,\mathrm{T};\mathrm{H}^1(\Omega_e))} \leqslant \mathrm{C},$$

since

$$\int_0^{\mathrm{T}} \|v_h(t)\|^2_{\mathrm{L}^2(\Gamma)}\, dt \leqslant \mathrm{T}\|v_h\|^2_{\mathrm{L}^\infty(0,\mathrm{T};\mathrm{L}^2(\Gamma))} < \infty, \qquad \text{from (2.76)},$$

which gives (2.64). Lastly, we prove the inequality (2.65). Write

$$\begin{aligned} \|v_h\|_{\mathrm{H}^{\frac{1}{2}}(\Gamma)} &= \|u_{ih} - u_{eh}\|_{\mathrm{H}^{\frac{1}{2}}(\Gamma)} \\ &\leqslant \|u_{ih}\|_{\mathrm{H}^{\frac{1}{2}}(\Gamma)} + \|u_{eh}\|_{\mathrm{H}^{\frac{1}{2}}(\Gamma)} \\ &\leqslant \mathrm{C}\left(\|u_{ih}\|_{\mathrm{H}^1(\Omega_i)} + \|u_{eh}\|_{\mathrm{H}^1(\Omega_e)} \right), \end{aligned} \tag{2.77}$$

thanks to the continuity of trace operators defined in (2.41) and (2.42), respectively. We then deduce the following bound in $\mathrm{L}^2(0, \mathrm{T}; \mathrm{H}^{\frac{1}{2}}(\Gamma))$ for v_h:

$$\|v_h\|_{\mathrm{L}^2(0,\mathrm{T};\mathrm{H}^{\frac{1}{2}}(\Gamma))} \leqslant \mathrm{C}_4, \tag{2.78}$$

for some constant $\mathrm{C}_4 > 0$. □

2.3 Error Estimates in Space

In this section, we estimate the error between the solutions of the semidiscrete and continuous problems (2.46) and (2.10), respectively. Proceeding as in [74], we write the error as a sum of two terms which are then bounded separately:

$$u_h - u = (u_h - \mathrm{P}_h u) + (\mathrm{P}_h u - u) = \theta + \rho, \tag{2.79}$$

where P_h denotes a projection of W onto $\mathrm{V}_h^i \times \mathrm{V}_h^e$ defined by

$$\begin{aligned}\int_{\Omega_i} \sigma_i \nabla \mathrm{P}_h u_i \cdot \nabla \chi_{ih} \quad + \quad \int_{\Omega_e} \sigma_e \nabla \mathrm{P}_h u_e \cdot \nabla \chi_{eh} + \int_\Gamma \left(\mathrm{P}_h u_i - \mathrm{P}_h u_e\right)\left(\chi_{ih} - \chi_{eh}\right) = \\ \int_{\Omega_i} \sigma_i \nabla u_i \cdot \nabla \chi_{ih} \quad + \quad \int_{\Omega_e} \sigma_e \nabla u_e \cdot \chi_{eh} + \int_\Gamma \left(u_i - u_e\right)\left(\chi_{ih} - \chi_{eh}\right), \quad \forall \chi_h \in \mathrm{W}_h.\end{aligned}$$

Due to the jump on the interface Γ, P_h is not a standard projection operator.
The space W defined in Section 2.1 is equipped with the norm

$$|||u|||_{\mathrm{W}} = \left(\|u_i\|^2_{\mathrm{H}^1(\Omega_i)} + \|u_e\|^2_{\mathrm{H}^1(\Omega_e)} + \|u_i - u_e\|^2_{\mathrm{L}^2(\Gamma)}\right)^{\frac{1}{2}}. \tag{2.80}$$

Before stating the main result of this section, we shall prove that the projection operator P_h is well defined. For a given $u \in \mathrm{W}$, let us set

$$\begin{aligned} a\left(w_h, \chi_h\right) &= \int_{\Omega_i} \sigma_i \nabla w_{ih} \cdot \nabla \chi_{ih} + \int_{\Omega_e} \sigma_e \nabla w_{eh} \cdot \nabla \chi_{eh} + \int_\Gamma \left(w_{ih} - w_{eh}\right)\left(\chi_{ih} - \chi_{eh}\right) \\ l(\chi_h) &= a\left(u, \chi_h\right) = \int_{\Omega_i} \sigma_i \nabla u_i \cdot \nabla \chi_{ih} + \int_{\Omega_e} \sigma_e \nabla u_e \cdot \chi_{eh} + \int_\Gamma v\left(\chi_{ih} - \chi_{eh}\right), \end{aligned}$$

where $w_h, \chi_h \in \mathrm{W}_h$ and $v = u_i - u_e$. For a given $u \in \mathrm{W}$, let us consider the following problem:

$$\begin{cases} \text{find} \;\; \mathrm{P}_h u \in \mathrm{W}_h \quad \text{such that} \\ \qquad a\left(\mathrm{P}_h u, \chi_h\right) = l(\chi_h) \quad \text{for all } \chi_h \in \mathrm{W}_h. \end{cases} \tag{2.81}$$

The following lemma will be useful to prove the existence and uniqueness of the solution of (2.81).

Lemma 2.3.1 (Petree-Tartar). *Let* $\mathrm{X}, \mathrm{Y}, \mathrm{Z}$ *be three Banach spaces. Let* $\mathrm{A} \in \mathcal{L}\left(\mathrm{X}, \mathrm{Y}\right)$ *be an injective operator and* $\mathrm{T} \in \mathcal{L}\left(\mathrm{X}, \mathrm{Z}\right)$ *be a compact operator. If there exists* $C > 0$ *such that:*

$$C\|x\|_{\mathrm{X}} \leq \|\mathrm{A}x\|_{\mathrm{Y}} + \|\mathrm{T}x\|_{\mathrm{Z}}.$$

Then, $Im(A)$ *is closed. Equivalently, there exists* $\alpha > 0$ *such that:*

$$\forall x \in \mathrm{X}, \quad \alpha\|x\|_{\mathrm{X}} \leq \|\mathrm{A}x\|_{\mathrm{Y}}. \tag{2.82}$$

For the proof of this lemma, see e.g.[20, Lemma A.38 pp.469].
To prove the coercivity of $a(\cdot,\cdot)$, we establish (2.82). We use the following lemma:

Lemma 2.3.2. *Let $w \in \mathrm{W}$ be arbitrary. There exists a constant $\alpha > 0$ sucht that*

$$\alpha |||w|||^2_{\mathrm{W}} \leqslant \|\nabla w_e\|^2_{\mathrm{L}^2(\Omega_e)} + \|\nabla w_i\|^2_{\mathrm{L}^2(\Omega_i)} + \|w_i - we\|^2_{\mathrm{L}^2(\Gamma)}. \tag{2.83}$$

Proof. We consider the following three Banach spaces:

$$\begin{cases} \mathrm{X} = \mathrm{W} \\ \mathrm{Y} = \mathrm{L}^2(\Omega_i) \times \mathrm{L}^2(\Omega_e) \times \mathrm{L}^2(\Gamma), \\ \mathrm{Z} = \mathrm{L}^2(\Omega_i) \times \mathrm{L}^2(\Omega_e). \end{cases} \tag{2.84}$$

Further, we consider the following operator:

$$\begin{aligned} \mathrm{A}\colon \mathrm{X} &\longrightarrow \mathrm{Y} \\ w &\mapsto \left(\nabla w_i, \nabla w_e, w_{i_{|\Gamma}} - w_{e_{|\Gamma}}\right). \end{aligned}$$

Clearly, A is a continuous linear operator. We claim that A is injective. In fact, assume that

$$\begin{cases} \nabla w_i = 0 & \text{a.e in} \quad \Omega_i, \\ \nabla w_e = 0 & \text{a.e in} \quad \Omega_e, \\ w_i = w_e & \text{a.e on} \quad \Gamma. \end{cases}$$

Then,

$$\begin{cases} w_{i_{|\Omega_i}} = C_i & \text{a.e in} \quad \Omega_i, \\ w_{e_{|\Omega_e}} = C_e & \text{a.e in} \quad \Omega_e, \\ C_i = C_e & \text{a.e on} \quad \Gamma. \end{cases}$$

where C_i and C_e are constants. Since $\int_{\Omega_e} w_e \, dx = 0$, $w_e|_{\Omega_e} = C_e$ a.e, and $\mu(\Omega_e) \neq 0$, it follows that $u_e = 0$ in Ω_e a.e. Therefore, $C_e = 0 = C_i$ and $u_i = 0$ in Ω_i a.e.
On the other hand, we consider the operator below:

$$\begin{aligned} \mathrm{T}\colon \mathrm{X} &\longrightarrow \mathrm{Z} \\ w &\mapsto (w_i, w_e). \end{aligned}$$

Clearly, T is a compact operator, see e.g.[1, 8]. It remains to prove that there exists $C > 0$ such that

$$|||w|||_{\mathrm{W}} \leq \|\mathrm{A}w\|_{\mathrm{Y}} + \|\mathrm{T}w\|_{\mathrm{Z}}.$$

We have

$$\begin{aligned}
|||w|||_{\mathrm{W}}^2 &= \|w_i\|_{\mathrm{H}^1(\Omega_i)}^2 + \|w_e\|_{\mathrm{H}^1(\Omega_e)}^2 + \|w_i - w_e\|_{\mathrm{L}^2(\Gamma)}^2 \\
&= \|w_i\|_{\mathrm{L}^2(\Omega_i)}^2 + \|\nabla w_i\|_{\mathrm{L}^2(\Omega_i)}^2 + \|w_e\|_{\mathrm{L}^2(\Omega_e)}^2 + \|\nabla w_e\|_{\mathrm{L}^2(\Omega_e)}^2 \\
&+ \|w_i - w_e\|_{\mathrm{L}^2(\Gamma)}^2 \\
&= \|\mathrm{A}w\|_{\mathrm{Y}}^2 + \|\mathrm{T}w\|_{\mathrm{Z}}^2 \\
&\leq \left(\|\mathrm{A}w\|_{\mathrm{Y}} + \|\mathrm{T}w\|_{\mathrm{Z}}\right)^2.
\end{aligned}$$

Consequently,

$$|||w|||_{\mathrm{X}} \leq \|\mathrm{A}w\|_{\mathrm{Y}} + \|\mathrm{T}w\|_{\mathrm{Z}},$$

with $C = 1$. Thanks to Lemma 2.3.1, there exists $\alpha > 0$, such that

$$\alpha|||w|||_{\mathrm{X}} \leq \|\mathrm{A}w\|_{\mathrm{Y}},$$

that is,

$$\begin{aligned}
\alpha\left(\|w_i\|_{\mathrm{H}^2(\Omega_i)}^2 + \|w_e\|_{\mathrm{H}^1(\Omega_e)}^2 + \|w_i - w_e\|_{\mathrm{L}^2(\Gamma)}^2\right) \leqslant \\
\|\nabla w_e\|_{\mathrm{L}^2(\Omega_e)}^2 + \|\nabla w_i\|_{\mathrm{L}^2(\Omega_i)}^2 + \|w_i - w_e\|_{\mathrm{L}^2(\Gamma)}^2.
\end{aligned}$$

□

Theorem 2.3.3. *The problem* (2.81) *has a unique solution.*

Proof. Let us show that:

i) The bilinear form $a(\cdot,\cdot)$ in (2.81) is continuous on $\mathrm{W} \times \mathrm{W}$ and coercive on W.

ii) The linear form $l(\cdot)$ in (2.81) is continuous on W.

i) Let $w, \varphi \in \mathrm{W}$ be arbitrary, we have

$$\begin{aligned}
|a(w,\varphi)| &\leqslant \mathrm{C}\|\nabla w_e\|_{\mathrm{L}^2(\Omega_e)}\|\nabla\varphi_e\|_{\mathrm{L}^2(\Omega_e)} + \mathrm{C}\|\nabla w_i\|_{\mathrm{L}^2(\Omega_i)}\|\nabla\varphi_i\|_{\mathrm{L}^2(\Omega_i)} \\
&+ \|w_i - w_e\|_{\mathrm{L}^2(\Gamma)}\|\varphi_i - \varphi_e\|_{\mathrm{L}^2(\Gamma)}, \\
&\leq \mathrm{C}\left(\|\nabla w_e\|_{\mathrm{L}^2(\Omega_e)}^2 + \|\nabla w_i\|_{\mathrm{L}^2(\Omega_i)}^2 + \|w_i - w_e\|_{\mathrm{L}^2(\Gamma)}^2\right)^{1/2} \\
&\quad \left(\|\nabla\varphi_e\|_{\mathrm{L}^2(\Omega_e)}^2 + \|\nabla\varphi_i\|_{\mathrm{L}^2(\Omega_i)}^2 + \|\varphi_i - \varphi_e\|_{\mathrm{L}^2(\Gamma)}^2\right)^{1/2} \\
&\leq \mathrm{C}|||w|||_{\mathrm{W}}|||\varphi|||_{\mathrm{W}},
\end{aligned}$$

where C is a given constant depending on $\operatorname*{ess\,sup}_{x\in\Omega_e}\sigma_e(x)$ and $\operatorname*{ess\,sup}_{x\in\Omega_i}\sigma_i(x)$. It follows that the bilinear form $a(\cdot,\cdot)$ is continuous on $\mathrm{W}\times\mathrm{W}$. In particular, $a(\cdot,\cdot)$ is continuous on $\mathrm{W}_h\times\mathrm{W}_h$.
Let us prove the coercivity of $a(\cdot,\cdot)$. Let $w\in\mathrm{W}$. We have

$$\begin{aligned} a\left(w,w\right) &= \int_{\Omega_i}\sigma_i\left|\nabla w_i\right|^2+\int_{\Omega_e}\sigma_e\left|\nabla w_e\right|^2+\int_{\Gamma}\left(w_i-w_e\right)^2 \\ &\geqslant \min\left(1,\beta\right)\left(\|\nabla w_e\|^2_{\mathrm{L}^2(\Omega_e)}+\|\nabla w_i\|^2_{\mathrm{L}^2(\Omega_i)}+\|w_i-w_e\|^2_{\mathrm{L}^2(\Gamma)}\right) \\ &\geqslant \nu|||w|||^2_{\mathrm{W}}, \quad \text{from (2.83)}, \end{aligned}$$

where $\nu=\alpha\min\left(1,\beta\right)>0$ and $\beta=\min\left(\operatorname*{ess\,inf}_{x\in\Omega_i}\sigma_i,\ \operatorname*{ess\,inf}_{x\in\Omega_e}\sigma_e\right)>0\cdot$ It follows that the bilinear form $a(\cdot,\cdot)$ is coercive on W, consequently on W_h as well.
ii) Let $\varphi=(\varphi_i,\varphi_e)\in\mathrm{W}$ be arbitrary and fix $u=(u_i,u_e)\in\mathrm{W}$. Using the continuity of the bilinear form $a(\cdot,\cdot)$, we have

$$|l(\varphi)| \leqslant \mathrm{C}|||w|||_{\mathrm{W}}|||\varphi|||_{\mathrm{W}}\cdot$$

Therefore, the variational formulation problem (2.81) has a unique solution thanks to the Lax-Milgram theorem. □

The following lemma due to Céa will be useful in the sequel.

Lemma 2.3.4. *Let $u\in\mathrm{W}$. Let $\nu>0$ and $M>0$ be the coercivity and continuity constants of the bilinear form $a(\cdot,\cdot)$ defined above (2.81), respectively. Then*

$$|||u-\mathrm{P}_h u|||_{\mathrm{W}}\leqslant\sqrt{\frac{M}{\nu}}\inf_{\chi_h\in\mathrm{W}_h}|||u-\chi_h|||_{\mathrm{W}}\cdot \tag{2.85}$$

Proof. From (2.81), we subtract the bilinear form $a\left(\mathrm{P}_h u,\chi_h\right)$ from the linear form $l(\chi_h)=a\left(u,\chi_h\right)$. Then,

$$a(u-\mathrm{P}_h u,\chi_h) = 0, \qquad \forall\chi_h\in\mathrm{W}_h\cdot \tag{2.86}$$

Let $\chi_h\in\mathrm{W}_h$ be arbitrary, then

$$\begin{aligned} a(u-\chi_h,u-\chi_h) &= a(u-\mathrm{P}_h u+\mathrm{P}_h u-\chi_h,u-\mathrm{P}_h u+\mathrm{P}_h u-\chi_h) \\ &= a(u-\mathrm{P}_h u,u-\mathrm{P}_h u)+a(\mathrm{P}_h u-\chi_h,\mathrm{P}_h u-\chi_h), \end{aligned}$$

taking into account (2.86) and the symmetry of $a(\cdot,\cdot)$. It follows that

$$a(u-\mathrm{P}_h u,u-\mathrm{P}_h u)=\inf_{\chi_h\in\mathrm{W}_h}\left\{a(u-\chi_h,u-\chi_h)\right\}\cdot$$

The continuity and coercivity of the bilinear form $a(\cdot,\cdot)$ yield

$$\nu|||u-\mathrm{P}_h u|||_{\mathrm{W}}^2 \leq M \inf_{\chi_h\in \mathrm{W}_h}\left\{|||u-\chi_h|||_{\mathrm{W}}^2\right\} \Longrightarrow |||u-\mathrm{P}_h u|||_{\mathrm{W}} \leq \sqrt{\frac{M}{\nu}} \inf_{\chi_h\in \mathrm{W}_h}\{|||u-\chi_h|||_{\mathrm{W}}\}.$$

□

Let us write the error as in (2.79), that is,

$$u_h - u \;=\; (u_h-\mathrm{P}_h u)+(\mathrm{P}_h u-u)=\theta+\rho.$$

Let us set

$$\theta \;=\; \begin{cases} \theta_i = u_{ih}-\mathrm{P}_h u_i, \quad \text{in } \Omega_i, \\ \theta_e = u_{eh}-\mathrm{P}_h u_e, \quad \text{in } \Omega_e, \end{cases} \tag{2.87}$$

$$\rho \;=\; \begin{cases} \rho_i = \mathrm{P}_h u_i - u_i, \quad \text{in } \Omega_i, \\ \rho_e = \mathrm{P}_h u_e - u_e, \quad \text{in } \Omega_e, \end{cases} \tag{2.88}$$

$$\begin{cases} \theta^{\Gamma} = \theta_i-\theta_e = v_h-(\mathrm{P}_h u_i-\mathrm{P}_h u_e), \quad \text{on } \Gamma, \\ \rho^{\Gamma} = \mathrm{P}_h u_i-\mathrm{P}_h u_e - v, \quad \text{on } \Gamma, \end{cases} \tag{2.89}$$

where $v_h = u_{ih}-u_{eh}$ and $v=u_i-u_e$. The following error estimates hold:

Proposition 2.3.5. *Let $u\in \mathrm{W}$. We assume that $u_i\in \mathrm{H}^{l+1}(\Omega_i)$ and $u_e\in \mathrm{H}^{l+1}(\Omega_e)$ for $1\leqslant l\leqslant d$. Then,*

$$\|\rho_e\|_{\mathrm{H}^1(\Omega_e)} \;\leq\; Ch^l\left(|u_e|_{\mathrm{H}^{l+1}(\Omega_e)}+|u_i|_{\mathrm{H}^{l+1}(\Omega_i)}\right), \tag{2.90}$$

$$\|\rho_i\|_{\mathrm{H}^1(\Omega_i)} \;\leq\; Ch^l\left(|u_e|_{\mathrm{H}^{l+1}(\Omega_e)}+|u_i|_{\mathrm{H}^{l+1}(\Omega_i)}\right), \tag{2.91}$$

$$\|\rho^{\Gamma}\|_{\mathrm{L}^2(\Gamma)} \;\leq\; Ch^l\left(|u_e|_{\mathrm{H}^{l+1}(\Omega_e)}+|u_i|_{\mathrm{H}^{l+1}(\Omega_i)}\right), \tag{2.92}$$

where $|\cdot|_{\mathrm{H}^l(\Omega)}$ is the $\mathrm{H}^l(\Omega)$ seminorm defined in (2.40) and $\mathrm{C}>0$ is some constant independent of the meshsize.

Proof. Let $\chi_h=(\chi_{ih},\chi_{eh})\in \mathrm{W}_h$ be arbitrary. We have

$$|||u-\chi_h|||_{\mathrm{W}}^2 = \|u_e-\chi_{eh}\|_{\mathrm{H}^1(\Omega_e)}^2+\|u_i-\chi_{ih}\|_{\mathrm{H}^1(\Omega_i)}^2+\|(u_i-u_e)-(\chi_{ih}-\chi_{eh})\|_{\mathrm{L}^2(\Gamma)}^2.$$

Taking $\chi_{ih} = \Pi_{\mathrm{h}}^{\mathrm{i}} u_i$ and $\chi_{eh} = \Pi_{\mathrm{h}}^{\mathrm{e}} u_e$, where $\Pi_{\mathrm{h}}^{\mathrm{e}}$ and $\Pi_{\mathrm{h}}^{\mathrm{i}}$ are the Lagrange interpolation operators mentioned above (2.38) and (2.39), respectively. It follows that

$$\begin{aligned}
\inf_{\chi_h \in \mathrm{W}_h} \left\{ |||u - \chi_h|||_{\mathrm{W}}^2 \right\} &\leqslant \|u_e - \Pi_{\mathrm{h}}^{\mathrm{e}} u_e\|_{\mathrm{H}^1(\Omega_e)}^2 + \|u_i - \Pi_{\mathrm{h}}^{\mathrm{i}} u_i\|_{\mathrm{H}^1(\Omega_i)}^2 \\
&+ \|(u_i - u_e) - (\Pi_{\mathrm{h}}^{\mathrm{i}} u_i - \Pi_{\mathrm{h}}^{\mathrm{e}} u_e)\|_{\mathrm{L}^2(\Gamma)}^2, \\
&\leqslant \|u_e - \Pi_{\mathrm{h}}^{\mathrm{e}} u_e\|_{\mathrm{H}^1(\Omega_e)}^2 + \|u_i - \Pi_{\mathrm{h}}^{\mathrm{i}} u_i\|_{\mathrm{H}^1(\Omega_i)}^2 \\
&+ 2\|u_i - \Pi_h^i u_i\|_{\mathrm{L}^2(\Gamma)}^2 + 2\|u_e - \Pi_h^e u_e\|_{\mathrm{L}^2(\Gamma)}^2 \\
&\leqslant \mathrm{C} \left(\|u_e - \Pi_{\mathrm{h}}^{\mathrm{e}} u_e\|_{\mathrm{H}^1(\Omega_e)}^2 + \|u_i - \Pi_{\mathrm{h}}^{\mathrm{i}} u_i\|_{\mathrm{H}^1(\Omega_i)}^2 \right)
\end{aligned}$$

for some constant $\mathrm{C} > 0$, thanks to the inequalities (2.41) and (2.42). It follows that

$$\begin{aligned}
\inf_{\chi_h \in \mathrm{W}_h} \left\{ |||u - \chi_h|||_{\mathrm{W}} \right\} &\leq \mathrm{C} \left(\|u_e - \Pi_{\mathrm{h}}^{\mathrm{e}} u_e\|_{\mathrm{H}^1(\Omega_e)} + \|u_i - \Pi_{\mathrm{h}}^{\mathrm{i}} u_i\|_{\mathrm{H}^1(\Omega_i)} \right) \\
&\leq \mathrm{C} h^l \left(|u_e|_{\mathrm{H}^{l+1}(\Omega_e)} + |u_i|_{\mathrm{H}^{l+1}(\Omega_i)} \right),
\end{aligned}$$

for some constant $\mathrm{C} > 0$, thanks to the inequalities (2.38) and (2.39). On account of the inequality (2.85), the following error estimate holds

$$|||\rho|||_{\mathrm{W}} \leq \mathrm{C} h^l \left(|u_e|_{\mathrm{H}^{l+1}(\Omega_e)} + |u_i|_{\mathrm{H}^{l+1}(\Omega_i)} \right), \tag{2.93}$$

for some constant $\mathrm{C} > 0$. From (2.93), we deduce the error estimates (2.90)-(2.92). □

Let us recall the following space-time domains defined above

$$\begin{aligned}
\mathcal{Q}_i &= \Omega_i \times]0, \mathrm{T}[, \\
\mathcal{Q}_e &= \Omega_e \times]0, \mathrm{T}[, \\
\Sigma &= \Gamma \times]0, \mathrm{T}[.
\end{aligned}$$

It is worth remembering that there are isometric isomorphisms from $\mathrm{L}^2\left(0, \mathrm{T}; \mathrm{L}^2(\Omega_i)\right)$ and $\mathrm{L}^2\left(0, \mathrm{T}; \mathrm{L}^2(\Omega_e)\right)$ to $\mathrm{L}^2\left(\mathrm{Q}_i\right)$ and $\mathrm{L}^2\left(\mathrm{Q}_e\right)$, respectively.

Theorem 2.3.6. *Let u and u_h be the solutions of (2.10) and (2.46). Let us assume that $u_{i,e} \in \mathrm{H}^1(0, \mathrm{T}; \mathrm{H}^{l+1}(\Omega_{i,e}))$ for $1 \leq l \leq d$. There exists a positive constant C depending only on T, and L_f the Lipschitz constant of f, such that*

$$\begin{aligned}
\|\nabla(u_i - u_{ih})\|_{\mathrm{L}^2(\mathrm{Q}_i)}^2 + \|\nabla(u_e - u_{eh})\|_{\mathrm{L}^2(\mathrm{Q}_e)}^2 &\leqslant \mathrm{C} h^{2l} \int_0^{\mathrm{T}} \left(|u_e|_{\mathrm{H}^{l+1}(\Omega_e)}^2 + |u_i|_{\mathrm{H}^{l+1}(\Omega_i)}^2 \right) dt \\
&+ \mathrm{C} h^{2l} \int_0^{\mathrm{T}} \left(\left| \frac{\partial u_e}{\partial t} \right|_{\mathrm{H}^{l+1}(\Omega_e)}^2 + \left| \frac{\partial u_i}{\partial t} \right|_{\mathrm{H}^{l+1}(\Omega_i)}^2 \right) dt.
\end{aligned} \tag{2.94}$$

$$\|v - v_h\|^2_{\mathrm{L}^2(\Gamma)} \leqslant Ch^{2l} \int_0^{\mathrm{T}} \left(|u_e|^2_{\mathrm{H}^{l+1}(\Omega_e)} + |u_i|^2_{\mathrm{H}^{l+1}(\Omega_i)} + \left| \frac{\partial u_e}{\partial t} \right|^2_{\mathrm{H}^{l+1}(\Omega_e)} + \left| \frac{\partial u_i}{\partial t} \right|^2_{\mathrm{H}^{l+1}(\Omega_i)} \right). \quad (2.95)$$

Proof. With the error written as in (2.79) it suffices, in view of Proposition 2.3.5, to bound $\theta = u_h - \mathrm{P}_h u$.
Let $\chi_h \in \mathrm{W}_h$.

$$\begin{aligned}
(\partial_t (\theta_i - \theta_e), \chi_{ih} - \chi_{eh})_\Gamma \quad + \quad & a(\theta, \chi_h) = \int_\Gamma \partial_t (\theta_i - \theta_e)(\chi_{ih} - \chi_{eh}) + \int_{\Omega_i} \sigma_i \nabla\theta_i \cdot \nabla\chi_{ih} \\
& + \int_{\Omega_e} \sigma_e \nabla\theta_e \cdot \nabla\chi_{eh} + \int_\Gamma (\theta_i - \theta_e)(\chi_{ih} - \chi_{eh}) \\
= \quad & \int_\Gamma \partial_t v_h (\chi_{ih} - \chi_{eh}) + \int_{\Omega_i} \sigma_i \nabla u_{ih} \cdot \nabla\chi_{ih} \\
& + \int_{\Omega_e} \sigma_e \nabla u_{eh} \cdot \nabla\chi_{eh} + \int_\Gamma v_h (\chi_{ih} - \chi_{eh}) \\
& - \int_\Gamma \partial_t (P_h u_i - P_h u_e)(\chi_{ih} - \chi_{eh}) - \int_{\Omega_i} \sigma_i \nabla P_h u_i \cdot \nabla\chi_{ih} \\
& - \int_{\Omega_e} \sigma_e \nabla P_h u_e \cdot \nabla\chi_{eh} - \int_\Gamma (P_h u_i - P_h u_e)(\chi_{ih} - \chi_{eh}) \\
= \quad & - \int_\Gamma f(v_h)(\chi_{ih} - \chi_{eh}) + \int_{\Omega_i} \mathrm{I}_{i,stim}\chi_{ih} + \int_{\Omega_e} \mathrm{I}_e \chi_{eh} + \int_{\Gamma_e} g_e \chi_{eh} \\
& + \int_\Gamma v_h (\chi_{ih} - \chi_{eh}) - \int_\Gamma \partial_t (P_h u_i - P_h u_e)(\chi_{ih} - \chi_{eh}) \\
& - \int_{\Omega_i} \sigma_i \nabla u_i \cdot \nabla\chi_{ih} - \int_{\Omega_e} \sigma_e \nabla u_e \cdot \nabla\chi_{eh} - \int_\Gamma v (\chi_{ih} - \chi_{eh}) \\
= \quad & \int_\Gamma \partial_t v (\chi_{ih} - \chi_{eh}) + \int_\Gamma (f(v) - f(v_h))(\chi_{ih} - \chi_{eh}) \\
& + \int_\Gamma (v_h - v)(\chi_{ih} - \chi_{eh}) - \int_\Gamma \partial_t (P_h u_i - P_h u_e)(\chi_{ih} - \chi_{eh}).
\end{aligned}$$

We have for all $\chi_h \in \mathrm{W}_h$,

$$\begin{aligned}
(\partial_t (\theta_i - \theta_e), \chi_{ih} - \chi_{eh})_\Gamma \quad + \quad & a(\theta, \chi_h) = -\left(\partial_t \rho^\Gamma, \chi_{ih} - \chi_{eh}\right)_\Gamma + (v_h - v, \chi_{ih} - \chi_{eh})_\Gamma \\
+ \quad & (f(v) - f(v_h), \chi_{ih} - \chi_{eh})_\Gamma, \qquad (2.96)
\end{aligned}$$

where $\rho^\Gamma = P_h u_i - P_h u_e - v$. Setting $\chi_h = \theta$ in (2.96) yields

$$\begin{aligned}\frac{1}{2}\frac{d}{dt}\|\theta^\Gamma\|^2_{\mathrm{L}^2(\Gamma)} &+ \beta\left(\|\nabla\theta_i\|^2_{\mathrm{L}^2(\Omega_i)} + \|\nabla\theta_e\|^2_{\mathrm{L}^2(\Omega_e)}\right) + \|\theta^\Gamma\|^2_{\mathrm{L}^2(\Gamma)} \leq \|\partial_t\rho^\Gamma\|_{\mathrm{L}^2(\Gamma)}\|\theta^\Gamma\|_{\mathrm{L}^2(\Gamma)}\\ &+ \mathrm{L}_f\|v_h - v\|_{\mathrm{L}^2(\Gamma)}\|\theta^\Gamma\|_{\mathrm{L}^2(\Gamma)} + \|v_h - v\|_{\mathrm{L}^2(\Gamma)}\|\theta^\Gamma\|_{\mathrm{L}^2(\Gamma)}\\ &\leq \|\partial_t\rho^\Gamma\|_{\mathrm{L}^2(\Gamma)}\|\theta^\Gamma\|_{\mathrm{L}^2(\Gamma)} + (1+\mathrm{L}_f)\,\|\theta^\Gamma\|^2_{\mathrm{L}^2(\Gamma)} + (1+\mathrm{L}_f)\,\|\rho^\Gamma\|_{\mathrm{L}^2(\Gamma)}\|\theta^\Gamma\|_{\mathrm{L}^2(\Gamma)}\\ &\leq \frac{5}{4}(1+\mathrm{L}_f)\,\|\theta^\Gamma\|^2_{\mathrm{L}^2(\Gamma)} + 2\,(1+\mathrm{L}_f)\,\|\rho^\Gamma\|^2_{\mathrm{L}^2(\Gamma)} + \frac{2}{(1+\mathrm{L}_f)}\|\partial_t\rho^\Gamma\|^2_{\mathrm{L}^2(\Gamma)},\end{aligned}$$

using Young inequality. Then,

$$\begin{aligned}\frac{1}{2}\frac{d}{dt}\|\theta^\Gamma\|^2_{\mathrm{L}^2(\Gamma)} &+ \beta\left(\|\nabla\theta_i\|^2_{\mathrm{L}^2(\Omega_i)} + \|\nabla\theta_e\|^2_{\mathrm{L}^2(\Omega_e)}\right) \leqslant \frac{1}{4}(1+5\mathrm{L}_f)\,\|\theta^\Gamma\|^2_{\mathrm{L}^2(\Gamma)}\\ &+ \mathrm{C}_1\|\partial_t\rho^\Gamma\|^2_{\mathrm{L}^2(\Gamma)} + \mathrm{C}_2\|\rho^\Gamma\|^2_{\mathrm{L}^2(\Gamma)},\end{aligned} \tag{2.97}$$

for some constants $\mathrm{C}_1, \mathrm{C}_2 > 0$. It follows from the previous inequality that

$$\frac{d}{dt}\|\theta^\Gamma\|^2_{\mathrm{L}^2(\Gamma)} \leqslant \frac{(1+5\mathrm{L}_f)}{2}\|\theta^\Gamma\|^2_{\mathrm{L}^2(\Gamma)} + \mathrm{C}_1\|\partial_t\rho^\Gamma\|^2_{\mathrm{L}^2(\Gamma)} + \mathrm{C}_2\|\rho^\Gamma\|^2_{\mathrm{L}^2(\Gamma)}. \tag{2.98}$$

From (2.98), we deduce that

$$\frac{d}{dt}\left(e^{-0.5\left(1+5\mathrm{L}_f\right)t}\|\theta^\Gamma\|^2_{\mathrm{L}^2(\Gamma)}\right) \leqslant \mathrm{C}e^{-0.5\left(1+5\mathrm{L}_f\right)t}\left[\|\partial_t\rho^\Gamma\|^2_{\mathrm{L}^2(\Gamma)} + \|\rho^\Gamma\|^2_{\mathrm{L}^2(\Gamma)}\right]. \tag{2.99}$$

By integrating (2.99) with respect to time, we obtain that

$$\|\theta^\Gamma(t)\|^2_{\mathrm{L}^2(\Gamma)} \leqslant \mathrm{C}\left[\|\theta^\Gamma(0)\|^2_{\mathrm{L}^2(\Gamma)} + \|\partial_t\rho^\Gamma\|^2_{\mathrm{L}^2(0,\mathrm{T};\mathrm{L}^2(\Gamma))} + \|\rho^\Gamma\|^2_{\mathrm{L}^2(0,\mathrm{T};\mathrm{L}^2(\Gamma))}\right], \tag{2.100}$$

for $a.e.t \in (0,\mathrm{T})$ and for some constant $\mathrm{C} > 0$ depending on L_f and T. From (2.97) , we have

$$\begin{aligned}2\beta\int_0^\mathrm{T}\left(\|\nabla\theta_i\|^2_{\mathrm{L}^2(\Omega_i)} + \|\nabla\theta_e\|^2_{\mathrm{L}^2(\Omega_e)}\right)dt &\leqslant \|\theta^\Gamma(0)\|^2_{\mathrm{L}^2(\Gamma)} + \frac{(1+\mathrm{L}_f)}{2}\int_0^\mathrm{T}\|\theta^\Gamma\|^2_{\mathrm{L}^2(\Gamma)}\,dt\\ &+ \mathrm{C}_1\int_0^\mathrm{T}\|\partial_t\rho^\Gamma\|^2_{\mathrm{L}^2(\Gamma)}\,dt + \mathrm{C}_2\int_0^\mathrm{T}\|\rho^\Gamma\|^2_{\mathrm{L}^2(\Gamma)}\,dt.\end{aligned}$$

Thus,

$$\begin{aligned}\int_0^\mathrm{T}\left(\|\nabla\theta_i\|^2_{\mathrm{L}^2(\Omega_i)} + \|\nabla\theta_e\|^2_{\mathrm{L}^2(\Omega_e)}\right)dt &\leqslant \mathrm{C}\left[\|\theta^\Gamma(0)\|^2_{\mathrm{L}^2(\Gamma)} + \|\partial_t\rho^\Gamma\|^2_{\mathrm{L}^2(0,\mathrm{T};\mathrm{L}^2(\Gamma))}\right]\\ &+ \mathrm{C}\|\rho^\Gamma\|^2_{\mathrm{L}^2(0,\mathrm{T};\mathrm{L}^2(\Gamma))},\end{aligned} \tag{2.101}$$

where $\mathrm{C} > 0$ is a constant that depends on T, β and L_f. In addition,

$$\begin{aligned}
\|\theta^{\Gamma}(0)\|_{\mathrm{L}^2(\Gamma)} &= \|v_h(0) - (\mathrm{P}_h u_i(0) - \mathrm{P}_h u_e(0))\,\|_{\mathrm{L}^2(\Gamma)} \\
&\leqslant \|v_h(0) - v(0)\|_{\mathrm{L}^2(\Gamma)} + \|v(0) - (\mathrm{P}_h u_i(0) - \mathrm{P}_h u_e(0))\,\|_{\mathrm{L}^2(\Gamma)} \\
&= \|v_h(0) - v(0)\|_{\mathrm{L}^2(\Gamma)} + \|\rho^{\Gamma}(0)\|_{\mathrm{L}^2(\Gamma)} \\
&\leq \mathrm{C}h^l \left(|u_e(0)|_{\mathrm{H}^{l+1}(\Omega_e)} + |u_i(0)|_{\mathrm{H}^{l+1}(\Omega_i)}\right), \qquad (2.102)
\end{aligned}$$

using (2.92) together with the continuity of the trace operator and the interpolation error estimates (2.38) and (2.39). From (2.92), we deduce that

$$\|\partial_t \rho^{\Gamma}\|^2_{\mathrm{L}^2(\Gamma)} \leqslant \mathrm{C}h^{2l} \left(\left| \frac{\partial u_e}{\partial t} \right|^2_{\mathrm{H}^{l+1}(\Omega_e)} + \left| \frac{\partial u_i}{\partial t} \right|^2_{\mathrm{H}^{l+1}(\Omega_i)} \right) \qquad (2.103)$$

Plugging (2.92), (2.102) and (2.103) in (2.100) and (2.101) yield, respectively,

$$\|\theta^{\Gamma}(t)\|^2_{\mathrm{L}^2(\Gamma)} \leqslant \mathrm{C}h^{2l} \int_0^{\mathrm{T}} \left(|u_e|^2_{\mathrm{H}^{l+1}(\Omega_e)} + |u_i|^2_{\mathrm{H}^{l+1}(\Omega_i)} + \left| \frac{\partial u_e}{\partial t} \right|^2_{\mathrm{H}^{l+1}(\Omega_e)} + \left| \frac{\partial u_i}{\partial t} \right|^2_{\mathrm{H}^{l+1}(\Omega_i)} \right) dt \qquad (2.104)$$

$$\begin{aligned}
\int_0^{\mathrm{T}} \left(\|\nabla \theta_i\|^2_{\mathrm{L}^2(\Omega_i)} + \|\nabla \theta_e\|^2_{\mathrm{L}^2(\Omega_e)} \right) dt &\leqslant \mathrm{C}h^{2l} \int_0^{\mathrm{T}} \left(|u_e|^2_{\mathrm{H}^{l+1}(\Omega_e)} + |u_i|^2_{\mathrm{H}^{l+1}(\Omega_i)} \right) dt \qquad (2.105) \\
&\quad + \mathrm{C}h^{2l} \int_0^{\mathrm{T}} \left(\left| \frac{\partial u_e}{\partial t} \right|^2_{\mathrm{H}^{l+1}(\Omega_e)} + \left| \frac{\partial u_i}{\partial t} \right|^2_{\mathrm{H}^{l+1}(\Omega_i)} \right) dt.
\end{aligned}$$

Further, we have

$$\|v - v_h\|^2_{\mathrm{L}^2(\Gamma)} \leqslant \mathrm{C} \left(\|\theta^{\Gamma}(t)\|^2_{\mathrm{L}^2(\Gamma)} + \|\rho^{\Gamma}(t)\|^2_{\mathrm{L}^2(\Gamma)} \right). \qquad (2.106)$$

The error estimate (2.95) is obtained by plugging (2.104) and (2.92) in (2.106).
We are now in position to prove the error estimate (2.94). We have

$$\begin{aligned}
\|\nabla(u_i - u_{ih})\|^2_{\mathrm{L}^2(\mathrm{Q}_i)} &+ \|\nabla(u_e - u_{eh})\|^2_{\mathrm{L}^2(\mathrm{Q}_e)} \leqslant \int_0^{\mathrm{T}} \left(\|\nabla \theta_i\|_{\mathrm{L}^2(\Omega_i)} + \|\nabla \rho_i\|_{\mathrm{L}^2(\Omega_i)} \right)^2 \\
&+ \int_0^{\mathrm{T}} \left(\|\nabla \theta_e\|_{\mathrm{L}^2(\Omega_e)} + \|\nabla \rho_e\|_{\mathrm{L}^2(\Omega_e)} \right)^2 \\
&\leqslant \mathrm{C} \int_0^{\mathrm{T}} \left(\|\nabla \theta_i\|^2_{\mathrm{L}^2(\Omega_i)} + \|\nabla \rho_i\|^2_{\mathrm{L}^2(\Omega_i)} + \|\nabla \theta_e\|^2_{\mathrm{L}^2(\Omega_e)} + \|\nabla \rho_e\|^2_{\mathrm{L}^2(\Omega_e)} \right)
\end{aligned}$$

The error estimate (2.94) is derived by substituting (2.90),(2.91) and (2.105) in the previous inequality. □

2.3.1 Numerical Tests with a Manufactured Solution

To evaluate the convergence of the spatial semi-discretization applied to the problem (2.1)-(2.6), we use the method of manufactured solutions, see e.g [58]. We apply the $\mathbb{P}_1$ finite element method. We investigate the accuracy of the numerical method using mesh refinement. We consider a 2D domain consisting of the single cell Ω_i surrounded by the extracellular domain Ω_e, see (2.3):

$$\begin{aligned} \Omega_i &= (10,110)\times(10,30)\,, \\ \Omega_e &= [(0,120)\times(0,40)]\setminus\overline{\Omega}_i\cdot \end{aligned}$$

We assume that the conductivities σ_i and σ_e are scalar and we let $\sigma_i = \sigma_e = 1$. We

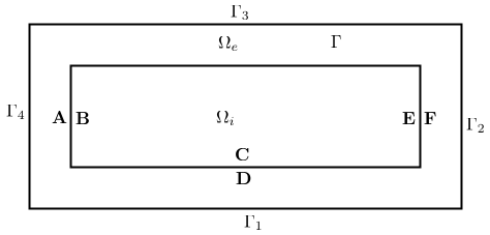

Figure 2.3: Sketch of $\Omega = \Omega_i \cup \Omega_e \cup \Gamma$, $\Gamma = \overline{\Omega}_i \cap \overline{\Omega}_e$.

implement our methods using the software Freefem++ and UMFPACK for solving linear systems.

Our choice for the ionic model falls on a variant of the MS model described in Section 1.3 and initially introduced by Djabella et al. [18].

$$\frac{\partial v}{\partial t} = f(v,w) + \mathrm{I}_{stim}(t), \quad \text{with} \quad f(v,w) = \frac{1}{\tau_{in}} w v^2 (1-v) - \frac{1}{\tau_{out}} v, \tag{2.107}$$

$$\frac{\partial w}{\partial t} = g(v,w), \ \text{with} \ \ g(v,w) = \frac{1}{\tau_k}\left[(1-w_k)\,(1-w) - w_k w\right], \tag{2.108}$$

$$\begin{aligned} \tau_k(v, v_{gate}) &= \tau_{open} + (\tau_{close} - \tau_{open})\, w_k(v, v_{gate}) \\ w_k(v, v_{gate}) &= \frac{1}{2}(1 + \tanh(k(v - v_{gate}))), \end{aligned}$$

where k is a given parameter. In our calculation, we choose $k = 5, \tau_{open} = 120\mathtt{ms}, \tau_{close} = 150\mathtt{ms}, \tau_{in} = 0.3\mathtt{ms}, \tau_{out} = 6\mathtt{ms}$ and $v_{gate} = 0.13$. This value provides a solution that is

close to the solution of the standard MS model [45]. We consider the following activation function

$$\delta(t) = \frac{1}{1+e^{-at}},$$

for some real number a, and we let

$$\begin{aligned} u_{i,ex}(x,y,t) &= 2\delta(t) + \varepsilon\left[(x-x_0)^p + (y-y_0)^p\right], && (2.109)\\ u_{e,ex}(x,y,t) &= \delta(t) + \varepsilon\left[(x-x_0)^p + (y-y_0)^p\right], && (2.110)\\ v_{ex}(x,y,t) &= \delta(t), && (2.111)\\ w_{ex}(x,y,t) &= 2\delta(-t), && (2.112) \end{aligned}$$

where $p \geqslant 2$ is a given interger, (x_0, y_0) are the coordinates of the center of Ω_i, ε is a given parameter that controls the magnitude of $z = (x-x_0)^p + (y-y_0)^p$. Figure 2.4 shows contour and 3D plots of the manufactured solution for $p = 2$. The stimulation currents $\mathrm{I}_{i,stim}$ and $\mathrm{I}_{e,stim}$ becomes:

$$\begin{aligned} \mathrm{I}_{i,ex} &= \varepsilon p(p-1)\left[(x-x_0)^{p-2} + (y-y_0)^{p-2}\right] && (2.113)\\ \mathrm{I}_{e,ex} &= \varepsilon p(p-1)\left[(x-x_0)^{p-2} + (y-y_0)^{p-2}\right]. && (2.114) \end{aligned}$$

The problem (2.1)-(2.6) is then modified with source terms

$$\begin{aligned} -\nabla\cdot(\sigma_i\nabla u_i) &= \mathrm{I}_{i,ex} \quad \text{in } \Omega_i, && (2.115)\\ -\nabla\cdot(\sigma_e\nabla u_e) &= \mathrm{I}_{e,ex} \quad \text{in } \Omega_e, && (2.116)\\ \sigma_e\nabla u_e\cdot n_e &= -\sigma_i\nabla u_i\cdot n_i = \mathrm{I}_m \quad \text{on } \Gamma, && (2.117)\\ s(x,y,t) &= \frac{\partial v}{\partial t} + f(v,w) - \mathrm{I}_m \quad \text{on } \Gamma, && (2.118)\\ v &= u_i - u_e \quad \text{on} \quad \Gamma, && (2.119)\\ \sigma_e\nabla u_e\cdot n_e &= g_{e,ex} \quad \text{on} \quad \Gamma_e, && (2.120) \end{aligned}$$

where $p \geqslant 2$. It follows that

$$\begin{aligned} s(x,y,t) &= a\delta(t)(1-\delta(t)) + f(v_{ex}, w_{ex}) - \sigma_e\nabla u_{e,ex}\cdot n_e,\\ g_{e,ex}(x,y,t) &= \sigma_e\nabla u_{e,ex}\cdot n_e, \end{aligned}$$

where the function $f(v,w)$ is defined in (2.107). The variational formulations (2.115)-(2.120) reads

$$\begin{aligned} \int_{\Omega_e}\sigma_e\nabla u_e(t)\cdot\nabla\varphi_e &- \int_\Gamma\left(\frac{\partial v(t)}{\partial t} + f(v(t),w(t))\right)\varphi_e = \int_{\Omega_e}\mathrm{I}_{e,ex}\varphi_e + \int_{\Gamma_e} g_{e,ex}\varphi_e\\ &- \int_\Gamma s(x,y,t)\varphi_e, && (2.121) \end{aligned}$$

$$\int_{\Omega_i} \sigma_i \nabla u_i(t) \cdot \nabla \varphi_i + \int_{\Gamma} \left(\frac{\partial v(t)}{\partial t} + f(v(t), w(t)) \right) \varphi_i = \int_{\Omega_i} \mathrm{I}_{i,ex} \varphi_i + \int_{\Gamma} s(x, y, t) \varphi_i, \quad (2.122)$$

$$\int_{\Gamma} \frac{\partial w(t)}{\partial t} \varphi - \int_{\Gamma} g(v(t), w(t)) \varphi = \int_{\Gamma} \frac{\partial w_{ex}(t)}{\partial t} \varphi - \int_{\Gamma} g(v_{ex}(t), w_{ex}(t)) \varphi, \quad (2.123)$$

for a.e. $t \in [0, \mathrm{T}]\cdot$ We approximate the time derivatives, $\frac{\partial v}{\partial t}$ and $\frac{\partial w}{\partial t}$, using the second order backward finite difference formula, that is,

$$\frac{\partial v}{\partial t} \approx \frac{3v^n - 4v^{n-1} + v^{n-2}}{2\Delta t}, \quad (2.124)$$

$$\frac{\partial w}{\partial t} \approx \frac{3w^n - 4w^{n-1} + w^{n-2}}{2\Delta t} \quad (2.125)$$

The nonlinear terms f, g, $\mathrm{I}_{i,ex}$ and $\mathrm{I}_{i,ex}$ are extrapolated at $t = t^n$ as follows

$$\begin{aligned} f(v^n, w^n) &\approx 2f(v^{n-1}, w^{n-1}) - f(v^{n-2}, w^{n-2}) \\ g(v^n, w^n) &\approx 2g(v^{n-1}, w^{n-1}) - g(v^{n-2}, w^{n-2}) \\ \mathrm{I}^n_{i,ex} &\approx 2\mathrm{I}^{n-1}_{i,ex} - \mathrm{I}^{n-2}_{i,ex}, \\ \mathrm{I}^n_{e,ex} &\approx 2\mathrm{I}^{n-1}_{e,ex} - \mathrm{I}^{n-2}_{e,ex}, \end{aligned}$$

where $v^n \approx v(t_n), w^n \approx w(t_n), \mathrm{I}^n_{e,ex} = \mathrm{I}_{e,ex}(t_n), \mathrm{I}^n_{i,ex} = \mathrm{I}_{i,ex}(t_n), t_n = n\Delta t$, and $\Delta t = \frac{\mathrm{T}}{N}$ is the time step. This method is known as the second order semi-implicit backward differentiation formula (SBDF2) [3, 4, 63] and will be discussed later.

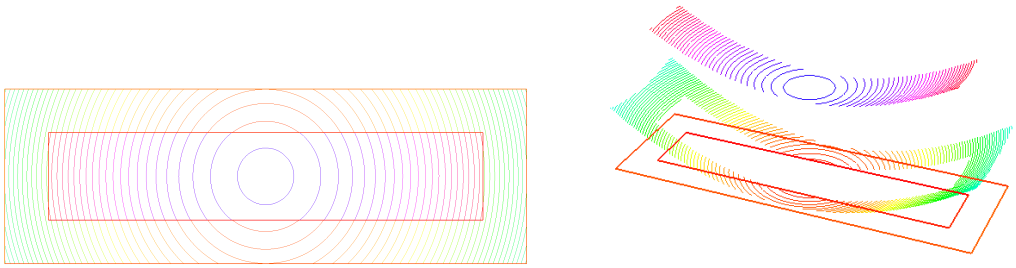

Figure 2.4: Contour plot and 3D graph of the manufactured solution for $p = 2$.

We estimate the errors between the fully discretized solutions $u^N_{i,h}, u^N_{e,h}$, v^N_h, and w^N_h and the exact solution $u_{i,ex}, u_{e,ex}, v_{ex}$, and w_{ex}, respectively. We compute the $\mathrm{L}^2 -$ norms, $\|u^N_{i,h} - u_{i,ex}\|_{\mathrm{L}^2(\Omega_i)}$, $\|u^N_{e,h} - u_{e,ex}\|_{\mathrm{L}^2(\Omega_e)}$, $\|v^N_h - v_{ex}\|_{\mathrm{L}^2(\Gamma)}$ and $\|w^N_h - w_{ex}\|_{\mathrm{L}^2(\Gamma)}$, as well as the $\mathrm{H}^1 -$ norms $\|\nabla u^N_{e,h} - \nabla u_{e,ex}\|_{\mathrm{L}^2(\Omega_e)}$ and $\|\nabla u^N_{i,h} - \nabla u_{i,ex}\|_{\mathrm{L}^2(\Omega_i)}$, at the final time

$\mathrm{T} = N \times \Delta t = 0.8\mathtt{ms}$. In our computation, we take $\varepsilon = 0.0001$ and we let $a = 8$ to achieve a faster transient. The domains Ω_e and Ω_i consist of $(16n) \times (4n)$ and $(8n) \times (2n)$ nodes on the sides of the subdomains, respectively, where n is a given integer. The mesh is fixed, unstructured and conformal on the interface Γ, see Figure 2.5. The computation

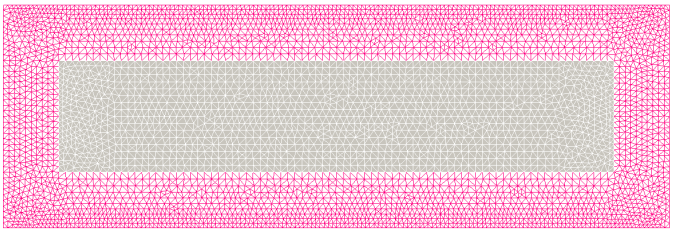

Figure 2.5: A 2D mesh of the domains Ω_e and Ω_i for $n = 10$.

is performed for different spatial resolutions and time steps. Since we are interested in semidiscretization error in space, we shall determine a time step Δt for which the time error is significantly smaller than the space error. We fix $n = 10$. Starting with $\Delta t = 0.001$, we decrease the time-step Δt till the error in time is negligeable compared to the error in space. Table 2.1 shows that Δt should be selected smaller than 0.0001 for the variables u_i, u_e and v. To study the convergence in space, we increase n. To ensure that the error in space remains dominant, we decrease Δt simultaneously. We assume that the error in space is proportional to h^q, where q is the convergence rate that can be estimated thanks to the formula

$$q \approx \frac{\log\left(|\mathrm{E}_{2h}/\mathrm{E}_h|\right)}{\log(2)}, \tag{2.126}$$

where E_h is the error associated to the mesh size h. Table 2.2 reports the results of the convergence tests on the variables u_e, u_e, v and w. We observe that the convergence rate is two for the error in the L^2-norm for both $u_{e,h}$ and $u_{i,h}$, while it is between 1 and 2 on the variables v and w. Therefore, the rate of convergence obtained from our numerical test is better than what is shown in the theoretical estimate (2.95) for the L^2-norm of the error on v. From Table 2.3, we observe that a first order convergence is achieved in the H^1-norm for the variables $u_{e,h}$ and $u_{i,h}$, which is in agreement with the theoretical estimates (2.94).

Table 2.1: L^2 norm errors with fixed $n = 10$, at the final time $T = N \times \Delta t = 0.8\texttt{ms}$.

n	Δt	$\|u_{e,h}^N - u_{e,ex}\|_{0,\Omega_e}$	$\|u_{i,h}^N - u_{i,ex}\|_{0,\Omega_i}$	$\|v_h^N - v_{ex}\|_{0,\Gamma}$	$\|w_h^N - w_{ex}\|_{0,\Gamma}$
10	1.0e-03	5.25545e-04	6.47831e-04	2.25664e-04	1.91362e-06
10	5.0e-04	5.25544e-04	6.24351e-04	2.25007e-04	4.78142e-07
10	2.5e-04	5.25545e-04	6.18681e-04	2.24936e-04	1.19556e-07
10	1.25e-04	5.25543e-04	6.17272e-04	2.24917e-04	3.01018e-08

Table 2.2: L^2 norm errors with convergence rates in parentheses, at $T = N \times \Delta t = 0.8\texttt{ms}$.

n	Δt	$\|u_{e,h}^N - u_{e,ex}\|_{0,\Omega_e}$	$\|u_{i,h}^N - u_{i,ex}\|_{0,\Omega_i}$	$\|v_h^N - v_{ex}\|_{0,\Gamma}$	$\|w_h^N - w_{ex}\|_{0,\Gamma}$
10	1.0e-04	5.25543e-04	6.17104e-04	2.24914e-04	1.94744e-08
20	5.0e-5	1.30516e-04(2.00)	1.49744e-04 (2.04)	6.04427e-05(1.89)	4.93266e-09(1.89)
40	2.5e-05	3.16817e-05(2.04)	4.01872e-05 (1.89)	2.35998e-05(1.36)	1.32895e-09(1.89)
80	1.25e-05	7.15588e-06(2.15)	8.87071e-06 (2.18)	8.41393e-06(1.48)	3.81054e-10(1.80)

Table 2.3: H^1 semi-norm errors with convergence rates in parentheses.

n	Δt	$\|\nabla u_{e,h}^N - \nabla u_{e,ex}\|_{0,\Omega_e}$	$\|\nabla u_{i,h}^N - \nabla u_{i,ex}\|_{0,\Omega_i}$
10	1.0e-04	3.80101e-03	3.84055e-03
20	5.0e-5	1.901220e-03 (0.99)	1.93780e-03 (0.99)
40	2.5e-05	9.433090e-04 (1.01)	9.66920e-04 (1.00)
80	1.25e-05	4.74793 e-04 (0.99)	4.88733e-04 (0.98)

The unusual coupling of PDEs and ODEs on the boundary makes the microscopic model challenging to solve numerically. To get around this difficulty, we reformulated the model on the interface using a Steklov-Poincaré operator. We discretized the model in space using FEM. We proved the existence of semi-discrete solution and we derived stability and error estimates for FEM. From the numerical tests, the convergence rate is two for the error in the L^2-norm for the potentials $u_{i,h}$ and $u_{e,h}$, while it is between one and two on the potential v and gating variable w. The theoretical estimates guarantee a convergence rate of at least one for the error in the L^2-norm on the membrane potential v. The theoretical analysis of the L^2-norm errors on the variables $u_{i,h}$ and $u_{e,h}$ was not investigated. However, a first order convergence is achieved in the H^1-norm for the variables $u_{e,h}$ and $u_{i,h}$, which is in agreement with the theoretical estimates.

Chapter 3

Time-Stepping Methods for the Cardiac Microscopic Problem

In this chapter, we introduce different time-stepping methods applied to the microscopic model. We obtain theoretical error estimates in space and time, respectively, and we check if these are achieved in numerical computations. In Section 3.1, we present the microscopic model. In Section 3.2, we derive a variational formulation of the model. In Section 3.3, we present a variety of time-discretization schemes used in this thesis. In Section 3.4, we prove the well-posedness of semi-discrete problems. In Sections 3.5 and 3.6, we show convergence and error estimates in space and time, respectively. In Section 3.7, we discuss the resolution of the linear and nonlinear algebraic systems resulting from the fully discretized problem. Finally in Section 3.8, we present numerical results.

3.1 Microscopic Model

We recall the following nondimensional microscopic model

$$
\begin{aligned}
-\nabla \cdot (\sigma_i \nabla u_i) &= \mathrm{I}_{i,stim} \quad \text{in } \Omega_i, && (3.1)\\
-\nabla \cdot (\sigma_e \nabla u_e) &= \mathrm{I}_{e,stim} \quad \text{in } \Omega_e, && (3.2)\\
\mathrm{I}_m &:= \frac{\partial v}{\partial t} + f(v,w) \quad \text{on } \Gamma, && (3.3)\\
\sigma_e \nabla u_e \cdot n_e &= -\sigma_i \nabla u_i \cdot n_i = \mathrm{I}_m \quad \text{on } \Gamma, && (3.4)\\
v &= u_i - u_e \quad \text{on} \quad \Gamma, && (3.5)\\
\sigma_e \nabla u_e \cdot n_e &= g_e \quad \text{on} \quad \Gamma_e, && (3.6)
\end{aligned}
$$

where $\mathrm{I}_{i,stim}$ and $\mathrm{I}_{e,stim}$ are the stimulation currents applied on Ω_i and Ω_e, respectively, w is the gating variable, f represents the ionic current through the cellular membrane Γ, and g_e is a given function on $\Gamma_e = \partial\Omega_e \setminus \Gamma$. The model is coupled with the following system of ordinary differential equations

$$\frac{\partial w}{\partial t} = g(v, w) \quad \text{on} \quad \Gamma, \tag{3.7}$$

where g models the dynamics of the gating variables, w. For a rigorous mathematical analysis regarding the well-posedness of the model, see e.g. [24, 79].

3.2 Variational Formulation

In this subsection, we define a functional framework within which we derive the variational formulation of the nondimensional problem (3.1)-(3.6). It is worth recalling that the solution of the problem is defined up to the addition of constants. More specifically, if (u_i, u_e) is a solution of the problem, then $(u_i + c, u_e + c)$ is also a solution. To fix additive constants, we assume that the mean of the extracellular potential u_e is zero, that is,

$$\int_{\Omega_e} u_e dx = 0. \tag{3.8}$$

Next we consider the following spaces

$$\begin{cases} u_i(t) \in \mathrm{H}^1(\Omega_i), \\ u_e(t) \in \mathrm{H}^1(\Omega_e)/\mathbb{R}, \\ v(t) = u_i(t) - u_e(t) \in \mathrm{H}^{\frac{1}{2}}(\Gamma), \end{cases}$$

for a.e $t \in]0, T[$.
Multiplying the equation (3.1) by the test function φ_e, then integrating by parts on Ω_e, we have for a.e. $t \in [0, \mathrm{T}]$,

$$\int_{\Omega_e} \sigma_e \nabla u_e(t) \cdot \nabla \varphi_e - \int_{\Gamma_e} \sigma_e \nabla u_e(t) \cdot n_e \varphi_e = \int_{\Omega_e} \mathrm{I}_{e,stim}(t)\varphi_e + \int_{\Gamma_e} g_e \varphi_e. \tag{3.9}$$

On account of the boundary conditions (3.4) and (3.6), the equation (3.9) becomes

$$\int_{\Omega_e} \sigma_e \nabla u_e(t) \cdot \nabla \varphi_e - \int_{\Gamma} \left(\frac{\partial v(t)}{\partial t} + f(v(t), w(t)) \right) \varphi_e = \int_{\Omega_e} \mathrm{I}_{e,stim}(t)\varphi_e + \int_{\Gamma_e} g_e \varphi_e. \tag{3.10}$$

Similarly,

$$\int_{\Omega_i} \sigma_i \nabla u_i(t) \cdot \nabla \varphi_i + \int_{\Gamma} \left(\frac{\partial v(t)}{\partial t} + f(v(t), w(t)) \right) \varphi_i = \int_{\Omega_i} \mathrm{I}_{i,stim}(t) \varphi_i. \tag{3.11}$$

$$\int_{\Gamma} \frac{\partial w(t)}{\partial t} \psi = \int_{\Gamma} g(v(t), w(t)) \psi, \tag{3.12}$$

for a.e $t \in [0, \mathrm{T}]$, where $\dfrac{\partial v}{\partial t}$ is the weak derivative of v and $\Gamma_e = \partial\Omega_e \setminus \Gamma$. We assume for a.e. $t \in [0, \mathrm{T}]$ that $f(v(t), w(t)) \in \mathrm{L}^2(\Gamma)$ provided $v(t), w(t) \in \mathrm{L}^2(\Gamma)$, $\mathrm{I}_{e,stim}(t)$ and $\mathrm{I}_{i,stim}(t)$ belong to $\mathrm{L}^2(\Omega_e)$ and $\mathrm{L}^2(\Omega_i)$, respectively. In addition, the intracellular and extracellular conductivities σ_i and σ_e satisfy the condition

$$\beta = \min \left(\operatorname*{ess\,inf}_{x \in \Omega_i} \sigma_i, \ \operatorname*{ess\,inf}_{x \in \Omega_e} \sigma_e \right) > 0, \tag{3.13}$$

where the notation ess inf stands for the essential infimum.
For the convergence analysis of the model, we assume that the functions f and g satisfy a global Lipschitz condition with constants L_f and L_g, respectively, that is, for all v_1, v_2, w_1 and w_2 in $\mathbb{R}$

$$|f(v_1, w_1) - f(v_2, w_2)| \leq \mathrm{L}_f \{ |v_1 - v_2| + |w_1 - w_2| \}, \tag{3.14}$$

$$|g(v_1, w_1) - g(v_2, w_2)| \leq \mathrm{L}_g \{ |v_1 - v_2| + |w_1 - w_2| \}. \tag{3.15}$$

In addition, we assume that the stimulation currents $\mathrm{I}_{i,stim}$ and $\mathrm{I}_{e,stim}$ are Lipschitz in t, uniformly in Ω_i and Ω_e, respectively. Thus, there exist Lipschitz constants $\mathrm{L}_i > 0$ and $\mathrm{L}_e > 0$ such that

$$|\mathrm{I}_{e,stim}(x, t_1) - \mathrm{I}_{e,stim}(x, t_2)| \leq \mathrm{L}_e |t_1 - t_2|, \quad \forall t_1, t_2 \in \mathbb{R}, \quad \forall x \in \Omega_e \tag{3.16}$$

$$|\mathrm{I}_{i,stim}(x, t_1) - \mathrm{I}_{i,stim}(x, t_2)| \leq \mathrm{L}_i |t_1 - t_2|, \quad \forall t_1, t_2 \in \mathbb{R}, \quad \forall x \in \Omega_i. \tag{3.17}$$

From now on, we set

$$\mathrm{L}_0 = \max(\mathrm{L}_f, \mathrm{L}_g); \qquad \mathrm{L}_1 = \max(\mathrm{L}_i, \mathrm{L}_e). \tag{3.18}$$

These assumptions on the functions $f, g, \mathrm{I}_{e,stim}$ and $\mathrm{I}_{i,stim}$ ensure the existence of a weak solution to the miscroscopic problem (3.10)-(3.12), see e.g. [5]. From now on, we consider the following Neumann boundary conditions on Γ_e:

$$\sigma_e \nabla u_e \cdot n_e = 0 \quad \text{on} \quad \Gamma_e.$$

3.3 Time-Discretization Schemes

In this section, we consider a variety of time-stepping methods. These include implicit, semi-implicit and Godunov splitting methods. The semi-implicit methods are also known as semi-explicit or implicit-explicit (IMEX) methods. For a given problem involving a linear and non-linear terms, IMEX methods solve the linear and non-linear parts implicitly and explicitly, respectively. A detailed discussion about IMEX methods can be found in [3, 4, 63]. We use the Forward Backward Euler (FBE) method and the second order Semi-Implicit Backward Differentiation Formula (SBDF2) as representatives of the IMEX methods. Fully implicit methods studied are the Backward Euler (BE) method and second order Backward Differentiation Formula (BDF2). The presentation here is motivated by the formulation in [21, 61].
From now on, the following notations will be used

$$v^n \approx v(t_n),\ w^n \approx w(t_n),\ u_i^n \approx u_i^n(t_n),\ u_e^n \approx u_e^n(t_n),\ \mathrm{I}_{i,e,stim}^n = \mathrm{I}_{i,e,stim}(t_n),\ t_n = n\Delta t,$$

where $\Delta t = \frac{\mathrm{T}}{N}$ is the time step.

3.3.1 Backward Euler Method

From equations (3.10) - (3.12), we have

$$\int_{\Omega_e} \sigma_e \nabla u_e^n \cdot \nabla \varphi_e - \int_\Gamma \frac{v^n - v^{n-1}}{\Delta t}\varphi_e - \int_\Gamma f(v^n, w^n)\varphi_e = \int_{\Omega_e} \mathrm{I}_{e,stim}^n \varphi_e, \tag{3.19}$$

$$\int_{\Omega_i} \sigma_i \nabla u_i^n \cdot \nabla \varphi_i + \int_\Gamma \frac{v^n - v^{n-1}}{\Delta t}\varphi_i + \int_\Gamma f(v^n, w^n)\varphi_i = \int_{\Omega_i} \mathrm{I}_{i,stim}^n \varphi_i, \tag{3.20}$$

$$\int_\Gamma \frac{w^n - w^{n-1}}{\Delta t}\varphi = \int_\Gamma g(v^n, w^n)\varphi, \tag{3.21}$$

for $n \in \{1, 2, \cdots, N\}$. Throughout this section, $v^n = u_i^n - u_e^n$ so that the resulting problems are consistent.

3.3.2 Forward Backward Euler Method

Starting from (3.19) - (3.21), we take the nonlinear terms f and g at the previous time step $t = t^{n-1}$ to make the global system linear, which gives

$$\begin{aligned}
\int_{\Omega_e} \sigma_e \nabla u_e^n \cdot \nabla \varphi_e - \int_\Gamma \frac{v^n - v^{n-1}}{\Delta t} \varphi_e &= \int_{\Omega_e} \mathrm{I}_{e,stim}^{n-1} \varphi_e + \int_\Gamma f(v^{n-1}, w^{n-1}) \varphi_e, \quad (3.22)\\
\int_{\Omega_i} \sigma_i \nabla u_i^n \cdot \nabla \varphi_i + \int_\Gamma \frac{v^n - v^{n-1}}{\Delta t} \varphi_i &= \int_{\Omega_i} \mathrm{I}_{i,stim}^{n-1} \varphi_i - \int_\Gamma f(v^{n-1}, w^{n-1}) \varphi_i, \quad (3.23)\\
\int_\Gamma \frac{w^n - w^{n-1}}{\Delta t} \varphi &= \int_\Gamma g(v^{n-1}, w^{n-1}) \varphi, \quad (3.24)
\end{aligned}$$

for $n \in \{1, 2, \cdots, N\}$.

3.3.3 Godunov Time-Splitting Method

The operator splitting (or fractional step) method consists in decomposing complex coupled systems of PDEs into simpler sub-problems, see e.g. [54, 70]. These sub-problems are then treated individually. To introduce the Godunov splitting method, we consider an initial value problem

$$\begin{cases} \frac{du}{dt} &= \mathrm{L}u, \\ u(0) &= u_0, \end{cases} \quad (3.25)$$

where u_0 is a given initial condition and L is a differential operator that can be split into a sum of two or more components. We consider the simple case

$$\mathrm{L} = \mathrm{L}_1 + \mathrm{L}_2.$$

Let Δt be a small time step. An approximate solution at time $t = \Delta t$ may be computed by first solving the problem

$$\begin{cases} \frac{dv}{dt} &= \mathrm{L}_1(v) \\ v(0) &= u_0, \end{cases} \quad (3.26)$$

for $t \in [0, \Delta t]$. Thereafter, we solve the problem

$$\begin{cases} \frac{dw}{dt} &= \mathrm{L}_2(w) \\ w(0) &= v(\Delta t), \end{cases} \quad (3.27)$$

for $t \in [0, \Delta t]$, using as initial condition the solution of the system (3.26). The solution $w(\Delta t)$ is a consistent approximation of the solution $u(\Delta t)$, see e.g.[71]. The method

is known as Godunov splitting and is first order accurate in time step Δt. The Godunov splitting method applied to (3.1)-(3.6) and (3.7), consists of the following two sub-problems: In the first substep of the method, we update the solutions for the membrane potential, v, and gating variable, w, by solving the following system of ODEs

$$\int_\Gamma \frac{v^* - v^{n-1}}{\Delta t}\varphi = -\int_\Gamma f(v^{n-1}, w^{n-1})\varphi, \tag{3.28}$$

$$\int_\Gamma \frac{w^n - w^{n-1}}{\Delta t}\varphi = \int_\Gamma g(v^{n-1}, w^{n-1})\varphi\cdot \tag{3.29}$$

In the next substep, we solve the following variational formulation

$$\int_{\Omega_e} \sigma_e \nabla u_e^n \cdot \nabla \varphi_e - \int_\Gamma \frac{v^n - v^*}{\Delta t}\varphi_e = \int_{\Omega_e} \mathrm{I}_{e,stim}^{n-1}\varphi_e, \tag{3.30}$$

$$\int_{\Omega_i} \sigma_i \nabla u_i^n \cdot \nabla \varphi_i + \int_\Gamma \frac{v^n - v^*}{\Delta t}\varphi_i = \int_{\Omega_i} \mathrm{I}_{i,stim}^{n-1}\varphi_i \tag{3.31}$$

where $v^n = u_i^n - u_e^n$ for $n \in \{1, 2, \cdots, N\}$, assuming for each time step that the solution $v^{n-1} = u_i^{n-1} - u_e^{n-1}$ is known for $t = t_{n-1}$ on Γ.

Remark 3.3.4. *In this thesis, we solve the first step of the Godunov splitting method using the forward Euler method. Therefore, the Godunov method is equivalent to the FBE method. It should be mentioned that any other appropriate ODE solver, such as the Runge-Kutta method, could be used, in which case the Godunov method and FBE would no longer be equivalent.*

3.3.5 Second Order Backward Differentiation Formula

Backward differentiation formulas are popular multistep methods to solve stiff ODE problems. From the BE scheme (3.19)-(3.21), we approximate the time derivative, $\frac{\partial v}{\partial t}$, using the current value v^n and two previously computed approximations, v^{n-1} and v^{n-2}, that is,

$$\frac{\partial v}{\partial t} \approx \frac{3v^n - 4v^{n-1} + v^{n-2}}{2\Delta t},$$

which yields

$$\int_{\Omega_e} \sigma_e \nabla u_e^n \cdot \nabla \varphi_e - \int_\Gamma \frac{3v^n - 4v^{n-1} + v^{n-2}}{2\Delta t}\varphi_e - \int_\Gamma f(v^n, w^n)\varphi_e = \int_{\Omega_e} \mathrm{I}_{e,stim}^{n}\varphi_e, \tag{3.32}$$

$$\int_{\Omega_i} \sigma_i \nabla u_i^n \cdot \nabla \varphi_i + \int_\Gamma \frac{3v^n - 4v^{n-1} + v^{n-2}}{2\Delta t}\varphi_i + \int_\Gamma f(v^n, w^n)\varphi_i = \int_{\Omega_i} \mathrm{I}_{i,stim}^{n}\varphi_i, \tag{3.33}$$

$$\int_\Gamma \frac{3w^n - 4w^{n-1} + w^{n-2}}{2\Delta t}\varphi = \int_\Gamma g(v^n, w^n)\varphi\cdot \tag{3.34}$$

for $n \in \{2, \cdots, N\}$. The backward Euler scheme is used in the first time step.

3.3.6 Second Order Semi-implicit Backward Differentiation Formula

If in the BDF2 scheme (3.32)-(3.34), the nonlinear terms f, g, and $\mathrm{I}^n_{i,e,stim}$ are extrapolated at $t = t^n$ as follows

$$\begin{aligned} f(v^n, w^n) &\approx 2f(v^{n-1}, w^{n-1}) - f(v^{n-2}, w^{n-2}) \\ g(v^n, w^n) &\approx 2g(v^{n-1}, w^{n-1}) - g(v^{n-2}, w^{n-2}) \\ \mathrm{I}^n_{i,e,stim} &\approx 2\mathrm{I}^{n-1}_{i,e,stim} - \mathrm{I}^{n-2}_{i,e,stim}, \end{aligned}$$

we get the following SBDF2 scheme, see e.g. [3, 4, 63]

$$\begin{aligned} \int_{\Omega_e} \sigma_e \nabla u_e^n \cdot \nabla \varphi_e - \int_\Gamma \frac{3v^n - 4v^{n-1} + v^{n-2}}{2\Delta t}\varphi_e &- \int_\Gamma 2f(v^{n-1}, w^{n-1})\varphi_e \\ + \int_\Gamma f(v^{n-2}, w^{n-2})\varphi_e &= \int_{\Omega_e} (2\mathrm{I}^{n-1}_{e,stim} - \mathrm{I}^{n-2}_{e,stim})\varphi_e, \quad (3.35) \\ \int_{\Omega_i} \sigma_i \nabla u_i^n \cdot \nabla \varphi_i + \int_\Gamma \frac{3v^n - 4v^{n-1} + v^{n-2}}{2\Delta t}\varphi_i &+ \int_\Gamma 2f(v^{n-1}, w^{n-1})\varphi_i \\ - \int_\Gamma f(v^{n-2}, w^{n-2})\varphi_i &= \int_{\Omega_i} (2\mathrm{I}^{n-1}_{i,stim} - \mathrm{I}^{n-2}_{i,stim})\varphi_i, \quad (3.36) \\ \int_\Gamma \frac{3w^n - 4w^{n-1} + w^{n-2}}{2\Delta t}\varphi = \int_\Gamma 2g(v^{n-1}, w^{n-1})\varphi &- \int_\Gamma g(v^{n-2}, w^{n-2})\varphi \cdot \quad (3.37) \end{aligned}$$

for $n \in \{2, \cdots, N\}$. The forward backward Euler scheme is used in the first time step.

3.4 Well-Posedness of the Time Semi-Discrete Problems

In the following, we are concerned with the well-posedness of the above semi-discrete problems. We only focus on the FBE method We define a convenient functional framework to prove the existence and uniqueness of the solution through classical results. The space W is equipped with the norm defined in (2.80):

$$|||u|||_{\mathrm{W}} = \left(\|u_i\|^2_{\mathrm{H}^1(\Omega_i)} + \|u_e\|^2_{\mathrm{H}^1(\Omega_e)} + \|u_i - u_e\|^2_{\mathrm{L}^2(\Gamma)} \right)^{\frac{1}{2}},$$

for all $u = (u_i, u_e) \in \mathrm{W}$.
By adding up equations (3.22) and (3.23) , we obtain

$$\begin{aligned} \Delta t \int_{\Omega_e} \sigma_e \nabla u_e^n \cdot \nabla \varphi_e \;\; + \;\; & \Delta t \int_{\Omega_i} \sigma_i \nabla u_i^n \cdot \nabla \varphi_i + \int_\Gamma (u_i^n - u_e^n)(\varphi_i - \varphi_e) \\ = \;\; & \int_\Gamma v^{n-1}(\varphi_i - \varphi_e) + \Delta t \int_{\Omega_i} \mathrm{I}_{i,stim}^{n-1} \varphi_i + \Delta t \int_{\Omega_e} \mathrm{I}_{e,stim}^{n-1} \varphi_e \\ - \;\; & \Delta t \int_\Gamma f(v^{n-1}, w^{n-1})(\varphi_i - \varphi_e), \end{aligned} \tag{3.38}$$

for all $u = (u_i, u_e)$, $\varphi = (\varphi_i, \varphi_e) \in \mathrm{W}$, where $v^n = u_i^n - u_e^n$, and v^{n-1} is the previous known value which can be obtained by recurrence from the initial value v^0.
The variational problem reads:

$$\begin{cases} \text{find} \;\; u^n = (u_i^n, u_e^n) \in \mathrm{W} \quad \text{such that} \\ \qquad a(u^n, \varphi) = l(\varphi) \quad \text{for all } \varphi \in \mathrm{W}, \end{cases} \tag{3.39}$$

where

$$\begin{cases} a(u^n, \varphi) = \Delta t \left(\displaystyle\int_{\Omega_e} \sigma_e \nabla u_e^n \cdot \nabla \varphi_e + \int_{\Omega_i} \sigma_i \nabla u_i^n \cdot \nabla \varphi_i \right) \\ \qquad\qquad + \displaystyle\int_\Gamma (u_i^n - u_e^n)(\varphi_i - \varphi_e), \\ l(\varphi) = \displaystyle\int_\Gamma v^{n-1}(\varphi_i - \varphi_e) + \Delta t \int_{\Omega_i} \mathrm{I}_{i,stim}^{n-1} \varphi_i + \Delta t \int_{\Omega_e} \mathrm{I}_{e,stim}^{n-1} \varphi_e \\ \qquad\qquad - \Delta t \displaystyle\int_\Gamma f(v^{n-1}, w^{n-1})(\varphi_i - \varphi_e), \end{cases} \tag{3.40}$$

for all $u^n = (u_i^n, u_e^n) \in \mathrm{W}$ and $\varphi = (\varphi_i, \varphi_e) \in \mathrm{W}$.

Theorem 3.4.1. *Under the hypothesis that* $\mathrm{I}_{i,stim}^{n-1} \in \mathrm{L}^2(\Omega_i)$, $\mathrm{I}_{e,stim}^{n-1} \in \mathrm{L}^2(\Omega_e)$, *and* $f(v^{n-1}, w^{n-1}) \in \mathrm{L}^2(\Gamma)$ *provided* v^{n-1} *and* w^{n-1} *are in* $\mathrm{L}^2(\Gamma)$, *the problem* (3.39) *has a unique solution.*

Proof. By reasoning as in Theorem 2.3.3, we show that the bilinear form $a(\cdot,\cdot)$ in (3.40) is continuous on $\mathrm{W} \times \mathrm{W}$ and coercive on W.
Let us show that the linear form $l(\cdot)$ in (3.40) is continuous on W. Let $\varphi = (\varphi_i, \varphi_e) \in \mathrm{W}$. Using assumptions on the stimulation currents $\mathrm{I}_{i,stim}^{n-1}$ and $\mathrm{I}_{e,stim}^{n-1}$ and the Cauchy-Schwarz

inequality, we have

$$\begin{aligned}
|l(\varphi)| &\leq \int_\Gamma |v^{n-1}||\varphi_i - \varphi_e|\,dx + \Delta t \int_{\Omega_i} |\mathrm{I}_{i,stim}^{n-1}||\varphi_i|\,dx + \Delta t \int_{\Omega_e} |\mathrm{I}_{e,stim}^{n-1}||\varphi_e|\,dx \\
&+ \Delta t \int_\Gamma |f(v^{n-1}, w^{n-1})||\varphi_i - \varphi_e|\,dx \\
&\leq \|v^{n-1}\|_{0,\Gamma}\|\varphi_i - \varphi_e\|_{0,\Gamma} + \Delta t\|\mathrm{I}_{i,stim}^{n-1}\|_{0,\Omega_i}\|\varphi_i\|_{0,\Omega_i} + \Delta t\|\mathrm{I}_{e,stim}^{n-1}\|_{0,\Omega_e}\|\varphi_e\|_{0,\Omega_e} \\
&+ \Delta t\|f^{n-1}\|_{0,\Gamma}\|\varphi_i - \varphi_e\|_{0,\Gamma} \\
&\leq C\|\varphi\|_{\mathrm{W}},
\end{aligned}$$

where $f^{n-1} = f(v^{n-1}, w^{n-1})$ and $C > 0$ is a constant. Therefore, the variational formulation problem (3.39) has a unique solution thanks to the Lax-Milgram theorem. □

3.5 Convergence and Error Estimate in Space

We assume that the domain Ω is covered by a regular mesh $\mathcal{T}_h$ of triangles of maximum diameter h, conformal on the interface Γ, see Section 2.1.2 and Figure 2.1. We focus on the FBE method. We replace the Hilbert space W used in the formulation (3.39) by a subspace W_h of finite dimension. The problem posed over W_h reads

$$\begin{cases} \text{Find} \quad u_h = (u_{ih}, u_{eh}) \in \mathrm{W}_h \quad \text{such that} \\ \qquad\qquad a\,(u_h, \varphi_h) = l(\varphi_h), \quad \text{for all} \quad \varphi_h \in \mathrm{W}_h, \end{cases} \tag{3.41}$$

where $a(\cdot,\cdot)$ and $l(\cdot)$ are defined as in (3.40). The existence and uniqueness of the solution of (3.41) follow from the Lax-Milgram theorem applied to W_h. We now estimate the error $|||u - u_h|||_{\mathrm{W}}$, where u is the solution of (3.39) and u_h is the solution of (3.41). Let us denote by $\nu > 0$ the coercivity constant and $M > 0$ the continuity constant of the bilinear form $a(\cdot,\cdot)$, that is,

$$\begin{aligned}
|a\,(u, \varphi)| &\leq M|||u|||_W|||\varphi|||_{\mathrm{W}} \\
a\,(u, u) &\geq \nu|||u|||_{\mathrm{W}}^2,
\end{aligned}$$

for all $u, \varphi \in \mathrm{W}$. The following lemma due to Céa shows that the error $|||u - u_h|||_{\mathrm{W}}$ can be bounded uniformly with respect to the subspace W_h by the distance between u and W_h.

Lemma 3.5.1. *Let u and u_h be the solution of (3.39) and (3.41), respectively. Then*

$$|||u - u_h|||_{\mathrm{W}} \leq \sqrt{\frac{M}{\nu}} \inf_{v_h \in \mathrm{W}_h} |||u - v_h|||_{\mathrm{W}}. \tag{3.42}$$

The proof of this lemma can be found in [8, 20].

Proposition 3.5.2. *Let $u = (u_i, u_e) \in \mathrm{W}$ and $u_h = (u_{ih}, u_{eh}) \in \mathrm{W}_h$ be the solutions of the problems (3.39) and (3.41), respectively. We assume that $u_i \in \mathrm{H}^{l+1}(\Omega_i)$ and $u_e \in \mathrm{H}^{l+1}(\Omega_e)$ for $1 \leqslant l \leqslant d$. The following error estimates hold:*

$$\begin{aligned}
\|u_e - u_{eh}\|_{\mathrm{H}^1(\Omega_e)} &\leq \mathrm{C}h^l \left(|u_e|_{\mathrm{H}^{l+1}(\Omega_e)} + |u_i|_{\mathrm{H}^{l+1}(\Omega_i)}\right), && (3.43)\\
\|u_i - u_{ih}\|_{\mathrm{H}^1(\Omega_i)} &\leq \mathrm{C}h^l \left(|u_e|_{\mathrm{H}^{l+1}(\Omega_e)} + |u_i|_{\mathrm{H}^{l+1}(\Omega_i)}\right), && (3.44)\\
\|(u_i - u_e) - (u_{ih} - u_{eh})\|_{\mathrm{L}^2(\Gamma)} &\leq \mathrm{C}h^l \left(|u_e|_{\mathrm{H}^{l+1}(\Omega_e)} + |u_i|_{\mathrm{H}^{l+1}(\Omega_i)}\right), && (3.45)
\end{aligned}$$

for some constant $\mathrm{C} > 0$.

Proof. Let $\chi_h = (\chi_{ih}, \chi_{eh}) \in \mathrm{W}_h$ be arbitrary. We then have

$$|||u - \chi_h|||^2_{\mathrm{W}} = \|u_e - \chi_{eh}\|^2_{\mathrm{H}^1(\Omega_e)} + \|u_i - \chi_{ih}\|^2_{\mathrm{H}^1(\Omega_i)} + \|(u_i - u_e) - (\chi_{ih} - \chi_{eh})\|^2_{\mathrm{L}^2(\Gamma)}.$$

Then

$$\begin{aligned}
\inf_{\chi_h \in \mathrm{W}_h} \left\{|||u - \chi_h|||^2_{\mathrm{W}}\right\} &\leq \|u_e - \mathit{\Pi}^{\mathrm{e}}_{\mathrm{h}} u_e\|^2_{\mathrm{H}^1(\Omega_e)} + \|u_i - \mathit{\Pi}^{\mathrm{i}}_{\mathrm{h}} u_i\|^2_{\mathrm{H}^1(\Omega_i)}\\
&+ \|(u_i - u_e) - (\mathit{\Pi}^{\mathrm{i}}_{\mathrm{h}} u_i - \mathit{\Pi}^{\mathrm{e}}_{\mathrm{h}} u_e)\|^2_{\mathrm{L}^2(\Gamma)},\\
&\leq \|u_e - \mathit{\Pi}^{\mathrm{e}}_{\mathrm{h}} u_e\|^2_{\mathrm{H}^1(\Omega_e)} + \|u_i - \mathit{\Pi}^{\mathrm{i}}_{\mathrm{h}} u_i\|^2_{\mathrm{H}^1(\Omega_i)}\\
&+ 2\|u_i - \mathit{\Pi}^{i}_{h} u_i\|^2_{\mathrm{L}^2(\Gamma)} + 2\|u_e - \mathit{\Pi}^{e}_{h} u_e\|^2_{\mathrm{L}^2(\Gamma)}\\
&\leq \mathrm{C}\left(\|u_e - \mathit{\Pi}^{\mathrm{e}}_{\mathrm{h}} u_e\|^2_{\mathrm{H}^1(\Omega_e)} + \|u_i - \mathit{\Pi}^{\mathrm{i}}_{\mathrm{h}} u_i\|^2_{\mathrm{H}^1(\Omega_i)}\right).
\end{aligned}$$

for some constant $\mathrm{C} > 0$, thanks to the inequalities (2.41) and (2.42). It follows that

$$\begin{aligned}
\inf_{\chi_h \in \mathrm{W}_h} \left\{|||u - \chi_h|||_{\mathrm{W}}\right\} &\leq \mathrm{C}\left(\|u_e - \mathit{\Pi}^{\mathrm{e}}_{\mathrm{h}} u_e\|_{\mathrm{H}^1(\Omega_e)} + \|u_i - \mathit{\Pi}^{\mathrm{i}}_{\mathrm{h}} u_i\|_{\mathrm{H}^1(\Omega_i)}\right)\\
&\leq \mathrm{C}h^l \left(|u_e|_{\mathrm{H}^{l+1}(\Omega_e)} + |u_i|_{\mathrm{H}^{l+1}(\Omega_i)}\right),
\end{aligned}$$

for some constant $\mathrm{C} > 0$, thanks to the inequalities (2.38) and (2.39). On account of the inequality (3.42), the following error estimate holds

$$|||u - u_h|||_{\mathrm{W}} \leq \mathrm{C}h^l \left(|u_e|_{\mathrm{H}^{l+1}(\Omega_e)} + |u_i|_{\mathrm{H}^{l+1}(\Omega_i)}\right), \qquad (3.46)$$

for some constant $\mathrm{C} > 0$. From (3.46), we deduce the error estimates (3.43)-(3.45) on u_i, u_e and $u_i - u_e$, respectively. □

3.6 Convergence and Error Estimate in Time

In this section, we obtain error estimates for the semi-discrete in time formulations presented above. These estimates also hold for the fully discretized problem since the space $\mathrm{H}^1(\Omega_i) \times \mathrm{H}^1(\Omega_e)$ can be replaced by any finite dimensional subspace $\mathrm{V}_h^i \times \mathrm{V}_h^e$. All error estimates then hold with the same upper bounds and constants. We will focus on BE, FBE, and BDF2 methods, respectively. The error estimation for the semi-discretized problems through the SBDF2 method can also be investigated by combining the techniques used for FBE and BDF2 schemes. For the analysis below, we assume that $g_e = 0$ on Γ_e and $v, w \in \mathrm{H}^1(0, \mathrm{T}; \mathrm{L}^2(\Gamma))$.

3.6.1 Convergence Analysis of the Backward Euler Method

We first obtain an error estimate for the semi-discretization in time through the BE method given in (3.19)-(3.21). The main difficulties lie in the need for handling boundary and volumic terms, and the fact that the finite difference in time appears only on the interface Γ. Care is also required for the nonlinear terms in f and g.
By subtracting equation (3.19) from equation (3.10) and setting

$$e^n = v^n - v(t_n); \quad e_i^n = u_i^n - u_i(t_n); \quad e_e^n = u_e^n - u_e(t_n), \tag{3.47}$$

we have,

$$\begin{aligned} \int_{\Omega_e} \sigma_e \nabla e_e^n \cdot \nabla \varphi_e - \int_\Gamma \left[\frac{v^n - v^{n-1}}{\Delta t} - v_t(t_n) \right] \varphi_e \; &- \; \int_\Gamma [f(v^n, w^n) - f(v(t_n), w(t_n))] \varphi_e \\ &= \; 0. \end{aligned} \tag{3.48}$$

Using Taylor's series, we have

$$v_t(t_n) = \frac{v(t_n) - v(t_{n-1})}{\Delta t} + \frac{\Delta t}{2} v_{tt}(\xi^n), \tag{3.49}$$

where ξ^n is some point between t_{n-1} and t_n. Substituting (3.49) in (3.48) and considering (3.47), we write

$$\begin{aligned} \int_{\Omega_e} \sigma_e \nabla e_e^n \cdot \nabla \varphi_e - \int_\Gamma \left[\frac{e^n - e^{n-1}}{\Delta t} \right] \varphi_e - \int_\Gamma [f(v^n, w^n) - f(v(t_n), w(t_n))] \varphi_e \\ = -\frac{\Delta t}{2} \int_\Gamma v_{tt}(\xi^n) \varphi_e. \end{aligned} \tag{3.50}$$

Similarly, we have on Ω_i

$$\int_{\Omega_i} \sigma_i \nabla e_i^n \cdot \nabla \varphi_i + \int_\Gamma \left[\frac{e^n - e^{n-1}}{\Delta t}\right] \varphi_i + \int_\Gamma [f(v^n, w^n) - f(v(t_n), w(t_n))]\varphi_i = \frac{\Delta t}{2} \int_\Gamma v_{tt}(\xi^n)\varphi_i. \quad (3.51)$$

Adding up the equations (3.50) and (3.51) and we write

$$\int_{\Omega_e} \sigma_e \nabla e_e^n \cdot \nabla \varphi_e + \int_{\Omega_i} \sigma_i \nabla e_i^n \cdot \nabla \varphi_i + \int_\Gamma \left[\frac{e^n - e^{n-1}}{\Delta t}\right] (\varphi_i - \varphi_e) + \int_\Gamma [f(v^n, w^n) - f(v(t_n), w(t_n))](\varphi_i - \varphi_e) = \frac{\Delta t}{2} \int_\Gamma v_{tt}(\xi^n)(\varphi_i - \varphi_e). \quad (3.52)$$

Subtracting equation (3.21) from equation (3.12) and setting

$$e_w^n = w^n - w(t_n), \quad (3.53)$$

give

$$\int_\Gamma (e_w^n - e_w^{n-1})\psi = \Delta t \int_\Gamma (g(v^n, w^n) - g(v(t_n), w(t_n)))\psi + \frac{\Delta t^2}{2} \int_\Gamma w_{tt}(\xi_1^n)\psi, \quad (3.54)$$

considering (3.49) and (3.53).

3.6.2 A Priori Error Estimates

In this section, we derive some a priori estimates on e^n, e_i^n, e_e^n and e_w^n. The a priori estimates will be proved thanks to the following lemma.

Lemma 3.6.1 (Discrete Gronwall Lemma)**.** *Assume that k_n is a non-negative sequence, and that the sequence φ_n satisfies*

$$\varphi_0 \leq g_0, \quad \varphi_n \leq g_0 + \sum_{m=0}^{n-1} P_m + \sum_{m=0}^{n-1} k_m \varphi_m, \quad n \geq 1.$$

If $g_0 \geq 0$ and $P_m \geq 0$ for $m \geq 0$, then

$$\varphi_n \leq \left[g_0 + \sum_{m=0}^{n-1} P_m\right] \exp\left(\sum_{m=0}^{n-1} k_m\right), \quad n \geq 1.$$

The proof of this lemma can be found in [54].

The following a priori estimates hold.

Proposition 3.6.2. *Let* $n \in \{1, 2, \cdots, N\}$. *Assume that* $v, w \in \mathrm{C}^2([0, \mathrm{T}]; \mathrm{L}^2(\Gamma))$, $\|e^0\|_{\mathrm{L}^2(\Gamma)} = 0$, *and* $\|e_w^0\|_{\mathrm{L}^2(\Gamma)} = 0$, *and that there exists a constant* $0 < \alpha_2 < 1$ *such that* $\Delta t < \dfrac{1-\alpha_2}{\mathrm{L}_0}$. *Then*

$$\|e^n\|_{\mathrm{L}^2(\Gamma)} + \|e_w^n\|_{\mathrm{L}^2(\Gamma)} \leq \frac{\mathrm{T}^{\frac{1}{2}}\Delta t C_4}{\alpha_2}\left(\|v_{tt}\|_{\mathrm{L}^2(0,\mathrm{T},\mathrm{L}^2(\Gamma))} + \|w_{tt}\|_{\mathrm{L}^2(0,\mathrm{T},\mathrm{L}^2(\Gamma))}\right)\exp\left(\frac{\mathrm{TL}_0}{\alpha_2}\right), \tag{3.55}$$

$$\sum_{n=1}^{N}\Delta t\left(\int_{\Omega_e}|\nabla e_e^n|^2 + \int_{\Omega_i}|\nabla e_i^n|^2\right) \leq \mathrm{C}_6\Delta \mathrm{t}^2\left(\|v_{tt}\|_{\mathrm{L}^2(0,\mathrm{T},\mathrm{L}^2(\Gamma))} + \|w_{tt}\|_{\mathrm{L}^2(0,\mathrm{T},\mathrm{L}^2(\Gamma))}\right)^2, \tag{3.56}$$

for some constants $C_4 > 0$, $C_6 > 0$, $\mathrm{T} = N\Delta t$, *and* $\mathrm{L}_0 = \max(\mathrm{L}_f, \mathrm{L}_g)$.

Proof. Let us prove the inequality (3.55). Setting $\varphi_i = e_i^n$ and $\varphi_e = e_e^n$ in (3.52), we have

$$\begin{aligned}&\Delta t\int_{\Omega_e}\sigma_e|\nabla e_e^n|^2 + \Delta t\int_{\Omega_i}\sigma_i|\nabla e_i^n|^2 + \int_\Gamma|e^n|^2 - \int_\Gamma e^{n-1}e^n\\ &+ \Delta t\int_\Gamma[f(v^n, w^n) - f(v(t_n), w(t_n))]e^n = \frac{\Delta t^2}{2}\int_\Gamma v_{tt}(\xi^n)e^n.\end{aligned}$$

Then

$$\begin{aligned}\Delta t\int_{\Omega_e}\sigma_e|\nabla e_e^n|^2 + \Delta t\int_{\Omega_i}\sigma_i|\nabla e_i^n|^2 + \int_\Gamma|e^n|^2 \;&\leq\; \int_\Gamma|e^{n-1}e^n| + \frac{\Delta t^2}{2}\int_\Gamma|v_{tt}(\xi^n)e^n|\\ &+\; \Delta t\int_\Gamma|f(v^n, w^n) - f(v(t_n), w(t_n))||e^n|.\end{aligned}$$

Considering (3.14), we have

$$\begin{aligned}\Delta t\int_{\Omega_e}\sigma_e|\nabla e_e^n|^2 + \Delta t\int_{\Omega_i}\sigma_i|\nabla e_i^n|^2 + \int_\Gamma|e^n|^2 \;&\leq\; \int_\Gamma|e^{n-1}e^n| + \frac{\Delta t^2}{2}\int_\Gamma|v_{tt}(\xi^n)e^n|\\ &+ \Delta t\int_\Gamma \mathrm{L}_f|v^n - v(t_n)||e^n| \;+\; \Delta t\int_\Gamma \mathrm{L}_f|w^n - w(t_n)||e^n|,\end{aligned}$$

that is,

$$\begin{aligned}\Delta t\int_{\Omega_e}\sigma_e|\nabla e_e^n|^2 + \Delta t\int_{\Omega_i}\sigma_i|\nabla e_i^n|^2 + \int_\Gamma|e^n|^2 \;&\leq\; \int_\Gamma|e^{n-1}e^n| + \frac{\Delta t^2}{2}\int_\Gamma|v_{tt}(\xi^n)e^n|\\ &+ \Delta t\int_\Gamma \mathrm{L}_f|e^n|^2 \;+\; \Delta t\int_\Gamma \mathrm{L}_f|e_w^n e^n|.\end{aligned} \tag{3.57}$$

From (3.57), we obtain

$$\int_\Gamma|e^n|^2 \;\leq\; \int_\Gamma|e^{n-1}e^n| + \frac{\Delta t^2}{2}\int_\Gamma|v_{tt}(\xi^n)e^n| + \Delta t\mathrm{L}_f\int_\Gamma|e^n|^2 + \Delta t\mathrm{L}_f\int_\Gamma|e_w^n e^n|.$$

Thanks to Cauchy-Schwarz inequality, we obtain

$$\begin{aligned}\|e^n\|^2_{\mathrm{L}^2(\Gamma)} &\leq \|e^{n-1}\|_{\mathrm{L}^2(\Gamma)}\|e^n\|_{\mathrm{L}^2(\Gamma)} + \frac{\Delta t^2}{2}\|v_{tt}(\xi^n)\|_{\mathrm{L}^2(\Gamma)}\|e^n\|_{\mathrm{L}^2(\Gamma)} + \Delta t \mathrm{L}_f\|e^n\|^2_{\mathrm{L}^2(\Gamma)} \\ &+ \Delta t \mathrm{L}_f\|e^n\|_{\mathrm{L}^2(\Gamma)}\|e^n_w\|_{\mathrm{L}^2(\Gamma)}.\end{aligned}$$

Then,

$$\|e^n\|_{\mathrm{L}^2(\Gamma)} \leq \|e^{n-1}\|_{\mathrm{L}^2(\Gamma)} + \frac{\Delta t^2}{2}\|v_{tt}(\xi^n)\|_{\mathrm{L}^2(\Gamma)} + \Delta t \mathrm{L}_f\|e^n\|_{\mathrm{L}^2(\Gamma)} + \Delta t \mathrm{L}_f\|e^n_w\|_{\mathrm{L}^2(\Gamma)} \cdot \quad (3.58)$$

Setting $\varphi = e^n_w$ in (3.54) and considering (3.15) we have

$$\int_\Gamma |e^n_w|^2 \leq \int_\Gamma |e^{n-1}_w e^n_w| + \frac{\Delta t^2}{2}\int_\Gamma |w_{tt}(\xi^n_1)e^n_w| + \Delta t \mathrm{L}_g \int_\Gamma |e^n_w|^2 + \Delta t \mathrm{L}_g \int_\Gamma |e^n_w e^n| \cdot \quad (3.59)$$

Applying the Cauchy-Schwarz inequality, (3.59) becomes,

$$\begin{aligned}\|e^n_w\|^2_{\mathrm{L}^2(\Gamma)} &\leq \|e^{n-1}_w\|_{\mathrm{L}^2(\Gamma)}\|e^n_w\|_{\mathrm{L}^2(\Gamma)} + \frac{\Delta t^2}{2}\|w_{tt}(\xi^n_1)\|_{\mathrm{L}^2(\Gamma)}\|e^n_w\|_{\mathrm{L}^2(\Gamma)} + \Delta t \mathrm{L}_g\|e^n_w\|^2_{\mathrm{L}^2(\Gamma)} \\ &+ \Delta t \mathrm{L}_g\|e^n_w\|_{\mathrm{L}^2(\Gamma)}\|e^n\|_{\mathrm{L}^2(\Gamma)} \cdot \quad (3.60)\end{aligned}$$

Hence,

$$\|e^n_w\|_{\mathrm{L}^2(\Gamma)} \leq \|e^{n-1}_w\|_{\mathrm{L}^2(\Gamma)} + \frac{\Delta t^2}{2}\|w_{tt}(\xi^n)\|_{\mathrm{L}^2(\Gamma)} + \Delta t \mathrm{L}_g\|e^n_w\|_{\mathrm{L}^2(\Gamma)} + \Delta t \mathrm{L}_g\|e^n\|_{\mathrm{L}^2(\Gamma)} \cdot \quad (3.61)$$

Adding the inequalities (3.58) and (3.61), we have

$$\begin{aligned}\|e^n\|_{\mathrm{L}^2(\Gamma)} + \|e^n_w\|_{\mathrm{L}^2(\Gamma)} &\leq \|e^{n-1}\|_{\mathrm{L}^2(\Gamma)} + \|e^{n-1}_w\|_{\mathrm{L}^2(\Gamma)} + \frac{\Delta t^2}{2}\|v_{tt}(\xi^n)\|_{\mathrm{L}^2(\Gamma)} \\ &+ \frac{\Delta t^2}{2}\|w_{tt}(\xi^n_1)\|_{\mathrm{L}^2(\Gamma)} + \Delta t \mathrm{L}_0\left(\|e^n\|_{\mathrm{L}^2(\Gamma)} + \|e^n_w\|_{\mathrm{L}^2(\Gamma)}\right). \quad (3.62)\end{aligned}$$

From the latter inequality, we have

$$\begin{aligned}\sum_{k=1}^n \left(\|e^k\|_{\mathrm{L}^2(\Gamma)} + \|e^k_w\|_{\mathrm{L}^2(\Gamma)}\right) \leq & \sum_{k=1}^n \left(\|e^{k-1}\|_{\mathrm{L}^2(\Gamma)} + \|e^{k-1}_w\|_{\mathrm{L}^2(\Gamma)}\right) + \frac{\Delta \mathrm{t}^2}{2}\sum_{k=1}^N \|v_{tt}(\xi^n)\|_{\mathrm{L}^2(\Gamma)} \\ &+ \frac{\Delta t^2}{2}\sum_{k=1}^N \|w_{tt}(\xi^n_1)\|_{\mathrm{L}^2(\Gamma)} + \Delta t L_0 \sum_{k=1}^n \left(\|e^k\|_{\mathrm{L}^2(\Gamma)} + \|e^k_w\|_{\mathrm{L}^2(\Gamma)}\right) \cdot\end{aligned}$$

Then,

$$\begin{aligned}\|e^n\|_{\mathrm{L}^2(\Gamma)} + \|e^n_w\|_{\mathrm{L}^2(\Gamma)} &\leq \|e^0\|_{\mathrm{L}^2(\Gamma)} + \|e^0_w\|_{\mathrm{L}^2(\Gamma)} + \frac{1}{2}\sum_{k=1}^N \left(\Delta t^{\frac{1}{2}}\|v_{tt}(\xi^k)\|_{\mathrm{L}^2(\Gamma)}\right)\left(\Delta t^{\frac{3}{2}}\right) \\ &+ \frac{1}{2}\sum_{k=1}^N \left(\Delta t^{\frac{1}{2}}\|w_{tt}(\xi^k_1)\|_{\mathrm{L}^2(\Gamma)}\right)\left(\Delta t^{\frac{3}{2}}\right) \\ &+ \Delta t \mathrm{L}_0 \sum_{k=1}^n \left(\|e^k\|_{\mathrm{L}^2(\Gamma)} + \|e^k_w\|_{\mathrm{L}^2(\Gamma)}\right) \cdot\end{aligned}$$

Applying the discrete Cauchy-Schwarz inequality and using that $\|e^0\|_{\mathrm{L}^2(\Gamma)} = 0$ and $\|e_w^0\|_{\mathrm{L}^2(\Gamma)} = 0$, give

$$\begin{aligned}\|e^n\|_{\mathrm{L}^2(\Gamma)} + \|e_w^n\|_{\mathrm{L}^2(\Gamma)} &\leq \frac{1}{2}\left(\sum_{k=1}^{N}\Delta t\|v_{tt}(\xi^k)\|^2_{\mathrm{L}^2(\Gamma)}\right)^{\frac{1}{2}}\left(\sum_{k=1}^{N}\Delta t^3\right)^{\frac{1}{2}}\\ &+ \frac{1}{2}\left(\sum_{k=1}^{N}\Delta t\|w_{tt}(\xi_1^k)\|^2_{\mathrm{L}^2(\Gamma)}\right)^{\frac{1}{2}}\left(\sum_{k=1}^{N}\Delta t^3\right)^{\frac{1}{2}}\\ &+ \Delta t\mathrm{L}_0\sum_{k=1}^{n}\left(\|e^k\|_{\mathrm{L}^2(\Gamma)} + \|e_w^k\|_{\mathrm{L}^2(\Gamma)}\right).\end{aligned}$$

Then,

$$\begin{aligned}(1-\Delta t\mathrm{L}_0)\left(\|e^n\|_{\mathrm{L}^2(\Gamma)} + \|e_w^n\|_{\mathrm{L}^2(\Gamma)}\right) &\leq \mathrm{T}^{\frac{1}{2}}\Delta tC_4\left(\|v_{tt}\|_{\mathrm{L}^2(0,\mathrm{T},\mathrm{L}^2(\Gamma))} + \|w_{tt}\|_{\mathrm{L}^2(0,\mathrm{T},\mathrm{L}^2(\Gamma))}\right)\\ &+ \Delta t\mathrm{L}_0\sum_{k=1}^{n-1}\left(\|e^k\|_{\mathrm{L}^2(\Gamma)} + \|e_w^k\|_{\mathrm{L}^2(\Gamma)}\right), \qquad (3.63)\end{aligned}$$

for some constant $C_4 > 0$.
Using the constant α_2 from the hypothesis, we get

$$\begin{aligned}\|e^n\|_{\mathrm{L}^2(\Gamma)} + \|e_w^n\|_{\mathrm{L}^2(\Gamma)} &\leq \frac{\mathrm{T}^{\frac{1}{2}}\Delta tC_4}{\alpha_2}\left(\|v_{tt}\|_{\mathrm{L}^2(0,\mathrm{T},\mathrm{L}^2(\Gamma))} + \|w_{tt}\|_{\mathrm{L}^2(0,\mathrm{T},\mathrm{L}^2(\Gamma))}\right)\\ &+ \frac{\Delta tL_0}{\alpha_2}\sum_{k=1}^{n-1}\left(\|e^k\|_{\mathrm{L}^2(\Gamma)} + \|e_w^k\|_{\mathrm{L}^2(\Gamma)}\right).\end{aligned}$$

Finally, applying Lemma 3.6.1, we obtain

$$\begin{aligned}\|e^n\|_{\mathrm{L}^2(\Gamma)} + \|e_w^n\|_{\mathrm{L}^2(\Gamma)} &\leq \frac{\mathrm{T}^{\frac{1}{2}}\Delta\mathrm{tC}_4}{\alpha_2}\left(\|v_{tt}\|_{\mathrm{L}^2(0,\mathrm{T},\mathrm{L}^2(\Gamma))} + \|w_{tt}\|_{\mathrm{L}^2(0,\mathrm{T},\mathrm{L}^2(\Gamma))}\right)\exp\left(\sum_{\mathrm{k}=1}^{\mathrm{n}-1}\frac{\Delta\mathrm{tL}_0}{\alpha_2}\right)\\ &\leq \frac{\mathrm{T}^{\frac{1}{2}}\Delta tC_4}{\alpha_2}\left(\|v_{tt}\|_{\mathrm{L}^2(0,\mathrm{T},\mathrm{L}^2(\Gamma))} + \|w_{tt}\|_{\mathrm{L}^2(0,\mathrm{T},\mathrm{L}^2(\Gamma))}\right)\exp\left(\frac{\mathrm{TL}_0}{\alpha_2}\right).\end{aligned}$$

Let us prove the inequality (3.56). From (3.57), we have

$$\begin{aligned}\Delta t\int_{\Omega_e}\sigma_e|\nabla e_e^n|^2 + \Delta t\int_{\Omega_i}\sigma_i|\nabla e_i^n|^2 + \|e^n\|^2_{\mathrm{L}^2(\Gamma)} &\leq \|e^n\|_{\mathrm{L}^2(\Gamma)}\|e^{n-1}\|_{\mathrm{L}^2(\Gamma)}\\ &+ \frac{\Delta t^2}{2}\|v_{tt}(\xi^n)\|_{\mathrm{L}^2(\Gamma)}\|e^n\|_{\mathrm{L}^2(\Gamma)} + \Delta t\mathrm{L}_f\|e^n\|^2_{\mathrm{L}^2(\Gamma)}\\ &+ \Delta t\mathrm{L}_f\|e^n\|_{\mathrm{L}^2(\Gamma)}\|e_w^n\|_{\mathrm{L}^2(\Gamma)}. \qquad (3.64)\end{aligned}$$

Adding up the inequalities (3.60) and (3.64), we write

$$\begin{aligned}\beta\Delta t\int_{\Omega_e}|\nabla e_e^n|^2 \;+\; \beta\Delta t\int_{\Omega_i}|\nabla e_i^n|^2+\|e^n\|^2_{\mathrm{L}^2(\Gamma)}+\|e_w^n\|^2_{\mathrm{L}^2(\Gamma)} \;\leq\; \|e^n\|_{\mathrm{L}^2(\Gamma)}\|e^{n-1}\|_{\mathrm{L}^2(\Gamma)}\\ +\;\Delta t\mathrm{L}_0\|e_w^n\|^2_{\mathrm{L}^2(\Gamma)}+\Delta t\mathrm{L}_0\|e^n\|^2_{\mathrm{L}^2(\Gamma)}+\|e_w^{n-1}\|_{\mathrm{L}^2(\Gamma)}\|e_w^n\|_{\mathrm{L}^2(\Gamma)}\\ +\;2\Delta t\mathrm{L}_0\|e^n\|_{\mathrm{L}^2(\Gamma)}\|e_w^n\|_{\mathrm{L}^2(\Gamma)}+\frac{1}{2}\left(\Delta t^{\frac{3}{2}}\|v_{tt}(\xi^n)\|_{\mathrm{L}^2(\Gamma)}\right)\left(\Delta t^{\frac{1}{2}}\|e^n\|_{\mathrm{L}^2(\Gamma)}\right)\\ +\;\frac{1}{2}\left(\Delta t^{\frac{3}{2}}\|w_{tt}(\xi_1^n)\|_{\mathrm{L}^2(\Gamma)}\right)\left(\Delta t^{\frac{1}{2}}\|e_w^n\|_{\mathrm{L}^2(\Gamma)}\right),\end{aligned}$$

where β is defined as in (3.13). Using Young's inequality,

$$\begin{aligned}\beta\Delta t\int_{\Omega_e}|\nabla e_e^n|^2 \;+\; \beta\Delta t\int_{\Omega_i}|\nabla e_i^n|^2 \;\leq\; \frac{1}{2}\|e^{n-1}\|^2_{\mathrm{L}^2(\Gamma)}+\frac{1}{2}\|e_w^{n-1}\|^2_{\mathrm{L}^2(\Gamma)}-\frac{1}{2}\|e^n\|^2_{\mathrm{L}^2(\Gamma)}\\ -\;\frac{1}{2}\|e_w^n\|^2_{\mathrm{L}^2(\Gamma)}+\left(\frac{1}{4}+2L_0\right)\Delta t\|e^n\|^2_{\mathrm{L}^2(\Gamma)}\\ +\;\left(\frac{1}{4}+2L_0\right)\Delta t\|e_w^n\|^2_{\mathrm{L}^2(\Gamma)}+\frac{\Delta t^3}{4}\|v_{tt}(\xi^n)\|^2_{\mathrm{L}^2(\Gamma)}\\ +\;\frac{\Delta t^3}{4}\|w_{tt}(\xi_1^n)\|^2_{\mathrm{L}^2(\Gamma)}.\end{aligned}$$

Then,

$$\begin{aligned}\beta\sum_{n=1}^{N}\Delta t\int_{\Omega_e}|\nabla e_e^n|^2 \;+\; \beta\sum_{n=1}^{N}\Delta t\int_{\Omega_i}|\nabla e_i^n|^2 \;\leq\; \frac{1}{2}\sum_{n=1}^{N}\left(\|e^{n-1}\|^2_{\mathrm{L}^2(\Gamma)}+\|e_w^{n-1}\|^2_{\mathrm{L}^2(\Gamma)}\right)\\ -\;\frac{1}{2}\sum_{n=1}^{N}\left(\|e^n\|^2_{\mathrm{L}^2(\Gamma)}+\|e_w^n\|^2_{\mathrm{L}^2(\Gamma)}\right)+\left(\frac{1}{4}+2L_0\right)\Delta t\sum_{n=1}^{N}\|e^n\|^2_{\mathrm{L}^2(\Gamma)}\\ +\;\left(\frac{1}{4}+2L_0\right)\Delta t\sum_{n=1}^{N}\|e_w^n\|^2_{\mathrm{L}^2(\Gamma)}+\frac{\Delta t^2}{4}\sum_{n=1}^{N}\Delta t\|v_{tt}(\xi^n)\|^2_{\mathrm{L}^2(\Gamma)}\\ +\;\frac{\Delta t^2}{4}\sum_{n=1}^{N}\Delta t\|w_{tt}(\xi_1^n)\|^2_{\mathrm{L}^2(\Gamma)}.\end{aligned}$$

We obtain

$$\begin{aligned}\sum_{n=1}^{N}\beta\Delta t\int_{\Omega_e}|\nabla e_e^n|^2 \;+\; \sum_{n=1}^{N}\beta\Delta t\int_{\Omega_i}|\nabla e_i^n|^2 \;\leq\; \frac{1}{2}\left(\|e^0\|^2_{\mathrm{L}^2(\Gamma)}+\|e_w^0\|^2_{\mathrm{L}^2(\Gamma)}\right)\\ -\;\frac{1}{2}\left(\|e^N\|^2_{\mathrm{L}^2(\Gamma)}+\|e_w^N\|^2_{\mathrm{L}^2(\Gamma)}\right)+\left(\frac{1}{4}+2L_0\right)\Delta t\sum_{n=1}^{N}\|e^n\|^2_{\mathrm{L}^2(\Gamma)}\\ +\;\left(\frac{1}{4}+2L_0\right)\Delta t\sum_{n=1}^{N}\|e_w^n\|^2_{\mathrm{L}^2(\Gamma)}+C_5\Delta t^2\left\|v_{tt}\right\|^2_{\mathrm{L}^2(0,\mathrm{T},\mathrm{L}^2(\Gamma))}\\ +\;C_5\Delta t^2\left\|w_{tt}\right\|^2_{\mathrm{L}^2(0,\mathrm{T},\mathrm{L}^2(\Gamma))},\end{aligned}$$

for some constants $C_5 > 0$.
Using $\|e^0\|_{\mathrm{L}^2(\Gamma)} = 0$ and $\|e_w^0\|_{\mathrm{L}^2(\Gamma)} = 0$ and considering the a priori error estimate (3.55), it follows that

$$\sum_{n=1}^{N} \Delta t \int_{\Omega_e} |\nabla e_e^n|^2 + \sum_{n=1}^{N} \Delta t \int_{\Omega_i} |\nabla e_i^n|^2 \leq \frac{\Delta t^2 C_5}{\beta} \left(\|v_{tt}\|^2_{\mathrm{L}^2(0,\mathrm{T},\mathrm{L}^2(\Gamma))} + \|w_{tt}\|^2_{\mathrm{L}^2(0,\mathrm{T},\mathrm{L}^2(\Gamma))} \right) + \frac{\Delta t^2 \mathrm{T}^2 C_4^2}{\beta \alpha_2^2} \left(\frac{1}{4} + 2L_0 \right) \left(\|v_{tt}\|_{\mathrm{L}^2(0,\mathrm{T},\mathrm{L}^2(\Gamma))} + \|w_{tt}\|_{\mathrm{L}^2(0,\mathrm{T},\mathrm{L}^2(\Gamma))} \right)^2 \exp\left(\frac{2\mathrm{T}L_0}{\alpha_2} \right).$$

Finally,

$$\sum_{n=1}^{N} \Delta t \int_{\Omega_e} |\nabla e_e^n|^2 + \sum_{n=1}^{N} \Delta t \int_{\Omega_i} |\nabla e_i^n|^2 \leq C_6 \Delta \mathrm{t}^2 \left(\|v_{tt}\|_{\mathrm{L}^2(0,\mathrm{T},\mathrm{L}^2(\Gamma))} + \|w_{tt}\|_{\mathrm{L}^2(0,\mathrm{T},\mathrm{L}^2(\Gamma))} \right)^2,$$

where $C_6 = \max\left(\frac{C_5}{\beta}, \frac{\mathrm{T}^2 C_4^2}{\beta \alpha_2^2} \left(\frac{1}{4} + 2L_0 \right) \exp\left(\frac{2\mathrm{T}L_0}{\alpha_2} \right) \right)$. □

3.6.3 Convergence Analysis of FBE Method

We next obtain an error estimate for the FBE method given in (3.22)-(3.24). The nonlinear terms in f and g are now handled explicitely, which requires some changes in the derivation. The stability condition is slightly modified compared to the BE scheme. Further, the error estimate possesses an extra term in $\Delta t^{2-\epsilon}$ for any $\epsilon > 0$.
By subtracting equation (3.22) from equation (3.10), we have on account of (3.47),

$$\int_{\Omega_e} \sigma_e \nabla e_e^n \cdot \nabla \varphi_e - \int_{\Gamma} \left[\frac{v^n - v^{n-1}}{\Delta t} - v_t(t_n) \right] \varphi_e - \int_{\Gamma} [f(v^{n-1}, w^{n-1}) - f(v(t_n), w(t_n))] \varphi_e = \int_{\Omega_e} (\mathrm{I}_{e,stim}^{n-1} - \mathrm{I}_{e,stim}(t_n)) \varphi_e \cdot \quad (3.65)$$

Using Taylor's series, we have

$$v_t(t_n) = \frac{v(t_n) - v(t_{n-1})}{\Delta t} + \frac{\Delta t}{2} v_{tt}(\xi^n) \cdot \quad (3.66)$$

where ξ^n, is some point between t_{n-1} and t_n. Combining (3.65) and (3.66), and taking into consideration (3.47), we write

$$\int_{\Omega_e} \sigma_e \nabla e_e^n \cdot \nabla \varphi_e - \int_{\Gamma} \left[\frac{e^n - e^{n-1}}{\Delta t} \right] \varphi_e = \int_{\Gamma} [f(v^{n-1}, w^{n-1}) - f(v(t_{n-1}), w(t_{n-1}))] \varphi_e + \int_{\Gamma} [f(v(t_{n-1}), w(t_{n-1})) - f(v(t_n), w(t_n))] \varphi_e - \frac{\Delta t}{2} \int_{\Gamma} v_{tt}(\xi^n) \varphi_e + \int_{\Omega_e} [\mathrm{I}_{e,stim}^{n-1} - \mathrm{I}_{e,stim}(t_{n-1})] \varphi_e + [\mathrm{I}_{e,stim}(t_{n-1}) - \mathrm{I}_{e,stim}(t_n)] \varphi_e \cdot \quad (3.67)$$

Similarly, we have on Ω_i

$$\begin{aligned}\int_{\Omega_i}\sigma_i\nabla e_i^n\cdot\nabla\varphi_i \;+\; \int_\Gamma\left[\frac{e^n-e^{n-1}}{\Delta t}\right]\varphi_i &= -\int_\Gamma[f(v^{n-1},w^{n-1})-f(v(t_{n-1}),w(t_{n-1}))]\varphi_i\\ -\int_\Gamma[f(v(t_{n-1}),w(t_{n-1}))-f(v(t_n),w(t_n))]\varphi_i &+\frac{\Delta t}{2}\int_\Gamma v_{tt}(\xi^n)\varphi_i\\ +\int_{\Omega_i}[\mathrm{I}_{i,stim}^{n-1}-\mathrm{I}_{i,stim}(t_{n-1})]\varphi_i &+\int_{\Omega_i}[\mathrm{I}_{i,stim}(t_{n-1})-\mathrm{I}_{i,stim}(t_n)]\varphi_i\cdot\end{aligned}\tag{3.68}$$

Adding up the equations (3.67) and (3.68) we have

$$\begin{aligned}\int_{\Omega_e}\sigma_e\nabla e_e^n\cdot\nabla\varphi_e \;+\; \int_{\Omega_i}\sigma_i\nabla e_i^n\cdot\nabla\varphi_i+\int_\Gamma\left[\frac{e^n-e^{n-1}}{\Delta t}\right](\varphi_i-\varphi_e)&\\ =\; -\int_\Gamma[f(v^{n-1},w^{n-1})-f(v(t_{n-1}),w(t_{n-1}))](\varphi_i-\varphi_e)&\\ -\int_\Gamma[f(v(t_{n-1}),w(t_{n-1}))-f(v(t_n),w(t_n))](\varphi_i-\varphi_e)&\\ +\frac{\Delta t}{2}\int_\Gamma v_{tt}(\xi^n)(\varphi_i-\varphi_e)+\int_{\Omega_i}[\mathrm{I}_{i,stim}(t_{n-1})-\mathrm{I}_{i,stim}(t_n)]\varphi_i&\\ +\int_{\Omega_e}[\mathrm{I}_{e,stim}(t_{n-1})-\mathrm{I}_{e,stim}(t_n)]\varphi_e\cdot&\end{aligned}\tag{3.69}$$

Further, by subtracting equation (3.21) from equation (3.12), we have on account of (3.53) and (3.66),

$$\int_\Gamma(e_w^n-e_w^{n-1})\psi \;=\; \Delta t\int_\Gamma(g(v^{n-1},w^{n-1})-g(v(t_n),w(t_n)))\psi+\frac{\Delta t^2}{2}\int_\Gamma w_{tt}(\xi_1^n)\psi,$$

then

$$\begin{aligned}\int_\Gamma(e_w^n-e_w^{n-1})\psi \;=\; \Delta t\int_\Gamma(g(v^{n-1},w^{n-1})-g(v(t_{n-1}),w(t_{n-1})))\psi+\frac{\Delta t^2}{2}\int_\Gamma w_{tt}(\xi_1^n)\psi&\\ +\;\Delta t\int_\Gamma(g(v(t_{n-1}),w(t_{n-1}))-g(v(t_n),w(t_n)))\psi\cdot&\end{aligned}\tag{3.70}$$

3.6.4 A Priori Error Estimates

The following a priori estimates hold for e^n, e_i^n, e_e^n and e_w^n,

Proposition 3.6.3. *Let $\epsilon>0$ be fixed. Assume that $v,w\in\mathrm{C}^2([0,\mathrm{T});\mathrm{L}^2(\Gamma))$, $\|e^0\|_{\mathrm{L}^2(\Gamma)}=0$, and $\|e_w^0\|_{\mathrm{L}^2(\Gamma)}=0$, and that there exist constants $0<\alpha_3<1$ and $0<\alpha_4<\beta$ such*

that $\Delta t < \min\left(1, \dfrac{1-\alpha_3}{\frac{1}{\alpha}+4\mathrm{L}_0+\frac{1}{2}}\right)$ *and* $\Delta t^{\epsilon} < 2\alpha(\beta-\alpha_4)$. *Then*

$$\begin{aligned}\|e^n\|_{\mathrm{L}^2(\Gamma)} + \|e_w^n\|_{\mathrm{L}^2(\Gamma)} &\leq \Delta t C_{15}\left(\|v_{tt}\|^2_{\mathrm{L}^2(0,\mathrm{T},\mathrm{L}^2(\Gamma))} + \|w_{tt}\|^2_{\mathrm{L}^2(0,\mathrm{T},\mathrm{L}^2(\Gamma))}\right)^{\frac{1}{2}} \exp\left(\frac{\mathrm{T}C_9}{2\alpha_3}\right)\\ &+ \Delta t C_{16}\left(\|v_t\|^2_{\mathrm{L}^2(0,\mathrm{T},\mathrm{L}^2(\Gamma))} + \|w_t\|^2_{\mathrm{L}^2(0,\mathrm{T},\mathrm{L}^2(\Gamma))}\right)^{\frac{1}{2}} \exp\left(\frac{\mathrm{T}C_9}{2\alpha_3}\right)\\ &+ \Delta t^{1-\frac{\epsilon}{2}} C_{17} \exp\left(\frac{\mathrm{T}C_9}{2\alpha_3}\right), \end{aligned} \tag{3.71}$$

$$\begin{aligned}\sum_{n=1}^{N}\Delta t\int_{\Omega_e}|\nabla e_e^n|^2 + \sum_{n=1}^{N}\Delta t\int_{\Omega_i}|\nabla e_i^n|^2 &\leq \mathrm{C}_{23}\Delta \mathrm{t}^2\left(\|v_{tt}\|^2_{\mathrm{L}^2(0,\mathrm{T},\mathrm{L}^2(\Gamma))} + \|w_{tt}\|^2_{\mathrm{L}^2(0,\mathrm{T},\mathrm{L}^2(\Gamma))}\right)\\ &+ C_{24}\Delta t^2\left(\|v_t\|^2_{\mathrm{L}^2(0,\mathrm{T},\mathrm{L}^2(\Gamma))} + \|w_t\|^2_{\mathrm{L}^2(0,\mathrm{T},\mathrm{L}^2(\Gamma))}\right)\\ &+ C_{25}\Delta t^{2-\epsilon}, \end{aligned} \tag{3.72}$$

for some constants $C_i > 0$, $\quad i \in \{9, 15, 16, 17, 23, 24, 25\}$, *provided* $\mathrm{T} = N\Delta t$, $\mathrm{L}_0 = \max(\mathrm{L}_f, \mathrm{L}_g)$ *and* α *is as in* (2.82).

Proof. Let us start with the inequality (3.71). Setting $\varphi_i = e_i^n$ and $\varphi_e = e_e^n$ in (3.69), we have

$$\begin{aligned}\Delta t\int_{\Omega_e}\beta|\nabla e_e^n|^2 &+ \Delta t\int_{\Omega_i}\beta|\nabla e_i^n|^2 + \int_{\Gamma}|e^n|^2 - \int_{\Gamma}e^{n-1}e^n\\ &\leq -\Delta \mathrm{t}\int_{\Gamma}[f(v^{n-1},w^{n-1}) - f(v(t_{n-1}),w(t_{n-1}))]e^n\\ &\quad -\Delta t\int_{\Gamma}[f(v(t_{n-1}),w(t_{n-1})) - f(v(t_n),w(t_n))]e^n\\ &\quad +\frac{\Delta \mathrm{t}^2}{2}\int_{\Gamma}v_{tt}(\xi^n)e^n + \Delta t\int_{\Omega_i}[\mathrm{I}_{i,stim}(t_{n-1}) - \mathrm{I}_{i,stim}(t_n)]e_i^n\\ &\quad +\Delta t\int_{\Omega_e}[\mathrm{I}_{e,stim}(t_{n-1}) - \mathrm{I}_{e,stim}(t_n)]e_e^n. \end{aligned}$$

Considering (3.14), (3.16) and (3.17), it follows that

$$\begin{aligned}\Delta t\int_{\Omega_e}\beta|\nabla e_e^n|^2 &+ \Delta t\int_{\Omega_i}\beta|\nabla e_i^n|^2 + \int_{\Gamma}|e^n|^2 \leq \int_{\Gamma}|e^{n-1}e^n| + \Delta \mathrm{t}\int_{\Gamma}\mathrm{L}_f|v^{n-1} - v(t_{n-1})||e^n|\\ &+ \Delta t\int_{\Gamma}\mathrm{L}_f|w^{n-1} - w(t_{n-1})||e^n| + \Delta t\int_{\Gamma}\mathrm{L}_f|v(t_{n-1}) - v(t_n)||e^n|\\ &+ \Delta t\int_{\Gamma}\mathrm{L}_f|w(t_{n-1}) - w(t_n)||e^n| + \frac{\Delta t^2}{2}\int_{\Gamma}|v_{tt}(\xi^n)e^n| + \Delta t^2\int_{\Omega_i}\mathrm{L}_i|e_i^n|\\ &+ \Delta t^2\int_{\Omega_e}\mathrm{L}_e|e_e^n|. \end{aligned} \tag{3.73}$$

Considering (3.49) and applying Young's inequality to the last two terms of (3.73), yield,

$$\begin{aligned}\Delta t\int_{\Omega_e}\beta|\nabla e_e^n|^2 \;+\; \Delta t\int_{\Omega_i}\beta|\nabla e_i^n|^2+\int_\Gamma|e^n|^2 &\le \int_\Gamma|e^{n-1}e^n|+\Delta \mathrm{t}\int_\Gamma \mathrm{L}_0|e^{n-1}e^n|\\ &+\Delta \mathrm{t}\int_\Gamma \mathrm{L}_0|e_w^{n-1}e^n|+\Delta t^2\int_\Gamma \mathrm{L}_0|v_t(\delta_1^n)e^n|+\Delta t^2\int_\Gamma \mathrm{L}_0|w_t(\delta_2^n)e^n|\\ &+\frac{\Delta t^2}{2}\int_\Gamma|v_{tt}(\xi^n)e^n|+\frac{\Delta t^{3-\epsilon}\mathrm{L}_1^2|\Omega_i|}{2}+\frac{\Delta t^{3-\epsilon}\mathrm{L}_1^2|\Omega_e|}{2}\\ &+\frac{\Delta t^{1+\epsilon}}{2}\left(\int_{\Omega_i}|e_i^n|^2+\int_{\Omega_e}|e_e^n|^2\right),\end{aligned}\tag{3.74}$$

for any fixed $\epsilon>0$, where $\delta_i^n=\delta_i^n(x)$, $i=1,2$, $x\in\Gamma$, are some points between t_{n-1} and t_n. The notations $|\Omega_i|$ and $|\Omega_e|$ stand for the Lebesgue measure of Ω_i and Ω_e, respectively. Considering the inequality (2.83) resulting from Petree-Tartar Lemma 2.3.1, (3.74) becomes

$$\begin{aligned}\Delta t\int_{\Omega_e}\beta|\nabla e_e^n|^2 \;+\; \Delta t\int_{\Omega_i}\beta|\nabla e_i^n|^2+\int_\Gamma|e^n|^2 &\le \int_\Gamma|e^{n-1}e^n|+\Delta \mathrm{t}\int_\Gamma \mathrm{L}_0|e^{n-1}e^n|\\ &+\Delta \mathrm{t}\int_\Gamma \mathrm{L}_0|e_w^{n-1}e^n|+\Delta t^2\int_\Gamma \mathrm{L}_0|v_t(\delta_1^n)e^n|+\Delta t^2\int_\Gamma \mathrm{L}_0|w_t(\delta_2^n)e^n|\\ &+\frac{\Delta t^2}{2}\int_\Gamma|v_{tt}(\xi^n)e^n|+\frac{\Delta t^{3-\epsilon}\mathrm{L}_1^2|\Omega_e|}{2}+\frac{\Delta t^{3-\epsilon}\mathrm{L}_1^2|\Omega_i|}{2}\\ &+C_7\Delta t^{1+\epsilon}\int_{\Omega_e}|\nabla e_e^n|^2+C_7\Delta t^{1+\epsilon}\int_{\Omega_i}|\nabla e_i^n|^2+C_7\Delta t^{1+\epsilon}\int_\Gamma|e^n|^2,\end{aligned}\tag{3.75}$$

for $C_7=\dfrac{1}{2\alpha}>0$. Applying Cauchy-Schwarz inequality to (3.75), it follows that

$$\begin{aligned}(\beta-C_7\Delta t^\epsilon)\left(\Delta t\int_{\Omega_e}|\nabla e_e^n|^2+\Delta t\int_{\Omega_i}|\nabla e_i^n|^2\right)+\int_\Gamma|e^n|^2 \;&\le\; \|e^{n-1}\|_{\mathrm{L}^2(\Gamma)}\|e^n\|_{\mathrm{L}^2(\Gamma)}\\ &+\Delta t\mathrm{L}_0\|e^{n-1}\|_{\mathrm{L}^2(\Gamma)}\|e^n\|_{\mathrm{L}^2(\Gamma)}+\Delta t\mathrm{L}_0\|e_w^{n-1}\|_{\mathrm{L}^2(\Gamma)}\|e^n\|_{\mathrm{L}^2(\Gamma)}\\ &+\Delta \mathrm{t}^2\mathrm{L}_0\|v_t(\delta_1^n)\|_{\mathrm{L}^2(\Gamma)}\|e^n\|_{\mathrm{L}^2(\Gamma)}+\Delta t^2\mathrm{L}_0\|w_t(\delta_2^n)\|_{\mathrm{L}^2(\Gamma)}\|e^n\|_{\mathrm{L}^2(\Gamma)}\\ &+\frac{\Delta t^2}{2}\|v_{tt}(\xi^n)\|_{\mathrm{L}^2(\Gamma)}\|e^n\|_{\mathrm{L}^2(\Gamma)}+\frac{\Delta t^{3-\epsilon}\mathrm{L}_1^2|\Omega_e|}{2}+\frac{\Delta t^{3-\epsilon}\mathrm{L}_1^2|\Omega_i|}{2}+C_7\Delta t\|e^n\|_\Gamma^2.\end{aligned}$$

provided $\Delta t < 1$. Using the constant α_4 from the hypothesis, we write

$$\begin{aligned}\alpha_4\Delta t\int_{\Omega_e}|\nabla e_e^n|^2 \;+\; & \alpha_4\Delta t\int_{\Omega_i}|\nabla e_i^n|^2+\int_\Gamma|e^n|^2 \;\le\; \|e^{n-1}\|_{\mathrm{L}^2(\Gamma)}\|e^n\|_{\mathrm{L}^2(\Gamma)}\\ &+\Delta t\mathrm{L}_0\|e^{n-1}\|_{\mathrm{L}^2(\Gamma)}\|e^n\|_{\mathrm{L}^2(\Gamma)}+\Delta t\mathrm{L}_0\|e_w^{n-1}\|_{\mathrm{L}^2(\Gamma)}\|e^n\|_{\mathrm{L}^2(\Gamma)}\\ &+\Delta \mathrm{t}^2\mathrm{L}_0\|v_t(\delta_1^n)\|_{\mathrm{L}^2(\Gamma)}\|e^n\|_{\mathrm{L}^2(\Gamma)}+\Delta t^2\mathrm{L}_0\|w_t(\delta_2^n)\|_{\mathrm{L}^2(\Gamma)}\|e^n\|_{\mathrm{L}^2(\Gamma)}\\ &+\frac{\Delta t^2}{2}\|v_{tt}(\xi^n)\|_{\mathrm{L}^2(\Gamma)}\|e^n\|_{\mathrm{L}^2(\Gamma)}+\frac{\Delta t^{3-\epsilon}\mathrm{L}_1^2|\Omega_e|}{2}+\frac{\Delta t^{3-\epsilon}\mathrm{L}_1^2|\Omega_i|}{2}\\ &+C_7\Delta t\|e^n\|_\Gamma^2.\end{aligned}$$

It follows that

$$\begin{aligned}\|e^n\|^2_{\mathrm{L}^2(\Gamma)} \;\le\; & \|e^{n-1}\|_{\mathrm{L}^2(\Gamma)}\|e^n\|_{\mathrm{L}^2(\Gamma)}+\Delta t\mathrm{L}_0\|e^{n-1}\|_{\mathrm{L}^2(\Gamma)}\|e^n\|_{\mathrm{L}^2(\Gamma)}+\Delta t\mathrm{L}_0\|e_w^{n-1}\|_{\mathrm{L}^2(\Gamma)}\|e^n\|_{\mathrm{L}^2(\Gamma)}\\ &+\Delta \mathrm{t}^2\mathrm{L}_0\|v_t(\delta_1^n)\|_{\mathrm{L}^2(\Gamma)}\|e^n\|_{\mathrm{L}^2(\Gamma)}+\Delta t^2\mathrm{L}_0\|w_t(\delta_2^n)\|_{\mathrm{L}^2(\Gamma)}\|e^n\|_{\mathrm{L}^2(\Gamma)}\\ &+\frac{\Delta t^2}{2}\|v_{tt}(\xi^n)\|_{\mathrm{L}^2(\Gamma)}\|e^n\|_{\mathrm{L}^2(\Gamma)}+\frac{\Delta t^{3-\epsilon}\mathrm{L}_1^2|\Omega_e|}{2}+\frac{\Delta t^{3-\epsilon}\mathrm{L}_1^2|\Omega_i|}{2}+C_7\Delta t\|e^n\|_\Gamma^2.\end{aligned}\tag{3.76}$$

Further, setting $\varphi = e_w^n$ in (3.70), using (3.15) and Cauchy-Schwarz inequality, we have

$$\begin{aligned}\|e_w^n\|^2_{\mathrm{L}^2(\Gamma)} \;\le\; & \|e_w^{n-1}\|_{\mathrm{L}^2(\Gamma)}\|e_w^n\|_{\mathrm{L}^2(\Gamma)}+\Delta t\mathrm{L}_0\|e^{n-1}\|_{\mathrm{L}^2(\Gamma)}\|e_w^n\|_{\mathrm{L}^2(\Gamma)}+\Delta t\mathrm{L}_0\|e_w^{n-1}\|_{\mathrm{L}^2(\Gamma)}\|e_w^n\|_{\mathrm{L}^2(\Gamma)}\\ &+\frac{\Delta t^2}{2}\|w_{tt}(\xi_1^n)\|_{\mathrm{L}^2(\Gamma)}\|e_w^n\|_{\mathrm{L}^2(\Gamma)}+\Delta t^2\mathrm{L}_0\|v_t(\delta_3^n)\|_{\mathrm{L}^2(\Gamma)}\|e_w^n\|_{\mathrm{L}^2(\Gamma)}\\ &+\Delta t^2\mathrm{L}_0\|w_t(\delta_4^n)\|_{\mathrm{L}^2(\Gamma)}\|e_w^n\|_{\mathrm{L}^2(\Gamma)}.\end{aligned}\tag{3.77}$$

Adding up the inequalities (3.76) and (3.77) and using the Young's inequality, we have

$$\begin{aligned}\|e^n\|^2_{\mathrm{L}^2(\Gamma)}+\|e_w^n\|^2_{\mathrm{L}^2(\Gamma)} \;\le\; & \|e^{n-1}\|^2_{\mathrm{L}^2(\Gamma)}+\|e_w^{n-1}\|^2_{\mathrm{L}^2(\Gamma)}+2\Delta t\mathrm{L}_0\left(\|e^{n-1}\|^2_{\mathrm{L}^2(\Gamma)}+\|e_w^{n-1}\|^2_{\mathrm{L}^2(\Gamma)}\right)\\ &+C_8\Delta t\left(\|e^n\|^2_{\mathrm{L}^2(\Gamma)}+\|e_w^n\|^2_{\mathrm{L}^2(\Gamma)}\right)+\frac{\Delta t^3}{2}\|v_{tt}(\xi^n)\|^2_{\mathrm{L}^2(\Gamma)}\\ &+\frac{\Delta t^3}{2}\|w_{tt}(\xi_1^n)\|^2_{\mathrm{L}^2(\Gamma)}+\Delta t^3\mathrm{L}_0\left(\|v_t(\delta_1^n)\|^2_{\mathrm{L}^2(\Gamma)}+\|v_t(\delta_3^n)\|^2_{\mathrm{L}^2(\Gamma)}\right)\\ &+\Delta t^3\mathrm{L}_0\left(\|w_t(\delta_2^n)\|^2_{\mathrm{L}^2(\Gamma)}+\|w_t(\delta_4^n)\|^2_{\mathrm{L}^2(\Gamma)}\right)\\ &+\Delta t^{3-\epsilon}\mathrm{L}_1^2|\Omega_e|+\Delta t^{3-\epsilon}\mathrm{L}_1^2|\Omega_i|,\end{aligned}\tag{3.78}$$

for some constant $C_8 = \left(\frac{1}{\alpha}+4\mathrm{L}_0+\frac{1}{2}\right) > 0$. Assuming $\|e^0\|_{\mathrm{L}^2(\Gamma)} = 0$ and $\|e_w^0\|_{\mathrm{L}^2(\Gamma)} = 0$,

and summing from 1 to n we write

$$\begin{aligned}(1-C_8\Delta t)\left(\|e^n\|^2_{\mathrm{L}^2(\Gamma)}+\|e^n_w\|^2_{\mathrm{L}^2(\Gamma)}\right) &\leq C_9\Delta t\sum_{k=1}^{n-1}\left(\|e^k\|^2_{\mathrm{L}^2(\Gamma)}+\|e^k_w\|^2_{\mathrm{L}^2(\Gamma)}\right)\\ &+ C_{10}\Delta t^2\left(\|v_{tt}\|^2_{\mathrm{L}^2(0,\mathrm{T},\mathrm{L}^2(\Gamma))}+\|w_{tt}\|^2_{\mathrm{L}^2(0,\mathrm{T},\mathrm{L}^2(\Gamma))}\right)\\ &+ C_{11}\Delta t^2\left(\|v_t\|^2_{\mathrm{L}^2(0,\mathrm{T},\mathrm{L}^2(\Gamma))}+\|w_t\|^2_{\mathrm{L}^2(0,\mathrm{T},\mathrm{L}^2(\Gamma))}\right)\\ &+ \Delta t^{2-\epsilon}\mathrm{L}_1^2\mathrm{T}|\Omega_e|+\Delta t^{2-\epsilon}\mathrm{L}_1^2\mathrm{T}|\Omega_i|,\end{aligned}$$

for some constants $C_9,\ C_{10},\ C_{11}>0$. Using the constant α_3 from the hypothesis, we have

$$\begin{aligned}\|e^n\|^2_{\mathrm{L}^2(\Gamma)}+\|e^n_w\|^2_{\mathrm{L}^2(\Gamma)} &\leq \frac{C_9\Delta t}{\alpha_3}\sum_{k=1}^{n-1}\left(\|e^k\|^2_{\mathrm{L}^2(\Gamma)}+\|e^k_w\|^2_{\mathrm{L}^2(\Gamma)}\right)\\ &+ C_{12}\Delta t^2\left(\|v_{tt}\|^2_{\mathrm{L}^2(0,\mathrm{T},\mathrm{L}^2(\Gamma))}+\|w_{tt}\|^2_{\mathrm{L}^2(0,\mathrm{T},\mathrm{L}^2(\Gamma))}\right)\\ &+ C_{13}\Delta t^2\left(\|v_t\|^2_{\mathrm{L}^2(0,\mathrm{T},\mathrm{L}^2(\Gamma))}+\|w_t\|^2_{\mathrm{L}^2(0,\mathrm{T},\mathrm{L}^2(\Gamma))}\right)\\ &+ C_{14}\Delta t^{2-\epsilon},\end{aligned}\tag{3.79}$$

for some constants $C_{12},\ C_{13}>0$, and $C_{14}=\dfrac{\mathrm{L}_1^2\mathrm{T}}{\alpha_3}\left(|\Omega_i|+|\Omega_e|\right)>0$. Applying Lemma 3.6.1, we obtain

$$\begin{aligned}\|e^n\|^2_{\mathrm{L}^2(\Gamma)}+\|e^n_w\|^2_{\mathrm{L}^2(\Gamma)} &\leq \Delta t^2C_{12}\left(\|v_{tt}\|^2_{\mathrm{L}^2(0,\mathrm{T},\mathrm{L}^2(\Gamma))}+\|w_{tt}\|^2_{\mathrm{L}^2(0,\mathrm{T},\mathrm{L}^2(\Gamma))}\right)\exp\left(\frac{\mathrm{T}C_9}{\alpha_3}\right)\\ &+ \Delta t^2C_{13}\left(\|v_t\|^2_{\mathrm{L}^2(0,\mathrm{T},\mathrm{L}^2(\Gamma))}+\|w_t\|^2_{\mathrm{L}^2(0,\mathrm{T},\mathrm{L}^2(\Gamma))}\right)\exp\left(\frac{\mathrm{T}C_9}{\alpha_3}\right)\\ &+ C_{14}\Delta t^{2-\epsilon}\exp\left(\frac{\mathrm{T}C_9}{\alpha_3}\right).\end{aligned}\tag{3.80}$$

Finally,

$$\begin{aligned}\|e^n\|_{\mathrm{L}^2(\Gamma)}+\|e^n_w\|_{\mathrm{L}^2(\Gamma)} &\leq \Delta tC_{15}\left(\|v_{tt}\|^2_{\mathrm{L}^2(0,\mathrm{T},\mathrm{L}^2(\Gamma))}+\|w_{tt}\|^2_{\mathrm{L}^2(0,\mathrm{T},\mathrm{L}^2(\Gamma))}\right)^{\frac{1}{2}}\exp\left(\frac{\mathrm{T}C_9}{2\alpha_3}\right)\\ &+ \Delta tC_{16}\left(\|v_t\|^2_{\mathrm{L}^2(0,\mathrm{T},\mathrm{L}^2(\Gamma))}+\|w_t\|^2_{\mathrm{L}^2(0,\mathrm{T},\mathrm{L}^2(\Gamma))}\right)^{\frac{1}{2}}\exp\left(\frac{\mathrm{T}C_9}{2\alpha_3}\right)\\ &+ \Delta t^{1-\frac{\epsilon}{2}}C_{17}\exp\left(\frac{\mathrm{T}C_9}{2\alpha_3}\right),\end{aligned}$$

for some constants $C_i>0,\ i\in\{15,16,17\}$.

Let us prove the inequality (3.72). Adding up the inequalities (3.76) and (3.77) and using

Young's inequality, we have

$$\begin{aligned}\alpha_4\Delta t\int_{\Omega_e}|\nabla e_e^n|^2 \;+\; \alpha_4\Delta t\int_{\Omega_i}|\nabla e_i^n|^2 \;\le\; & \frac{1}{2}\|e^{n-1}\|^2_{\mathrm{L}^2(\Gamma)}+\frac{1}{2}\|e_w^{n-1}\|^2_{\mathrm{L}^2(\Gamma)}-\frac{1}{2}\|e^n\|^2_{\mathrm{L}^2(\Gamma)}\\ &-\frac{1}{2}\|e_w^n\|^2_{\mathrm{L}^2(\Gamma)}+C_{18}\Delta t\left(\|e^n\|^2_{\mathrm{L}^2(\Gamma)}+\|e_w^n\|^2_{\mathrm{L}^2(\Gamma)}\right)\\ &+\Delta t\mathrm{L}_0\left(\|e^{n-1}\|^2_{\mathrm{L}^2(\Gamma)}+\|e_w^{n-1}\|^2_{\mathrm{L}^2(\Gamma)}\right)\\ &+\frac{\Delta t^3}{4}\left(\|v_{tt}(\xi^n)\|^2_{\mathrm{L}^2(\Gamma)}+\|w_{tt}(\xi_1^n)\|^2_{\mathrm{L}^2(\Gamma)}\right)\\ &+\frac{\Delta t^3\mathrm{L}_0}{2}\left(\|v_t(\delta_1^n)\|^2_{\mathrm{L}^2(\Gamma)}+\|v_t(\delta_3^n)\|^2_{\mathrm{L}^2(\Gamma)}\right)\\ &+\frac{\Delta t^3\mathrm{L}_0}{2}\left(\|w_t(\delta_2^n)\|^2_{\mathrm{L}^2(\Gamma)}+\|w_t(\delta_4^n)\|^2_{\mathrm{L}^2(\Gamma)}\right)\\ &+\frac{\Delta t^{3-\epsilon}\mathrm{L}_1^2|\Omega_e|}{2}+\frac{\Delta t^{3-\epsilon}\mathrm{L}_1^2|\Omega_i|}{2},\end{aligned}\tag{3.81}$$

for some constant $C_{18}>0$. Assuming that $\|e^0\|_{\mathrm{L}^2(\Gamma)}=0$ and $\|e_w^0\|_{\mathrm{L}^2(\Gamma)}=0$ and summing (3.81) from 1 to N yield

$$\begin{aligned}\sum_{n=1}^{N}\Delta t\int_{\Omega_e}|\nabla e_e^n|^2 \;+\; \sum_{n=1}^{N}\Delta t\int_{\Omega_i}|\nabla e_i^n|^2 \;\le\; & C_{19}\Delta t\sum_{n=1}^{N}\left(\|e^n\|^2_{\mathrm{L}^2(\Gamma)}+\|e_w^n\|^2_{\mathrm{L}^2(\Gamma)}\right)\\ &+C_{20}\Delta t^2\left(\|v_{tt}\|^2_{\mathrm{L}^2(0,\mathrm{T},\mathrm{L}^2(\Gamma))}+\|w_{tt}\|^2_{\mathrm{L}^2(0,\mathrm{T},\mathrm{L}^2(\Gamma))}\right)\\ &+C_{21}\Delta t^2\left(\|v_t\|^2_{\mathrm{L}^2(0,\mathrm{T},\mathrm{L}^2(\Gamma))}+\|w_t\|^2_{\mathrm{L}^2(0,\mathrm{T},\mathrm{L}^2(\Gamma))}\right)+C_{22}\Delta t^{2-\epsilon},\end{aligned}$$

for some constants C_{19}, C_{20}, $C_{21}>0$ and $C_{22}=\dfrac{\mathrm{L}_1^2\mathrm{T}}{2\alpha_4}\left(|\Omega_i|+|\Omega_e|\right)>0$. Considering the a priori estimate (3.71), we obtain

$$\begin{aligned}\sum_{n=1}^{N}\Delta t\int_{\Omega_e}|\nabla e_e^n|^2 \;+\; \sum_{n=1}^{N}\Delta t\int_{\Omega_i}|\nabla e_i^n|^2 \;\le\; & C_{23}\Delta t^2\left(\|v_{tt}\|^2_{\mathrm{L}^2(0,\mathrm{T},\mathrm{L}^2(\Gamma))}+\|w_{tt}\|^2_{\mathrm{L}^2(0,\mathrm{T},\mathrm{L}^2(\Gamma))}\right)\\ &+C_{23}\Delta t^2\left(\|v_t\|^2_{\mathrm{L}^2(0,\mathrm{T},\mathrm{L}^2(\Gamma))}+\|w_t\|^2_{\mathrm{L}^2(0,\mathrm{T},\mathrm{L}^2(\Gamma))}\right)+C_{23}\Delta t^{2-\epsilon},\end{aligned}\tag{3.82}$$

for some constant $C_{23}>0$.

□

Remark 3.6.5. *The choice of the stimulation currents,* $\mathrm{I}_{i,stim}^{n-1}$ *and* $\mathrm{I}_{e,stim}^{n-1}$ *at time* t_{n-1} *in*

the FBE scheme, yields only the convergence rate

$$\|e^n\|_{\mathrm{L}^2(\Gamma)} + \|e_w^n\|_{\mathrm{L}^2(\Gamma)} = \mathcal{O}(\Delta t^{1-\frac{\epsilon}{2}}),$$

$$\left(\sum_{n=1}^{N} \Delta t \int_{\Omega_e} |\nabla e_e^n|^2 + \sum_{n=1}^{N} \Delta t \int_{\Omega_i} |\nabla e_i^n|^2\right)^{\frac{1}{2}} = \mathcal{O}(\Delta t^{1-\frac{\epsilon}{2}}),$$

for a fixed $\epsilon > 0$. One can avoid this order reduction by considering in the discretization, the stimulation currents $\mathrm{I}_{i,stim}^n$ and $\mathrm{I}_{e,stim}^n$ at time t_n instead of $\mathrm{I}_{i,stim}^{n-1}$ and $\mathrm{I}_{e,stim}^{n-1}$ at time t_{n-1}.

3.6.6 Convergence Analysis of BDF2 Scheme

Finally, we derive an error estimate for the BDF2 method (3.32)-(3.34). The approximation of the time derivative, $\frac{\partial v}{\partial t}$, using the current value v^n and two previously computed approximations v^{n-1} and v^{n-2} in the BDF2 scheme, requires the analysis of a three-term recurrence compared to the two-term recurrence needed for the BE method. The finite difference in time appearing on the interface Γ needs to be treated with care. The stability condition is of the same type as that of the BE method. However, the error estimates exhibit third order derivative with respect to time of the variables v and w.
By subtracting equation (3.32) from equation (3.10), we have on account of (3.47),

$$\begin{aligned}\int_{\Omega_e} \sigma_e \nabla e_e^n \cdot \nabla \varphi_e \; - \; & \int_{\Gamma} \left[\frac{3v^n - 4v^{n-1} + v^{n-2}}{2\Delta t} - v_t(t_n)\right] \varphi_e \\ - \; & \int_{\Gamma} [f(v^n, w^n) - f(v(t_n), w(t_n)]\varphi_e = \int_{\Omega_e} (\mathrm{I}_{e,stim}^n - \mathrm{I}_{e,stim}(t_n))\varphi_e \cdot \end{aligned} \tag{3.83}$$

Using Taylor's series, we have

$$v_t(t_n) = \frac{3v(t_n) - 4v(t_{n-1}) + v(t_{n-2})}{2\Delta t} + \frac{\Delta t^2}{3} v_{ttt}(\xi^n), \tag{3.84}$$

where ξ^n is some point between t_{n-2} and t_n.
Replacing (3.84) in (3.83), we write

$$\begin{aligned}\int_{\Omega_e} \sigma_e \nabla e_e^n \cdot \nabla \varphi_e - \int_{\Gamma} \left[\frac{3e^n - 4e^{n-1} + e^{n-2}}{2\Delta t}\right] \varphi_e \; - \; & \int_{\Gamma} [f(v^n, w^n) - f(v(t_n), w(t_n))]\varphi_e \\ = \; & -\int_{\Gamma} \frac{\Delta t^2}{3} v_{ttt}(\xi^n)\varphi_e. \end{aligned} \tag{3.85}$$

Similarly,

$$\int_{\Omega_i} \sigma_i \nabla e_i^n \cdot \nabla \varphi_i + \int_\Gamma \left[\frac{3e^n - 4e^{n-1} + e^{n-2}}{2\Delta t}\right] \varphi_i \quad + \quad \int_\Gamma [f(v^n, w^n) - f(v(t_n), w(t_n))]\varphi_i$$
$$= \int_\Gamma \frac{\Delta t^2}{3} v_{ttt}(\xi_3^n)\varphi_i. \tag{3.86}$$

Adding equations (3.85) and (3.86), we write

$$\int_{\Omega_e} \sigma_e \nabla e_e^n \cdot \nabla \varphi_e \quad + \quad \int_{\Omega_i} \sigma_i \nabla e_i^n \cdot \nabla \varphi_i + \int_\Gamma \left[\frac{3e^n - 4e^{n-1} + e^{n-2}}{2\Delta t}\right] (\varphi_i - \varphi_e)$$
$$+ \quad \int_\Gamma [f(v^n, w^n) - f(v(t_n), w(t_n))] (\varphi_i - \varphi_e)$$
$$= \quad \int_\Gamma \frac{\Delta t^2}{3} v_{ttt}(\xi_3^n)(\varphi_i - \varphi_e) \cdot \tag{3.87}$$

Similarly, by subtracting equation (3.34) from equation (3.12), we have on account of (3.53) and (3.84),

$$\int_\Gamma (3e_w^n - 4e_w^{n-1} + e_w^{n-2})\varphi = 2\Delta t \int_\Gamma (g(v^n, w^n) - g(v(t_n), w(t_n))\varphi + \frac{2\Delta t^3}{3} \int_\Gamma w_{ttt}(\xi_4^n)\varphi. \tag{3.88}$$

3.6.7 A priori estimates

The following a priori estimates hold on e^n, e_i^n,e_e^n and e_w^n.

Proposition 3.6.4. *Let $n \in \{1, 2, \cdots, N\}$. Assume that $v, w \in \mathrm{C}^3([0, \mathrm{T}]; \mathrm{L}^2(\Gamma))$, $\|e^0\|_{\mathrm{L}^2(\Gamma)} = 0$, and $\|e_w^0\|_{\mathrm{L}^2(\Gamma)} = 0$, and that there exists a constant $0 < \alpha_5 < 1$ such that $\Delta t < \dfrac{1 - \alpha_5}{\frac{2}{3} + 8L_0}$. Then, the following a priori estimates hold*

$$\|e^n\|_{\mathrm{L}^2(\Gamma)} + \|e_w^n\|_{\mathrm{L}^2(\Gamma)} \quad \leq \quad C_{28}\Delta t^2 \left(\|v_{tt}(\xi_1^1)\|_{\mathrm{L}^2(\Gamma)} + \|w_{tt}(\xi_2^1)\|_{\mathrm{L}^2(\Gamma)}\right) \exp\left(\frac{TC_{25}}{2\alpha_5}\right)$$
$$+ \quad C_{29}\Delta t^2 \left(\|v_{ttt}\|_{\mathrm{L}^2(0,\mathrm{T},\mathrm{L}^2(\Gamma))} + \|w_{ttt}\|_{\mathrm{L}^2(0,\mathrm{T},\mathrm{L}^2(\Gamma))}\right) \exp\left(\frac{TC_{25}}{2\alpha_5}\right) \cdot \tag{3.89}$$

$$\sum_{n=2}^{N} \Delta t \left(\int_{\Omega_e} |\nabla e_e^n|^2 + \int_{\Omega_i} |\nabla e_i^n|^2\right) \quad \leq \quad C_{30}\Delta t^4 \left(\|v_{ttt}\|_{\mathrm{L}^2(0,\mathrm{T},\mathrm{L}^2(\Gamma))} + \|w_{ttt}\|_{\mathrm{L}^2(0,\mathrm{T},\mathrm{L}^2(\Gamma))}\right)^2 +$$
$$C_{31}\Delta t^4 \left(\|v_{tt}(\xi_1^1)\|_{\mathrm{L}^2(\Gamma)} + \|w_{tt}(\xi_2^1)\|_{\mathrm{L}^2(\Gamma)}\right)^2, \tag{3.90}$$

for some constants $C_{28}, C_{29}, C_{30}, C_{31} > 0$, *and* $\xi_i^1 = \xi_i^1(x)$, $x \in \Gamma$, $i = 1, 2$, *are some points between* t_0 *and* t_1.

Proof. Let us start with the inequality (3.89). Setting $\varphi_i = e_i^n$ and $\varphi_e = e_e^n$ in (3.87), we have

$$\begin{aligned} 4\Delta t \int_{\Omega_e} \sigma_e |\nabla e_e^n|^2 \;+\; 4\Delta t \int_{\Omega_i} \sigma_i |\nabla e_i^n|^2 + \int_\Gamma \left(6e^n - 8e^{n-1} + 2e^{n-2}\right) e^n \\ +\; 4\Delta t \int_\Gamma [f(v^n, w^n) - f(v(t_n), w(t_n))] e^n = \frac{4\Delta t^3}{3} \int_\Gamma v_{ttt}(\xi_3^n) e^n. \end{aligned}$$

Using the identity,

$$\begin{aligned} \left(6e^n - 8e^{n-1} + 2e^{n-2}\right) e^n &= (e^n)^2 - (e^{n-1})^2 + (2e^n - e^{n-1})^2 - (2e^{n-1} - e^{n-2})^2 \\ &+ (e^n - 2e^{n-1} + e^{n-2})^2, \end{aligned} \tag{3.91}$$

it follows that

$$\begin{aligned} 4\beta\Delta t \int_{\Omega_e} |\nabla e_e^n|^2 \;+\; 4\beta\Delta t \int_{\Omega_i} |\nabla e_i^n|^2 + \|e^n\|^2_{\mathrm{L}^2(\Gamma)} - \|e^{n-1}\|^2_{\mathrm{L}^2(\Gamma)} + \|2e^n - e^{n-1}\|^2_{\mathrm{L}^2(\Gamma)} \\ -\; \|2e^{n-1} - e^{n-2}\|^2_{\mathrm{L}^2(\Gamma)} + \|e^n - 2e^{n-1} + e^{n-2}\|^2_{\mathrm{L}^2(\Gamma)} \\ \leq\; 4\Delta t \mathrm{L}_f \|e^n\|^2_{\mathrm{L}^2(\Gamma)} + 4\Delta t \mathrm{L}_f \|e^n\|_{\mathrm{L}^2(\Gamma)} \|e_w^n\|_{\mathrm{L}^2(\Gamma)} \\ +\; \frac{4\Delta t^3}{3} \|v_{ttt}(\xi_3^n)\|_{\mathrm{L}^2(\Gamma)} \|e^n\|_{\mathrm{L}^2(\Gamma)}. \end{aligned} \tag{3.92}$$

We deduce from the previous inequality that,

$$\begin{aligned} \|e^n\|^2_{\mathrm{L}^2(\Gamma)} - \|e^{n-1}\|^2_{\mathrm{L}^2(\Gamma)} \;+\; \|2e^n - e^{n-1}\|^2_{\mathrm{L}^2(\Gamma)} - \|2e^{n-1} - e^{n-2}\|^2_{\mathrm{L}^2(\Gamma)} \\ \leq\; 4\Delta t \mathrm{L}_f \|e^n\|^2_{\mathrm{L}^2(\Gamma)} + 4\Delta t \mathrm{L}_f \|e^n\|_{\mathrm{L}^2(\Gamma)} \|e_w^n\|_{\mathrm{L}^2(\Gamma)} \\ +\; \frac{4\Delta t^3}{3} \|v_{ttt}(\xi_3^n)\|_{\mathrm{L}^2(\Gamma)} \|e^n\|_{\mathrm{L}^2(\Gamma)}. \end{aligned} \tag{3.93}$$

Setting $\varphi = e_w^n$ in (3.88), considering (3.15) and the identity (3.91), we write

$$\begin{aligned} \|e_w^n\|^2_{\mathrm{L}^2(\Gamma)} - \|e_w^{n-1}\|^2_{\mathrm{L}^2(\Gamma)} \;+\; \|2e_w^n - e_w^{n-1}\|^2_{\mathrm{L}^2(\Gamma)} - \|2e_w^{n-1} - e_w^{n-2}\|^2_{\mathrm{L}^2(\Gamma)} \\ +\; \|e_w^n - 2e_w^{n-1} + e_w^{n-2}\|^2_{\mathrm{L}^2(\Gamma)} \\ \leq\; 4\Delta t \mathrm{L}_g \|e_w^n\|^2_{\mathrm{L}^2(\Gamma)} + 4\Delta t \mathrm{L}_g \|e^n\|_{\mathrm{L}^2(\Gamma)} \|e_w^n\|_{\mathrm{L}^2(\Gamma)} \\ +\; \frac{4\Delta t^3}{3} \|w_{ttt}(\xi_4^n)\|_{\mathrm{L}^2(\Gamma)} \|e_w^n\|_{\mathrm{L}^2(\Gamma)}. \end{aligned} \tag{3.94}$$

Then,

$$\begin{aligned}\|e_w^n\|^2_{\mathrm{L}^2(\Gamma)} - \|e_w^{n-1}\|^2_{\mathrm{L}^2(\Gamma)} &+ \|2e_w^n - e_w^{n-1}\|^2_{\mathrm{L}^2(\Gamma)} - \|2e_w^{n-1} - e_w^{n-2}\|^2_{\mathrm{L}^2(\Gamma)} \\ &\leq 4\Delta t \mathrm{L}_g \|e_w^n\|^2_{\mathrm{L}^2(\Gamma)} + 4\Delta t \mathrm{L}_g \|e^n\|_{\mathrm{L}^2(\Gamma)} \|e_w^n\|_{\mathrm{L}^2(\Gamma)} \\ &+ \frac{4\Delta t^3}{3} \|w_{ttt}(\xi_4^n)\|_{\mathrm{L}^2(\Gamma)} \|e_w^n\|_{\mathrm{L}^2(\Gamma)}. \end{aligned} \tag{3.95}$$

Adding up the inequalities (3.93) and (3.95) and using Young's inequality, give

$$\begin{aligned}\|e^n\|^2_{\mathrm{L}^2(\Gamma)} + \|e_w^n\|^2_{\mathrm{L}^2(\Gamma)} &- \|e^{n-1}\|^2_{\mathrm{L}^2(\Gamma)} - \|e_w^{n-1}\|^2_{\mathrm{L}^2(\Gamma)} + \|2e^n - e^{n-1}\|^2_{\mathrm{L}^2(\Gamma)} \\ &+ \|2e_w^n - e_w^{n-1}\|^2_{\mathrm{L}^2(\Gamma)} - \|2e^{n-1} - e^{n-2}\|^2_{\mathrm{L}^2(\Gamma)} - \|2e_w^{n-1} - e_w^{n-2}\|^2_{\mathrm{L}^2(\Gamma)} \\ &\leq C_{25}\Delta t \left(\|e^n\|^2_{\mathrm{L}^2(\Gamma)} + \|e_w^n\|^2_{\mathrm{L}^2(\Gamma)} \right) \\ &+ \frac{2\Delta t^5}{3} \left(\|v_{ttt}(\xi_3^n)\|^2_{\mathrm{L}^2(\Gamma)} + \|w_{ttt}(\xi_4^n)\|^2_{\mathrm{L}^2(\Gamma)} \right), \end{aligned} \tag{3.96}$$

where $C_{25} = \left(\frac{2}{3} + 8\mathrm{L}_0\right) > 0$.
Summing up the previous inequality for $2 \leq \mathrm{k} \leq \mathrm{n} \leq \mathrm{N}$, we have

$$\begin{aligned}\|e^n\|^2_{\mathrm{L}^2(\Gamma)} + \|e_w^n\|^2_{\mathrm{L}^2(\Gamma)} &+ \|2e^n - e^{n-1}\|^2_{\mathrm{L}^2(\Gamma)} + \|2e_w^n - e_w^{n-1}\|^2_{\mathrm{L}^2(\Gamma)} \\ &\leq \|e^1\|^2_{\mathrm{L}^2(\Gamma)} + \|e_w^1\|^2_{\mathrm{L}^2(\Gamma)} + \|2e^1 - e^0\|^2_{\mathrm{L}^2(\Gamma)} + \|2e_w^1 - e_w^0\|^2_{\mathrm{L}^2(\Gamma)} \\ &+ \sum_{k=2}^{n} C_{25}\Delta t \left(\|e^k\|^2_{\mathrm{L}^2(\Gamma)} + \|e_w^k\|^2_{\mathrm{L}^2(\Gamma)} \right) \\ &+ \frac{2\Delta t^5}{3} \sum_{k=2}^{n} \left(\|v_{ttt}(\xi_3^n)\|^2_{\mathrm{L}^2(\Gamma)} + \|w_{ttt}(\xi_4^n)\|^2_{\mathrm{L}^2(\Gamma)} \right). \end{aligned}$$

Using $\|e^0\|_{\mathrm{L}^2(\Gamma)} = 0$ and $\|e_w^0\|_{\mathrm{L}^2(\Gamma)} = 0$, we obtain

$$\begin{aligned}(1 - C_{25}\Delta t) \left(\|e^n\|^2_{\mathrm{L}^2(\Gamma)} + \|e_w^n\|^2_{\mathrm{L}^2(\Gamma)} \right) &\leq 3 \left(\|e^1\|^2_{\mathrm{L}^2(\Gamma)} + \|e_w^1\|^2_{\mathrm{L}^2(\Gamma)} \right) \\ &+ \sum_{k=1}^{n-1} C_{25}\Delta t \left(\|e^k\|^2_{\mathrm{L}^2(\Gamma)} + \|e_w^k\|^2_{\mathrm{L}^2(\Gamma)} \right) \\ &+ \frac{2\Delta t^4}{3} \left(\|v_{ttt}\|^2_{\mathrm{L}^2(0,\mathrm{T},\mathrm{L}^2(\Gamma))} + \|w_{ttt}\|^2_{\mathrm{L}^2(0,\mathrm{T},\mathrm{L}^2(\Gamma))} \right). \end{aligned} \tag{3.97}$$

Second order BDF scheme is reduced to BE scheme in the first time step. Therefore, the term $\|e^1\|^2_{\mathrm{L}^2(\Gamma)} + \|e_w^1\|^2_{\mathrm{L}^2(\Gamma)}$ in (3.97) can be bounded using the inequality (3.62), that is,

$$(1 - \Delta t L_0) \left(\|e^1\|_{\mathrm{L}^2(\Gamma)} + \|e_w^1\|_{\mathrm{L}^2(\Gamma)} \right) \leq \frac{\Delta t^2}{2} \left(\|v_{tt}(\xi_1^1)\|_{\mathrm{L}^2(\Gamma)} + \|w_{tt}(\xi_2^1)\|_{\mathrm{L}^2(\Gamma)} \right),$$

where $\xi_i^1 = \xi_i^1(x),\ x \in \Gamma,\ i = 1, 2$, are some points between t_0 and t_1. Using the constant α_2 from Proposition 3.6.2, we write

$$\|e^1\|_{\mathrm{L}^2(\Gamma)} + \|e_w^1\|_{\mathrm{L}^2(\Gamma)} \leq \frac{\Delta t^2}{2\alpha_2}\left(\|v_{tt}(\xi_1^1)\|_{\mathrm{L}^2(\Gamma)} + \|w_{tt}(\xi_2^1)\|_{\mathrm{L}^2(\Gamma)}\right). \tag{3.98}$$

Replacing (3.98) in the inequality (3.97) yields,

$$\begin{aligned}(1 - C_{25}\Delta t)\left(\|e^n\|_{\mathrm{L}^2(\Gamma)}^2 + \|e_w^n\|_{\mathrm{L}^2(\Gamma)}^2\right) &\leq \frac{3\Delta t^4}{4\alpha_2^2}\left(\|v_{tt}(\xi_1^1)\|_{\mathrm{L}^2(\Gamma)} + \|w_{tt}(\xi_2^1)\|_{\mathrm{L}^2(\Gamma)}\right)^2 \\ &+ \sum_{k=1}^{n-1} C_{25}\Delta t\left(\|e^k\|_{\mathrm{L}^2(\Gamma)}^2 + \|e_w^k\|_{\mathrm{L}^2(\Gamma)}^2\right) + \frac{2\Delta t^4}{3}\left(\|v_{ttt}\|_{\mathrm{L}^2(0,\mathrm{T},\mathrm{L}^2(\Gamma))}^2\right) \\ &+ \frac{2\Delta t^4}{3}\left(\|w_{ttt}\|_{\mathrm{L}^2(0,\mathrm{T},\mathrm{L}^2(\Gamma))}^2\right).\end{aligned}$$

Using the constant α_5 from the hypothesis, it follows that

$$\begin{aligned}\|e^n\|_{\mathrm{L}^2(\Gamma)}^2 + \|e_w^n\|_{\mathrm{L}^2(\Gamma)}^2 &\leq \frac{3\Delta t^4}{4\alpha_2^2\alpha_5}\left(\|v_{tt}(\xi_1^1)\|_{\mathrm{L}^2(\Gamma)} + \|w_{tt}(\xi_2^1)\|_{\mathrm{L}^2(\Gamma)}\right)^2 \\ &+ \sum_{k=1}^{n-1}\frac{C_{25}\Delta t}{\alpha_5}\left(\|e^k\|_{\mathrm{L}^2(\Gamma)}^2 + \|e_w^k\|_{\mathrm{L}^2(\Gamma)}^2\right) \\ &+ \frac{2\Delta t^4}{3\alpha_5}\left(\|v_{ttt}\|_{\mathrm{L}^2(0,\mathrm{T},\mathrm{L}^2(\Gamma))}^2 + \|w_{ttt}\|_{\mathrm{L}^2(0,\mathrm{T},\mathrm{L}^2(\Gamma))}^2\right).\end{aligned}$$

Applying Lemma 3.6.1, we obtain

$$\begin{aligned}\|e^n\|_{\mathrm{L}^2(\Gamma)}^2 + \|e_w^n\|_{\mathrm{L}^2(\Gamma)}^2 &\leq C_{26}\Delta t^4\left(\|v_{tt}(\xi_1^1)\|_{\mathrm{L}^2(\Gamma)} + \|w_{tt}(\xi_2^1)\|_{\mathrm{L}^2(\Gamma)}\right)^2\exp\left(\frac{TC_{25}}{\alpha_5}\right) \\ &+ \mathrm{C}_{27}\Delta\mathrm{t}^4\left(\|v_{ttt}\|_{\mathrm{L}^2(0,\mathrm{T},\mathrm{L}^2(\Gamma))} + \|w_{ttt}\|_{\mathrm{L}^2(0,\mathrm{T},\mathrm{L}^2(\Gamma))}\right)^2\exp\left(\frac{\mathrm{TC}_{25}}{\alpha_5}\right),\end{aligned} \tag{3.99}$$

for some constants $C_i > 0,\ i = 26, 27$. Finally,

$$\begin{aligned}\|e^n\|_{\mathrm{L}^2(\Gamma)} + \|e_w^n\|_{\mathrm{L}^2(\Gamma)} &\leq C_{28}\Delta t^2\left(\|v_{tt}(\xi_1^1)\|_{\mathrm{L}^2(\Gamma)} + \|w_{tt}(\xi_2^1)\|_{\mathrm{L}^2(\Gamma)}\right)\exp\left(\frac{\mathrm{TC}_{25}}{2\alpha_5}\right) \\ &+ \mathrm{C}_{29}\Delta\mathrm{t}^2\left(\|v_{ttt}\|_{\mathrm{L}^2(0,\mathrm{T},\mathrm{L}^2(\Gamma))} + \|w_{ttt}\|_{\mathrm{L}^2(0,\mathrm{T},\mathrm{L}^2(\Gamma))}\right)\exp\left(\frac{\mathrm{TC}_{25}}{2\alpha_5}\right),\end{aligned}$$

for some constants $C_i > 0,\ i = 28, 29$.

Now, we are in position of proving the inequality (3.90). Applying Young's inequality to the sum of (3.92) and (3.94) and summing up from 2 to N, the resulting inequality

yield,

$$\begin{aligned} 4\beta\sum_{n=2}^{N}\Delta t\int_{\Omega_e}|\nabla e_e^n|^2 \;&+\; 4\beta\sum_{n=2}^{N}\Delta t\int_{\Omega_i}|\nabla e_i^n|^2+\|e^N\|^2_{\mathrm{L}^2(\Gamma)}+\|e_w^N\|^2_{\mathrm{L}^2(\Gamma)}+\|2e^N-e^{N-1}\|^2_{\mathrm{L}^2(\Gamma)}\\ &+\; \|2e_w^N-e_w^{N-1}\|^2_{\mathrm{L}^2(\Gamma)}-3\|e^1\|^2_{\mathrm{L}^2(\Gamma)}-3\|e_w^1\|^2_{\mathrm{L}^2(\Gamma)}\\ &\leq\; \frac{2\Delta \mathrm{t}^5}{3}\sum_{n=2}^{N}\left(\|v_{ttt}(\xi_3^n)\|^2_{\mathrm{L}^2(\Gamma)}+\|w_{ttt}(\xi_4^n)\|^2_{\mathrm{L}^2(\Gamma)}\right)\\ &+\; C_{25}\Delta t\sum_{n=2}^{N}\left(\|e^n\|^2_{\mathrm{L}^2(\Gamma)}+\|e_w^n\|^2_{\mathrm{L}^2(\Gamma)}\right), \end{aligned}$$

using $\|e^0\|_{\mathrm{L}^2(\Gamma)}=0$ and $\|e_w^0\|_{\mathrm{L}^2(\Gamma)}=0$.
Condidering (3.98) and (3.99) yield

$$\begin{aligned} \sum_{n=2}^{N}\Delta t\int_{\Omega_e}|\nabla e_e^n|^2+\sum_{n=2}^{N}\Delta t\int_{\Omega_i}|\nabla e_i^n|^2 \;&\leq\; C_{30}\Delta t^4\left(\|v_{ttt}\|_{\mathrm{L}^2(0,\mathrm{T},\mathrm{L}^2(\Gamma))}+\|w_{ttt}\|_{\mathrm{L}^2(0,\mathrm{T},\mathrm{L}^2(\Gamma))}\right)^2\\ &+\; C_{31}\Delta t^4\left(\|v_{tt}(\xi_1^1)\|_{\mathrm{L}^2(\Gamma)}+\|w_{tt}(\xi_2^1)\|_{\mathrm{L}^2(\Gamma)}\right)^2, \end{aligned}$$

for some constants $C_{30}, C_{31}>0$ and $\xi_i^1=\xi_i^1(x),\ i=1,2,\ x\in\Gamma$, are some point between t_0 and t_1. □

3.7 Resolution of the Linear and Nonlinear Algebraic Systems

In this section, we consider a spatial discretization of the model through finite element methods. Our choice falls on the standard $\mathbb{P}_d$ Lagrange finite element method [20]. Let $\mathcal{T}_h$ be a partition of the domain $\overline{\Omega}$ into triangular elements. In this context the parameter h corresponds to the maximal size of the elements in the triangulation $\mathcal{T}_h$. Let us assume that the partition $\mathcal{T}_h=\mathcal{T}_{ih}\cup\mathcal{T}_{eh}$, where $\mathcal{T}_{ih}$ and $\mathcal{T}_{eh}$ are triangular element meshes of Ω_i and Ω_e, respectively, and $\mathcal{T}_{ih}\cap\mathcal{T}_{eh}=\varnothing$. The meshes $\mathcal{T}_{ih}$ and $\mathcal{T}_{eh}$ can be conformal or nonconformal on the interface Γ.
Let us define the following space of continuous piecewise linear functions:

$$\mathrm{W}_h=\left\{(u_i,u_e)\in\mathrm{C}(\overline{\Omega}_i)\times\mathrm{C}(\overline{\Omega}_e):\ u_i|_{\mathrm{K}}\in\mathbb{P}_d(\mathrm{K}),\ \forall\mathrm{K}\in\mathcal{T}_{ih};\ u_e|_{\mathrm{K}}\in\mathbb{P}_d(\mathrm{K}),\ \forall\mathrm{K}\in\mathcal{T}_{eh}\right\},$$

where $\mathbb{P}_d(\mathrm{K})$ is the set of polynomials in two variables, with real coefficients and of degree at most d on K. Let us assume that $\{x_k\}_{1\leqslant k\leqslant \mathrm{N}_h}$ is the set of all geometrical nodes of

the mesh. Let $\{(\Phi_{i,l}, \Phi_{e,k}),\ 1 \leqslant l \leqslant \mathrm{N}_{ih},\ 1 \leqslant k \leqslant \mathrm{N}_{eh}\}$ be a basis of the space W_h, where N_{eh} and N_{ih} are the total number of vertices of the elements in $\mathcal{T}_{eh}$ and $\mathcal{T}_{ih}$, respectively, $\mathrm{N}_h = \mathrm{N}_{eh} + \mathrm{N}_{ih}$. The basis function $(\Phi_{i,l}, \Phi_{e,k})$ is associated with the vertices x_l and x_k, for $1 \leqslant l \leqslant \mathrm{N}_{ih}$ and $1 \leqslant k \leqslant \mathrm{N}_{eh}$, respectively. It satifies the following conditions:

$$\begin{aligned} \Phi_{i,l}(x_j) &= \delta_{lj}, \quad 1 \leqslant l, j \leqslant \mathrm{N}_{ih}, \\ \Phi_{e,k}(x_j) &= \delta_{kj}, \quad 1 \leqslant k, j \leqslant \mathrm{N}_{eh}. \end{aligned}$$

Let $\{\Phi_j,\ 1 \leqslant j \leqslant \mathrm{N}_h^\Gamma\}$ be the basis function associated with the vertices $\{x_j\}_{1 \leqslant j \leqslant \mathrm{N}_h^\Gamma}$, where N_h^Γ is the total number of vertices of the elements on Γ. We are now in position to address the fully discretized problem based on the variational formulation of the previous section. We focus on the BE and FBE methods, for which we transform the system into matrix forms. Discrete problems using the BDF2 and SBDF2 methods can also be presented in matrix forms with similar structures.

3.7.1 Backward Euler Method

Recall that for any element $K \in \mathcal{T}_h = \mathcal{T}_{ih} \cup \mathcal{T}_{eh}$, if x_l is not a vertex of K, then we have $\Phi_{i,l}(x) = 0 = \Phi_{e,l}(x)$ for all $x \in K$. By setting for $n \in \{0, 1, \cdots, N\}$,

$$\begin{aligned} u_i^n &= \sum_{j=1}^{\mathrm{N}_{ih}} u_{i,j}^n \Phi_{i,j}, \quad u_e^n = \sum_{j=1}^{\mathrm{N}_{eh}} u_{e,j}^n \Phi_{e,j}, \quad w^n = \sum_{j=1}^{\mathrm{N}_h^\Gamma} w_j^n \Phi_j, \\ v^n &= (u_i^n - u_e^n)|_\Gamma, \qquad \varphi_i = \Phi_{i,l}, \quad \varphi_e = \Phi_{e,l} \quad \varphi = \Phi_l, \end{aligned}$$

we can rewrite the equations (3.19)- (3.20) under the following matrix form:

$$\mathrm{A}\mathrm{U}^n = \mathrm{F}^n,$$

$$\mathrm{A} = \begin{pmatrix} \mathrm{A}_i & \mathrm{M}_{\mathrm{ie}} \\ \mathrm{M}_{\mathrm{ei}} & \mathrm{A}_e \end{pmatrix}, \quad \mathrm{U}^n = \begin{pmatrix} \mathrm{U}_i^n \\ \mathrm{U}_e^n \end{pmatrix}, \quad \mathrm{F}^n = \begin{pmatrix} \mathrm{F}_i^n \\ \mathrm{F}_e^n \end{pmatrix},$$

where

$$\begin{aligned} (\mathrm{A}_i)_{lj} &= \int_{\Omega_i} \sigma_i \nabla \Phi_{i,j} \cdot \nabla \Phi_{i,l} + \frac{1}{\Delta t} \int_\Gamma \Phi_{i,j} \Phi_{i,l}, \quad 1 \leqslant j, l \leqslant \mathrm{N}_{ih}, \\ (\mathrm{M}_{ie})_{lj} &= -\frac{1}{\Delta t} \int_\Gamma \Phi_{e,j} \Phi_{i,l}, \quad 1 \leqslant j \leqslant \mathrm{N}_{eh},\ 1 \leqslant l \leqslant \mathrm{N}_{ih}, \\ \mathrm{U}_i^n &= \left(u_{i,1}^n, \cdots, u_{i,\mathrm{N}_{ih}}^n\right)^{\mathrm{T}}, \quad \mathrm{U}_e^n = \left(u_{e,1}^n, \cdots, u_{e,\mathrm{N}_{eh}}^n\right)^{\mathrm{T}}, \\ (\mathrm{F}_i^n)_l &= \int_{\Omega_i} \mathrm{I}_{i,stim}^n \Phi_{i,l} - \int_\Gamma f(v_h^n, w_h^n) \Phi_{i,l} + \frac{1}{\Delta t} \int_\Gamma v_h^{n-1} \Phi_{i,l}, \quad 1 \leqslant l \leqslant \mathrm{N}_{ih}. \end{aligned}$$

Simirlarly, $(\mathrm{A}_e)_{lj}$, $(\mathrm{M}_{ei})_{lj}$ and F_e^n are obtained by replacing $\Phi_{i,j}$, $\Phi_{i,l}$, $\Phi_{e,j}$ and Ω_i by $\Phi_{e,j}$, $\Phi_{e,l}$,$\Phi_{i,j}$ and Ω_e, respectively.
Given an initial guess $\mathrm{U}^{n,0}$, we use Picard's iterative method to solve the system

$$\mathrm{AU}^{n,k} = \mathrm{F}^{n,k-1}, \quad 1 \leqslant k \leqslant \mathrm{m},$$

where $\mathrm{F}^{n,k-1}$ is obtained from F^n by replacing v^n and w^n by $v^{n,k-1}$ and $w^{n,k-1}$, respectively. The variable $w^{n,k}$ is updated by solving the system

$$\mathrm{M}_\Gamma w^{n,k} = \mathrm{G}^{n,k-1}, \quad 1 \leqslant k \leqslant \mathrm{m}, \tag{3.100}$$

where

$$\begin{aligned}
(\mathrm{M}_\Gamma)_{lj} &= \frac{1}{\Delta t}\int_\Gamma \Phi_j \Phi_l, \quad 1 \leqslant j,l \leqslant \mathrm{N}_h^\Gamma \\
\left(\mathrm{G}^{n,k-1}\right)_l &= \int_\Gamma g(v_h^{n,k-1}, w_h^{n,k-1})\Phi_l + \frac{1}{\Delta t}\int_\Gamma w_h^{n-1}\Phi_l, \quad 1 \leqslant l \leqslant \mathrm{N}_h^\Gamma, \\
w^{n,k} &= \left(w_1^{n,k}, \cdots, w_{\mathrm{N}_h^\Gamma}^{n,k}\right)^{\mathrm{T}}.
\end{aligned}$$

We compute the L^2-norm of the error between two successive iterates $U^{n,k}$ and $U^{n,k-1}$. We stop the iteration when it is less than the tolerance $\mathrm{TOL} = 10^{-10}$. It is worth recalling that the convergence of Picard's method is not guaranteed.

3.7.2 Forward Backward Euler Method

The finite element approximation of (3.22)- (3.23) reduces to solving the linear system

$$\begin{aligned}
\mathrm{AU}^n &= \mathrm{F}^{n-1}, \\
\mathrm{F}^{n-1} &= \begin{pmatrix} \mathrm{F}_i^{n-1} \\ \mathrm{F}_e^{n-1} \end{pmatrix}
\end{aligned} \tag{3.101}$$

where the matrix A and the vector U^n are defined as in the previous section. The components of the vector F^{n-1} are written as follows:

$$\begin{aligned}
\mathrm{F}_i^{n-1} &= \left(\int_{\Omega_i} \mathrm{I}_{i,stim}^{n-1}\Phi_{i,l} - \int_\Gamma f(v^{n-1}, w^{n-1})\Phi_{i,l} + \frac{1}{\Delta t}\int_\Gamma v^{n-1}\Phi_{i,l}\right)_{1\leqslant l\leqslant \mathrm{N}_{ih}}, \\
\mathrm{F}_e^{n-1} &= \left(\int_{\Omega_e} \mathrm{I}_{e,stim}^{n-1}\Phi_{e,l} + \int_\Gamma f(v^{n-1}, w^{n-1})\Phi_{e,l} - \frac{1}{\Delta t}\int_\Gamma v^{n-1}\Phi_{e,l}\right)_{1\leqslant l\leqslant \mathrm{N}_{eh}}.
\end{aligned}$$

The variable w^n is updated by solving the system of ODEs (3.24), which in matrix form reads:

$$\mathrm{M}_\Gamma W^n = \mathrm{G}^{n-1},$$

where M_Γ is the same as in (3.100) and $\mathrm{G}^{n,k-1}$ is replacing by G^{n-1}.

3.8 Numerical Results

In this section, we perform numerical tests to verify that the order of convergence of the numerical methods agrees with what is expected based on the above a priori analysis. We use the method of manufactured solutions [58] to obtain a closed-form solution for the problem (3.1)-(3.6). We compute the L^2- norm errors between the manufactured solution and the approximate solution at a fixed final time and for a given sequence of decreasing time steps. Next, we carry out the same work for a test case with all parameters and model data properly scaled to mimic a single cardiac cell. Numerical solutions with larger Δt are compared to a numerical reference solution computed with the second order SBDF2 method using a small time step. Finally, we compare the computational time needed both while varying the time step and to reach a certain level of error.
We consider a 2D domain consisting of an extracellular domain Ω_e and a single cell Ω_i. The domains Ω_i and Ω_e are defined as follows, see Figure 3.1,

$$\begin{aligned} \Omega_i &= (10, 110) \times (10, 30)\,, \\ \Omega_e &= [(0, 120) \times (0, 40)] \setminus \overline{\Omega}_i\cdot \end{aligned}$$

The parameter values used in the simulations are given in Table 3.1. We implement our

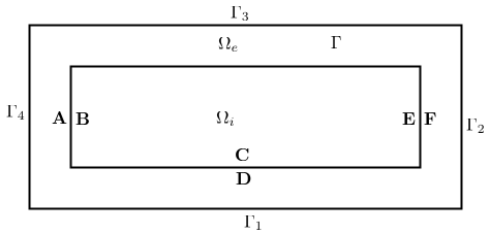

Figure 3.1: Sketch of $\Omega = \Omega_i \cup \Omega_e \cup \Gamma$, $\Gamma = \overline{\Omega}_i \cap \overline{\Omega}_e$, with points A&B, C&D, and E&F.

methods using the software Freefem++ and UMFPACK for solving linear systems.

Table 3.1: Parameter values used in the simulations.

Description	Parameters	Values	Units	References
Maximum potential	v_{max}	40	mV	[67, 71]
Resting potential	v_{rest}	-85	mV	[76, 32, 71]
Characteristic potential	v_m	125	mV	
Transmembrane capacitance	C_m	1	μF/cm^2	[76, 67, 80]
Intracellular conductivity	σ_i	3	mS/cm	[9, 67]
Extracellular conductivity	σ_e	20	mS/cm	[67, 68]
Characteristic time	T	1	ms	-
Characteristic length	L	10^{-4}	cm	-

3.8.1 Ionic Current Model

Our choice for the ionic model is based on a variant of the MS model described in Section 1.3 and initially introduced by Djabella et al. [18].

$$\frac{\partial v}{\partial t} = f(v,w) + \mathrm{I}_{stim}(t), \quad \text{with} \quad f(v,w) = \frac{1}{\tau_{in}} w v^2 (1-v) - \frac{1}{\tau_{out}} v, \tag{3.102}$$

$$\frac{\partial w}{\partial t} = g(v,w), \ \text{with} \ \ g(v,w) = \frac{1}{\tau_k} \left[(1-w_k)\,(1-w) - w_k w \right], \tag{3.103}$$

$$\begin{aligned} \tau_k(v, v_{gate}) &= \tau_{open} + (\tau_{close} - \tau_{open})\, w_k(v, v_{gate}) \\ w_k(v, v_{gate}) &= \frac{1}{2}(1 + \tanh(k(v - v_{gate}))), \end{aligned}$$

where k is a given parameter. The regularized MS model above shares the same characteristics as the standard MS model [45]. The main difference between both models is the introduction of the parameter k. The latter will be used to control the slope of the smooth function $w_k(v, v_{gate})$ seen as a regularized Heaviside function centered at $v = v_{gate}$. Throughout this chapter, we used the parameter values suggested by MS [45], see Table 3.2. The action potentials of the standard and regularized MS models with this set of parameters are illustrated in Figure 3.2. A value of $k = 5$ provides a solution that is close to the solution of the standard MS model.

Remark 3.8.2. *The function f fails to satisfy $f(v,w) \in \mathrm{L}^2(\Gamma)$ when v and w are only in $\mathrm{L}^2(\Gamma)$, because of the quadratic and cubic terms in v. For the latter reason, f does*

not satisfy the Lipschitz condition (3.14) *globally but only locally. This is good enough for the relevance of the theoretical error estimate because the solution remains bounded.*

Table 3.2: Parameter values in the MS model.

Parameters	τ_{in}	τ_{out}	τ_{open}	τ_{close}	v_{gate}
Values	0.3 ms	6 ms	120 ms	150 ms	0.13

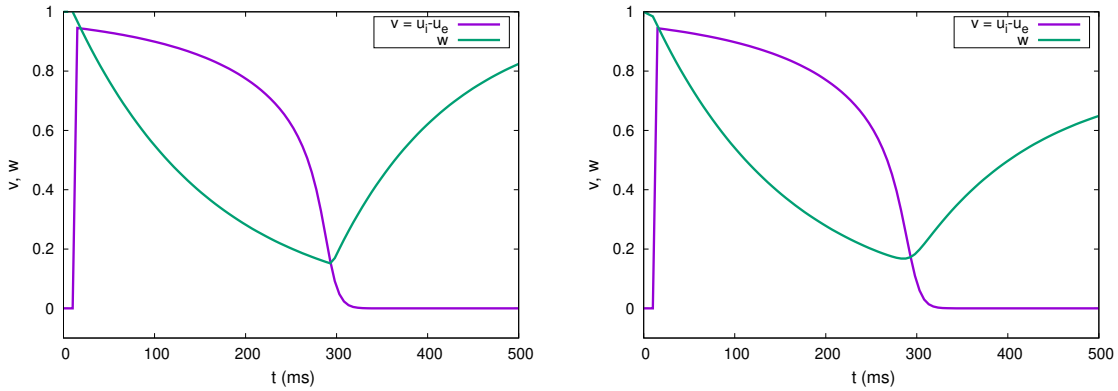

(a) AP of the original MS model.

(b) AP of the modified MS model with $k = 5$.

Figure 3.2: Action potential of both standard and regularized MS models.

3.8.3 Manufactured Solution

We assume that the conductivities σ_i and σ_e in the nondimensional problem (3.1)-(3.6) are scalar. We let $\sigma_i = \sigma_e = C_m = 1$, and set the stimulation currents $\mathrm{I}_{i,stim}$ and $\mathrm{I}_{e,stim}$ to zero, respectively. Considering the following activation function

$$\delta(t) = \frac{1}{1 + e^{-at}},$$

for some real number a, a manufactured solution of (3.1)-(3.6) is given by

$$u_{i,ex}(x, y, t) = 2\delta(t) + \varepsilon\left[(x - x_0) + (y - y_0)\right], \tag{3.104}$$

$$u_{e,ex}(x, y, t) = \delta(t) + \varepsilon\left[(x - x_0) + (y - y_0)\right], \tag{3.105}$$

$$v_{ex}(x, y, t) = \delta(t), \tag{3.106}$$

$$w_{ex}(x, y, t) = 2\delta(-t), \tag{3.107}$$

where (x_0, y_0) are the coordinates of the center of the cell Ω_i, $\varepsilon = \varepsilon(t)$ is a given function that controls the magnitude of the linear pertubation $z = (x - x_0) + (y - y_0)$. In our computation we assume $\varepsilon = 0.005$, and let $a = 8$ to achieve a faster transient. Considering the above manufactured solution, the problem (3.1)-(3.6) is modified with source terms

$$\begin{aligned}
-\nabla \cdot (\sigma_i \nabla u_i) &= 0 \quad \text{in } \Omega_i, && (3.108)\\
-\nabla \cdot (\sigma_e \nabla u_e) &= 0 \quad \text{in } \Omega_e, && (3.109)\\
s(x, y, t) &:= \frac{\partial v}{\partial t} + f(v, w) - \mathrm{I}_m \quad \text{on } \Gamma, && (3.110)\\
\sigma_e \nabla u_e \cdot n_e &= -\sigma_i \nabla u_i \cdot n_i = \mathrm{I}_m \quad \text{on } \Gamma, && (3.111)\\
v &= u_i - u_e \quad \text{on} \quad \Gamma, && (3.112)\\
\sigma_e \nabla u_e \cdot n_e &= g_e \quad \text{on} \quad \Gamma_e \cdot && (3.113)
\end{aligned}$$

It follows that

$$\begin{aligned}
s(x, y, t) &= a\delta(t)(1 - \delta(t)) + f(v_{ex}, w_{ex}) - \sigma_e \nabla u_{e_{ex}} \cdot n_e,\\
g_e(x, y, t) &= \sigma_e \nabla u_{e,ex} \cdot n_e,
\end{aligned}$$

where the function $f(v, w)$ is defined in (3.102). The variational formulations (3.10), (3.11) and (3.12) become, respectively,

$$\begin{aligned}
\int_{\Omega_e} \sigma_e \nabla u_e(t) \cdot \nabla \varphi_e \quad &- \quad \int_\Gamma \left(\frac{\partial v(t)}{\partial t} + f(v(t), w(t)) \right) \varphi_e \\
&= \int_{\partial\Omega_e \setminus \Gamma} g_e \varphi_e - \int_\Gamma s(x, y, t) \varphi_e, \qquad (3.114)
\end{aligned}$$

$$\int_{\Omega_i} \sigma_i \nabla u_i(t) \cdot \nabla \varphi_i + \int_\Gamma \left(\frac{\partial v(t)}{\partial t} + f(v(t), w(t)) \right) \varphi_i = \int_\Gamma s(x, y, t) \varphi_i, \qquad (3.115)$$

$$\int_\Gamma \frac{\partial w(t)}{\partial t} \varphi - \int_\Gamma g(v(t), w(t)) \varphi = \int_\Gamma \frac{\partial w_{ex}(t)}{\partial t} \varphi - \int_\Gamma g(v_{ex}(t), w_{ex}(t)) \varphi, \qquad (3.116)$$

for a.e. $t \in [0, \mathrm{T}]$. To handle the condition (3.8), we substract the average value of u_e at each time step during the computation. In the following, we denote by $u^h_{i,\Delta t}$, $u^h_{e,\Delta t}$, $v^h_{\Delta t}$, and $w^h_{\Delta t}$ the totally discrete variables associated to u_i, u_e, v, and w, respectively.

3.8.4 Convergence Tests with the Manufactured Solution

The convergence of the different numerical methods presented in Section 3.3 is now investigated. We choose a small final time T = 0.8ms, since the sharp rise of the manufactured solution occurs over a short time interval to mimick the cell depolarization. We compute the errors between the discretized solutions $u^h_{i,\Delta t}, u^h_{e,\Delta t}$, $v^h_{\Delta t}$, and $w^h_{\Delta t}$ and the exact solution $u_{i,ex}, u_{e,ex}, v_{ex}$, and w_{ex}, respectively. We compute the L^2-norms, $\|u^h_{i,\Delta t} - u_{i,ex}\|_{0,\Omega_i}$, $\|u^h_{e,\Delta t} - u_{e,ex}\|_{0,\Omega_e}$, $\|v^h_{\Delta t} - v_{ex}\|_{0,\Gamma}$ and $\|w^h_{\Delta t} - w_{ex}\|_{0,\Gamma}$ at the time t = 0.8ms. The domain $\Omega = \Omega_i \cup \Omega_e$ is discretized in space with 9088 triangles and 4745 vertices, on a fixed mesh, which corresponds to $(16n) \times (4n)$ and $(8n) \times (2n)$ nodes on the boundaries of the domains Ω_e and Ω_i, respectively, where $n = 10$. The mesh is unstructured and conformal on the interface Γ. The computation is performed for different choices of the time step Δt· Since the exact solution is $\mathbb{P}_1$ in space and is computed on $\mathbb{P}_1$ finite elements, the spatial discretization error is zero. We focus on the temporal discretization error. We assume that this error is proportional to Δt^q, where q is the convergence rate that can be estimated thanks to the formula

$$q \approx \frac{\log\left(|\mathrm{E}_{\Delta t_1}/\mathrm{E}_{\Delta t_2}|\right)}{\log\left(\Delta t_1/\Delta t_2\right)}, \tag{3.117}$$

where Δt_1 and Δt_2 are consecutive time-steps in a given sequence of decreasing time steps, and $\mathrm{E}_{\Delta t_1}$ and $\mathrm{E}_{\Delta t_2}$ are the corresponding errors. The results of the convergence tests are shown in Figure 3.3. These graphs illustrate how the errors on the variables, u_i, w and v, vary as the size of the time step decreases. In our computations, the error $\|u^h_{e,\Delta t} - u_{e,ex}\|_{0,\Omega_e}$ approches zero very quickly, therefore we do not plot the graph of the L^2-error on the variable u_e. Figures 3.3(a), 3.3(b) and 3.3(c) indicate that all numerical methods exhibit the expected order of convergence, when the time step Δt gets smaller. For first order methods, we observe that BE is twice as accurate as FBE and Godunov splitting on the variables u_i and v, for larger time steps. For smaller time steps and on the variable w, the three methods show the same level of accuracy. For second-order methods, we notice that BDF2 is two to three time more accurate on the variable u_i and v than SBDF2 for smaller time steps. On the variable w, SBDF2 is more than 10 times more accurate than BDF2 for larger Δt . For smaller Δt, we observe a superconvergence for the BDF2 method on the variable w. Globally, the BDF2 method is the most accurate of the two second order methods.

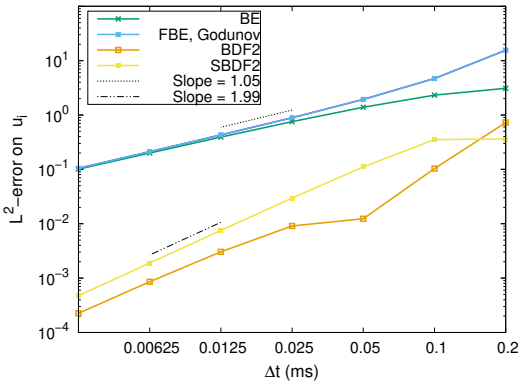

(a) L^2-norm error on the potential, u_i·

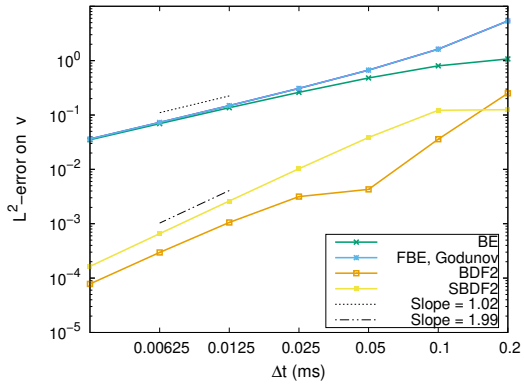

(b) L^2- norm error on the potential, v·

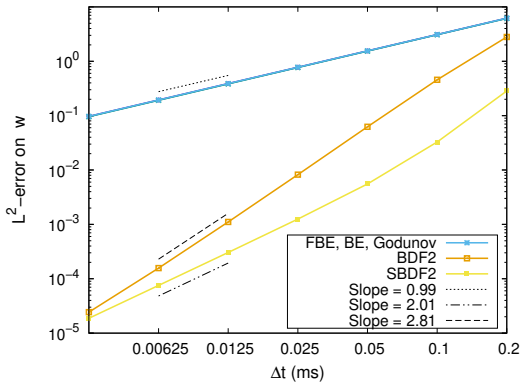

(c) L^2- norm error on the gating variable, w·

Figure 3.3: Graphs of the error as a function of the time step using the manufactured solution· In the upper panel, the graphs for the FBE and Godunov splitting methods are superposed. In the lower panel the graphs for the FBE, BE and Godunov splitting are superposed·

3.8.5 Convergence Tests with a Reference Solution

Using a manufactured solution, all methods studied showed their expected convergence order except on w where BDF2 shows a higher convergence order of 2.8. This time around, we would like to carry the same work as in the previous section using the solution of the physical problem (3.1)-(3.6) instead of a manufactured solution. Unfortunately, the exact solution for the physical problem is not available. We have to compute a reference solution using a very small time step, on a fixed mesh.

We first illustrate the evolution of the membrane potential over time. We use the second

order SBDF2 method and the time step $\Delta t = 0.001\texttt{ms}$. We visualize the propagation of an action potential in the cell Ω_i. In our study, the nondimensional potentials u_i, u_e, $v = u_i - u_e$ and the gating variable w vary from 0 to 1. We assume that the system starts in the stable equilibrium state, $(v, w) = (0, 1)$, as described by Mitchell and Schaeffer in [45]. We need an artificial external stimulus current, I_{stim}, to increase the voltage, v. We initiate an action potential by injecting a stimulus current of amplitude $A = 20\mu\texttt{A}$ near the membrane of the cell, see Figure 3.4. It is worth recalling that the stimulus current should be strong enough to raise the transmembrane potential above a certain value known as the threshold of excitation, so that the cell membrane can depolarize. The applied stimulation currents on Ω_e and Ω_i read as follows, respectively,

$$I_{e,stim}(x,y,t) = \begin{cases} -20\exp\left(\frac{-1}{R^2-|t-t_0|^2}\right)\exp\left(\frac{1}{R^2}\right), & |t-t_0| < R,\ |x-8.5| < 1, \quad \text{and} \\ & |y-20| < 10, \\ 0 & \text{otherwise}, \end{cases}$$

$$I_{i,stim}(x,y,t) = \begin{cases} 20\exp\left(\frac{-1}{R^2-|t-t_0|^2}\right)\exp\left(\frac{1}{R^2}\right), & |t-t_0| < R,\ |x-11.5| < 1, \ \text{and} \\ & |y-20| < 10, \\ 0 & \text{otherwise}, \end{cases}$$

where t_0 is the midpoint of the time interval $[-R + t_0, R + t_0]$, during which the stimulus is maintained, R is half the length of the interval. In our study, we set $t_0 = 10.5\texttt{ms}$ and

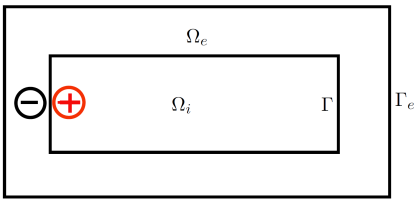

Figure 3.4: Stimulation currents on Ω_e and Ω_i.

$R = 0.3\texttt{ms}$. The potential v is initialized at 0. Figures 3.5 and 3.6 depict the evolution of the potentials u_i and u_e over the first $360\texttt{ms}$ out of $500\texttt{ms}$ for the whole simulation, in the domains Ω_e and Ω_i, respectively. Figure 3.6 shows in more details the spatial variation of the potential u_e at time $t = 10.55\texttt{ms}$ during the stimulation phase. The time $t = 10.22\texttt{ms}$ marks the beginning of the stimulations, both potentials u_i and u_e are around 0. The time interval $t = 10.4\texttt{ms}$ to $t = 10.8\texttt{ms}$ corresponds to the polarized state of the cell.

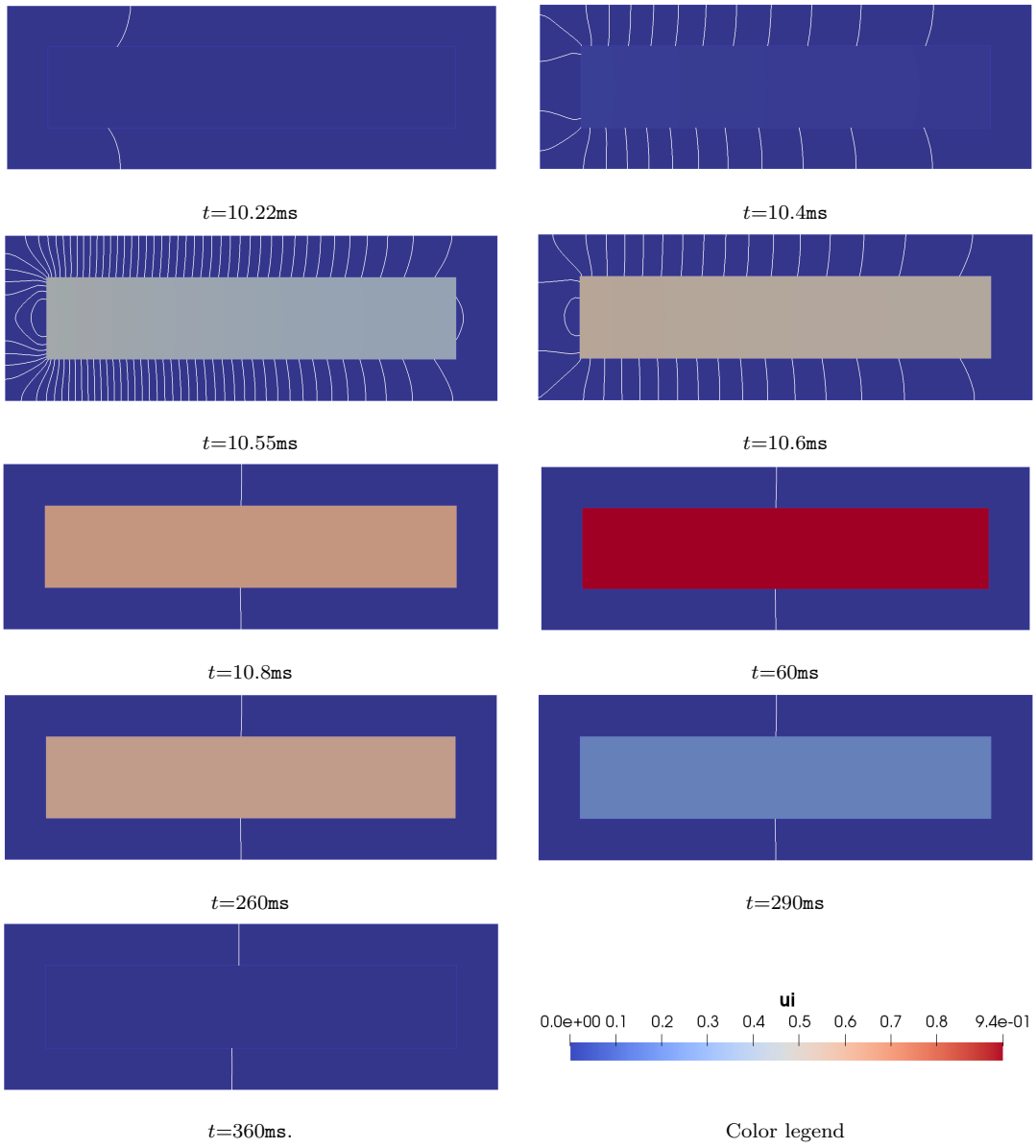

Figure 3.5: Evolution of the potentials u_i and u_e using SBDF2 method with Δt = 0.001ms

The potentials u_i and u_e have increased and are around 1 and 0.003, respectively. At t = 60 ms the depolarization of the cell is complete. The transmembrane potential is around 1. The cell slowly undergoes repolarization. From t = 260 ms to t = 290 ms, the transmembrane potential has decreased and is around 0.3. At time t = 360ms, the cell has returned to its resting state, except for the gating variable w that more slowly

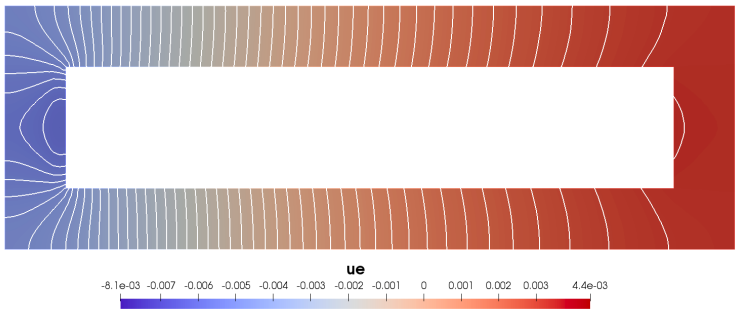

Figure 3.6: Potential u_e at time $t = 10.55\texttt{ms}$, using SBDF2 method with $\Delta\text{t} = 0.001\texttt{ms}$. The distance between any two consecutive contours is $\Delta u_e = 10^{-4}$.

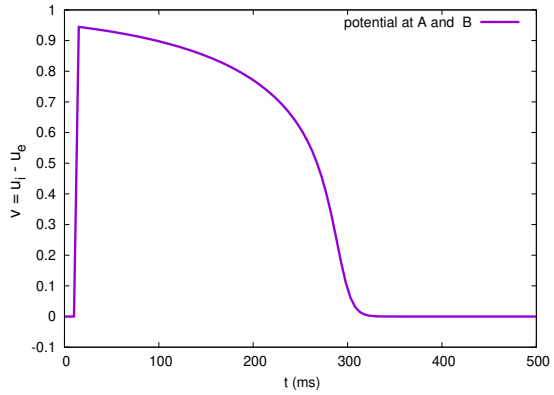

(a) Potential difference at A&B.

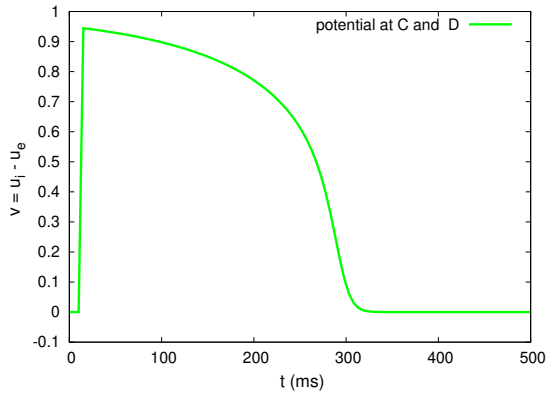

(b) Potential difference at C&D.

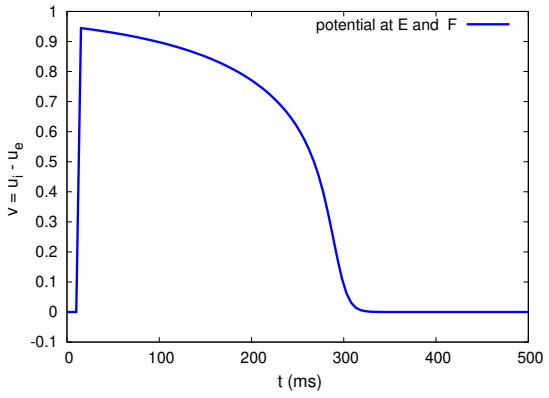

(c) Potential difference at E&F.

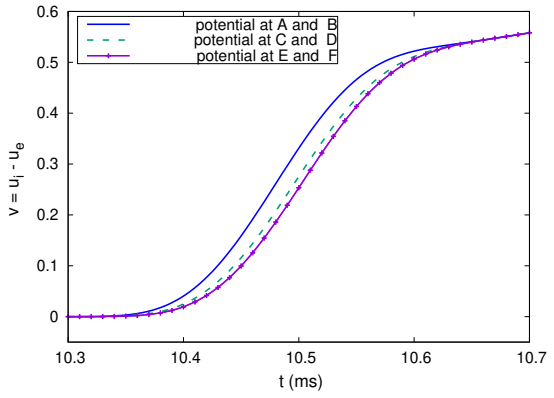

(d) Potential difference at A&B, C&D, and E&F.

Figure 3.7: Graphs of the transmembrane potential at points A&B, C&D, and E&F in the domain Ω, as a function of time.

returns to its equilibrium value (not shown).
Although Figures 3.5 and 3.6 help to illustrate the propagation of an action potential in the cell, they give little information regarding the evolution of the transmembrane potential over time. To address this limitation, we compute the potential difference over time between each pair of points A&B, C&D, and E&F, respectively. These points are chosen close enough to the membrane Γ, see Figure 3.1. Figures 3.7(a), 3.7(b) and 3.7(c) show the plot of the potential difference between A&B, C&D, and E&F, over time, respectively.
We notice that the stimulus produces an action potential with a profile similar to what is usually obtained with the MS model. The duration of the action potential is about 320$\mathtt{ms}$. Figure 3.7(d) is obtained by zooming in on Figures 3.7(a) to 3.7(c), during the stimulation. We observe that the graphs of the transmembrane potential at points A&B, C&D, and E&F slightly differ. That means the cell does not depolarize simultaneously. The difference between the solutions obtained with points A&B and E&F shows a lag of about 0.02$\mathtt{ms}$ on the depolarization time along a single cardiac cell.

Convergence tests

Based on the results obtained using a manufactured solution, we opted for computing a reference solution using a second order method. Figure 3.3 shows that the difference between the solutions obtained with SBDF2 and BDF2 methods is not significant for smaller time steps. Since the implicit BDF2 method requires a large computational time, we compute a reference solution using SBDF2 and a small time step $\Delta t = 10^{-5}\mathtt{ms}$. The domains Ω_e and Ω_i, consist of $(16n)\times(4n)$ and $(8n)\times(2n)$ nodes on the sides of each subdomain, respectively, where $n = 40$. We compute the L^2-errors, $\|u^h_{i,\Delta t} - u_{i,ref}\|_{0,\Omega_i}$, $\|u^h_{e,\Delta t} - u_{e,ref}\|_{0,\Omega_e}$, $\|v^h_{\Delta t} - v_{ref}\|_{0,\Gamma}$ and $\|w^h_{\Delta t} - w_{ref}\|_{0,\Gamma}$, between the approximate solution $u^h_{i,\Delta t}, u^h_{e,\Delta t}$, $v^h_{\Delta t}$, and $w^h_{\Delta t}$ and the reference solution $u_{i,ref}, u_{e,ref}, v_{ref}$, and w_{ref} at time $t = 0.8\mathtt{ms}$. To estimate the level of accuracy of the reference solution, we compute the solutions with the time steps $\Delta t = 10^{-5}\mathtt{ms}$, and $\Delta t = 10^{-4}\mathtt{ms}$. Next, we measure the distance in the L^2-norm between the two solutions for the variables u_i, v and w, respectively. The obtained values are drawn as horizontal dashed lines on the graphs in Figure 3.8. Below these lines, we cannot guarantee that the error between a given numerical solution and the reference solution is accurate or reliable. The threshold of accuracy for the variables u_i, v, and w is reached at 0.00045, 0.00016, and 1.09×10^{-5}, respectively.

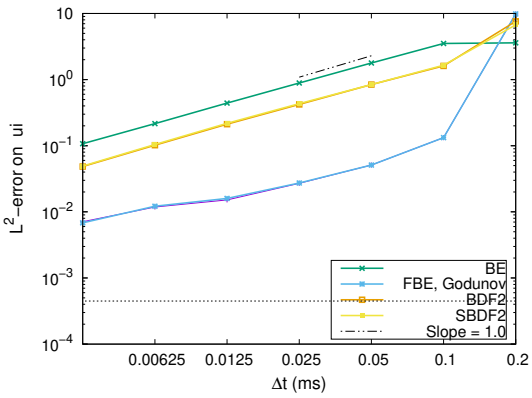

(a) L^2-norm error on the potential, u_i·

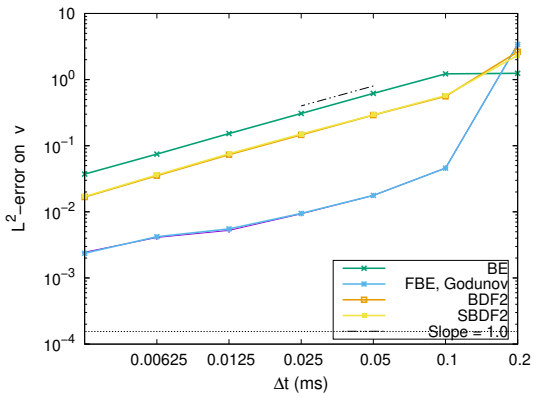

(b) L^2- norm error on the potential, v ·

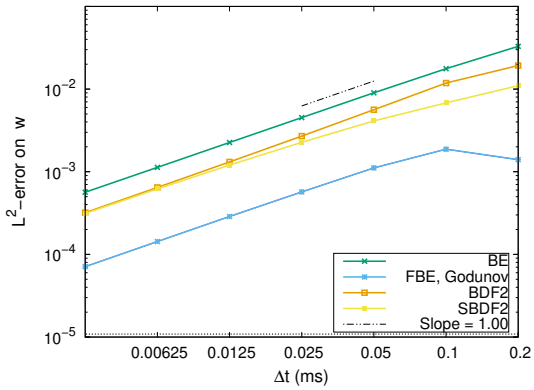

(c) L^2- norm error on the gating variable, w·

Figure 3.8: Convergence tests using the reference solution·

The results of the convergence tests are shown in Figure 3.8. We observe that on the variables u_i and v, the FBE and Godunov splitting methods show higher convergence orders for larger time steps. For smaller time steps, the convergence rate is between 0.7 and 0.8 except for the time steps 0.0125 and 0.00625 where the convergence order is 0.4, on the variables u_i and v. On the variable w, a first order convergence is achieved for both methods for smaller time steps. The BE scheme provides a convergence order of 1 on all variables. For the first order methods, we can see that the FBE method is surprisingly 10 to 20 times more accurate than the BE on the variables u_i, v and w. For the second order methods, the convergence order of the BDF2 and SBDF2 methods is about 2 on u_i and v, for larger time steps. For smaller time steps, the convergence orders of both methods go down to 1 on both variables. For the variable w, the BDF2

and SBDF2 methods only provide first order convergence for smaller time steps. Considering the size of the absolute error, the FBE method performs better than the BE, BDF2 and SBDF2 methods. Moreover, the BDF2 and SBDF2 methods perform better than the BE method. However, the BDF2 and SBDF2 methods fail to achieve second order convergence. Globally, the FBE is the most accurate, followed by second order methods, then by BE which is the least accurate. The implicit BDF2 method and the semi-implicit SBDF2 method have the same level of accuracy on u_i and v. On w BDF2 is slightly more accurate than SBDF2 for large time steps.
To illustrate the convergence of Picard method, we compute the L^2- norm of the error between two successive iterates. We stop the iteration when this error is less than the tolerance TOL $= 10^{-10}$. The graphs in Figure 3.9 are plots of the error with respect to the L^2-norm against the cumulative number of iterations. We show results for the BE method. We limit the number of iterations to 200. Figure 3.9(a) shows the plot using the manufactured solution. The peaks in the plot indicate changes in time steps. The maximum number of Picard iterations needed to reach the given tolerance is about 7. When using the reference solution, the convergence of the Picard method with the required accuracy is not obtained in 200 iterations at each time step, during the stimulation period. However, the difference between two successive iterates reduces about 4 magnitude order. The method converges after 6 iterations at the end of the stimulation, after about 1800 cumulative iterations, see Figure 3.9(b). In practice, one would be happy with a tolerance of 10^{-4} between successive iterates (an accuracy below the error with the reference solution, as shown on Figure 3.8) to limit the number of Picard iterations and reduce the computing time.

3.8.6 CPU requirements

The microscopic model is well suited to represent each individual cell in a more explicit and detailed framework. However, it can be computationally demanding as the number of cardiomyocytes in the simulation increases. To begin with, we compare the performance of the four aforementioned methods in terms of their computational efficiency during the stimulation of a portion of the cell up to T $= 0.8$`ms`. This time slot corresponds to the cell depolarization phase. Next, for each numerical method, we choose a target value of the L^2-error on the numerical solution and we track the time-step needed to achieve this level of accuracy as well as the computational time required for the simulation. Finally, we compute the total CPU efforts necessary for solving the problem (3.1)-(3.6) over a

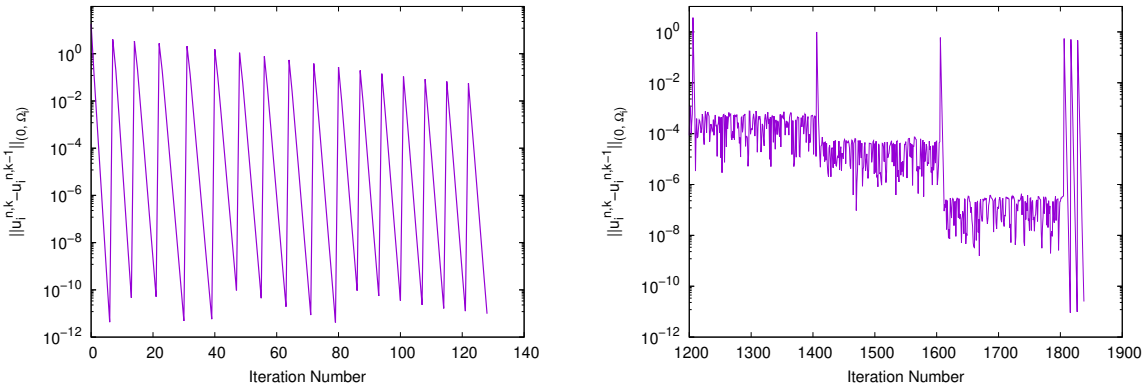

(a) L^2-error using the manufactured solution· (b) L^2-error using the reference solution·

Figure 3.9: Convergence of the Picard iterations using the manufactured solution(left) and the reference solution(right)·

whole action potential up to time T = 500ms.
Figure 3.10 reports the overall CPU time and CPU effort per time step of size $\Delta t = 0.0125ms$ needed during the stimulation, to reach the final time T = 0.8ms, respectively. We observe that the total CPU times for the fully-implicit BE and BDF2 schemes are

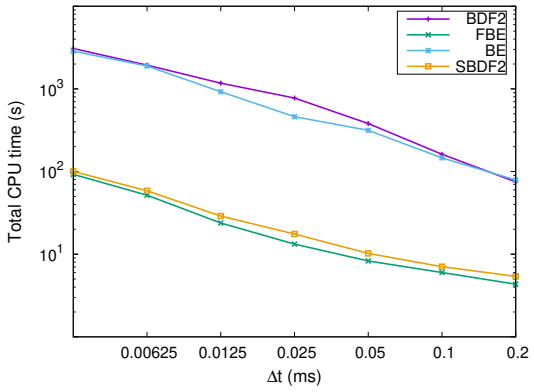

Schemes	$T_{CPU}/\Delta t$(s)
FBE	0.37
BE	14.42
BDF2	18.34
SBDF2	0.45

Figure 3.10: The left panel shows the graphs of the total CPU time needed to reach the final time T = 0.8ms, as a function of the time step. The right panel exhibits the CPU time per time step of size $\Delta t = 0.0125$ms for the same time slot.

about 10 to 50 times larger than those for the semi-implicit FBE and SBDF2 methods, durant the stimulation. Similarly, the CPU times per time step of size $\Delta t = 0.0125$ms for the BE and BDF2 methods are about 30 to 50 times greater than those for the

FBE and SBDF2 methods. Therefore, the FBE and SBDF2 methods are attractive as they take considerably less computing time than the BE and BDF2 methods. Further, FBE is more efficient than SBDF2 in terms of CPU time needed per time step. Using the Picard iterative method to solve the BE and BDF2 methods numerically requires large computational time. Solving the BE and BDF2 schemes using the Picard iterative method is computationally demanding. However, the efficiency of these methods can be improved by replacing Picard's method with a better iterative method, see [62].
Now, we choose the target values of L^2-errors on the variables u_i and v to be 0.1 and 0.04, respectively, for 0.4% relative L^2-error. They can be reached with any of the methods by properly choosing the time step. It should be mentioned that L^2-norms of the reference solutions $u_{i,ref}$, and v_{ref} are 27 and 9.3, respectively. Results are given in Table 3.3.

Table 3.3: Target values of L^2-errors on the variables u_i and v and CPU times.

Schemes	$\|u^h_{i,\Delta t} - u_{i,ref}\|_{0,\Omega_i}$	$\|v^h_{\Delta t} - v_{ref}\|_{0,\Gamma}$	Δt(ms)	T_{CPU}(s)	$T_{CPU}/\Delta t$(s)
FBE	0.1325	0.046	0.1	6.00	0.75
BE	0.1073	0.0372	0.003125	2857.73	11.16
BDF2	0.1017	0.0352	0.00625	1940.18	15.16
SBDF2	0.1043	0.0361	0.00625	58.46	0.46

The second and third columns in Table 3.3 are L^2-errors on the variables u_i and v, respectively, chosen close enough to the target value of the L^2-errors. The following columns give the corresponding time step Δt, the total CPU time of the simulation and the CPU time per time step of size Δt, respectively. The percent error on u_i, $\frac{\|u^h_{i,\Delta t}-u_{i,ref}\|_{0,\Omega_i}}{\|u_{i,ref}\|_{0,\Omega_i}} \times 100$, is around 0.5% for FBE and 0.4% for BE, BDF2 and SBDF2. The percent error on v, $\frac{\|v^h_{\Delta t}-v_{ref}\|_{0,\Gamma}}{\|v_{ref}\|_{0,\Gamma}} \times 100$, is around 0.5% for FBE and 0.4% for BE, BDF2 and SBDF2 methods. We see that the most efficient method is FBE, followed by the SBDF2 method. We observe that the total CPU time for the SBDF2 method is almost 10 times greater than that of the FBE method. This results from the fact that the SBDF2 method requires a smaller time step for the chosen error target values. However, the CPU time per time step is slightly lower than for FBE method. On average, the total CPU times for the fully-implicit BE and BDF2 schemes are 260 and 178 times greater than those for the FBE and SBDF2 methods, respectively. Similarly, on average the CPU times per time step for BE and BDF2 methods are 19 and 27 times greater than those for FBE and SBDF2 methods, respectively. In addition, both methods require a

smaller time step for the chosen L^2-error target values.
Figure 3.11 shows the plot of the total CPU costs needed to solve the problem over a single cell from time $t = 0\texttt{ms}$ to time $t = 500\texttt{ms}$, against the time step Δt. We use the semi-implicit FBE and SBDF2 methods, as the implicit BE and BDF2 methods require large computational time. We see that FBE is more efficient than SBDF2.

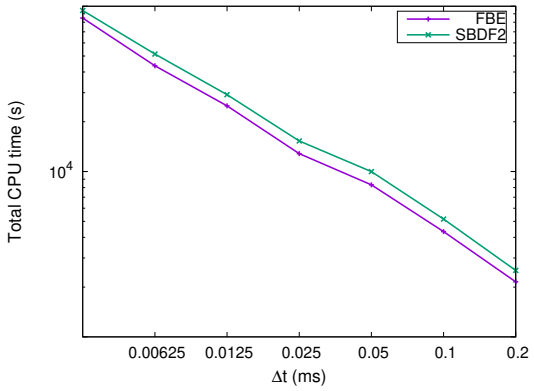

Schemes	Δt(ms)	T_{CPU}/Δt(s)
FBE	0.0125	0.38
SBDF2	0.0125	0.46

Figure 3.11: The left panel displays the graphs of the total CPU time needed to solve the problem over the single cell from time $t = 0\texttt{ms}$ to time $t = 500\texttt{ms}$ as a function of the time step Δt. The right panel shows the CPU time per time step of size $\Delta t = 0.0125\texttt{ms}$ for the same time slot.

Chapter 4

Microscopic Model for Two Cells Connected by a Gap Junction

In this chapter, we provide an exploratory study aiming at extending the methods used in Chapter 3 in the case of the multicellular model. We focus on the model consisting of two cells connected to each other by a gap junction. We first consider a fixed, unstructured fine mesh that is conformal on the interfaces. We apply the FBE method to the model and we visualize the propagation of the action potential in both cells. We then investigate the influence of the space discretization, the conformity and the non-conformity of the mesh on the solution to determine if the results are strongly mesh dependent or not. This will allow us to use meshes with as few nodes and elements as possible without altering the results. In addition to the FBE method, we solve the two-cell model using a time-splitting non-overlapping domain decomposition method (DDM). Finally, we compare the solutions obtained with both FBE and DDM methods. Section 4.1 introduces the model with gap junctions. Section 4.2 discusses the FBE method applied to model with a gap junction. Section 4.3 presents the DDM and test cases illustrating the convergence of the method.

4.1 Model with Gap Junctions

The model presented in this section is motivated by the work of [29, 67, 76]. We focus on the case of two cells, $\Omega_{i,k}$ for $k = 1, 2$, see Figure 4.1. We assume that both cells are coupled through a common gap junction, $\Gamma_{1,2}$, and are surrounded by a connected extracellular domain Ω_e. On the interface between Ω_e and $\Omega_{i,k}$, we define a cell membrane

Γ_k for $k = 1, 2$, respectively. The nondimensional model reads

$$
\begin{aligned}
-\nabla \cdot \sigma_e \nabla u_e &= \mathrm{I}_{e,stim} \quad \text{in} \quad \Omega_e, && (4.1)\\
-\nabla \cdot \sigma_i \nabla u_{i,k} &= \mathrm{I}_{ik,stim} \quad \text{in} \quad \Omega_{i,k}, && (4.2)\\
\mathrm{I}_{\mathrm{m,k}} &= \frac{\partial v_k}{\partial t} + f_k(v_k, w_k) \quad \text{on} \quad \Gamma_k, && (4.3)\\
n_e \cdot \sigma_e \nabla u_e &= -n_{i,k} \cdot \sigma_i \nabla u_{i,k} = \mathrm{I}_{\mathrm{m,k}} \quad \text{on} \quad \Gamma_k, && (4.4)\\
v_k &= u_{i,k} - u_e \quad \text{on} \quad \Gamma_k, && (4.5)\\
\mathrm{I}_{1,2} &= \frac{\partial v_{1,2}}{\partial t} + \mathrm{I}_{\mathrm{gap}} \quad \text{on} \quad \Gamma_{1,2}, && (4.6)\\
n_{i,2} \cdot \sigma_i \nabla u_{i,2} &= -n_{i,1} \cdot \sigma_i \nabla u_{i,1} = \mathrm{I}_{1,2} \quad \text{on} \quad \Gamma_{1,2}, && (4.7)\\
v_{1,2} &= u_{i,1} - u_{i,2} \quad \text{on} \quad \Gamma_{1,2}, && (4.8)\\
n_e \cdot \sigma_e \nabla u_e &= g_e \quad \text{on} \quad \partial\Omega_e \setminus (\Gamma_1 \cup \Gamma_2), && (4.9)
\end{aligned}
$$

where $k = 1, 2$, $u_{i,k}$ are the intracellular potentials, v_k are the membrane potentials, $v_{1,2}$ is the potential accross the gap junction $\Gamma_{1,2}$, $\mathrm{I}_{\mathrm{gap}}$ reperesents the current through the gap junction, w_k is the gating variable. We assume that the current through gap junction is a linear function of $v_{1,2}$

$$\mathrm{I}_{\mathrm{gap}}(v_{1,2}) = \mathrm{G}_{\mathrm{gap}} v_{1,2}, \tag{4.10}$$

where $\mathrm{G}_{\mathrm{gap}}$ is the conductance of the gap junction. The conductance $\mathrm{G}_{\mathrm{gap}}$ can be chosen time and voltage dependent, see [5, 15]. In our computations, we assume that $\mathrm{G}_{\mathrm{gap}}$ is constant. To ensure wellposedness of the problem (4.1)-(4.9), we assume the condition (3.8). As in previous chapters, the model is coupled with the following system of ordinary differential equations

$$\frac{\partial w_k}{\partial t} = g_k(v_k, w_k) \quad \text{on} \quad \Gamma_k, \tag{4.11}$$

where g_k models the dynamics of the gating variables, w_k for $k = 1, 2$.
In the following, we assume that $g_e = 0$ on $\partial\Omega_e \setminus (\Gamma_1 \cup \Gamma_2)$.

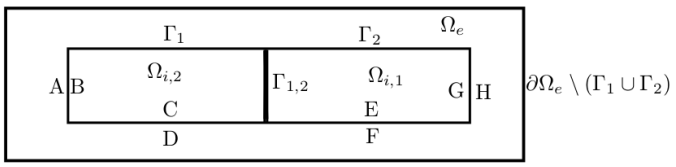

Figure 4.1: Sketch of a computational domain with two idealized cells, $\Omega_{i,1}$ and $\Omega_{i,2}$, connected by a gap junction $\Gamma_{1,2}$ and the surounding extracellular domain Ω_e.

4.2 Forward Backward Euler Method Applied to Model with a Gap Junction

As in Subsection 3.3.2, the nonlinear terms f_k and g_k as well as the linear function $\mathrm{I}_{\mathrm{gap}}$ are taken at the previous time step $t = t^{n-1}$. It follows that

$$\int_{\Omega_e} \sigma_e \nabla u_e^n \cdot \nabla \varphi_e - \sum_{k=1}^{2} \int_{\Gamma_k} \frac{v_k^n - v_k^{n-1}}{\Delta t} \varphi_e = \int_{\Omega_e} \mathrm{I}_{e,stim}^{n-1} \varphi_e + \sum_{k=1}^{2} \int_{\Gamma_k} f_k(v_k^{n-1}, w_k^{n-1}) \varphi_e, \tag{4.12}$$

$$\begin{aligned} \int_{\Omega_{i,1}} \sigma_i \nabla u_{i,1}^n \cdot \nabla \varphi_1 + \int_{\Gamma_1} \frac{v_1^n - v_1^{n-1}}{\Delta t} \varphi_1 + \int_{\Gamma_{1,2}} \frac{v_{1,2}^n - v_{1,2}^{n-1}}{\Delta t} \varphi_1 = \int_{\Omega_{i,1}} \mathrm{I}_{i1,stim}^{n-1} \varphi_1 \\ - \int_{\Gamma_1} f_1(v_1^{n-1}, w_1^{n-1}) \varphi_1 - \int_{\Gamma_{1,2}} \mathrm{I}_{\mathrm{gap}}(v_{1,2}^{n-1}) \varphi_1, \end{aligned} \tag{4.13}$$

$$\begin{aligned} \int_{\Omega_{i,2}} \sigma_i \nabla u_{i,2}^n \cdot \nabla \varphi_2 + \int_{\Gamma_2} \frac{v_2^n - v_2^{n-1}}{\Delta t} \varphi_2 - \int_{\Gamma_{1,2}} \frac{v_{1,2}^n - v_{1,2}^{n-1}}{\Delta t} \varphi_2 = \int_{\Omega_{i,2}} \mathrm{I}_{i2,stim}^{n-1} \varphi_2 \\ - \int_{\Gamma_2} f_2(v_2^{n-1}, w_2^{n-1}) \varphi_2 + \int_{\Gamma_{1,2}} \mathrm{I}_{\mathrm{gap}}(v_{1,2}^{n-1}) \varphi_2, \end{aligned} \tag{4.14}$$

$$\int_{\Gamma_k} \frac{w_k^n - w_k^{n-1}}{\Delta t} \varphi = \int_{\Gamma_k} g_k(v_k^{n-1}, w_k^{n-1}) \varphi, \tag{4.15}$$

for $n \in \{1, 2, \cdots, N\}$, where $v_k^n = u_{i,k}^n - u_e^n$ and $v_{1,2}^n = u_{i,1}^n - u_{i,2}^n$ for $k = 1, 2$.

4.2.1 Numerical Results

In this section, we attempt to extend the results of Section 3.8 to the two-cell case. We focus on visualizing the propagation of the action potential in both cells. We consider a 2D domain consisting of an extracellular domain Ω_e and two cells $\Omega_{i,k}, k = 1, 2$, connected by a gap junction $\Gamma_{1,2}$. The domains $\Omega_{i,k}$ and Ω_e are defined as follows, see Figure 4.1,

$$\begin{aligned} \Omega_{i,1} &= (10, 110) \times (10, 30)\,, \\ \Omega_{i,2} &= (110, 210) \times (10, 30)\,, \\ \Omega_e &= [(0, 220) \times (0, 40)] \setminus \overline{\Omega}_{i,1} \cup \overline{\Omega}_{i,2}. \end{aligned}$$

We use the first order FBE method (4.12)-(4.15), with linear finite elements (d=1). We set the final time T = 500`ms`. The domains Ω_e and $\Omega_{i,k}$, $k = 1, 2$, consist of $(20n) \times$

$(4n)$ and $(10n) \times (2n)$ nodes on the sides of each subdomain, respectively, where n is a given integer. In our computations, we consider a fixed, unstructured fine mesh that is conformal on the interfaces Γ_1 and Γ_2, see Figures 4.2 and 4.3. The coarse and fine meshes correspond to $n = 1$ and $n = 10$, respectively. The conductance of the gap junction is $\mathrm{G}_{gap} = \dfrac{1}{0.0015}$ as in [76]. The stimulation currents and the ionic current model are the same as those used in Section 3.8.

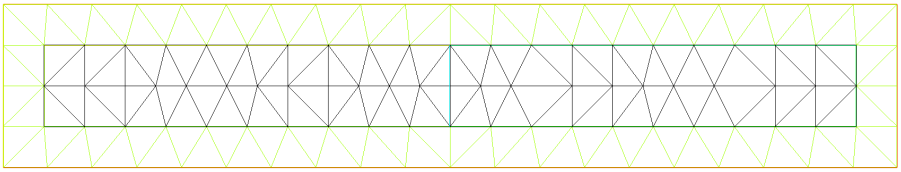

Figure 4.2: Sketch of a coarse conformal mesh on the interfaces Γ_1 and Γ_2, with $n = 1$.

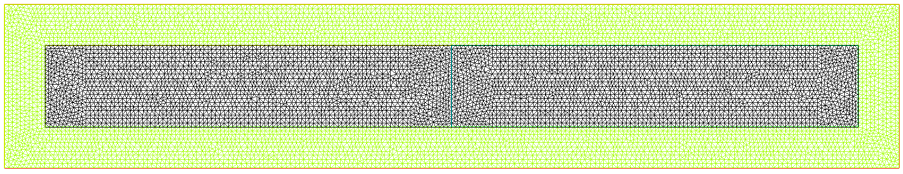

Figure 4.3: Sketch of a fine conformal mesh on the interfaces Γ_1 and Γ_2, with $n = 10$.

We visualize the propagation of an action potential in the cells $\Omega_{i,1}$ and $\Omega_{i,2}$. We use $\Delta\mathrm{t} = 0.001\mathtt{ms}$ as in Subsection 3.8.5. We initiate an action potential by injecting a stimulus current of amplitude $\mathrm{A} = 20\mu\mathtt{A}$ near the membrane of the cell, $\Omega_{i,1}$, see Figure 3.4. The simulation is triggered at $t = 10.30\mathtt{ms}$ and lasts $0.5\mathtt{ms}$. Figures 4.4 and 4.5 show the evolution of the potentials $u_{i,k}$ and u_e over the first $360\mathtt{ms}$, in the domains Ω_e and $\Omega_{i,k}$ for $k = 1, 2$, respectively. Figure 4.5 shows in more details the potential u_e at time $t = 10.5\mathtt{ms}$ during the stimulation phase. The time $t = 10.30\mathtt{ms}$ marks the beginning of the stimulation. The cells $\Omega_{i,1}$ and $\Omega_{i,2}$ are in a resting state. The potentials $u_{i,k}$ and u_e are around 0. At time $t = 10.4\mathtt{ms}$ the first cell $\Omega_{i,1}$ initiates the depolarization process. In time interval $t = 10.6\mathtt{ms}$ to $t = 10.8\mathtt{ms}$, cell $\Omega_{i,1}$ is already depolarized while cell $\Omega_{i,2}$ starts depolarizing. The potentials $u_{i,1}$ and $u_{i,2}$ have increased and are around 0.6 and 0.3, respectively. At $t = 60$ $\mathtt{ms}$ the depolarization of the cells $\Omega_{i,1}$ and $\Omega_{i,2}$ is complete. The transmembrane potentials $v_1 = u_{i,1} - u_e$ and $v_2 = u_{i,2} - u_e$ are around 1.

The cells $\Omega_{i,1}$ and $\Omega_{i,2}$ slowly undergo repolarization. From $t = 160$ ms to $t = 290$ ms, the transmembrane potentials v_1 and v_2 have decreased and are around 0.3. At time $t = 360$ms, both cells have returned to their resting states.

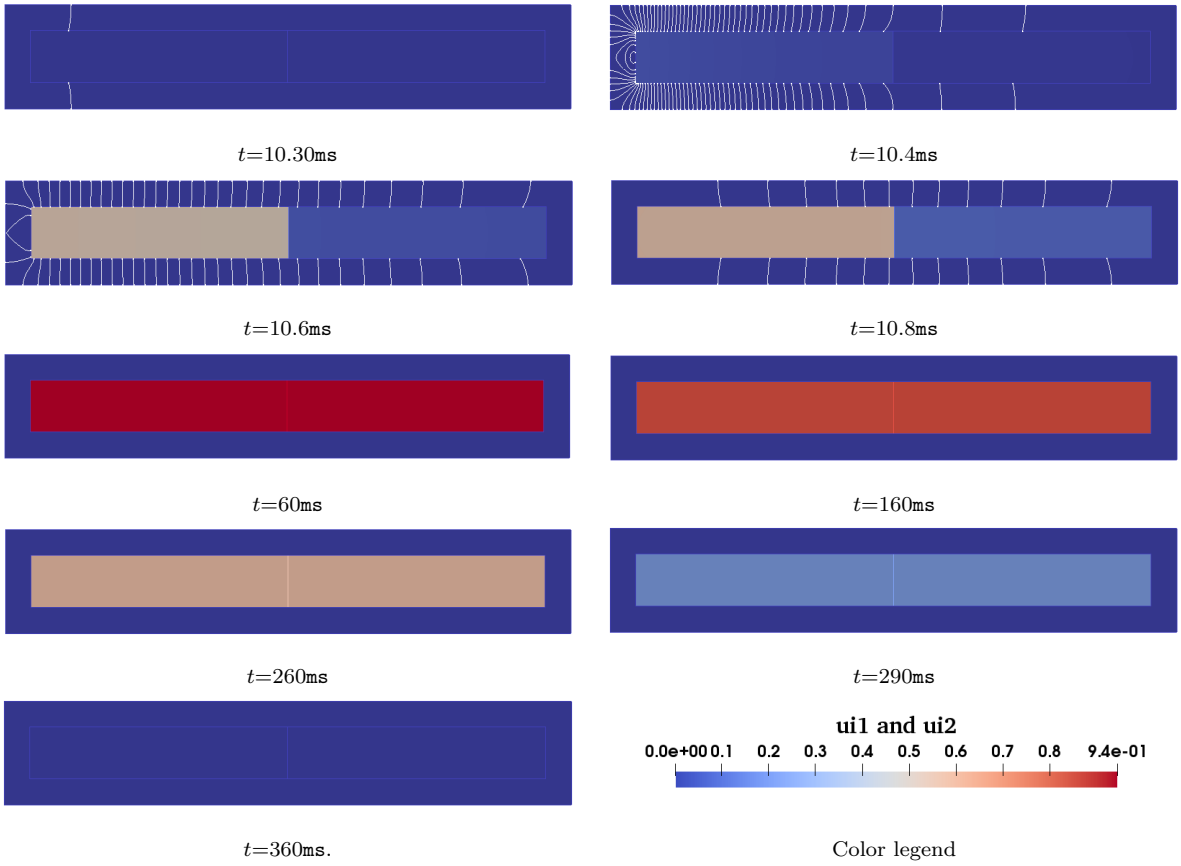

Figure 4.4: Time evolution of the potentials $u_{i,1}$ and $u_{i,2}$ using FBE method with $\Delta t = 0.001$ms, $n = 10$ and $d = 1$.

As in Section 3.8.5, we plot the potential difference over time between each pair of points A&B, C&D, E&F, and G&H, respectively. These points are chosen close enough to the membranes Γ_1 and Γ_2, see Figure 4.1. Figures 4.6(a) and 4.6(c) show the potential difference plots using coarse and fine meshes conformal on the interfaces Γ_1 and Γ_2, respectively. We notice that the stimulus produces an action potential with a profile similar to what is usually obtained with the MS model. We observe that the duration of the action potential is about 330ms, which is consitent with the previous visualization.

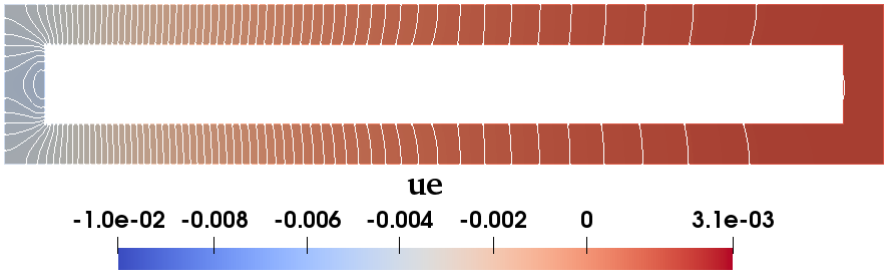

Figure 4.5: Potential u_e at time $t = 10.5\texttt{ms}$ using FBE method with $\Delta\text{t} = 0.001\texttt{ms}, n = 10$ and $d = 1$. The distance between any two consecutive contours is $\Delta u_e = 10^{-4}$.

Figures 4.6(b) and 4.6(d) are obtained by zooming in on Figures 4.6(a) and 4.6(c) during the stimulation, respectively. Using a coarse mesh, we observe a spike in the plots of the potential difference at points A&B and C&D for the first cell $\Omega_{i,1}$, see Figure 4.6(b).

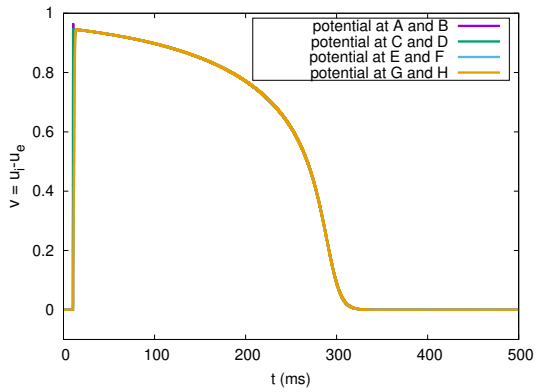

(a) Coarse and conformal mesh on Γ_1 and Γ_2.

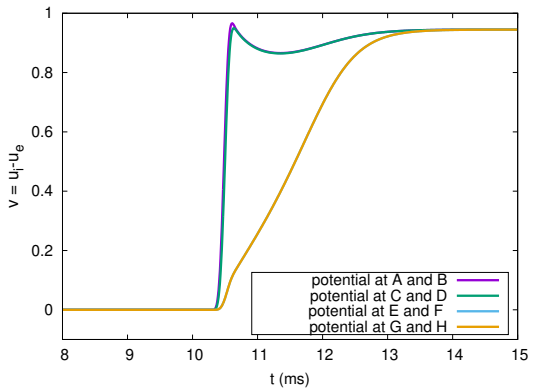

(b) Zoom in of Figure 4.6(a)

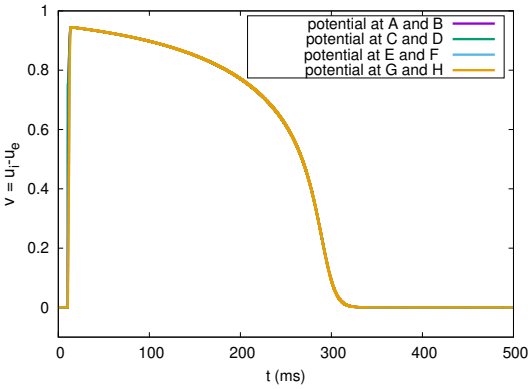

(c) Fine and conformal mesh on Γ_1 and Γ_2.

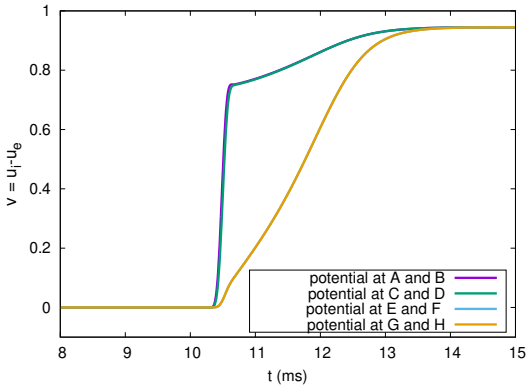

(d) Zoom in of Figure 4.6(c)

Figure 4.6: Graphs of the membrane potential at points A&B, C&D, E&F and G&H, as a function of time, using a conformal mesh on Γ_1 and Γ_2, with $\Delta t = 0.01\texttt{ms}$.

By using a finer mesh, the height of the spike is reduced. This leads to a longer depolarization phase in the case of the coarse mesh. The graphs of potential difference between the points E&F and G&H are identical for the second cell $\Omega_{i,2}$, while they slightly differ for the points A&B and C&D for the first cell $\Omega_{i,1}$, see Figures 4.6(b) and 4.6(d). We notice that the two cells do not depolarize simultaneously, which is in agreement with the previous visualization, see Figure 4.4 at time $t = 10.8\texttt{ms}$. There is a lag of about $1.2\texttt{ms}$ betweeen both cardiac cells during the depolarization phase. This lag can be due to the resistive gap junction $\Gamma_{1,2}$ that delays the depolarizing current flowing from the cell $\Omega_{i,1}$ to the cell $\Omega_{i,2}$.

Similarly, we consider coarse and fine meshes that are non-conformal on the interfaces Γ_1 and Γ_2. We plot the potential difference between the points A&B, C&D, E&F, and

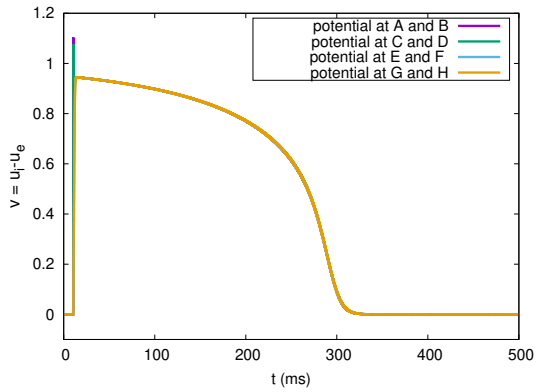

(a) Coarse and non conformal meshes on Γ_1 and Γ_2.

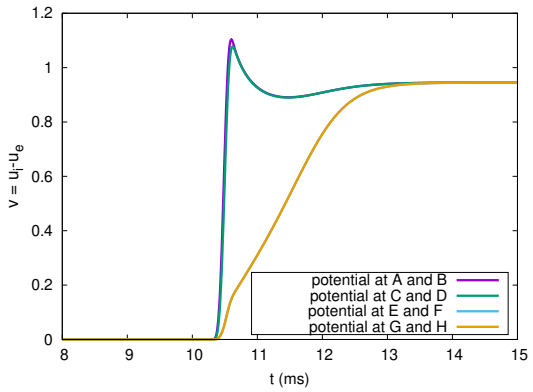

(b) Zoom in of Figure 4.6(b)

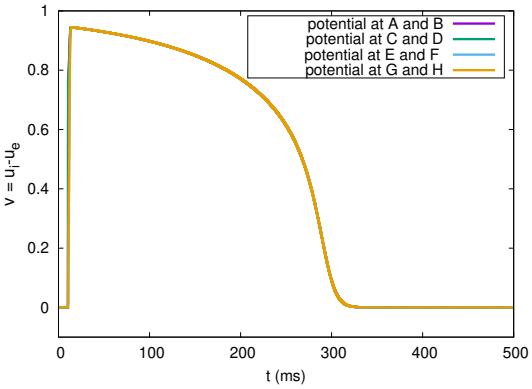

(c) Fine and non conformal meshes on Γ_1 and Γ_2.

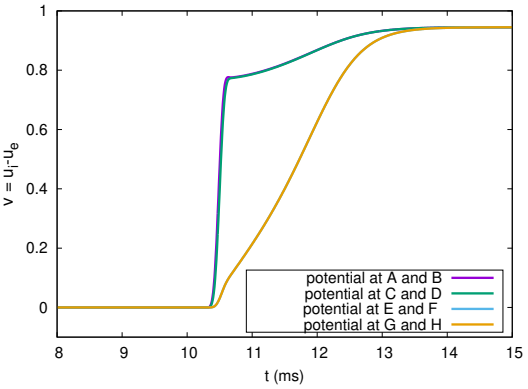

(d) Zoom in of Figure 4.7(c)

Figure 4.7: Graphs of the membrane potential at points A&B, C&D, E&F and G&H, as a function of time, using a non-conformal mesh on Γ_1 and Γ_2, with $\Delta t = 0.01\texttt{ms}$.

G&H, see Figures 4.7(a) and 4.7(c). Figures 4.7(b) and 4.7(d) are obtained by zooming in on Figures 4.7(a) and 4.7(c) during the stimulation, respectively. In the first cell $\Omega_{i,1}$, we see that transmembrane potentials experience an overshoot during the depolarization phase, when considering a coarse mesh, see Figure 4.7(b). Using a fine mesh, we see that the overshoot in the transmembrane potentials is eliminated, see Figure 4.7(d). During the stimulation phase, the difference between the solutions using fine and coarse meshes is 15% to 20% for about 1ms. Finally, we can conclude that the mesh resolution has a relatively important impact on simulation results, at least during the stimulation phase. We need to use a finer mesh, whether we consider a conformal or non-conformal mesh on interfaces Γ_1 and Γ_2.

4.3 Domain Decomposition Method

Domain decomposition methods (DDM) are iterative methods, which are based on the partition of the computational domain Ω, where the boundary value problem is set on two or more sub-domains which may or may not overlap. Then, discretized problems of smaller dimension are to be solved on each sub-domain, with iterations between these subproblems till convergence.
In this section, we present the DDM for a collection of isolated cells, that is, the cells are not connected by gap junctions. Afterwards, we choose model problems with known analytical solution to investigate the convergence of the method. Finally, we applied the DDM to two cells that are connected to each other by a gap junction.

4.3.1 DDM Applied to Isolated Cells

We assume that the computational domain $\Omega = \Omega_i \cup \Omega_e \cup \Gamma$ consists of p cells, where $\Omega_i = \cup_{j=1}^{p} \Omega_{i,j}$ and $\Omega_{i,j}, j = 1, \ldots, p$ are non-overlapping intracellular domains satisfying $\Omega_{i,j} \cap \Omega_{i,k} = \emptyset$ for $j \neq k$. The domain Ω_e is a connected extracellular space surrounding the cells. The cell membrane is denoted by Γ_j and is defined by $\Gamma_j = \overline{\Omega}_{i,j} \cap \overline{\Omega}_e$ for $j = 1, \ldots, p$. We set $\Gamma = \cup_{j=1}^{p} \Gamma_j$ and $\Gamma_e = \partial\Omega_e \setminus \Gamma$. The illustration of a two-dimensional version of this setup is given in the Figure 4.8.

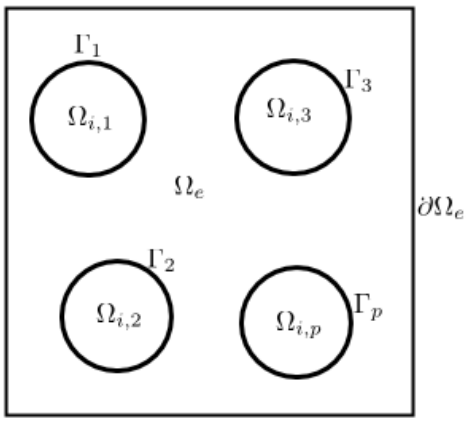

Figure 4.8: Sketch of the computational domain Ω with p intracellular spaces $\Omega_{i,j}$, $j = 1, \ldots, p$, that are surrounded by a connected extracellular space Ω_e.

We apply the DDM in the second substep of the Godunov time-splitting problem (3.28)-

(3.31). The algorithm for the time-splitting DDM reads as follows:

- In the first step, we update the solutions for the membrane potential, v, and gating variable, w, by solving the following system of ODEs on Γ

$$\int_\Gamma \frac{v^* - v^{n-1}}{\Delta t}\varphi = -\int_\Gamma f(v^{n-1}, w^{n-1})\varphi, \tag{4.16}$$

$$\int_\Gamma \frac{w^n - w^{n-1}}{\Delta t}\varphi = \int_\Gamma g(v^{n-1}, w^{n-1})\varphi\cdot \tag{4.17}$$

- For a given $u_i^{n,k-1}$, v^* and w^n, we solve for $u_e^{n,k}$ in the domain Ω_e the problem:

$$\int_{\Omega_e} \sigma_e \nabla u_e^{n,k}\cdot\nabla\varphi_e - \int_\Gamma \frac{u_i^{n,k-1} - u_e^{n,k}}{\Delta t}\varphi_e = \int_{\Omega_e} \mathrm{I}_{e,stim}^{n-1}\varphi_e - \int_\Gamma \frac{v^*}{\Delta t}\varphi_e \tag{4.18}$$

- Then we solve for $u_i^{n,k}$ in the domain Ω_i the problem

$$\int_{\Omega_i} \sigma_i \nabla u_i^{n,k}\cdot\nabla\varphi_i + \int_\Gamma \frac{u_i^{n,k} - u_e^{n,k}}{\Delta t}\varphi_i = \int_{\Omega_i} \mathrm{I}_{i,stim}^{n-1}\varphi_i + \int_\Gamma \frac{v^*}{\Delta t}\varphi_i, \tag{4.19}$$

- We repeat the two last steps with $k \longleftarrow k+1$, till $\|u_i^{n,k} - u_i^{n,k-1}\|_{0,\Omega_i} <$ TOL, and $u_e^{n,k} - u_e^{n,k-1}\|_{0,\Omega_e} <$ TOL,

for a given tolerance, TOL, where $k \geqslant 1$ is an integer denoting the DDM iteration count and $v^{n-1} = u_i^{n-1} - u_e^{n-1}$ and w^{n-1} are known for $t = t_{n-1}$ on Γ. The functions $\mathrm{I}_{e,stim}^{n-1}$, $\mathrm{I}_{i,stim}^{n-1}$ and g_e are in $\mathrm{L}^2(\Omega_e)$, $\mathrm{L}^2(\Omega_i)$ and $\mathrm{L}^2(\Gamma_e)$, respectively. We only need to initialize $u_i^{n,0}$ and we set $u_i^{0,0} = 0, \quad u_i^{n,0} = u_i^{n-1}$.

4.3.2 DDM Applied to the Model with Gap Junctions

The problem (4.1)-(4.9) is first decomposed into two sub-problems thanks to the operator splitting method introduced in Subsection 3.3.3. The algorithm for the time-splitting DDM reads as follows:

- We first solve for the membrane potential, v_k^*, and gating variable, w_k, the following system of ODEs on Γ_k

$$\int_{\Gamma_k} \frac{v_k^* - v_k^{n-1}}{\Delta t}\varphi_k = -\int_{\Gamma_k} f_k(v_k^{n-1}, w_k^{n-1})\varphi_k, \tag{4.20}$$

$$\int_{\Gamma_k} \frac{w_k^n - w_k^{n-1}}{\Delta t}\varphi_k = \int_{\Gamma_k} g_k(v_k^{n-1}, w_k^{n-1})\varphi_k\cdot \tag{4.21}$$

- For given $u_{i,k}^{n,j-1}$, v_k^* and w_k^n, we solve for $u_e^{n,j}$ in the domain Ω_e the problem:

$$\int_{\Omega_e} \sigma_e \nabla u_e^{n,j} \cdot \nabla \varphi_e - \sum_{k=1}^{2} \int_{\Gamma_k} \frac{u_{i,k}^{n,j-1} - u_e^{n,j}}{\Delta t} \varphi_e = \int_{\Omega_e} \mathrm{I}_e^{n-1} \varphi_e - \sum_{k=1}^{2} \int_{\Gamma_k} \frac{v_k^*}{\Delta t} \varphi_e \quad (4.22)$$

- We solve for $u_{i,1}^{n,j}$ in the domain $\Omega_{i,1}$ the problem

$$\begin{aligned} \int_{\Omega_{i,1}} \sigma_i \nabla u_{i,1}^{n,j} \cdot \nabla \varphi_1 + \int_{\Gamma_1} \frac{u_{i,1}^{n,j} - u_e^{n,j}}{\Delta t} \varphi_1 + \int_{\Gamma_{1,2}} \frac{v_{1,2}^{n,j}}{\Delta t} \varphi_1 + \int_{\Gamma_{1,2}} \mathrm{I}_{\mathrm{gap}}(v_{1,2}^{n,j}) \varphi_1 \\ = \int_{\Omega_{i,1}} \mathrm{I}_{i1,stim}^{n-1} \varphi_1 + \int_{\Gamma_1} \frac{v_1^*}{\Delta t} \varphi_1 + \int_{\Gamma_{1,2}} \frac{v_{1,2}^{n-1}}{\Delta t} \varphi_1, \end{aligned} \quad (4.23)$$

- We solve for $u_{i,2}^{n,j}$ in the domain $\Omega_{i,2}$ the problem

$$\begin{aligned} \int_{\Omega_{i,2}} \sigma_i \nabla u_{i,2}^{n,j} \cdot \nabla \varphi_2 + \int_{\Gamma_2} \frac{u_{i,2}^{n,j} - u_e^{n,j}}{\Delta t} \varphi_2 - \int_{\Gamma_{1,2}} \frac{v_{1,2}^{n,j}}{\Delta t} \varphi_2 - \int_{\Gamma_{1,2}} \mathrm{I}_{\mathrm{gap}}(v_{1,2}^{n,j}) \varphi_2 \\ = \int_{\Omega_{i,2}} \mathrm{I}_{i2,stim}^{n-1} \varphi_2 + \int_{\Gamma_1} \frac{v_2^*}{\Delta t} \varphi_2 - \int_{\Gamma_{1,2}} \frac{v_{1,2}^{n-1}}{\Delta t} \varphi_2, \end{aligned} \quad (4.24)$$

- We repeat the three last steps with $j \longleftarrow j+1$, till $\|u_{i,k}^{n,j} - u_{i,k}^{n,j-1}\|_{0,\Omega_{i,k}} <$ TOL and $\|u_e^{n,j} - u_e^{n,j-1}\|_{0,\Omega_e} <$ TOL for $k = 1, 2$, where TOL is a given tolerance, $j \geqslant 1$ is an integer denoted the DDM iteration count, $v_k^{n-1} = u_{i,k}^{n-1} - u_e^{n-1}$, w_k^{n-1} and $v_{1,2}^{n-1} = u_{i,1}^{n-1} - u_{i,2}^{n-1}$ are known for $t = t_{n-1}$ on Γ_k and $\Gamma_{1,2}$, respectively.

4.3.3 Numerical Results

We are interested in the convergence of the domain decomposition method (4.20)-(4.24). We estimate the error between two successive iterates of the DDM. We calculate the L^2-norm of the errors, $\|u_e^{n,k} - u_e^{n,k-1}\|_{0,\Omega_e}$ and $\|u_{i,j}^{n,k} - u_{i,j}^{n,k-1}\|_{0,\Omega_{i,j}}, j = 1, 2$, between two successive iterates $u_e^{n,k}$ and $u_e^{n,k-1}$, and $u_{i,j}^{n,k}$ and $u_{i,j}^{n,k-1}$, where $k \geq 1$ is the DDM iteration count. We limit the number of iterations to 50 and we stop the iteration when it is less than the tolerance TOL $= 10^{-10}$. We applied the method to the test case of Subsection 4.2.1. The graphs in Figures 4.9(a), 4.9(b) and 4.9(c) are the plot the L^2-norms of the errors $\|u_e^{n,k} - u_e^{n,k-1}\|_{0,\Omega_e}$, $\|u_{i,1}^{n,k} - u_{i,1}^{n,k-1}\|_{0,\Omega_{i,1}}$ and $\|u_{i,2}^{n,k} - u_{i,2}^{n,k-1}\|_{0,\Omega_{i,2}}$, respectively, against the cummulative number of iterations during the stimulation.
The peaks in the plot indicate changes in time steps. The maximum number of iterations

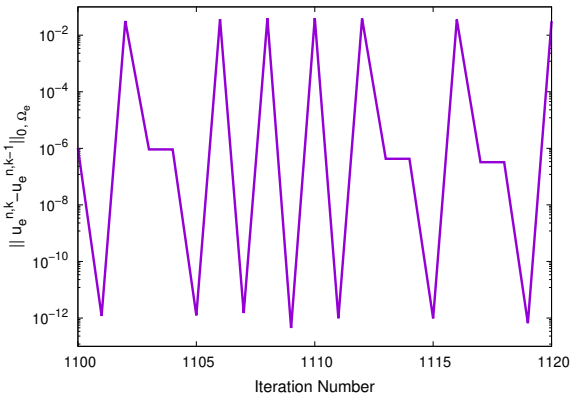

(a) Error $\|u_e^{n,k} - u_e^{n,k-1}\|_{0,\Omega_e}$

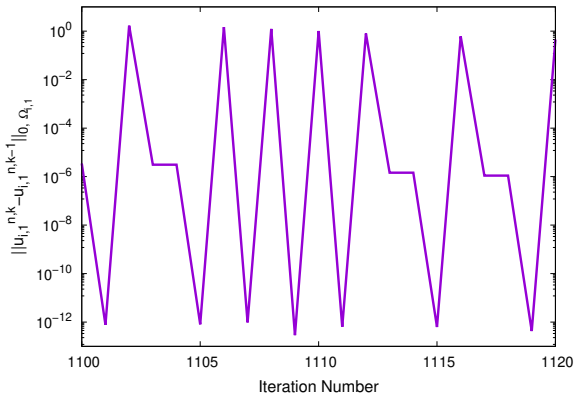

(b) Error $\|u_{i,1}^{n,k} - u_{i,1}^{n,k-1}\|_{0,\Omega_{i,1}}$

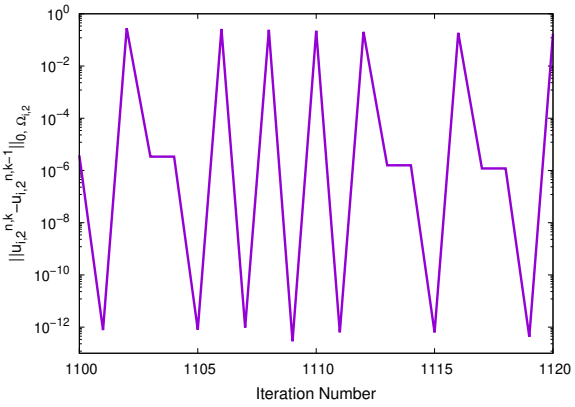

(c) Error $\|u_{i,2}^{n,k} - u_{i,2}^{n,k-1}\|_{0,\Omega_{i,2}}$

Figure 4.9: Convergence of the DDM, with $\Delta t = 0.01\texttt{ms}$.

needed to reach the given tolerance is about 6 per time step. After the stimulation phase, the DDM converges within 3 iterations. We want to understand the impact of doing only 3 iterations of DDM on the solution. Better yet, we want to see if the convergence of the DDM method is impacted by the number of iterations required. We will compare the solution obtained with three iterations of the DDM with the solution obtained with the FBE method involving no domain decomposition (as if we had let the DDM fully converges). We consider a fine mesh that is fixed, unstructured and conformal on the interfaces Γ_1 and Γ_2, see Figure 4.3. As before, we plot the potential difference over time between the points A&B (cell $\Omega_{i,1}$) and G&H (cell $\Omega_{i,2}$), using the FBE method and the DDM, see Figure 4.10(a). We see that the duration of the action potential is about

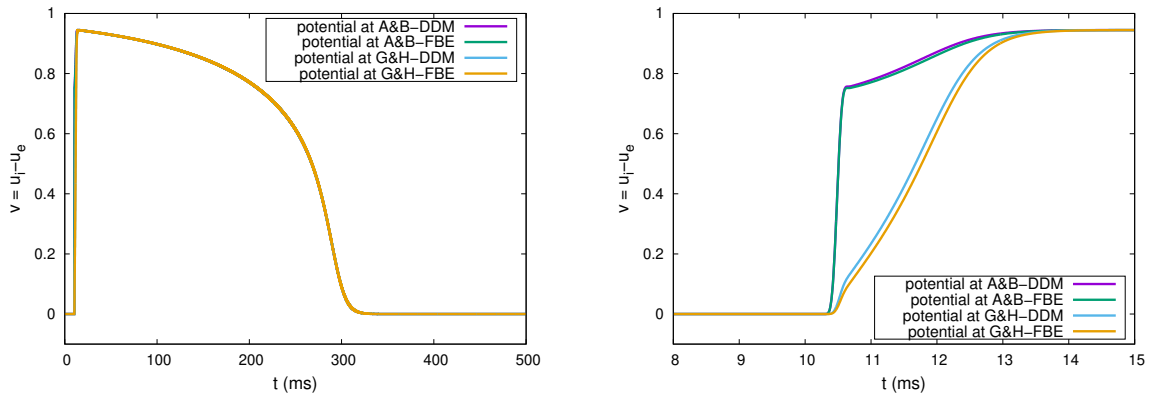

(a) Plots of the membrane potential against time using DDM and FBE.

(b) Zoom in of Figure 4.10(a)

Figure 4.10: Plots of the membrane potential at points A&B, C&D, E&F, and G&H against time, using the DDM on a fine and conformal mesh on Γ_1 and Γ_2, $\Delta t = 0.01\texttt{ms}$.

330ms as in Figure 4.6(c). Figure 4.10(b) is obtained by zooming in on Figure 4.10(a) during the stimulation. Figure 4.10(b) shows that the graphs of potential difference between the points A&B are almost identical for FBE and DDM methods. However, the plots of the transmembrane potential at the points G&H slightly differ. To understand this difference, we repeat the computations with a smaller time step $\Delta t = 0.001\texttt{ms}$, see Figure 4.11. Using the time step $\Delta t = 0.001\texttt{ms}$ the DDM provides the same solution as the Godunov splitting method which is equivalent to the FBE method. This confirms the fact that the DDM is capable of providing an accurate solution with a minimal number of sub-domain iterations, if any at all past the stimulation phase.

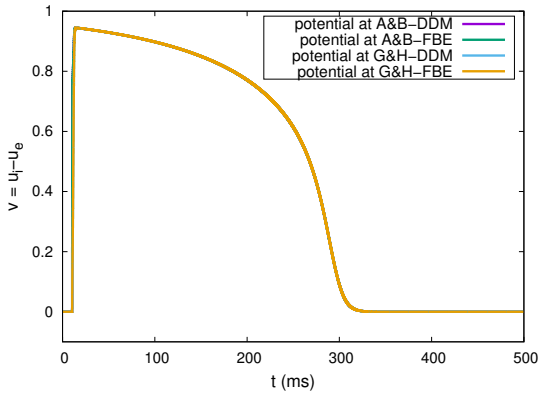

(a) Plots of the membrane potential against time using DDM and FBE.

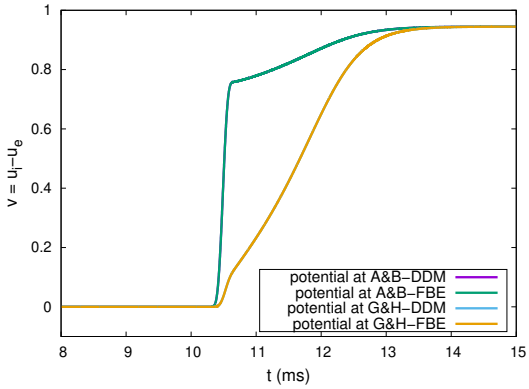

(b) Zoom in of Figure 4.11(a)

Figure 4.11: Plots of the membrane potential at points A&B, C&D, E&F, and G&H against time, using the DDM on a fine and conformal mesh on Γ_1 and Γ_2, $\Delta t = 0.001\texttt{ms}$.

Chapter 5

Conclusions and Perspectives

In this thesis, we have studied various numerical methods for solving the microscopic cardiac electrophysiology model. In Chapter 1, we performed a dimensional analysis of the model. The resulting nondimensional microscopic model can be coupled with any nondimensional ionic model. The nondimensionalization is essential for properly adjusting all the model parameters and obtaining physiologically relevant simulation results.
In Chapter 2, a key step in solving the microscopic model consisted in breaking it down into two problems using the Steklov-Poincaré operator. The first problem, made of coupled linear propagation problems in the domains Ω_i and Ω_e, was solved on an affine space that we properly defined. The second problem based on a nonlinear ODE system was solved on the interface Γ. This reformulation is crucial to solve the microscopic model numerically. In fact, the microscopic model is not a classical reaction-diffusion system as the time derivative only appears in a nonlinear ODE system defined on the cellular membrane, coupling the potential inside and outside the cell. We applied the finite element method for the spatial discretization of the microscopic model. We proved stability and error estimates for the finite element method. In theory, we expected a first order spatial convergence in the H^1- norm for the potentials $u_{e,h}$ and $u_{i,h}$, when using linear finite elements. The 2D numerical tests using a manufactured solution confirmed these theoretical predictions. The theoretical estimate of the L^2-norm of the error on the potential v predicts a convergence order of one. However, in practice we obtained an order of convergence between 1 and 2.
In Chapter 3, we introduced five time-stepping numerical methods for solving the microscopic model. These include FBE, BE, Godunov splitting, BDF2 and SBDF2. We used the Picard iterative method to solve the nonlinear algebraic system for the fully implicit

BE and BDF2 methods. Theoretically, we expected a first order convergence in time for the FBE, BE and Godunov splitting methods and a second order convergence for the BDF2 and SBDF2 methods. Numerical tests performed in 2D using a manufactured solution indicated that all numerical methods exhibit the expected order of convergence. However, when testing the methods using a reference solution computed with the SBDF2 scheme for a physiologically realistic problem, the BDF2 and SBDF2 only provide first order convergence. This inability to obtain the correct convergence orders using a reference solution is likely due to the stiffness of the system when using external stimulus current to depolarize the cell. In fact, the depolarization phase of the cell is the only time when the solution exhibits spatial variation. Consequently, for studying the order of accuracy of the method, it is sufficient to calculate the error right at the end of the depolarization phase. This phase is quite short and lasts only about 0.4 `ms` as shown in Figure 3.5. Therefore, second order methods have difficulty exhibiting their expected order of convergence over such a short time interval. Numerical results show that the FBE method is the best choice for solving the microscopic model, in terms of accuracy and computational cost.
In Chapter 4, we solved the model for two cells coupled through a common gap junction using FBE and a non-overlapping time-splitting domain decomposition method (DDM). We studied the influence of the spatial discretization (mesh size, conformal vs nonconformal mesh) on the propagation of the action potential. We found that the spatial discretization has a relatively important impact on simulation results, at least during the stimulation phase. Numerical experiments showed that the iteration of the DDM may not be needed at each time-step of the time-splitting method, yet DDM is able to provide an accurate solution with a minimal number of sub-domain iterations.

Further Research Directions

Real cardiac cells have much more complex tissue geometries including cylindrical shapes and transverse tubules (t-tubules) of the cardiomyocites. However in this thesis, we used rectangles to represent the cardiac cells. For further research, it would be interesting to extend our study to these types of geometries, and in particular to 3D geometries.

Ephaptic coupling is the mechanism by which action potential occurs in the absence of gap junction channels. As such, it is an important component of cardiac propagation in a healthy or diseased heart. Extending our work to the multi-cell model, which can take into account the ephaptic mechanism would be an interesting research question to

investigate.

The test cases considered here included only one or two cells. It would be interesting to increase the number of cells in the model and play with the geometrical structure. Since realistic simulations using the multi-cell model can be computationally demanding, incorporating more sophisticated techniques to solve the model using parallel computing can be an interesting future research direction.

The ionic current model that we used is based on a variant of the Mitchell-Shaeffer model. The latter model aims at reproducing the action potential, but uses a simplified formulation of the underlying physiological details. We could perform a similar study with more realistic ionic models, and investigate their impact on the evolution of the solution and the numerical efficiency of our methods.

Bibliography

[1] R.A. Adams and J.J.F. Fournier. *Sobolev Spaces*. Pure and Applied Mathematics. Elsevier Science, 2003.

[2] A. Agudelo-Toro and A. Neef. Computationally efficient simulation of electrical activity at cell membranes interacting with self-generated and externally imposed electric fields. *Journal of Neural Engineering*, 10(2):026019, 2013.

[3] Georgios Akrivis. Stability of implicit and implicit-explicit multistep methods for nonlinear parabolic equations. *IMA Journal of Numerical Analysis*, 38(4):1768–1796, 2017.

[4] U. M. Ascher, S. J. Ruuth, and B. T. R. Wetton. Implicit-explicit methods for time-dependent partial differential equations. *SIAM Journal on Numerical Analysis*, 32(3):797–823, 1995.

[5] Pierre-Elliott Bécue. *Modélisation et simulation de l'électrophysiologie cardiaque à l'échelle microscopique*. PhD thesis, Université de Bordeaux, France, 2018.

[6] G. W. Beeler and H. Reuter. Reconstruction of the action potential of ventricular myocardial fibres. *The Journal of Physiology*, 268(1):177–210, 1977.

[7] C. Bernardi, Y. Maday, and A.T Patera. Domain decomposition by the mortar element method. In *Asymptotic and Numerical Methods for Partial Differential Equations with Critical Parameters*, pages 269–286. Springer Netherlands, 1993.

[8] H. Brezis. *Functional Analysis, Sobolev Spaces and Partial Differential Equations*. Springer, 2010.

[9] A.M. Brown, K. S. Lee, and T. Powell. Voltage clamp and internal perfusion of single rat heart muscle cells. *The Journal of physiology*, 318:455–477, 1981.

[10] Philippe G. Ciarlet. *Finite Element Method for Elliptic Problems*. Society for Industrial and Applied Mathematics, USA, 2002.

[11] R. H. Clayton and A. V. Panfilov. A guide to modelling cardiac electrical activity in anatomically detailed ventricles. *Progress in Biophysics and Molecular Biology*, 96(1):19–43, 2008.

[12] E. D. Copene and J. P. Keener. Ephaptic coupling of cardiac cells through the junctional electric potential. *Journal of Mathematical Biology*, 57(2):265–284, 2008.

[13] C. Corrado and S. A. Niederer. A two-variable model robust to pacemaker behaviour for the dynamics of the cardiac action potential. *Mathematical Biosciences*, 281:46–54, 2016.

[14] M. Crouzeix and A.L. Mignot. *Analyse numérique des équations différentielles*, volume 1. Masson, Paris, 1984.

[15] A. Davidović, Y. Coudière, T. Desplantez, and C. Poignard. Microscopic modelling of the non-linear gap junction channels. In *2015 Computing in Cardiology Conference* (CinC), pages 425–428, 2015.

[16] D. DiFrancesco and D. Noble. A model of cardiac electrical activity incorporating ionic pumps and concentration changes. *Philosophical Transactions of the Royal Society of London. Series B, Biological Sciences*, 307(1133):353–398, 1985.

[17] I. Dione, J. Deteix, T. Briffard, E. Chamberland, and N. Doyon. Improved simulation of electrodiffusion in the node of ranvier by mesh adaptation. *PLOS ONE*, 11(8):1–22, 2016.

[18] K. Djabella, M. Landau, and M. Sorine. A two-variable model of cardiac action potential with controlled pacemaker activity and ionic current interpretation. *2007 46th IEEE Conference on Decision and Control*, pages 5186–5191, 2007.

[19] S. Domínguez, J. Reimer, K. R. Green, R. Zolfaghari, and R. J. Spiteri. A simulation-based method to study the lqt1 syndrome remotely using the EMI model. In *Emerging Technologies in Biomedical Engineering and Sustainable TeleMedicine*, pages 179–189. Springer International Publishing, 2021.

[20] A. Ern and J.L. Guermond. *Theory and Practice of Finite Elements*. Applied Mathematical Sciences. Springer New York, 2004.

[21] Marc Ethier and Yves Bourgault. Semi-implicit time-discretization schemes for the bidomain model. *Society for Industrial and Applied Mathematics*, 46(5):2443–2468, 2008.

[22] R. FitzHugh. Impulses and physiological states in theoretical models of nerve membrane. *Biophysical Journal*, 1:445–466, 1961.

[23] P.C. Franzone, L.F. Pavarino, and S. Scacchi. *Mathematical Cardiac Electrophysiology*, volume 13. Springer International Publishing, 2014.

[24] P.C. Franzone and Giuseppe Savaré. Degenerate evolution systems modeling the cardiac electric field at micro- and macroscopic level. In *Evolution Equations, Semi-Groups and Functional Analysis*, pages 49–78. Birkhäuser Basel, 2002.

[25] D. E. Goldman. Electrodiffusion in membranes. In *Membrane Transport: People and Ideas*, pages 251–259. Springer New York, 1989.

[26] E. Grandi, F.S. Pasqualini, and D. M. Bers. A novel computational model of the human ventricular action potential and calcium transient. *Journal of Molecular and Cellular Cardiology*, 48(1):112–121, 2010.

[27] A. L. Hodgkin and A. F. Huxley. A quantitative description of membrane current and its application to conduction and excitation in nerve. *The Journal of Physiology*, 117(4):500–544, 1952.

[28] K. H. Jæger, A. G. Edwards, W. R. Giles, and A. Tveito. From millimeters to micrometers; re-introducing myocytes in models of cardiac electrophysiology. *Frontiers in Physiology*, 12:763584, 2021.

[29] K. H. Jæger, A. G. Edwards, A. McCulloch, and A. Tveito. Properties of cardiac conduction in a cell-based computational model. *PLOS Computational Biology*, 15(5):1–35, 2019.

[30] K. H. Jæger, K. G. Hustad, X. Cai, and A. Tveito. Efficient numerical solution of the EMI model representing the extracellular space (E), cell membrane (M) and intracellular space (I) of a collection of cardiac cells. *Frontiers in Physics*, 8, 2021.

[31] K. H. Jæger and Aslak Tveito. Deriving the bidomain model of cardiac electrophysiology from a cell-based model; properties and comparisons. *Frontiers in Physiology*, 12:811029, 2022.

[32] D. A. Jaye, Y.-F. Xiao, and D. C. Sigg. Basic cardiac electrophysiology: excitable membranes. In *Cardiac Electrophysiology Methods and Models*, pages 41–51. Springer US, 2010.

[33] A.M. Katz. Mechanisms of disease-cardiac ion channels. *New England Journal of Medicine*, 328(17):1244–1251, 1993.

[34] J. Keener and J. Sneyd. *Mathematical Physiology: I: Cellular Physiology*. Springer, 2009.

[35] J. P. Keener. Modeling electrical activity of cardiac cells, two variable models. Available at, http://www.math.utah.edu/~keener/lectures/ionic_models/Two_variable_models/.

[36] J.P. Keener and J. Lin. Ephaptic coupling in cardiac myocytes. *IEEE Transactions on Biomedical Engineering*, 60(2):576–582, 2013.

[37] J.P. Keener and A. V. Panfilov. A biophysical model for defibrillation of cardiac tissue. *Biophysical Journal*, 71(3):1335–1345, 1996.

[38] P. Lee, M. Klos, C. Bollensdorff, L. Hou, P. Ewart, T. J. Kamp, J. Zhang, A. Bizy, G. Guerrero-Serna, P. Kohl, J. Jalife, and T.J. Herron. Simultaneous voltage and calcium mapping of genetically purified human induced pluripotent stem cell-derived cardiac myocyte monolayers. *Circulation Research*, 110(12):1556–1563, 2012.

[39] J. Lin and J. P. Keener. Modeling electrical activity of myocardial cells incorporating the effects of ephaptic coupling. *Proceedings of the National Academy of Sciences*, 107(49):20935–20940, 2010.

[40] J. Lin and J. P. Keener. Microdomain effects on transverse cardiac propagation. *Biophysical Journal*, 106(4):925–931, 2014.

[41] J.-L. Lions. *Quelques méthodes de résolution des problèmes aux limites non linéaires*. Etudes mathématiques. Dunod, 1969.

[42] J.-L. Lions and E. Magenes. *Problèmes aux limites non homogènes et applications*. Travaux et recherches mathématiques. Dunod, 1968.

[43] C. Luo and Y. Rudy. A dynamic model of the cardiac ventricular action potential. I. Simulations of ionic currents and concentration changes. *Circulation research*, 74(6):1071–1096, 1994.

[44] C. H. Luo and Y. Rudy. A model of the ventricular cardiac action potential: depolarization, repolarization, and their interaction. *Circulation Research*, 68(6):1501–1526, 1991.

[45] C.C. Mitchell and D.G. Schaeffer. A two-current model for the dynamics of cardiac membrane. *Bulletin of Mathematical Biology*, 65(5):767–793, 2003.

[46] Y. Mori and C. S. Peskin. A numerical method for cellular electrophysiology based on the electrodiffusion equations with internal boundary conditions at membranes. *Commun. Appl. Math. Comput. Sci.*, 4(1):85–134, 2009.

[47] J. Nagumo, S. Arimoto, and S. Yoshizawa. An active pulse transmission line simulating nerve axon. *Proceedings of the IRE*, 50(10):2061–2070, 1962.

[48] J. C. Neu and W. Krassowska. Homogenization of syncytial tissues. *Critical Reviews in Biomedical Engineering*, 21(2):137–199, 1993.

[49] Steven Niederer, Lawrence Mitchell, Nicolas Smith, and Gernot Plank. Simulating human cardiac electrophysiology on clinical time-scales. *Frontiers in Physiology*, 2, 2011.

[50] Lawrence Perko. *Differential Equations and Dynamical Systems*. Springer-Verlag, Berlin, Heidelberg, 1991.

[51] J. B. Picone, N. Sperelakis, and J. E. Mann. Expanded model of the electric field hypothesis for propagation in cardiac muscle. *Mathematical and Computer Modelling*, 15(8):17–35, 1991.

[52] J. Pods. A comparison of computational models for the extracellular potential of neurons. *Journal of Integrative Neuroscience*, 16, 2015.

[53] J. Pods, J. Schönke, and P. Bastian. Electrodiffusion models of neurons and extracellular space using the Poisson-Nernst-Planck equations - Numerical simulation of the intra- and extracellular potential for an axon model. *Biophysical Journal*, 105(1):242–254, 2013.

[54] A. Quarteroni and A. Valli. *Numerical Approximation of Partial Differential Equations*. Berlin, New York, Springer, 2nd edition, 1997.

[55] P. A. Raviart and J. M. Thomas. A mixed finite element method for second order elliptic problems. *Mathematical Aspects of Finite Element Methods*, 606:292–315, 1977.

[56] P.-A. Raviart and J.-M. Thomas. *Introduction à l'analyse numérique des équations aux dérivées partielles*. Masson, 1983.

[57] M. Rioux. *Numerical computations of action potentials for the heart-torso coupling problem*. PhD thesis, Université d'Ottawa, Canada, 2012.

[58] P. J. Roache. *Verification and Validation in Computational Science and Engineering*. Hermosa Publishers, 1998.

[59] S.F. Roberts, J.G. Stinstra, and C.S. Henriquez. Effect of nonuniform interstitial space properties on impulse propagation: A discrete multidomain model. *Biophysical Journal*, 95(8):3724–3737, 2008.

[60] S. Rohr. Role of gap junctions in the propagation of the cardiac action potential. *Cardiovascular Research*, 62(2):309–322, 2004.

[61] T. Roy, Y. Bourgault, and C. Pierre. Analysis of time-stepping methods for the monodomain model. *Computational and Applied Mathematics*, 39(230), 2020.

[62] Thomas Roy, Yves Bourgault, and Charles Pierre. Analysis of time-stepping methods for the monodomain model. *Computational and Applied Mathematics*, 39, 2017.

[63] S. J. Ruuth. Implicit-explicit methods for reaction-diffusion problems in pattern formation. *Journal of Mathematical Biology*, 34:148–176, 1995.

[64] L. F. Santana, E. P. Cheng, and W. J. Lederer. How does the shape of the cardiac action potential control calcium signaling and contraction in the heart? *Journal of Molecular and Cellular Cardiology*, 49(6):901–903, 2010.

[65] N. Sperelakis. An electric field mechanism for transmission of excitation between myocardial cells. *Circulation Research*, 91(11):985–987, 2002.

[66] N. Sperelakis and K. McConnell. Electric field interactions between closely abutting excitable cells. *IEEE Engineering in Medicine and Biology Magazine*, 21(1):77–89, 2002.

[67] J. Stinstra, R. MacLeod, and C. Henriquez. Incorporating histology into a 3D microscopic computer model of myocardium to study propagation at a cellular level. *Annals of Biomedical Engineering*, 38(4):1399–1414, 2010.

[68] J. G. Stinstra, B. Hopenfeld, and R. S. MacLeod. On the passive cardiac conductivity. *Annals of Biomedical Engineering*, 33(12):1743–1751, 2005.

[69] J. G. Stinstra, S. F. Roberts, J. B. Pormann, R. S. MacLeod, and C. S. Henriquez. A model of 3D propagation in discrete cardiac tissue. In *Computers in Cardiology 2006*, volume 33, pages 41–44, 2006.

[70] G. Strang. On the construction and comparison of difference schemes. *SIAM Journal on Numerical Analysis*, 5(3):506–517, 1968.

[71] J. Sundnes, G.T. Lines, X. Cai, B.F. Nielsen, K.A. Mardal, and A. Tveito. *Computing the Electrical Activity in the Heart*, volume 1. Springer Berlin Heidelberg, first edition, 2006.

[72] R. TannerThies. *Physiology - An Illustrated Review*. New York: Thieme, 2012.

[73] K. H. W. J. ten Tusscher, D. Noble, P. J. Noble, and A. V. Panfilov. A model for human ventricular tissue. *American Journal of Physiology-Heart and Circulatory Physiology*, 286(4):H1573–H1589, 2004.

[74] Vidar Thome. *Galerkin Finite Element Method for Parabolic Problems*, volume 1054. Springer-Verlag, 2006.

[75] L. Tung. *A Bi-domain model for describing ischemic myocardial D-C potentials*. PhD thesis, MIT, Cambridge, MA, 1978.

[76] A. Tveito, K.H. Jæger, M. Kuchta, K-A. Mardal, and M.E. Rognes. A cell-based framework for numerical modeling of electrical conduction in cardiac tissue. *Frontiers in Physics*, 5:48, 2017.

[77] A. Tveito, K.H. Jæger, G.T. Lines, L. Paszkowski, J. Sundnes, A.G. Edwards, T. Mki-Marttunen, G. Halnes, and G.T. Einevoll. An evaluation of the accuracy of classical models for computing the membrane potential and extracellular potential for neurons. *Frontiers in Computational Neuroscience*, 11:27, 2017.

[78] A. Tveito, K.-A. Mardal, and M. E. Rognes. *Modeling Excitable Tissue The EMI Framework*, volume 7. Springer International Publishing, Cham, 2021.

[79] M. Veneroni. Reaction diffusion systems for the microscopic cellular model of the cardiac electric field. *Mathematical Methods in the Applied Sciences*, 29(14):1631–1661, 2006.

[80] S. Weidmann. Electrical constants of trabecular muscle from mammalian heart. *The Journal of Physiology*, 210(4):1041–54, 1970.

[81] S. Weidmann and A.L. Hodgkin. The diffusion of radiopotassium across intercalated disks of mammalian cardiac muscle. *The Journal of Physiology*, 187(2):323–342, 1966.